1974

Quantitative Analysis of Respiratory Cell Activity

Charles Lewis Webber
Loyola University Chicago

QUANTITATIVE ANALYSIS OF RESPIRATORY CELL ACTIVITY

by

Charles Lewis Webber, Jr.

A Dissertation Submitted to the Faculty of the Graduate School
of Loyola University of Chicago in Partial Fulfillment
of the Requirements for the Degree of
Doctor of Philosophy

February, 1974

DEDICATION

I take great pleasure in dedicating this dissertation to my wife, Connie, in appreciation for her constant encouragement and positive attitude throughout the period of my graduate training.

ACKNOWLEDGEMENTS

The preparation of this dissertation would not have been possible without the help and encouragement of many individuals. I am greatly indebted to Dr. Walter C. Randall, Professor and Chairman of the Department of Physiology, for initially introducing me to physiological research four years ago. My sincerest appreciation is expressed to Dr. Clarence N. Peiss, Professor of Physiology and Associate Dean of the Graduate School, for directing this study and overseeing my training as a scientist. It is also a pleasure to acknowledge the expert technical assistance of Dr. Robert D. Wurster in neurophysiological problems and Dr. Robert D. McCook in computer software programming.

Thanks are extended to Miss Carol Ofenloch for her long patience in typing the text and labeling numerous graphs. I also appreciate the time that my wife, Connie, spent in locating references and proofreading portions of the dissertation.

BIOGRAPHY

Charles Lewis Webber, Jr., was born on July 26, 1947, in Bay Shore, Long Island, New York. He completed primary and secondary education requirements of the Sayville Public School system, graduating from high school in June, 1965, with a double diploma from the local district and New York State Board of Regents. He studied at Taylor University, Upland, Indiana, for the next four years and received the Bachelor of Arts degree, cum laude, in June, 1969, with a chemistry major and zoology minor.

Charles began graduate studies in June, 1969, in the Department of Physiology, Loyola University, Stritch School of Medicine, Maywood, Illinois, and was financially supported by a Research Training Grant of the National Institute of General Medical Sciences (NIGMS). After one year of study, he selected Dr. Clarence N. Peiss to direct his graduate training and research in the field of neural respiratory control. He also took advanced mathematics courses at Illinois Institute of Technology in Chicago.

BIOGRAPHY
(continued)

In June, 1970, Charles married Constance Anne Folkers, a 1969 Taylor graduate, from Minonk, Illinois. During his last three years of graduate training, his wife taught seventh grade language arts at Gurrie Junior High School in LaGrange, Illinois. The couple resided in Broadview, Illinois.

Charles has accepted an appointment as Postdoctoral Fellow at the Max-Planck-Gesellschaft, Bad Nauheim, Federal Republic of Germany, to continue studies on respiratory cell function with Prof. Dr. K. Pleschka. He holds associate memberships in the Society of the Sigma Xi, the American Physiological Society, and the Creation Research Society.

PUBLICATIONS

1. Webber, C.L., Jr. and C.N. Peiss. Computer analysis of activity patterns in single respiratory cells. Abstract, 1st Annual Society for Neuroscience, Washington, D.C., October, 1971.

2. Webber, C.L., Jr. and C.N. Peiss. Barbiturate induced apneusis in the cat. The Physiologist 15: 299, 1972.

TABLE OF CONTENTS

TABLE OF CONTENTS
(continued)

LIST OF TABLES

LIST OF TABLES
(continued)

LIST OF FIGURES

LIST OF FIGURES
(continued)

LIST OF FIGURES
(continued)

LIST OF FIGURES
(continued)

LIST OF FIGURES
(continued)

LIST OF FIGURES
(continued)

LIST OF FIGURES
(continued)

LIST OF FIGURES
(continued)

LIST OF PROGRAMS

LIST OF PROGRAMS
(continued)

Program Page

CHAPTER I

INTRODUCTION

Information transfer along central, efferent and afferent arcs of the respiratory system are coded in terms of interspike intervals of single unit spike discharges. At the output stage, respiratory muscles decode the neuronal signals into meaningful outputs of respiratory rate and depth, the two major determinants of alveolar ventilation. However, to follow dynamic changes in information flow in a control systems approach, it is necessary to evaluate mathematically the discharge patterns from various respiratory sub-systems. Comparison of such patterns can yield important information on transfer functions between various respiratory components. The plasticity of these functions during different ventilation demands can also be evaluated.

This study was designed to examine the discharge patterns of single respiratory neurons in the medulla over wide ranges of rate and depth. The combination of

new mathematical criteria and advanced computer techniques has revealed high neuronal correlates of respiratory rate and depth, identified as medullary outputs. This has been achieved by examination of thousands of interspike intervals, their distribution and sequencing.

CHAPTER II

LITERATURE REVIEW

A. Respiratory Areas of the Medulla

Numerous studies during the last century and a half have implicated the medulla as the primary control area responsible for genesis of the respiratory act. Many technical advances have been made in the study of this system, but differences in opinion concerning medullary organization still exist today. In general, opposing views can be grouped into two broad categories irrespective of the experimental technique or animal used. One theory maintains that respiratory neurons can be assigned specific anatomical localizations within the medullary architecture, with a definite segregation of inspiratory and expiratory neurons. The alternate theory maintains that respiratory cells are freely scattered and intermingled throughout the reticular formation and are functionally tied together via extensive synaptic interconnections. It is important to consider the

evidence for each of these views.

The discrete localization or center theory was the first to gain prominence. Lorry in 1760 (111) confirmed the work of Galen (65) by showing that section of the spinal cord at the first cervical segment immediately arrested respiration in the expiratory position of apnea. This indirectly demonstrated that the genesis of rhythmic respiratory movements was rostral to the cord. Legallois in 1812 (107) supplied the first direct evidence that the medulla possessed respiratory function by showing that rhythmic breathing persisted in young rabbits with removal of the cerebellum and part of the upper bulb. Flourens in 1842 (59) further localized this active lower bulbar region to a one millimeter area at the apex of the calamus scriptorius. Destruction of this "vital node" halted all respiratory movements. Flourens (60) later relocated the "vital node" 2.5 millimeters on either side of the midline at the level of the obex. In 1880, Marckwald and Kronecker (118) attempted to divide the respiratory center into inspiratory and expiratory portions, and Lumsden in 1923 (112, 113, 114) distinguished between an expiratory and gasping center in the medulla of the cat by means of transection procedures.

Active expiratory and inspiratory regions were

mapped with stereotaxic placement of stimulating electrodes. Pitts, Magoun and Ranson (145) explored the brainstem of the cat from the hypothalamus to the cervical cord with a bipolar stimulating electrode and were able to elicit maintained inspiratory or expiratory responses from the medulla. Since maximal responses could not be evoked either above or below the medulla, the authors claimed that their stimulations were selective for cell bodies and not fiber tracts. Expiratory responses were concentrated dorsal, rostral and medial to inspiratory responses, each occupying approximately 30 cubic millimeters of the reticular formation bilaterally, although some overlapping was observed. Pitts (140) reconfirmed functional subdivisions of the respiratory center into inspiratory and expiratory portions in a subsequent publication. Monnier (124) arrived at similar conclusions from his own work.

In the monkey, Beaton and Magoun (23) reported the existence of two discrete regions which when activated produced either inspiratory apneusis or expiratory apnea. The inspiratory activity was located dorsal and medial to the rostral half of the inferior olive. The expiratory activity surrounded the inspiratory field rostrally, caudally, laterally and dorsally. The authors concluded

that this mapping in the monkey corresponded to that in the cat as reported by Pitts et al.(145), but this is questionable. Amoroso, Bell and Rosenberg (6) completed a similar study in the sheep and found that respiratory responses were aggregated in the reticular formation of the medulla from the aroustic tubercles rostrally, to just behind the obex caudally. The expiratory region was located dorsal, anterior and lateral to the inspiratory region and both had bilateral representation. Ondina, Yamamoto and Masland (136) prepared stimulation maps of the rat brainstem. Respiratory regions identified by sustained inspiratory or expiratory apnea were clearly separated. The inspiratory center was found bilaterally above the rostral one-third of the inferior olive and the somewhat more diffuse expiratory center was located dorsal and caudal to the inspiratory center.

Localization of specific structures in the brainstem by the use of stimulating electrodes met with much criticism since such a large volume of tissue was activated. This technique was defended by Pitts (140) and Magoun and Beaton (115). The latter identified active respiratory sites in the medulla by stimulation, placed a lesion at the same locus and then restimulated. Lesions which extended no more than 0.7 millimeter from

the electrode tip abolished the respiratory response to the second stimulation. The authors used this as a measure of current spread during stimulation procedures.

Comroe (46) attempted to identify respiratory areas of the brainstem by microinjection of CO_2-bicarbonate solutions into the brain tissue, but met with serious problems localizing the stimulus to a small area. Nevertheless, general areas which yielded immediate hyperpneic responses corresponded to the inspiratory region of Pitts (140, 145). No expiratory responses were seen.

Evidence for separation of inspiratory and expiratory regions in the medulla has also come from extracellular recordings of single respiratory cell discharges. Nelson (127) found 110 single units in the cat and concluded that the expiratory area was dorsal to the inspiratory area. He was careful to record only from cell bodies which could be distinguished from fiber pathways by a technique of wave form identification. Haber, Kohn, Ngai, Holaday and Wang (79), however, suggested a new location for the expiratory center. Recording from single cells, these workers found that the inspiratory region in the cat corresponded to the stimulation maps of Pitts *et al.* (140, 145), but the expiratory region was located

more caudal with no difference in dorsal-ventral distribution of inspiratory and expiratory areas.

Woldring and Dirken (180) explored the brainstem of the rabbit with extracellular microelectrodes from the caudal border of the corpora quadrigemina to the exit level of the first spinal roots. They found respiratory activity only in an area extending from the obex to a plane 3 millimeters rostral to the obex. In this area, inspiratory and expiratory cells had a definite anatomical distribution. The inspiratory area was located 2.5 millimeters from the dorsal surface and was associated with the ventromedial reticular substance at the level of the vagal rootlets. The expiratory area was located 2.0 millimeters from the dorsal surface and was associated with the dorsolateral reticular formation. The expiratory area appeared to be connected with the spinal trigeminal root laterally and coursed parallel to the solitary tract medially. Batsel (14) published similar results from microelectrode recordings in the cat, dog and monkey. The medulla was explored from 6 millimeters rostral to 4 millimeters caudal to the obex and two bilateral groups of bulbar respiratory cells were identified. The larger area was located in and along the motor nuclei of the ninth and tenth cranial nerves.

The smaller area was located ventrolateral to the fasciculus solitarius, just rostral to the obex. Inspiratory and expiratory cells could not be separated in the dorsal-ventral direction, but the latter were found more frequently in the caudal medulla. Batsel (14) suggested that the recorded electrical activity came from closely packed cells indicative of specialized respiratory centers.

Merril (122) was able to distinguish between two major concentrations of respiratory cells in the medulla by mapping the data from each cat separately. One group was near the nucleus ambiguus and the other was associated with the solitary tract. Achard and Bucher (1) suggested that the lateral respiratory cells were not reticular cells, but rather nucleus ambiguus motorneurons. Von Baumgarten and Kanzow (19) recorded inspiratory potentials from the reticular formation just ventral to the tractus solitarius and 1-3 millimeters rostral to the obex. Nesland, Plum, Nelson and Siedler (129) occasionally recorded from expiratory and inspiratory cells at the same location, but reported that cells with expiratory phasings were localized more caudal and dorsal to the inspiratory cells.

In contrast to the foregoing, other experimental evidence suggests that medullary neurons are diffusely

organized and do not exhibit anatomical localization of inspiratory and expiratory areas. Longet in 1847 (110) showed that respiration was not affected by localized destruction of the pyramids and restiform bodies. However, destruction of the reticular formation at the same level immediately halted respiration. Gad and Marinesco in 1892 (64) confirmed this observation by cauterizing certain areas of the medulla. Only when the reticular substance of the floor of the fourth ventricle was destroyed did breathing stop. Arnheim (8) was also of the opinion that the bulbar neurons responsible for the generation of respiration were located diffusely in the reticular gray matter.

The stimulation technique has been used to show diffuse organization. Brookhart (34) stimulated the brainstem of dogs from 9 millimeters above to 6 millimeters below the obex with microelectrodes. With low voltage stimulations he got variable respiratory rate changes which were not correlated with any structure. The results failed to confirm the existence of compact inspiratory and expiratory centers described by Pitts et al. (140, 145) in the cat. Brookhart (34) suggested that the reticular formation was the seat of primary respiratory cells without detectable anatomical

differentiation of function. Liljestrand (108) studied in depth the respiratory movements which could be induced by stimulation of the medulla both electrically and chemically. He stated that inspiratory and expiratory areas were not separated and in his own words added, "Until further evidence of a respiratory centre has accumulated the term should be strictly defined when used, or otherwise it should be avoided."

Kim and Carpenter (100) used a different stimulation technique to induce respiratory movements. Ventilation changes comparable to electrical activation of the same area could be produced by injections of isotonic solutions of HCO_3^-, $HPC_4^=$ or citrate into the medullary reticular formation of the cat. The apneustic responses observed could be evoked from random reticular formation sites and the authors concluded that chemical stimulation of respiratory neurons represents a functionally non-specific phenomenon.

The extracellular recording technique has also been used to demonstrate diffuse medullary organization. Gesell, Bricker and Magee (70) published the first report of single respiratory cell recordings. The medulla, upper cervical cord, thalamus, hypothalamus, midbrain and pons of the dog were explored with bipolar needle

electrodes. Areas yielding rhythmic respiratory discharges were lesioned for histological identification. In all the regions examined, respiratory potentials were found most frequently in the reticular gray in the region of the obex, but no correlation could be made associating cell type with any one particular brainstem structure, either nucleus or tract. The organization of inspiratory and expiratory regions appeared to be diffuse. The authors commented that the reticular gray is influenced by every type of sensory signal, which may explain activation of the respiratory system during different situations. Amoroso, Bainbridge, Bell, Lawn and Rosenberg (5) used metal microelectrodes to study single respiratory cell discharges in the dog, cat and rat. These electrodes recorded from a brain tissue volume which was one thousandth of that activated by a small stimulating electrode. Because of this high specificity, respiratory potentials were difficult to locate. The authors wrote, "The scarcity of respiratory potentials in the reticular formation of the medulla suggests that generally this structure does not function as a whole but only in parts. It seems to act as a trigger, periodically firing spinal, phylogenetically older, neuronal aggregates which are ultimately responsible for the

coordinated respiratory movements."

Hukuhara, Nakayama and Okada (91) recorded respiratory potentials from the striae acousticae level in the lateral reticular formation of the dog and cat brain and suggested that this was the normal respiratory center. Although this localization did not agree with that of Gesell et al. (70), no differentiation of inspiratory and expiratory areas was possible. Hukuhara et al. (91) also discussed the coursing of centrifugal respiratory pathways through the lateral reticular formation of the medulla. Salmoiraghi and Burns (155) prepared a map of the brainstem localizing respiratory discharges in the cat. While no respiratory cells were found in the pons, potentials in phase with the respiratory cycle were localized in the medulla 2-4 millimeters below the dorsal surface on either side of the obex. Inspiratory and expiratory cells could not be anatomically distinguished and were sometimes found within 100 microns of each other. Brodie (31) reported that one electrode could record activity from both inspiratory and expiratory cells at the same time and concluded that these cell types were intermingled. Harris (81) came to the same conclusion.

Finally, von Baumgarten and Salmoiraghi (21)

studied the localization of respiratory neurons in the goldfish via electrical recording. They found that respiratory cells were bilaterally organized in narrow bands extending rostrally from the mid-vagal lobes. The cells with opposite phasing patterns corresponding to inspiratory and expiratory units were not segregated into different areas. The cells laid close to the segmental columns of the motor nuclei from the fifth to twelth cranial nerves.

Conclusions defining strict medullary organization of the respiratory system are difficult to make. From the clinical work of Baker, Matzke and Brown (11), respiratory failure during bulbar poliomyelitis definitely involves pathologic alterations in cells of the nucleus ambiguus although similar structural changes are also seen among other large and small reticular cells, many of which must also subserve a respiratory function. Weighing the evidence presented, it can be suggested that any concept of medullary organization must simultaneously explain the following two characteristics. First, inspiratory cells are anatomically scattered throughout the medullary reticular formation apparently without any logical ordering. Second, inspiratory and expiratory divisions of the respiratory system each function in a

highly integrated fashion. Obviously, the respiratory representation in the medulla poses interesting structure-function problems.

B. Apneusis

Knowledge concerning the organization of the brainstem respiratory system has been extended by many studies into the phenomenon of apneusis. It is now clear that medullary structures alone are not responsible for the coordinated act of respiration. The pons appears to contain two general populations of neurons which influence medullary respiratory cell discharge to respiratory motorneurons.

It is interesting that the definition of apneusis has slowly changed in the literature. When the concept was first introduced (116, 117) it was associated with maximal inspiratory cramps which were maintained until the preparation died from asphxia. Later, apneusis was described as an abnormal respiratory pattern characterized by periodic escape from sustained inspiratory efforts (26, 87, 112). Workers attributed this pattern to a specific cyclic function of the respiratory system which could be maintained for long periods of time. Other investigators (112) redefined apneusis as cyclic submaximal inspiratory holds. This, along with the

observation that apneusis was not a permanent pattern, prompted the suggestion that apneusis was the result of non-specific facilitation of medullary respiratory areas (26, 87). These differences in length and depth of inspiratory holds and duration of apneusis are a reflection of the various techniques used to induce this unusual breathing pattern.

Marckwald in 1887 (116) and 1890 (117) observed long inspiratory cramps in vagotomized rabbits if the brainstem was transected just behind the posterior colliculi. These inspiratory holds continued uninterrupted until asphyxial death if the trigeminal nerves were damaged. Vagotomy in preparations with transections placed just in front of the posterior colliculi failed to develop the characteristic inspiratory movement. Breathing simply became deeper and slower as seen after vagotomy in animals with intact brainstems. Marckwald (116, 117) concluded that the posterior colliculi contained a center inhibitory to inspiration. Loewy in 1888 (109) confirmed this observation.

Lumsden (112, 113, 114), using the transection technique, made major contributions on pontine organization. In one paper (112) he showed that vagotomy in cats with brainstem sectioned immediately behind the

posterior colliculi did not produce the inspiratory cramps described by Marckwald (116, 117). The inspiratory holds or apneusis, as Lumsden (112) called them (Greek for a holding of the breath), occurred only in cats with transections a few millimeters below the upper border of the pons when the vagi were cut. This apneusis was converted into a gasping respiration when another transection was introduced below the striae acousticae. The conclusions were obvious. That is, the lower pons contained an apneustic center which drove the gasping center of the medulla continuously when inhibition from the pneumotaxic center in the upper pons and vagi were removed. In another article, Lumsden (113) discussed his concept of an expiratory center in the medulla in order to explain active forced expirations and summarized his thoughts in a third publication (114) relating vagal impulses to central respiratory organization and rhythmic breathing.

An alternate view of apneusis was presented by Henderson and Sweet (83) and Hess (85) who suggested that the phenomenon was a manifestation of decerebrate rigidity. The authors explained that the apneusis they saw in mid-pontine cats with cold blocked vagi was due to tonic activity of medullary centers released from red nucleus inhibition by severing of the rubro-spinal

tracts. The vagi were believed to inhibit inspiration via direct inhibition of the general brainstem facilitatory mechanism. Hoff and Breckenridge (26, 87) also concluded that apneusis was best regarded as decerebrate rigidity of the respiratory system. They made the following major observations in the dog and cat. First, apneusis was not permanent as suggested by Marckwald (116, 117), but was an oscillating respiratory pattern. Second, apneusis was not total since alternating inspiration-expiration efforts were often seen superimposed on apneustic breaths. Third, as preparations deteriorated, apneusis was replaced by relatively normal respiratory patterns. Last, apneusis could be abolished by separation of the medulla from the pons as described by Lumsden (112). Breckenridge, Hoff and Smith (28) also showed that intravenously administered myanesin, a drug which blocks decerebrate rigidity, also converted apneustic breathing into normal respiratory patterns.

Stella (167) refuted the conclusions of Henderson and Sweet (83), Hess (85) and Hoff and Breckenridge (26, 87) and maintained that apneusis was a specific respiratory event. He showed that elimination of the red nucleus and/or posterior colliculi did not alter normal respiratory patterns. Apneusis resulted only when the upper pons

was removed in vagotomized preparations. This confirmed the inhibitory function of the upper pons (pneumotaxic area) first introduced by Lumsden (112). Stella (167) also demonstrated that apneusis was not dependent on proprioceptive reflexes from the respiratory muscles by showing that apneusis persisted in a deafferented brainstem preparation. This, of course, differentiated apneusis from decerebrate rigidity, since the latter could be terminated by dorsal root section.

Wang, Ngai and Frumin (176) reexamined the results of Breckenridge, Hoff, and Smith (28) who abolished both decerebrate rigidity and apneusis with myanesin. By using low doses of this drug, Wang et al. (176) were able to differentially block body rigidity without altering the apneustic breathing pattern. The authors interpreted these results as inferring that apneusis and decerebrate rigidity were two separate phenomena. Ondina, Yamamoto and Masland (136) qualified these results by suggesting that if apneusis were a phenomenon of bulbar facilitation, the sources of this facilitation did not lie in the same cells as those which facilitated the postural musculature. They demonstrated that in the rat, an animal which rarely displays decerebrate rigidity, apneusis can readily be induced by brainstem transection

at the mid-pons level and vagotomy without the manifestation of body rigidity.

Electrophysiological evidence supports the notion of a pontine apneustic area. Ngai and Wang (135) used the stimulation technique in cats with intact brainstems. They found that stimulation from a level 3 millimeters behind the rostral border of the pons extending caudally to the trapezoid body interrupted rhythmic respiration with a maximal inspiratory movement. The active brainstem area corresponded to Lumsden's (112) apneustic center. Kahn and Wang (96) recorded from single inspiratory and expiratory cells in midpontine cats and monitored the phrenic discharge. After vagotomy, inspiratory cells and phrenic patterns became continuous as apneustic breathing was initiated. Expiratory cells discharged only during the brief interruptions of inspiratory holds. In a central vagal stimulation study, Kerr, Dunlop, Best and Mullner (99) assigned the apneustic area to a supramedullary level at the origin of the eight cranial nerve just lateral to the midline. The authors suggested that the apneustic area may have some involvement with the vestibular system.

The removal of pneumotaxic and vagal inhibitions is important for the unmasking of apneustic drive.

Consequently, apneusis has been used as an endpoint in vagotomized preparations to locate pneumotaxic areas in the upper pons by tissue destruction. Pitts, Magoun and Ranson (147) made bilateral electrolytic lesions in the cat brainstem with stereotaxic placement of electrodes and localized the pneumotaxic area to the tegmentum of the upper few millimeters of the pons. Lesions in the inferior colliculi and red nuclei did not result in apneusis thereby refuting the work of Marckwald (116, 117) and Henderson and Sweet (83) respectively. Tang and Ruch (172) localized the pneumotaxic area in the dorsolateral portion of the rostral pons by suction destruction or electrolysis. Tang (170) later refined the location to the extreme dorsolateral portion of the anterior pontine tegmentum, the isthmus. Ngai and Wang (134) associated the pneumotaxic region with the dorsolateral reticular formation since stimulation in this area accelerated respiratory rate and destruction led to apneusis when the vagi were cut. Johnson (93) found similar results and placed the pneumotaxic area in the latero-dorsal tegmental nucleus or locus coeruleus. Baxter and Olszewski (22) also suggested that the cells of the locus coeruleus nucleus formed a major part of the pneumotaxic area.

Using the above localization data for the pneumotaxic center, St. John, Glasser and King (151) placed chronic lesions in the dorsolateral pontine regions of the cat. Rhythmic respiration was observed in all cats after recovery from anesthesia, but when the vagi were severed up to thirteen weeks later, cats with pneumotaxic center lesions immediately developed apneustic patterns. Cats with control lesions a few millimeters anterior or posterior to the pneumotaxic level did not develop apneusis. The authors concluded that their lesions chronically knocked out pneumotaxic participation in the genesis of eupnea. St. John, Glasser and King (152) later showed that vagotomized cats with chronic pneumotaxic lesions were capable of normal respiratory rhythmicity when awake. This demonstrated that higher regions of the central nervous system could maintain respiratory rhythmicity in the absence of pneumotaxic or vagi inhibitions.

From these accumulated data it has been concluded that the pneumotaxic and apneustic areas of the brainstem are directly involved with respiratory mechanisms. Unlike medullary inspiratory and expiratory areas, the pontine regions appear to be anatomically discrete.

The length and depth of apneustic breaths depend

on a number of factors besides the removal of pneumotaxic and vagal afferent inhibition. Additional factors to be considered are the chemical status of the preparation, integrity of cerebellar structures and the anesthetic drug type and level.

Stella (168) produced apneustic breathing in cats by transecting at the mid-pontine region and cold-blocking the vagus nerves. When the CO_2 content of the inhaled air was elevated to 8-10%, apneustic breaths became much deeper and prolonged. These results could be duplicated by using a rebreathing procedure. Hoff and Breckenridge (87) found that peripheral chemoreceptor stimulation by carotid occlusion prolonged or intensified the apneustic pattern in dogs. Also, vagotomy failed to induce apneusis in mid-pontine dogs with carotid denervation. The authors suggested from these results that apneusis derives from the interplay of peripheral carotid body and central lower pontine factors.

Ngai (130) determined the O_2 consumption, arterial blood pH, $PaCO_2$, PaO_2 and O_2 saturation during apneustic breathing in cats. Compared with control respiratory values, apneusis induced a respiratory acidosis with no change in the PaO_2 or O_2 consumption (cats breathed oxygen rich mixtures). Administration of 10% CO_2 increased the

depth of each apneustic breath and accelerated the apneustic cycle. The latter finding is in disagreement with that reported by Stella (168). Since this response persisted after carotid denervation, Ngai (130) concluded that apneustic cycling was probably due to the elevated arterial CO_2 tensions and was independent of the peripheral chemoreceptors.

Katz, Ngai, Nahas and Wang (98) studied the effect of pH alterations on apneusis. Two agents which elevate the pH (THAM, an organic buffer, and sodium bicarbonate) were infused intravenously in mid-pontine vagotomized cats displaying apneustic respiration. Neither agent altered the depth of apneusis, but THAM decreased the apneustic cycling while sodium bicarbonate increased the cycling. These apparently conflicting results were explained on the basis of possible differential distribution of the two agents across cell membranes. The authors suggested that if this were the case, the intracellular pH may be the critical factor for modulation of apneusis.

The effect of cyanide on apneusis was studied by Brodie and Borison (32). They showed that cyanide can convert apneustic breathing into a gasping pattern, a response which was independent of peripheral chemoreceptor

denervation. Ngai (130) reported that intracarotid injection of sodium cyanide can accelerate apneustic cycling thus demonstrating that cyanide does exert a peripheral influence also.

Although it is not commonly recognized, the cerebellum appears to have some connections with the brainstem respiratory system. Henderson and Sweet (83) mentioned that cerebellectomy could produce apneusis which disappeared after a short period. Using mid-pontine cats, Glasser, Tippett and Davidian (76) studied respiratory pattern changes during cerebellar depression induced by several techniques: occlusion of the cerebellar arteries, procaine or xylocaine application to the surface or subcortex of the cerebellum, or removal of part or all of the cerebellum by suction. Irrespective of the method used, cerebellar depression in mid-pontine cats with intact vagi led to a fall in respiratory rate and an increase in respiratory depth to the point of apneusis in many cases. The authors concluded that the cerebellum exerted a tonic inhibitory influence on the brainstem respiratory mechanism. The inhibition might have arisen in the anterior and posterior lobes of the corpus cerebelli, but brainstem projections were unknown. Another interesting report from Gesell, Bricker and Magee (70)

suggested that the cerebellum may contribute to the integration of the respiratory act. They were able to locate three single cell potentials in the region of the brachium conjunctivum (superior cerebellar penduncle) which had respiratory discharge patterns. It is possible that these were efferent fiber tracts from the cerebellum to the pons or medulla mediating respiratory inhibition.

There is a considerable body of evidence which indicates that high levels of barbiturate can convert normal respiratory patterns into apneustic ones even when all brainstem structures and vagi are intact. Harris and Borison (82) anesthetized cats with 36 mg/Kg pentobarbital and stimulated inspiratory regions of the medulla during pentobarbital titration until the spontaneous respiration was arrested. With progressively higher doses, the threshold to produce apneusis via medullary stimulation consistently decreased. At an accumulated dose of 45 mg/Kg pentobarbital, the respiratory cycle was lengthened with a progressive increase in the expiratory phase. With higher doses approaching the respiratory depression level of pentobarbital (mean 50 mg/Kg, range 33-70 mg/Kg) inspiratory holds of apneusis were observed in preparations with intact brainstems and vagus nerves. These results showed that pentobarbital selectively depressed systems

which were inhibitory to inspiration. The inspiratory apparatus was presumably depressed to some extent since apneustic breaths were of low amplitude.

A similar study was done by Ngai (131) who extended stimulation sites to the pons during pentobarbital accumulation in the midcollicular, vagotomized cat. At doses from 24 to 30 mg/Kg the inspiratory movements became apneustic in type except for a greatly reduced depth. At this same dose level, stimulation of the pneumotaxic region failed to accelerate respiratory rate as in control cases, but central vagal stimulation was still effective. The author concluded that pentobarbital produced apneusis in the decerebrate vagotomized cat by blocking pneumotaxic inhibition of the apneustic areas. Comparison of Ngai's (131) data with those of Harris and Borison (82) reveals that the pneumotaxic mechanism is more sensitive to pentobarbital depression than is vagal afferent feedback. St. John, Glasser and King (151) reported that cats with chronic pneumotaxic lesions, anesthetized with 35 mg/Kg pentobarbital, repeatedly had bouts of apneusis following small additional doses of pentobarbital and bilateral vagotomy. A similar prolongation of the inspiratory phase with thiopental has been published by Brodie (31).

Korczyn, Leibowitz and Bergmann (104) studied the

effect of pentobarbitone dose level on the respiratory response evoked by sciatic nerve stimulation. Control responses ranging from acceleration at low frequency stimulation to deceleration of breathing at high frequency stimulation could all be blocked by high doses of the barbiturate. These data parallel the blockade of vagal inhibition in the experiments of Harris and Borison (82) who observed apneusis in vagi intact cats with high doses of pentobarbital.

Robson, Houseley and Solis-Quiroga (148) studied barbiturate effects on respiration at the single neuron level. Successive increments of sodium pentobarbital or sodium thiopental in cats caused either the inspiratory or expiratory cell discharges to fire continuously. The inspiratory cell pattern resembled that of apneusis. The authors explained that the elevated excitatory firing of expiratory cells was due to barbiturate arrest of mutually inhibitory pathways between inspiratory and expiratory neurons.

Finally, Naifeh, Huggins and Hoff (125) studied respiratory pattern changes in crocodiles during pentobarbital accumulation. The authors termed this technique "anesthetic dissection," but were not able to induce apneusis as observed in other animal preparations under

similar conditions. These results were explained by Naifeh, Huggins and Hoff (126) in another publication in which serial transections were made in the crocodile brainstem. No evidence was found for an apneustic area in this animal. This is a good example of species differentiation in brainstem organization of the respiratory control system.

C. Medullary Outputs

The primary function of respiration is to maintain arterial blood oxygen, carbon dioxide and hydrogen ion concentrations in homeostatic proportions. To do this, metabolic drives determine the proper alveolar ventilation for the situation at hand by adjustment of respiratory rate and tidal volume, the two outputs from the brainstem respiratory complex. Although there are numerous respiration rate - tidal volume combinations which can generate a specific alveolar ventilation, workers such as Rohrer (149) and Otis, Fenn and Rahn (137) have suggested that the respiratory frequency is selected so as to minimize the amount of work expended by the respiratory musculature. Alternately, Mead (120, 121) has proposed that breathing is adjusted to minimize the muscle force instead of the work. In either case, any acute or chronic change in the mechanical properties of the chest or lung should manifest itself by a different optimal

breathing frequency. Also, removal of major compliance feedback via vagotomy should increase the work of breathing. Zechman, Salzano and Hall (184) confirmed this by showing that the regulation of rate and depth of breathing was less efficient when pulmonary afferents were blocked. Salzano and Hall (157) later reported that vagal reflexes did not influence the work of breathing during severe hypoxia or hypocapnia as much as they did during normal or obstructive breathing.

It is difficult to rank medullary outputs in order of primary (active) or secondary (passive) control. Many experiments have shown that rate and depth components are highly integrated and only a few have succeeded in separating the outputs into two component systems. The following discussion will consider system interactions responsible for the genesis of rate and depth outputs.

The respiratory rate output presents itself as a two-fold problem. First, generation of the basis rhythmicity must be explained and second, basic mechanisms which modulate this rhythm need to be examined. Hoff and Breckenridge (88) have classified breathing into three normal patterns (eupnea, sighing and panting) and three abnormal patterns (Cheyne-Stokes, Biots and apneusis). Each pattern is characterized by a specific rate-depth

combination which derives from medullary, pontine and vagal afferent interactions.

A large body of experimental evidence suggests that respiratory systems of the medulla are spontaneously rhythmic. One of the first observations came from Lumsden (112) who showed that medullary cats gasped rhythmically. Stella (167) reported that regular and smooth respiration was seen in the cat after thorough deafferentation of the medullary centers and concluded that the pattern was due to automaticity of the centers involved. Hoff and Breckenridge (87) showed that a dog can continue to breath for 5 to 6 hours in an approximately normal fashion after having been deprived of all pontine and vagal connections. The authors suggested that the rhythm was maintained via reciprocal innervation of inspiratory and expiratory neurons. In another paper, Breckenridge and Hoff (26) repeated these experiments in the cat. Again, medullary preparations showed rates and depths similar to those seen in midcollicular preparations before vagotomy. The authors concluded that medullary centers were automatic and were regulated only secondarily by facilitatory and inhibitory areas of the brain. Breckenridge and Hoff (27) later showed that breathing could be maintained reflexly when medullary centers were depressed to apnea

following drug administration or anoxia.

Other workers have agreed that the medulla possesses inherent rhythmicity. Ngai, Frumin and Wang (133) wrote, "The medullary respiratory centers have an autonomous rhythm when released from the influence of pneumotaxic and other pontine centers and afferent vagal impulses." Tang (170) wrote, "It thus appears that vagal and pneumotaxic afferent influx is not the sole determinant of respiratory periodicity for rhythmic breathing persists after elimination of such influx."

Brodie and Borison (33) attempted to study the relationship between gasping mechanisms and the generation of other rhythmic forms of respiration. In decerebrate cats, gasping could be induced by stimulation of the floor of the fourth ventricle a few millimeters rostral to the obex. Since ablation of Pitts' (145) expiratory region did not abolish this gasping response, the workers suggested that the gasping rhythm was not due to reciprocal connections between inspiratory and expiratory neurons. An alternate interpretation is that all expiratory cells were not destroyed.

Ondina, Yamamoto and Masland (136) observed the medullary rat for a prolonged time and described the development of respiratory incoordination or ataxia

consisting of a dissociation of inspiration-expiration sequencing. The authors suggested that this might have been due to altered linkage between loosely associated inspiratory and expiratory systems in the cat medulla.

In a series of stimulation experiments, Borison (25) described a spasmodic respiratory response which could be evoked from activation of the dorsolateral region of the myelencephelon. The response consisted of a series of strong inspiratory and expiratory movements every one to four seconds. Borison (25) suggested that medullary cats without pontine and vagal connections may rhythmically breathe or gasp because of oscillatory drives from this spasmodic center.

Other workers have suggested that gasping is not a normal respiratory pattern. Hukuhara and Nakayama (90) showed that eupneic-like gasping did not develop immediately following isolation of the medulla, but depended on deterioration of the animal. Barcroft (13) described gasping as an all or none type of breathing in which inspiratory depth appeared to be maximum. Brodie and Borison (32) showed that gasping rate was not increased by chemoreceptor activation at low PaO_2. Ngai (130) showed that gasping provided inadequate ventilation for the cat, resulting in respiratory acidosis. From this

evidence it is concluded that medullary areas are spontaneously rhythmic, but the isolated medulla is incapable of providing adequate ventilation.

Kahn and Wang (96) emphasized that pontine circuits must be accounted for in any explanation of the genesis of eupneic respiration. Coordinated oscillations of pontine and medullary structures was demonstrated by Adrian and Buytendijk (4) in isolated goldfish brains. They recorded gross potential discharges from the vagal lobes which oscillated at frequencies close to the gill movement rhythm in the intact fish. This paper demonstrated that rhythmicity can be present in the absence of afferent input, although the frequency did depend on the O_2 and CO_2 tensions in the surrounding fluid.

Mechanical afferent input can be eliminated by pharmacological blockade of the respiratory musculature. Von Baumgarten and Salmoiraghi (21) recorded rhythmic cell discharges from respiratory neurons in goldfish treated with succinycholine to produce myoneural block. Gesell, Atkinson and Brown (69) showed that curare-induced motor paralysis in the dog did not block rhythmic phrenic discharges. Kahn and Wang (94) reported the same results in gallamine-blocked cats. Joels and Samueloff (92) found that the recurrent laryngeal nerve still

exhibited rhythmic bursts of action potentials in the dog and cat whose respiratory movements had been blocked with succinlycholine.

While there is general agreement that midcollicular-decerebrate and vagotomized preparations exhibit rhythmic respiratory movements, the mechanism for the genesis of these oscillations is still disputed, mainly due to differences of opinion on pontine-medullary organization. Lumsden (113) attributed rhythmicity in the mammal to an interaction between his apneustic and expiratory centers which were both under the control of the higher pneumotaxic center. He suggested that the gasping center was overridden by pontine influence when both pons and medulla were intact.

Pitts, Magoun and Ranson (147) suggested that medullary centers were not inherently rhythmic since their medullary cats displayed apneusis. Rhythmic breathing was believed to be due to periodic inhibition of the tonically active inspiratory areas via pneumotaxic or vagal afferent feedback. Although rhythmicity could be explained on the basis that the pneumotaxic system was either spontaneously rhythmic or reflexly activated via proprioceptive afferents like the vagal mechanism, the authors favored the concept that the inspiratory area

sent collaterals up to the pneumotaxic region to activate inhibitory outflow. The reciprocal interchange between these two areas could produce rhythmic respiration even when the vagi were severed.

Wang, Ngai and Frumin (176) modified the schema of Pitts et al. (147), in whose experiments a portion of the lower pontine area had been left intact in the preparation of medullary animals. Wang et al. (176) made a definite distinction between the apneustic region of the lower pons and the medullary inspiratory area. Rhythmicity was believed to result from periodic inhibition of the apneustic region by vagal afferents and by the pneumotaxic area which was activated via apneustic center output. The authors suggested that inspiratory areas of the medulla, passive by themselves, were driven by apneustic outflow.

The pneumotaxic region may exert some modulatory control on respiratory rate since both Ngai and Wang (134) and Johnson (93) have shown that stimulation of the dorsolateral reticular formation of the pons accelerated respiratory rate. Kahn and Wang (95) studied the role of the pneumotaxic area in the establishment of rhythmicity by examining phrenic nerve discharges. Bilateral vagotomy had only slight effect on the phrenic discharge

pattern. Mid-pontine transection, however, greatly modified the discharge which became semi-continuous, yet still oscillatory. It was concluded that the pneumotaxic center provided important information for respiratory manifestation of eupnea and rate-setting control. Cohen and Gootman (44) suggested that the pneumotaxic region may be involved in reverberating mechanisms of respiratory rhythmicity in the brainstem.

Further evidence of pneumotaxic function has come from two different laboratories although both substantiate each other. First, Bertrand and Hugelin (24) delivered single or double stimuli, given at random within the respiratory cycle, to the nucleus parabrachialis medialis of the upper lateral pons. They found that the phrenic discharge could be synchronized by this pneumotaxic stimulation suggesting direct excitation of a self-reexciting system acting as a pacemaker. Cohen (43) brought the evidence one step further and was able to differentiate between two pneumotaxic functions: (1) stimulation of the dorsolateral pons facilitated phrenic discharge with earlier burst termination and decreased the expiratory phase; (2) stimulation of the ventrolateral pons reduced the phrenic discharge with an even earlier burst termination and prolonged the expiratory phase. The phase

switching response was shown to be dependent on stimulus current, frequency, total number of stimuli, and the timing of stimulation in relation to the respiratory cycle. Cohen (43) concluded that the pneumotaxic region may function to smooth transitions from inspiration to expiration and vice versa.

Tang (171) reported that destruction of the pneumotaxic center in cats with intact vagi depressed the depth response to CO_2. The respiration rate increase evoked by CO_2 was essentially unaffected. Tang (171) suggested that the pneumotaxic mechanism was responsible for depth modulation and could maintain constant rates in absence of vagal feedback. The pneumotaxic control was believed to operate through the apneustic system. St. John (150) confirmed this observation in conscious cats with either unilateral or bilateral chronic lesions placed in the pneumotaxic region. These cats displayed diminished tidal volume responses to hypercapnia. The tidal volume response to hypoxia was unaffected, however, and St. John (150) concluded that other regions of the central nervous system had tidal volume regulating capability in the conscious animal.

For a long time it has been recognized that bilateral vagotomy results in slower and deeper breathing.

As early as 1868, Hering and Breuer (84) and Breuer (29) demonstrated that inflation and deflation reflexes were mediated via vagal afferents and concluded that the oscillatory nature of breathing was regulated by pulmonary reflexes. Widdicomb (178, 179) has reviewed a multiplicity of reflexes which are carried in the vagu nerves, but one, the inflation reflex, has prime importance in directly modifying respiratory rate and depth. Consequently, much evidence has been complied on this reflex concerning receptor site, afferent path, anatomical and functional central projections and involvement in rate and depth control.

Receptors mediating the inflation reflex have been found in the small and large air passages in the lungs. Whitteridge and Bülbring (177) assigned a bronchial or bronchiolar location to the receptors and Hammouda and Wilson (80) showed reflex inhibition of inspiration by tracheal distension. Davis, Fowler and Lambert (49) found that many pulmonary afferents exhibited discharge patterns which paralleled airway pressures more closely than lung volume changes and concluded that the receptors were located in the air passages. An interesting confirmation of this came from Aviado and Schmidt (10) who showed that steam inhalation blocked the inflation reflex

without any apparent alveolar damage.

The afferent nervous pathway for the inflation reflex has been established as vagal. Hering and Breuer (84) and Steffensen, Brookhart and Gesell (166) showed that the inflation reflex could be blocked in the dog, cat and rabbit by cooling the vagi to 8°C while other vagal reflexes were left unimpaired. Paintal (138) identified fibers mediating the inflation reflex as belonging to the Aα and Aβ groups. Einthoven (52) in 1908, studied vagal afferent action currents from the cut peripheral vagus nerve with the string galvanometer and showed that discharge frequency increased with inflation of the lungs. Adrian (2) recorded from single inflation afferents using the new fiber splitting technique. Discharges were identified by lung inflation and receptors were found to be slowly-adapting to maintained lung inflations. Knowlton and Larrabee (103) confirmed this observation, but also described a second rapidly-adapting receptor discharge.

Inflation afferents project to the brainstem in the rostral vagal rootlets and distribute to the vagal nucleus and solitary tract of the cat as shown by Foley and DuBois (61). Wyss (182) showed that central vagal stimulation responses could be blocked by localized lesions in the tractus solitarius. He concluded that the

tractus solitarius is probably the locus proper of vagal respiratory reflex centers. Harris (81) applied single shocks to the vagi and recorded maximal evoked potentials in the medullary tractus solitarius, nucleus solitarius and nucleus ambiguus. Wyss, Andereggen and Oberholzer (183) suggested that the afferent fibers synapse in the solitary nucleus and then travel caudally in the solitary tract. Culberson and Kimmel (48) found degenerated vagal afferents which coursed dorsomedially through the medulla, passed through the spinal trigeminal tract and entered the tractus solitarius. These connections may interface respiratory reflex afferents with inspiratory and/or expiratory areas of the medulla.

Other workers believe that vagal afferent fibers project to the apneustic region in the lower pons. Kerr, Dunlop, Best and Mullner (99) observed that apneustic patterns in mid-pontine vagotomized rabbits could easily be modified by central vagal stimulation. Wang, Ngai and Frumin (176) found that vagotomy failed to alter gasping patterns in medullary cats. However, Hoff and Breckenridge (88) showed that vagotomy could release eupnea by increasing rate and depth, provided vagal inflow was initially intact in the medullary dog. Finally, Ngai and Wang (135) showed that upper pontine transection or removal of the

pneumotaxic area had very little effect on activity of the inflation reflex. From all of this evidence, it is believed that respiratory vagal afferents have an influence confined to medullary and lower pontine brainstem structures.

Evidence has accumulated that vagal afferents affect both the inspiratory and expiratory phases of respiration. Wyss (181) was able to produce opposite respiratory responses in the monkey by stimulating the central vagus at different frequencies. Low frequency stimulations (30-80 Hz) caused slight but distinct inspiratory effects with rate acceleration. High frequency stimulations (100-400 Hz) caused marked respiratory slowing with shifts favoring expiratory movements. These results were ascribed to selective activation of the inflation and deflation reflexes respectively. Pitts, Magoun and Ranson (146), using constant stimulating frequency of 240 Hz were able to evoke inspiratory or expiratory movements, respectively, by low or high intensity stimulation of the central vagus of the cat. In either case, stimulation of the inspiratory or expiratory center would override vagal stimulation effects. Pitts et al. (146) discussed results in terms of reciprocal inhibition between inspiratory and expiratory systems.

Gesell and Worzniak (74) made the comment that either inspiration or expiration may coincide with pulmonary inflation by a pump. Dirken and Woldring (51) investigated this further by occlusion of the airways during either the inspiratory or expiratory phase of spontaneous respiration in the rabbit. Occlusion during inspiration led to a gradual decrease in lung volume with a subsequent decrease in vagal afferent discharge frequency. Occlusion during expiration produced just the opposite results. Also, inspiratory occlusion tended to elevate the discharge frequency of expiratory cells, but had no effect on inspiratory cell frequency. Blockade of the vagus by anelectrotonus depressed expiratory discharges but enhanced inspiratory discharges. Stimulation of the central vagus at 9 Hz depressed inspiratory cells and at 200 Hz inspiratory cells were completely inhibited. Expiratory cells tended to go into continuous patterns during vagal stimulation at both frequencies. Dirken et al. (51) came to the conclusion that vagal afferents activate expiratory cells, while they reciprocally inhibit inspiratory cells.

Finally, Gesell, Atkinson and Brown (69) suggested that the act of respiration may be coordinated by vagal afferents that shift their drive to the quiescent medullary

center. This could explain the smooth transition between inspiratory and expiratory phases.

The vagal inflation reflex is of prime importance for control of rate and depth mechanisms. Gesell, Steffensen and Brookhart (73) concluded that, "The pulmonary vagi exercise two diametrically opposite functions: curtailment of the central respiratory discharge which reduces the depth of breathing, and acceleration of the inspiratory act, which allows increased depth of breathing." Tang (171) found that CO_2 administration failed to induce a rate change if the vagi were severed. Only changes in depth were observed. In the absence of pneumotaxic circuits, vagal afferents maintained a relatively constant depth during respiratory stimulation. Von Euler, Herrero and Wexler (55) also reported that the increase in respiratory rate during CO_2 stimulation depended on intact vagal mechanisms. The conclusions of Nesland, Plum, Nelson and Siedler (129) were identical.

Shannon, Zechman and Frazier (162) studied the first-breath response of inspiratory cells during mechanical loading in cats. In preparations with intact vagi, elevation of the resistance or elastance led to an increased depth and decreased rate of respiration, which were paralleled by increased frequency and increased

duration of single cell discharges. Vagotomy abolished the single cell changes during loading, but depth increases were still present. The authors concluded that the vagi were the only source of sensory information for activation of medullary inspiratory neurons during mechanical loading. Increase in depth in vagotomized preparations was believed to be due to modulation at the spinal cord level involving facilitation of external intercostal motor activity by their muscle spindles during loading. This conclusion was confirmed by Shannon and Zechman (161).

Finally, Fallert and Mühlemann (57) studied entrainment of respiratory centers during pump inflation with different tidal volumes and frequencies in the intact rabbit. Elevation of inflation volume increased the frequency range to which the rabbit would entrain. Small frequency ranges correlated with small volume inflations. The authors concluded that the Hering-Breuer reflex was important for determination of respiratory rates and depths.

D. Discharge Patterns

The ability to monitor single cell activity from the central nervous system has been of great value in the study of respiratory control. Various testing

procedures have been introduced whereby primary respiratory neurons can be distinguished from other cell types. Qualitative and quantitative assessment of respiratory cell discharge patterns have yielded satisfactory neural correlates of respiratory rate and tidal volume outflows from medullary structures. Consequently, numerous respiratory cell subtypes have been described and new theories on respiratory rhythmicity have been introduced.

Single respiratory potentials can be recorded from the medulla by using glass or metal microelectrodes (12, 20, 62, 78, 89). Gesell, Bricker and Magee (70) first reported that finding extracellular respiratory discharges was slow and tedious work. Von Baumgarten (16) found only 23 cells with 900 penetrations using 25 microelectrodes. Salmoiraghi and von Baumgarten (154) worked for a year and were successful in penetrating only eight respiratory cells for intracellular recording. Once located, extracellular respiratory potentials can be recorded for extended periods of time. Brodie (31) reported that he could usually hold cells for 30-60 minutes. Occasionally, cells were observed for more than seven hours.

Positive identification of primary respiratory neurons is based on phasing and spiking characteristics of the discharges and modification of patterns during

various testing procedures. Although both tonic and phasic cells may function in respiratory systems, the phasic cells have been classified as primary respiratory cell candidates since they fire during one phase of respiration and are quiescent during the alternate phase. Classically, respiratory neurons are grouped into inspiratory or expiratory categories. Tonic cells can show a frequency peaking in phase with the respiratory cycle, but these cells never become quiescent.

Care must be taken to show that phasic discharges do not arise from movement artifacts. Various techniques have been used to eliminate mechanical movement. Von Baumgarten, Kanzow, Koepchen and Timm (20) covered the brainstem with a thick layer of stiff agar jelly before recording respiratory potentials. Batsel (15) reported that cisternal drainage resulting from compression of the abdomen and chest was equal to or superior to the use of agar to arrest movements. Batsel (14) also found that cells responding to fluctuations in the blood pressure, which has a slow oscillating component in phase with respiration, could not be recorded from for a long time. Artifacts from this source were eliminated because of their instability. Cohen (39, 40, 41) used cats with neuromuscular blockade to avoid movement potentials. Movements

due to pump inflations were minimized by using preparations with a pneumothorax. Finally, von Baumgarten (17) introduced a floating electrode technique which permitted recording of respiratory potentials from moving brainstems.

Probably the best way to screen out rhythmic discharges due to movement is by examination of the spike potentials. Dirken and Woldring (51) and Hukuhara, Nakayama and Okada (91) used constant spike amplitude as their criterion. Any modulation of amplitude in phase with the respiratory cycle must be due to cell movement in relation to electrode tip position in the potential fields around active cells. Also, differences in spike amplitude can be used as a check against recording from more than one cell at the same time.

The phasing of periodic discharges is important in respiratory cell identification. Amoroso, Bainbridge, Bell, Lawn and Rosenberg (5) accepted as primary respiratory neurons only those discharges which preceded muscular electrical activity and which fired throughout the inspiratory or expiratory phase. Special care must be taken in identification when rhythmic potentials are found in the region of the solitary tract or nucleus since they may arise from vagal afferents or vagal motorneurons. The former are easily identified by their phase

spanning patterns as shown by Adrian (2), but the latter are more difficult to distinguish. Eyzaquirre and Taylor (56) showed that vagal motorneurones had discharge patterns paralleling phrenic bursts. Some had expiratory phasing patterns. In addition, von Baumgarten and Kanzow (19) described two respiratory cell types in the region of the tractus solitarius, neither of which were vagal afferents or vagal motorneurones. Both had inspiratory patterns, but lung inflation led to an inhibition of one and an excitation of the other.

When recording respiratory discharges it is important that the potentials arise from cell bodies. It is possible that ascending afferent and descending efferent traffic may carry respiratory potentials along fiber tracts which traverse medullary regions. These, of course, cannot be considered as primary respiratory potentials. Various techniques have been used to differentiate between cell body and fiber tract recordings. Due to differences in diameters, Cohen and Wang (45) suggested that cell bodies have a higher current output than single fibers. For this reason, potentials from the former have larger amplitudes (47) and longer durations (30, 79) than the latter and are found more frequently. Since the recording volume of steel microelectrodes with tip diameters

of 10-40 microns is only 5×10^{-3} cubic millimeters (5), fiber potentials are more susceptible to electrode movement than cell body potentials. For example, von Baumgarten and Salmoiraghi (21) concluded that they were recording from a cell body if the microelectrode could be moved 30-100 microns without losing the potential. Haber, Kohn, Ngai, Holaday and Wang (79) could not record respiratory activity from the caudal medulla and suggested that their microelectrodes were sensitive only to cell body potentials.

Nelson (127) and Cohen and Wang (45) introduced a new criterion and claimed that sources of unit activity could be distinguished on the basis of spike polarity. Pure negative or positive-negative waves were believed to arise from cell bodies. These were the most common. Pure positive or positive-negative-positive triphasic spikes were believed to arise from axons or fiber tracts.

Cells with respiratory characteristics may not always function in the respiratory complex and are therefore probably not primary respiratory neurons. Scheibel and Scheibel (158) observed reticular cells for many hours and reported that some non-respiratory cells assumed activity characteristics resembling respiratory patterns. The authors concluded that such neurons may function in different

neural nets at different periods of time. Gesell, Bricker and Magee (70) found that respiratory discharges may differ considerably in frequency and may vanish and reappear under modifying conditions. This indicated that the reticular formation could command recruitment and adjustment of respiratory cell patterns. Cohen (38) described periodic discharges recorded in the isolated pons which resembled respiratory discharges in both burst duration and firing frequency. On close examination, however, these cells were not locked to the respiratory cycle, but tended to drift in random patterns. This demonstrated that cells in the reticular formation could exhibit similar respiratory patterns without having any known respiratory function.

Elementary descriptions of respiratory cell discharge patterns have most commonly included measurements of the number of action potentials per burst (spikes per train), the discharge duration (train length) and the average discharge frequency. It has been implied that increases in these parameters for inspiratory cells correlate with deeper respiratory movements. Pitts (141) stimulated the inspiratory region of the medulla with various intensity and frequency combinations and found increased firing frequency of single motor units and motor unit

recruitment from the subliminal fringe of the phrenic population. Adrian and Bronk (3) found a linear relationship between interpleural pressure and stimulation frequency of the phrenic from 20-50 Hz. Integrated total phrenic nerve activity has subsequently been shown to be proportional to the tidal volume (39, 50, 58). Eldridge (53) recently demonstrated that integration of the phrenic signals during the 100 milliseconds coincident with the peak of inspiration is the best neural analog of tidal volume over wide ranges of tidal volume and respiratory rate.

Nesland, Plum, Nelson and Siedler (129), studying inspiratory cell patterns, introduced the product of spikes per train times respiration rate and showed that this spike output increased proportionally with elevation in minute ventilation. For example, CO_2 administration in intact cats led to increases in depth and rate of respiration, increase in mean frequency discharge, and decrease in train length. Spikes per train remained constant. Parameter changes due to alteration of respiratory rate were prevented by vagotomy. In vagotomized cats, CO_2 administration induced pure depth changes with corresponding increases in mean frequency discharge and spikes per train. Train length did not change. It was also shown that hypoxia produced less consistent responses than CO_2

administration. Hyperoxia depressed all parameters and some cells were completely inhibited. Nesland et al. (129) concluded, "It appears that the medullary respiratory neuron population regulates the magnitude of ventilation primarily by changes in the impulse frequency and total number of discharges of already active cells rather than by increasing or decreasing the number of cells actively discharging during each breath."

Nelson (127) recognized the importance of sampling from many respiratory cells to "resynthesize" characteristics of the whole population. Discharge parameters from inspiratory and expiratory cells were examined at different respiratory rates and the following conclusions were made. The train length is directly proportional to the respiratory cycle time. The spikes per train are proportional to the train length. The spike frequency is proportional to the spikes per train. Dirken and Woldring (51) confirmed the train length-spikes per train length relationship for expiratory cells at a constant discharge frequency. Cohen (41) confirmed the spikes per train-inspiratory phase duration relationship for inspiratory cells in lung inflation studies. Brodie (31) studied discharge patterns in inspiratory cells during modification of the spontaneous respiratory rate with drugs.

Thiopental, a respiratory depressant to both rate and amplitude, increased the spikes per train and burst duration but slightly decreased the discharge frequency. Cyanide, a respiratory stimulant, reversed all the responses. Brodie (31) concluded that respiration rate and train length were reciprocally related while respiration rate and discharge frequency were directly related.

Wang and Ngai (175) have stated that respiratory rate is probably determined by the rate of depolarization of respiratory neurons. In this case, measurements of spikes per train, train length and mean discharge frequencies fail to account for dynamic changes that take place in burst discharges during depolarization of respiratory cells. To quantitate these dynamic events, frequency modulation curves have been constructed where the instantaneous spike frequency is plotted as a function of time. Salmoiraghi and Burns (155) showed that respiratory cells fired in non-regular patterns, necessitating curve fitting for single burst discharges.

Gesell, Magee and Bricker (72) reported that inspiratory cells exhibited a slowly augmenting pattern in which the spike frequency consistently increased as the train progressed. The frequency discharge rapidly decreased just prior to the off-phase for the cell. This

frequency pattern correlated with tidal movement of air. Two expiratory patterns were described. One was a steady state discharge in which expiratory cells fired with a constant frequency throughout the whole train. The other pattern showed a rapid increase in frequency which slowly declined before the cells turned off. Similar discharge patterns were found at all points along the respiratory arc from the respiratory muscles through the central nervous system and back along sensory nerves. These parallel patterns suggested serial linking between stations of the respiratory mechanism. Gesell, Atkinson and Brown (69) restudied respiratory discharge patterns in muscle-blocked dogs. No alteration in inspiratory patterns were seen, suggesting that the frequency modulation of these cells was of central origin. Expiratory cell patterns were all of the steady state type. The authors suggested that the rapidly augmenting expiratory patterns might have been due to reflex modification of the basic steady state pattern. Gesell and Worzniak (74) supported this suggestion by showing that steady state expiratory cell patterns could be converted into rapidly augmenting patterns during spontaneous respiration or into slowly augmenting patterns during pump inflation.

Dirken and Woldring (51) studied the frequency

curves of inspiratory cells, expiratory cells and vagal afferents. Decreasing lung volume by tracheal blockade in mid-inspiration caused inhibition of vagal afferent frequency discharge and drop in the respiratory rate. The time course of frequency modulation in inspiratory cells was unaltered except for the duration of inspiration, which was increased. Vagal blockade by anelectrotonus, however, depressed the initial rate of change in frequency in the same cells. Assuming that rate of frequency change depends on the rate of depolarization in respiratory cells, a depression in the latter can be associated with low respiratory rates after vagotomy.

Hukuhara, Nakayama and Okada (91) described frequency modulation patterns of inspiratory and expiratory cells in cats and dogs. The basic patterns observed agreed with those of Gesell et al. (72) and up to four variations were noted for both cell types. Variations ranged from slowly and rapidly augmenting discharges to steady state patterns. The authors attributed variations in starting time, spike frequency and number of spikes per train to differences in thresholds throughout both inspiratory and expiratory populations.

Von Baumgarten, Balthasar and Koepchen (18) and Salmoiraghi and von Baumgarten (154) studied intracellular

discharge patterns from inspiratory and expiratory neurons. Burst discharges were initiated by a spontaneous depolarization of the resting membrane potential which continued to depolarize slowly until the burst was terminated. Inspiratory cells showed a frequency increase paralleling the degree of membrane depolarization. The authors suggested that the high depolarization level at the end of each spike train reflected a maximum threshold, above which the cells could not generate additional action potentials. This self-limiting theory quickly replaced the suggestion of Burns (35) that spike discharges terminated because of fatigue. Batsel (15) argued against the latter view by pointing out that respiratory cells could be driven at higher than normal rates for long periods of time without any sign of fatigue. Also, Robson, Houseley and Solis-Quiroga (148) showed that respiratory cells could fire continuously after barbiturate administration.

Salmoiraghi (153) proposed a theory for rhythmicity of breathing based on three excitatory mechanisms: (1) increased firing frequency of inspiratory cells, as the cycle progressed, depended on self-reexciting mechanisms within the inspiratory population; (2) concurrent decreased probability of expiratory cell firing was attributed

to reciprocal inhibition; (3) increased firing thresholds of inspiratory neurons explained transition from inspiration to expiration. This cyclic exchange between inspiratory and expiratory populations was expected to continue as long as the three postulated mechanisms were intact.

Although Waldron (174) has reported that distinct categories of activity patterns could not be distinguished within the inspiratory group, other investigators have described many respiratory cell subtypes. Cells have been classified into no less than eight categories based on phasing pattern differences with the respiratory cycle (14, 15, 40, 41, 42, 45, 128, 169, 173). It is interesting that cells do not change their phasing during CO_2 administration, lung inflation or other procedures. Most workers, led by Cohen (43), have assumed that these different respiratory cell patterns reflected differences in function. Elaborate theories on the genesis of respiratory rhythm have subsequently been devised. Batsel (15) concluded that the bulbar respiratory center may exhibit rhythmicity due to the differences in onset time of discharges of the various early inspiratory cells. Temporal overlapping of different subgroups was believed to smooth the transition between respiratory phases.

Nesland and Plum (128) suggested that any hypothesis

on respiratory oscillation derived from the interrelationships among functionally different subgroups within the medullary inspiratory and expiratory populations required three assumptions. First, one active subgroup must activate another quiescent subgroup. Second, one active subgroup must inhibit another active subgroup. Third, activity must be found within at least one subgroup at any point in time. Cohen (42) used these criteria and proposed a model for genesis of respiratory rhythmicity based on respiratory cell subtype response to CO_2, lung inflation and brainstem electrical stimulation. The schema was constructed around a master oscillatory loop which paralleled the inspiratory and expiratory neurons of Salmoiraghi and Burns (36, 155, 156). Three other loops had direct influence on the master loop. One, consisting of expiratory-inspiratory neurons, initiated inspiration. The other two loops inhibited inspiration and expiration respectively. Inspiratory units activated by lung inflation might function in the inspiratory inhibitory loop, but oscillation did not depend on vagal innervation.

CHAPTER III

METHODS

A. Surgical Preparation

Mongrel cats anesthetized intraperitoneally with 30 mg/Kg sodium pentobarbital (Nembutal, Abbott Laboratories) were used exclusively in this study. The cats had a mean weight of 2.7 Kg (range 1.6 to 4.9 Kg) and there was no sex discrimination. Cats were placed on a Gorman-Rupp Industries, Inc., Model M11 warm water circulated pad which was driven by a Model K-1-3 water heater-pump. Rectal temperatures, which were monitored with a Yellow Springs Instrument Company, Inc., Model 46 TUC Tele-thermometer, were maintained at 37 $\pm$ 2°C. Surgical preparations and instrument calibrations were usually completed within 2 hours. Most cats remained remarkably stable for more than 8 hours and breathed spontaneously throughout the duration of the experiment.

Four surgical incisions were made. First, the femoral triangle was exposed to permit catheterization of the

femoral artery and vein with PE100 polyethelene tubing. Catheter tips were advanced to the abdominal aorta for blood pressure recording and inferior vena cava for drug injections, respectively.

Second, a four or five centimeter midline incision was made through the ventral cervical neck skin and sternomastoid muscle. Reflection of the sternohyoid muscle exposed the trachea for intubation with a quarter-inch polypropylene (Nalgene) Y-tube. The cervical vagosympathetic nerves were isolated and loosely ligatured with umbilical tape. In some experiments loose triple zero silk ligatures were placed around each cervical carotid artery for bilateral carotid occlusions or tugs.

Third, after mounting the cat in David Kopf 1530 Stereotaxic Frame Assembly, a small incision was made through the skin of the left lateral thoracic cage and the pectoralis minor muscle was separated by blunt dissection. A transthoracic needle was inserted through the serratus ventralis and internal intercostal muscles at the fourth or fifth rib interspace. This probe was used for intrapleural pressure recording.

The last surgical procedure involved exposure of medullary brainstem structures. A dorsal midline incision was made through the skin of the head extending three to

four centimeters rostal and caudal to the occipital crest. The lambdoidal ridge was exposed by separation of the cut skin interfaces with retractors. A National cautery was used to separate neck muscles (clavotrapezius, levator auris longus, epicranius occipitalis, auricularis superior, abductor auris longus, abductor auris brevis and temporalis muscles). Some muscles were removed and other were retracted until the caudal interparietal and occipital bone surfaces were laid bare. The exposed dura mater between the occipital bone and the atlas vertebra was ruptured resulting in a free flow of cerebral spinal fluid. Portions of the occipital bone were removed with Rongeur forceps carefully inserted above but never touching the dorsal surface of the medulla. Medullary brainstem structures from the first cervical nerve to the cerebellar border were exposed. The posterior lobes of the cerebellum were also uncovered for suction removal of the whole cerebellum if necessary. In most experiments, however, the entire cerebellum was left intact. Frequent application of 0.9% saline solution prevented the brain tissue from drying out. In some cases, the spontaneous flow of cerebrospinal fluid provided satisfactory irrigation of the fourth ventricle.

B. Data Acquisition

The interconnections of the electronic equipment used to monitor and store on-line analog data are presented schematically in Figure 1. A Grass Model 7 Polygraph strip chart recorder was used to record four physiological parameters. In the first channel, airflow velocity was measured with a Fleisch pneumotachograph connected in series with one arm of the trachael Y-cannula. The opposite arm was blocked with U-screw clamp occlusion of a rubber tube extension. During movement of air through the pneumotachograph the small pressure gradient produced across a metal honeycomb grid was detected by a Grass Model PT5A differential volumetric pressure transducer. The device was calibrated and found to be linear with airflow velocities up to 110 cc/second in accordance with Poiseuille's Law. This was the upper limit for airflows in most experimental cases.

Intrapleural pressure was monitored on the second polygraph channel. A 15 gauge needle beveled at the tip with sideports along its shaft was inserted across the lateral thoracic wall at the fourth or fifth rib interspace. An elliptical copper plate attached to the needle shaft at a 45° angle limited the probe's insertion distance to 2.5 centimeters. Skin flaps were pulled

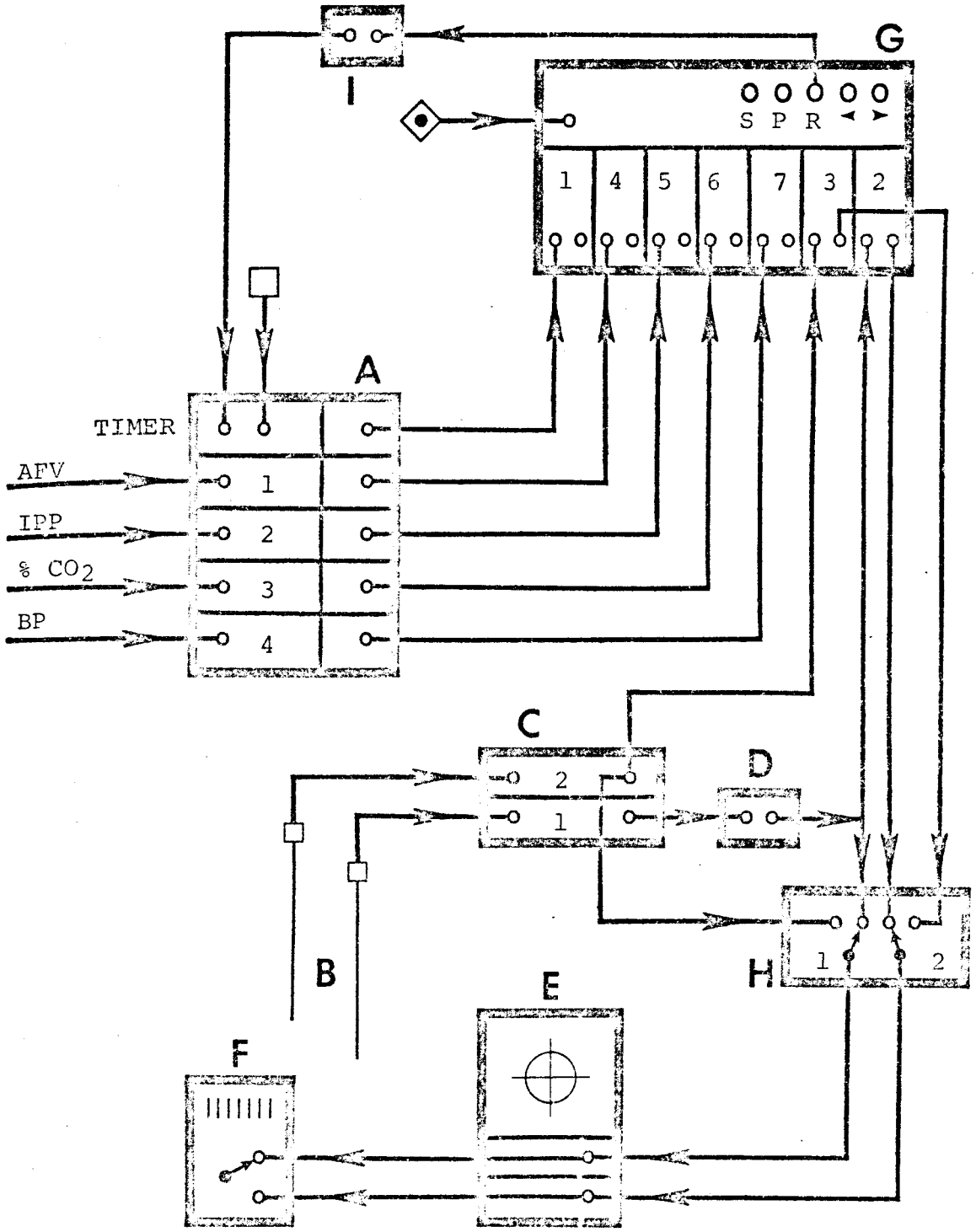

Figure 1. Instrumental schematic: A. polygraph; B. microelectrodes; C. preamplifier; D. 60 Hz filter; E. oscilloscope; F. audioamplifier; G. tape recorder; H. switching network; I. current amplifier.

together over this plate to seal any air leaks and maintain the needle in an approximate parallel apposition with the lung. Air pressure fluctuations were recorded with a Statham P23Dc pressure transducer which was initially calibrated with a water manometer.

The third polygraph channel monitored the end expiratory % CO_2. A short length of tygon tubing was attached to the exit port of the pneumotachograph to support a PE260 CO_2 sampling catheter in the center of the airflow profile. A Beckman microcatheter sample pump continuously drew a small fraction of the expired air through the detector head of a Beckman LB-1 Medical Gas Analyzer. Using an infrared absorption technique, a voltage signal related to the % CO_2 of the sample was obtained. This curvilinear signal was processed with a Beckman linearizer before going to the polygraph. At the beginning of each experiment the CO_2 channel was calibrated with a CO_2 reference gas (Matheson Gas Products). The linearizer was periodically adjusted for linearity.

Finally, the blood pressure was recorded on the fourth polygraph channel. A Statham PE23Gb pressure transducer attached to an intra-aortic PE100 catheter filled with 0.9% non-heprinized saline was used for this measurement. The catheter was kept clot-free by frequent

flushings with saline. The blood pressure transducer was initially calibrated with a mercury manometer.

The last physiologic parameter examined in this study was the extracellular electrical activity of single respiratory neurons in the medulla. As shown in Figure 1, potentials were recorded with microelectrodes, AC amplified (2 channel capacity) and filtered. In early experiments, glass micropipettes filled with 3 molar sodium chloride solution were used. With the exception of one cell, however, all single cell potentials analyzed in this study were recorded with Green's (78) metal microelectrodes. Steel insect pins were etched to fine tip diameters in 12 molar hydrochloric acid using a 6.3 volt A.C. source. The electrodes were insulated with clear Insl-X E33 solution and baked in an oven overnight. Tip dimensions were measured with a Carl Zeiss microscope (X10) and Vickers A.E.I. image splitting eyepiece (X10) and ranged from 1-5 microns. Corresponding electrical impedances, checked on a General Radio Company Type 1650-A impedance bridge, ranged from 80-5 megohms respectively.

Microelectrodes were mounted on a Kopf 1460 electrode carrier fitted with a Kopf 1206 reduction drive and were slowly advanced through medullary brain tissue in 10 micron steps. No attempt was made to cut away the pia

mater. Single cell potentials picked up by the microelectrodes were in the 200-800 microvolt range. These potentials were amplified about 2000 times with a Grass DP9B dual channel AC preamplifier (single-ended input, cathode follower mode). The signal-to-noise ratio was maximized by keeping input leads short, use of shielding, establishment of common grounds between the amplifier and cat, and signal filtering. The low and high half amplitude frequency filters on the amplifier were set at 0.1 and 40 K Hz respectively. A 60 Hz notch filter, shown in Figure 2A, was constructed to eliminate line noise. The frequency response curve of this filter, which is plotted on a log scale in Figure 2B, shows maximum attenuation at 60 Hz. Experimental tests demonstrated that peak-to-peak voltages of single respiratory spike potentials were not attenuated by filtering. Filtered waveforms were more biphasic than nonfiltered signals and the former displayed a small leading phase shift (less than 0.2 millisecond). Neither of these changes affected the validity of data collection or spike train analysis used in this study.

Amplified and filtered single cell discharges were monitored on-line. Potentials were displayed on a Tetronix type 502A dual-beam oscilloscope and were audio-amplified on a Grass AM7 audio-monitor as shown in Figure 1. Both

A

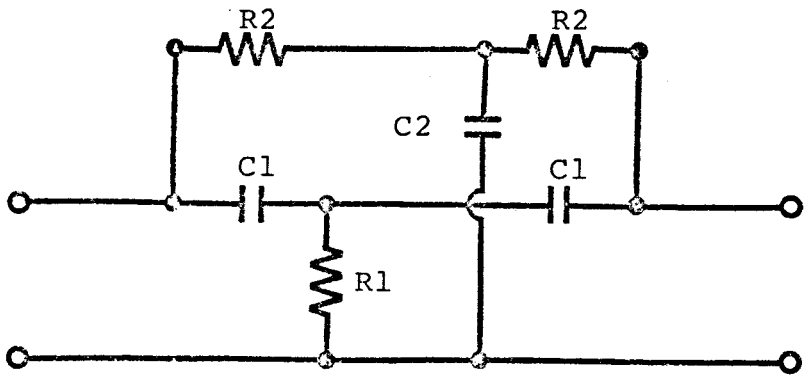

R1=3.92 K
R2=7.50 K
C1=0.350 μfd
C2=0.689 μfd

R2=2R1
C2=2C1

$f=[2\pi(R2)(C1)]^{-1}$

B

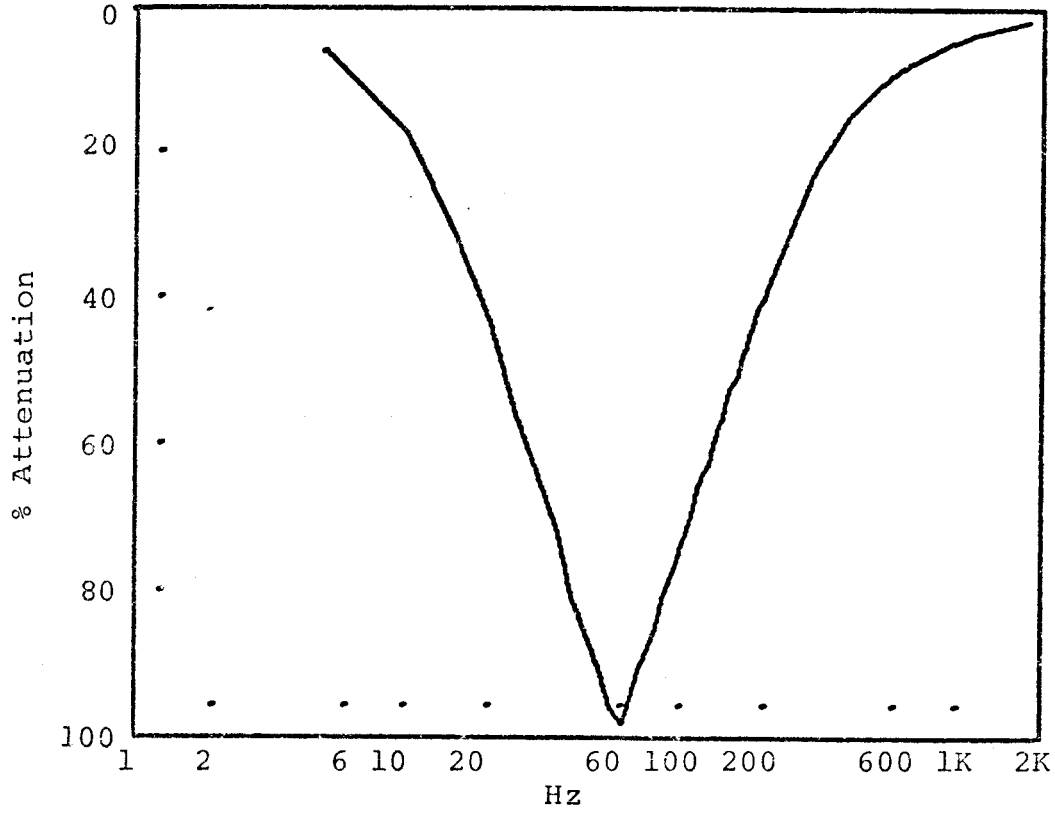

Figure 2. Parallel T notch filter: A. schematic diagram; B. frequency response curve.

of these instruments played important roles in the positive identification of single respiratory cell discharges.

Whenever a single respiratory cell potential of good amplitude was found, on line data from both this cell and from the polygraph were stored on a seven channel Philips ANA-LOG 7 tape recorder as shown in Figure 1. The tape recorder was operated at 3-3/4 inches per second in the FM mode. During a recording procedure, single cell data were immediately played back to the oscilloscope and audio-monitor to determine the quality of the recorded signal. A switching network permitted various combinations of data review when recordings from two different cells were obtained at the same time.

Finally, a current amplifier was constructed which sensed current flow in the "record light" logic circuit of the tape recorder. Whenever the recorder was storing analog data, this device closed a relay which caused a downward identification mark to be placed on the polygraph strip chart. An upward deflection on the polygraph event marker channel was activated by a remote foot switch to identify experimental manipulations. Other features including voice description on the tape (channel 8) and digital tape counter were also useful in locating single cell discharges during data analysis.

C. Experimental Manipulations

After a cat was surgically prepared and all polygraph channels were calibrated, a microelectrode search for respiratory potentials was started. Strict stereotaxic coordinates were not used, but by following the map of Salmoiraghi and Burns (155) with the obex as a reference point, respiratory cells could be found. Care was taken in the identification of cells as primary respiratory neurons. Many types of potential discharges were found in the medulla, but only those showing an on-off firing pattern in phase with the respiratory cycle (airflow, intrapleural pressure and % CO_2 oscillations) were considered as primary respiratory cell candidates. Some of these potentials were rejected for various reasons. Potentials whose amplitude fluctuated as a function of the respiratory cycle were eliminated because of the possibility that they were generated by movement artifacts. Potentials with uniform spike height showing highly irregular or high frequency discharges (instantaneous frequencies over 200 Hz) were rejected since more than one cell was probably present. Finally, potentials showing phase-spanning patterns were rejected since they may have been vagal afferent in origin. Only those potentials of constant amplitude exhibiting pure inspiratory or pure expiratory phasings were recorded

as primary respiratory neurons. These potentials were believed to be derived from cell bodies since no respiratory discharges could be found from the lower medulla to the upper cord where respiratory efferents are known to pass.

When a respiratory cell was found and positively identified, a control record was stored on magnetic tape. Various manipulations of the respiratory system were then performed to induce alterations in the discharge pattern. In general, procedures were used which evoked changes in respiratory rate and depth. Single cell data were obtained in both vagi-intact and vagotomized preparations.

Increases in respiratory rate were induced by intravenous injection of doxapram hydrochloride (Dopram, A.H. Robins Company). Respiratory rate was readily depressed by sodium pentobarbital or sodium pentothal (Pentothal, Abbott Laboratories). In a few cases, high respiratory rates arose spontaneously during exposure of the medulla. This acceleration was probably due to warming of brainstem structures. Other procedures, including CO_2 administration, anterior hypothalamic heating and intravenous injections of morphine sulfate (U.S.P.) were tried in several cats, but associated rate changes, if any, were not consistent.

Respiration depth was increased by increasing airflow

resistance. For this procedure, the cross-sectional area of the pneumotachograph exit port was decreased by known fractions with calibrated resistance plugs. It was very difficult to retain single unit recordings during induced depth changes. Either the cell would be lost because of movement problems or other cells would be recruited, thus masking the original discharge. For this reason, data obtained with airflow resistance plugs will not be presented.

Finally, other studies were designed to examine the correlation between apneustic breaths and barbiturate level in the spontaneously breathing cat. This phenomenon was studied at the single cell level and apneustic thresholds were evaluated by cerebellectomy and bilateral carotid occlusion. Data obtained from this work was important for the interpretation of single cell discharge pattern changes during barbiturate titration.

CHAPTER IV

DATA ANALYSIS

A. PDP-12 Overview

The general objective of this study was to investigate interspike interval distribution and sequencing of single respiratory cell discharges at various steady state breathing frequencies and depths. A Digital Equipment Corporation PDP-12 (Programmed Data Processor-12) general purpose laboratory computer was programmed to process off-line analog tape data of single cell activity. For each steady state observation, thousands of interspike intervals were examined and manipulated to construct histogram and interspike interval modulation curves. The latter involved a new mathematical technique devised by the author to quantitate ordering of interspike intervals during burst discharges. In addition to powerful software capabilities, a full array of PDP-12 output options was available to the user: CRT display; LA-30 Decwriter (Digital Equipment Corporation) hard copy printing; DP-1 Complot

(Houston Instrument, Baush and Lomb) digital increment plotting; LINC magnetic tape storage.

Communication with the PDP-12 computer was accomplished with essentially three programming languages. The first two are machine language in format and actually represent the two mode operation capacity of the PDP-12. The first or LINC-8 (Laboratory INstrument Computer) mode activates peripherals including analog to digital conversion, sense switch lines, relay buffers, CRT display and auxiliary LINC tape storage. The second or PDP-8 mode provides for extended arithmetic element (EAE) operations, real-time clock programming, digital incremental plotting and Decwriter input-output. While each mode has its own complete instruction set, both modes are given equal status by the single central processor. This permits rapid switching between modes under program control. Also, the 1.6 micro-second memory access time of the PDP-12 permits fast execution of individual instructions. This speed is advantageous for rapid analog to digital conversions.

FOCAL (Formulating On-line Calculations in Algebraic Language) was the third programming language used. This is a conversational language that permits on-line user-machine interaction and resembles FORTRAN IV (FORmula TRANslation version IV) in power for calculation of complex

mathematical expressions. Two FOCAL systems, FOCAL-12 and FOCALPL (plot), were utilized respectively to retrieve and manipulate data stored on magnetic tape from machine language programs and to graphically plot calculated parameters located on digital tape.

Two major disadvantages are associated with FOCAL. First, FOCAL programs are limited in length since the FOCAL interpreter, a machine language program itself, takes up a large portion of the PDP-12 8K core memory. Second, execution of individual FOCAL program instructions is slow since each mnemonic code command must be interpreted into machine language binary each time it is performed. Under the conditions of this study, these disadvantages were by no means limiting.

B. Machine Language Programs

1. ERASE

For convenience and speed of data handling, data were stored on LINC magnetic tape of standard format. Each tape was marked off into 1000_8 (512_{10}) blocks, each block containing 400_8 (256_{10}) 12-bit words. Prior to data storage, program ERASE was run to store a zero in each of the $131,072_{10}$ (512_{10} x 256_{10}) 12-bit words. By this procedure, new and old tapes could be cleared of all digital values before proceeding with other programs. Program ERASE along

with the programs discussed below are listed in the Appendix for reference.

2. DATA

Program DATA was written in machine language making free use of both LINC and PDP-8 modes. As outlined in the Appendix (Table VII), program instructions were located in the lower 4K memory of the PDP-12 and data were stored in the upper 4K memory. An abbreviated logic flow diagram of the program instructions is presented in Figure 3. The logic is represented by three major loops (A,B,C) and calculation (CALC) procedures between loops B and C. To facilitate understanding of data handling by program DATA, each of these four program sections will be discussed in relation to a real physiological input signal. The reader should be able to trace data processing of the analog respiratory cell discharge input to the final digitalized output before proceeding to higher levels of data analysis.

Inspiratory and expiratory cell discharges were examined in this study, and two representative cells are shown in Figure 4A and 4B respectively (35 mm records from a Grass Kymograph Model C4N Camera). Both cells were obtained from different cats, each of which was breathing at a rate of 30 breaths per minute. It can be seen that the inspiratory cell is in phase with the fall in the intrapleural pressure

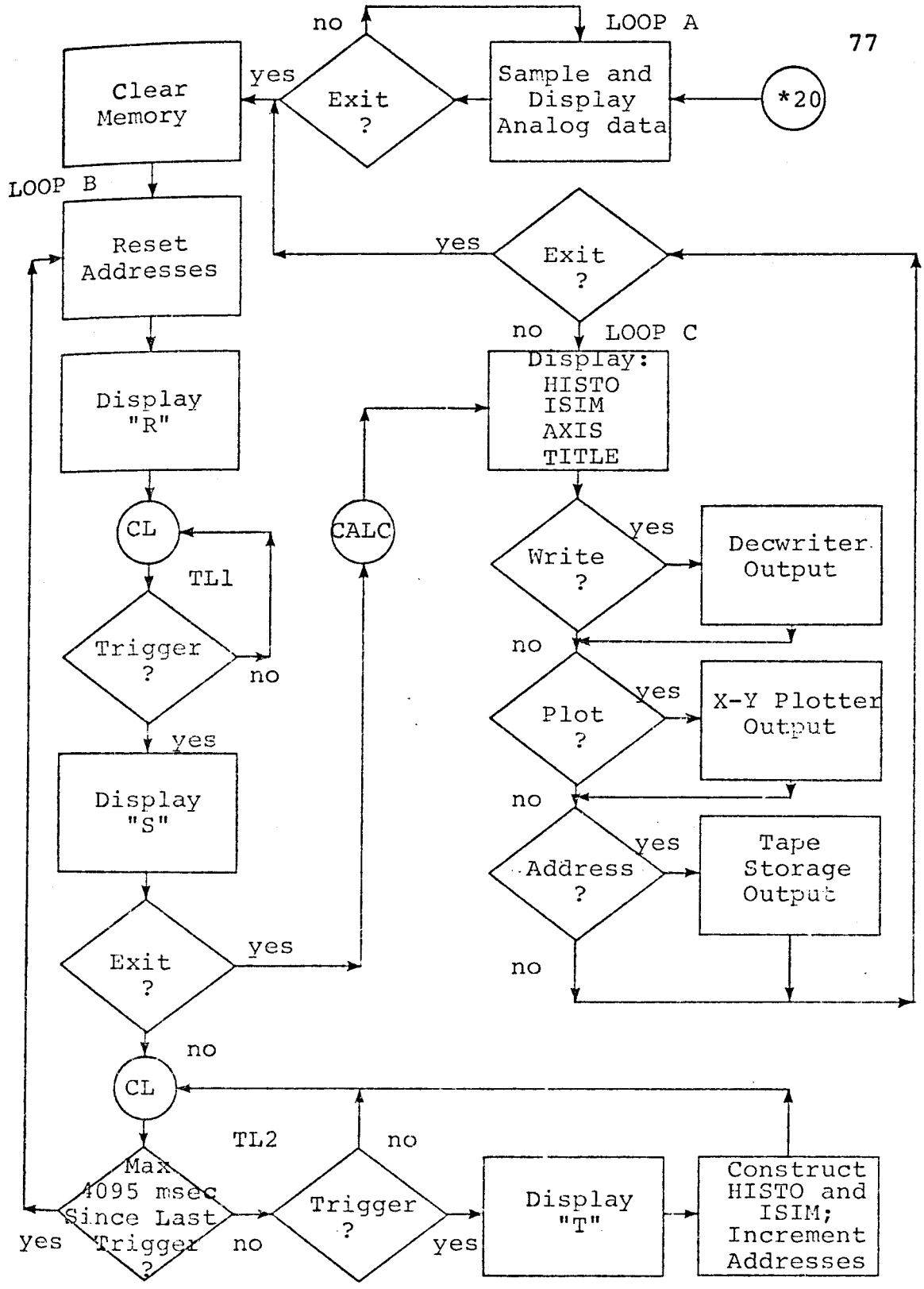

Figure 3. Program DATA flow chart. See text for details.

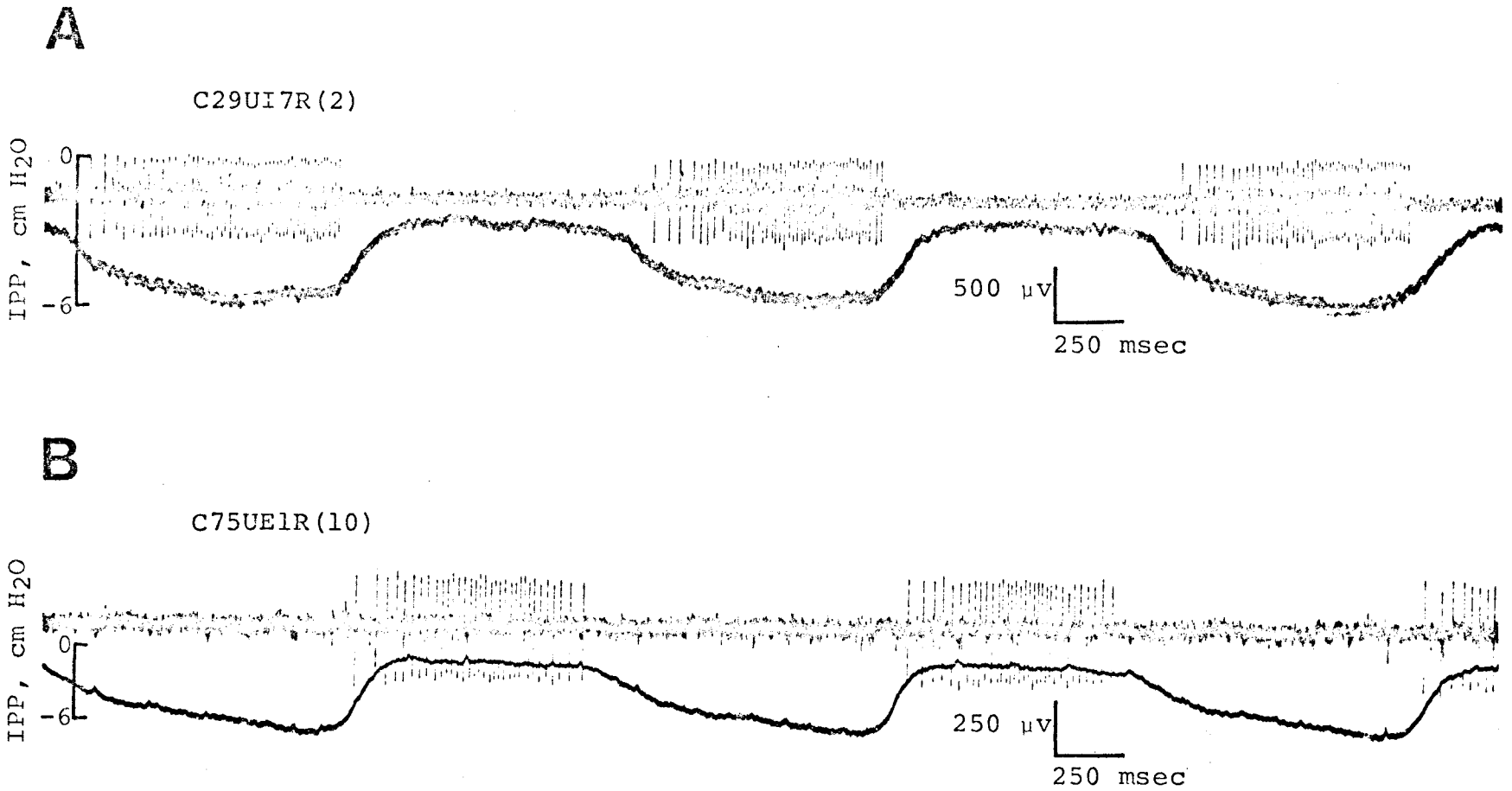

Figure 4. Representative examples of single cell analog data: A. inspiratory cell; B. expiratory cell. Lower tracing in each panel is intrapleural pressure (IPP).

while the expiratory cell is 180° out of phase. The inspiratory signal C29UI7R(2) of Figure 4A will be processed step by step in the discussion that follows.

The analog respiratory discharge was played back to the PDP-12 computer four times slower than record speed. In loop A of program DATA (Figure 3) the signal was digitalized and displayed on the CRT for assessment of signal quality. The sample rate was determined by the clock logic which halted program flow until a predetermined amount of time had elapsed. The KW12 real time clock, a crystal-controlled pulse generator oscillating at 400K Hz, was programmed to give a basic clock overflow count rate of 0.4 millisecond. This rate, coupled with the fourfold slow-down of the tape transport, established a simulated sampling rate of 0.1 millisecond per sample or 10 samples per millisecond.

Loop A was programmed to sample and store 1000_8 points before displaying the stored data on the CRT. The display therefore corresponded to a 51.2 millisecond segment (1000_8 samples x ($512_{10}/1000_8$) x 0.1 msec/sample) of the respiratory cell discharge. The memory was constantly updated causing the CRT to flash at about 5 Hz ($[0.0512 \text{ sec} \times 4]^{-1}$) although any segment could be frozen on the CRT for close analysis via sense switch control. After a signal

was judged to be satisfactory for computer analysis, exit from loop A was manually controlled under sense switch selection. Between loops A and B, the upper 4K of core memory was cleared along with various constants. Certain addresses were also reset to appropriate values.

The overall responsibility of loop B was to construct histogram and interspike interval modulation curves from the analog signal. The logic centered around detection of action potentials, measurement of interspike interval times and proper memory storage of interval times in various combinations for histogram and interval sequence analysis.

The PDP-12 computer is equipped with a Schmitt trigger. This device senses potentials whose amplitude exceed a manually set threshold and hence would appear ideal for action potential detection. The Schmitt trigger, however, has several disadvantages when used to detect the action potentials recorded in this study. For this reason a software rate-of-rise trigger was designed which proved highly reliable in action potential identification. The rate-of-rise trigger diagrammed in Figure 5 operated as follows. Analog sampling in loop B occurred at a constant simulated rate of 0.1 millisecond per sample as determined by the clock logic (CL). At this rate, action potentials

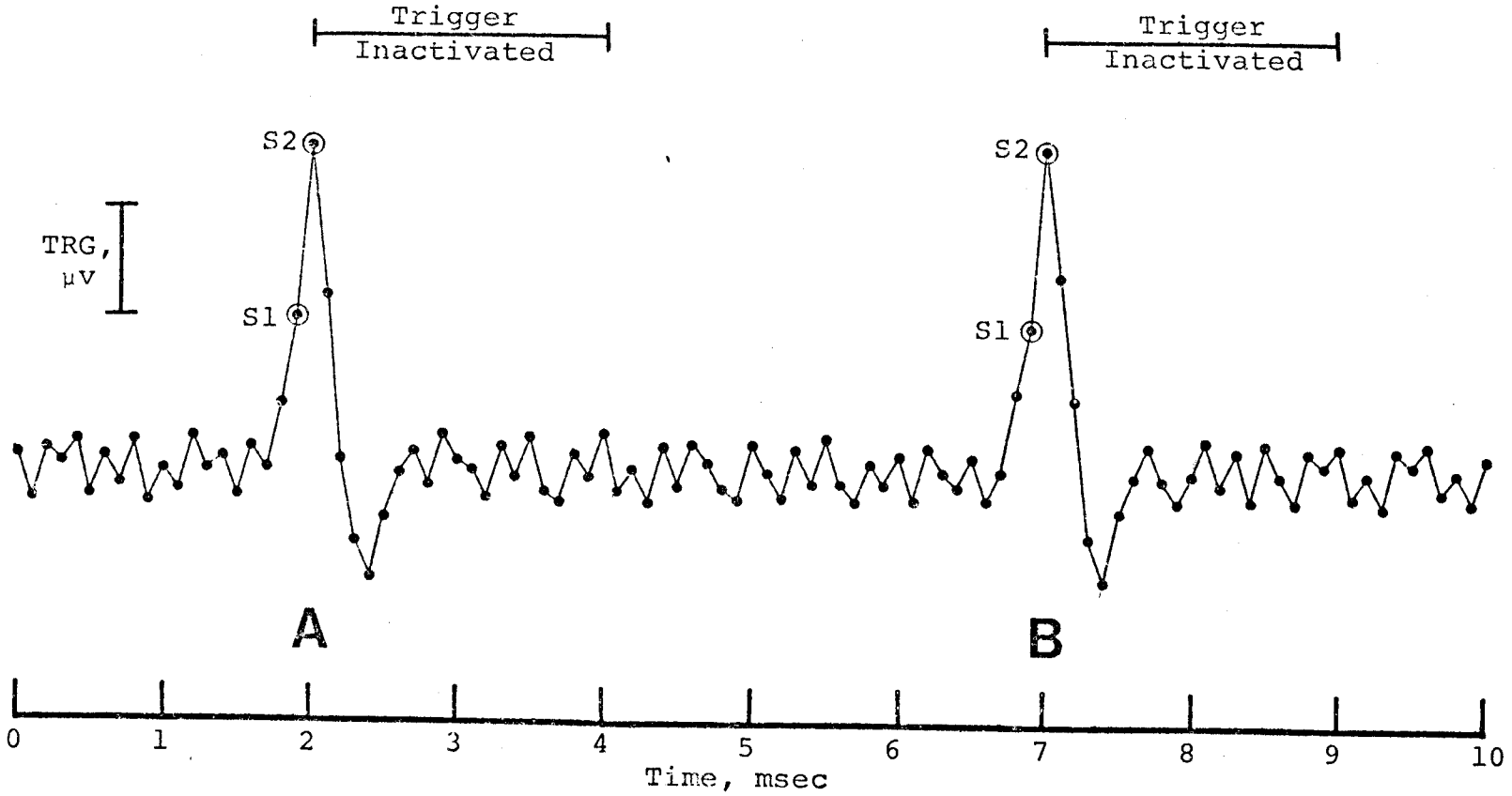

Figure 5. Technique for detection of action potentials. Dots represent digitalized 0.1 msec samples of analog signal. The change in voltage ($\Delta S=S2-S1$) per unit time represents a signal exceeding the trigger (TRG) level ($\Delta S>TRG$). This identifies an action potential (A or B) and inactivates the trigger logic for the next 2 msec.

1 millisecond in duration could be sampled 10 times. Since the sample rate was constant, the vertical distance between samples was proportional to the rate of potential change. Therefore, by testing for vertical separation between successive samples, action potentials could easily be detected even when the signal to noise ratio was as low as 2:1 and when slow baseline shifts were present. The trigger level (TRG) was manually adjusted until a "T" flashed on the CRT in synchrony with the audio amplified action potentials. The trigger operated only on the rising phase of action potentials. After a trigger occurred, 2 milliseconds elapsed before the trigger was "activated" again. This eliminated the possibility of generating two trigger pulses from a single biphasic action potential.

Interspike interval times were calculated to the nearest 0.1 millisecond by counting the elapsed time between action potential triggers. In short, a trigger caused the accumulated time of the previous interval to be stored with subsequent resetting of the interval counter. In Figure 5, for example, action potential A resets the counter to 0.0 milliseconds. Detection of action potential B 5.0 milliseconds later terminates the accumulation of interval time. The A-B interspike interval is stored as 5.0 milliseconds and the counter is reset for the next interval.

Histogram analysis has been a popular approach to quantitation of electrophysiological data from single neurons (66, 67). In this study, a 100 millisecond interval histogram was constructed by accumulating 500-4000 intervals, the number under manual selection. The histogram had 125 bins each of 0.8 millisecond width. The histogram plot for inspiratory cell C29UI7R(2) is presented in Figure 6A in which the terminal 30 milliseconds have been deleted. In Figure 6B the same data are plotted on an expanded scale. As consistent with all units studied, the distribution of interspike intervals for this cell shows unimodal peaking and is skewed to the right, favoring longer intervals. Parrot and Fleming (139) attempted to associate this characteristic shape of the respiratory interspike interval histogram with random Poisson processes. Although this has been done for non-respiratory discharges of truly random patterns (68, 106, 165), it is difficult to assign such random mechanisms to respiratory cells which possess predictable discharges. Against the random approach, Marczynski and Sherry (119) suggested that time-locked patterns which repeat over and over again with a sequential arrangement of adjacent intervals can best be described by the autocorrelation function. High correlations for respiratory cells (R.A. Mitchell - unpublished

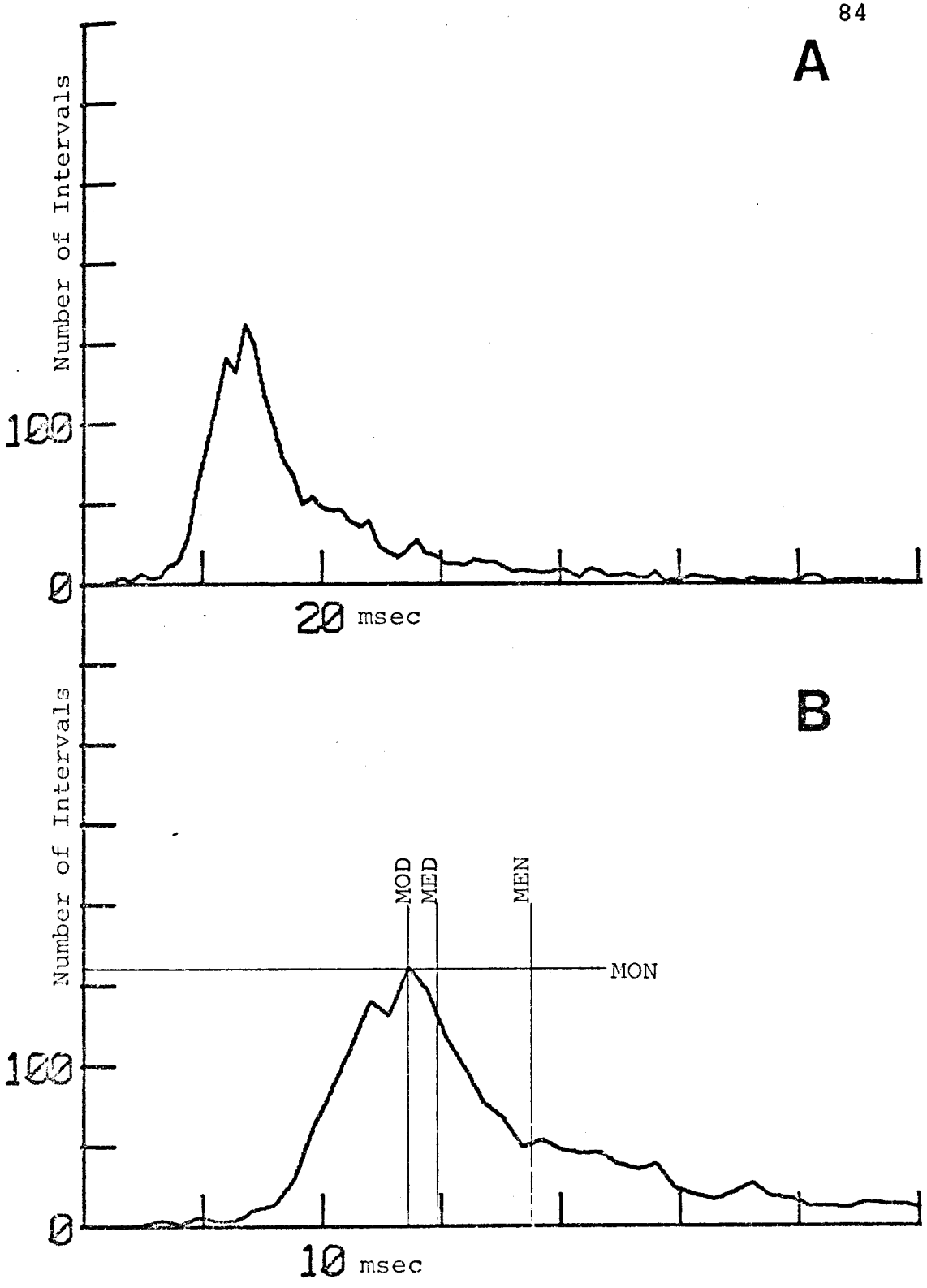

Figure 6. A. Interspike interval histogram derived from inspiratory cell C29UI7R(2) in Figure 4A. B. Same histogram on an expanded time scale showing mean (MEN), median (MED), mode (MOD) and number of intervals at the mode (MON). The histogram is made up of 2000 intervals.

observations) are certainly not indicative of random ordering of intervals. The interdependence series matrix method introduced by Sherry, Marczynski and Wolf (163) may also be useful in establishing a relationship between a specific interval and an interval removed by a fixed number of other intervals for respiratory train analysis.

A cumulative histogram or ogive curve is plotted in Figure 7 for inspiratory cell C29UI7R(2). The plot is linear on a log scale indicative of exponential processes operating in interval distribution. Similar plots are found for both Poisson and normal distribution functions. A horizontal line has been drawn at the 50% level and a vertical line intercepting the curve at this same level has been extended to the time scale. By definition, the interpolated time of 14.8 milliseconds corresponds to the median interval time. From Figure 6B, it can be seen that the median time is longer than the mode time. Also, the mean interval time is longer than median time. These relationships establish the skewing characteristics of the interspike interval histogram to the right.

For discharges that have random arrangement of intervals, quantification of cell output is satisfactorily completed by histogram analysis and measurement of standard

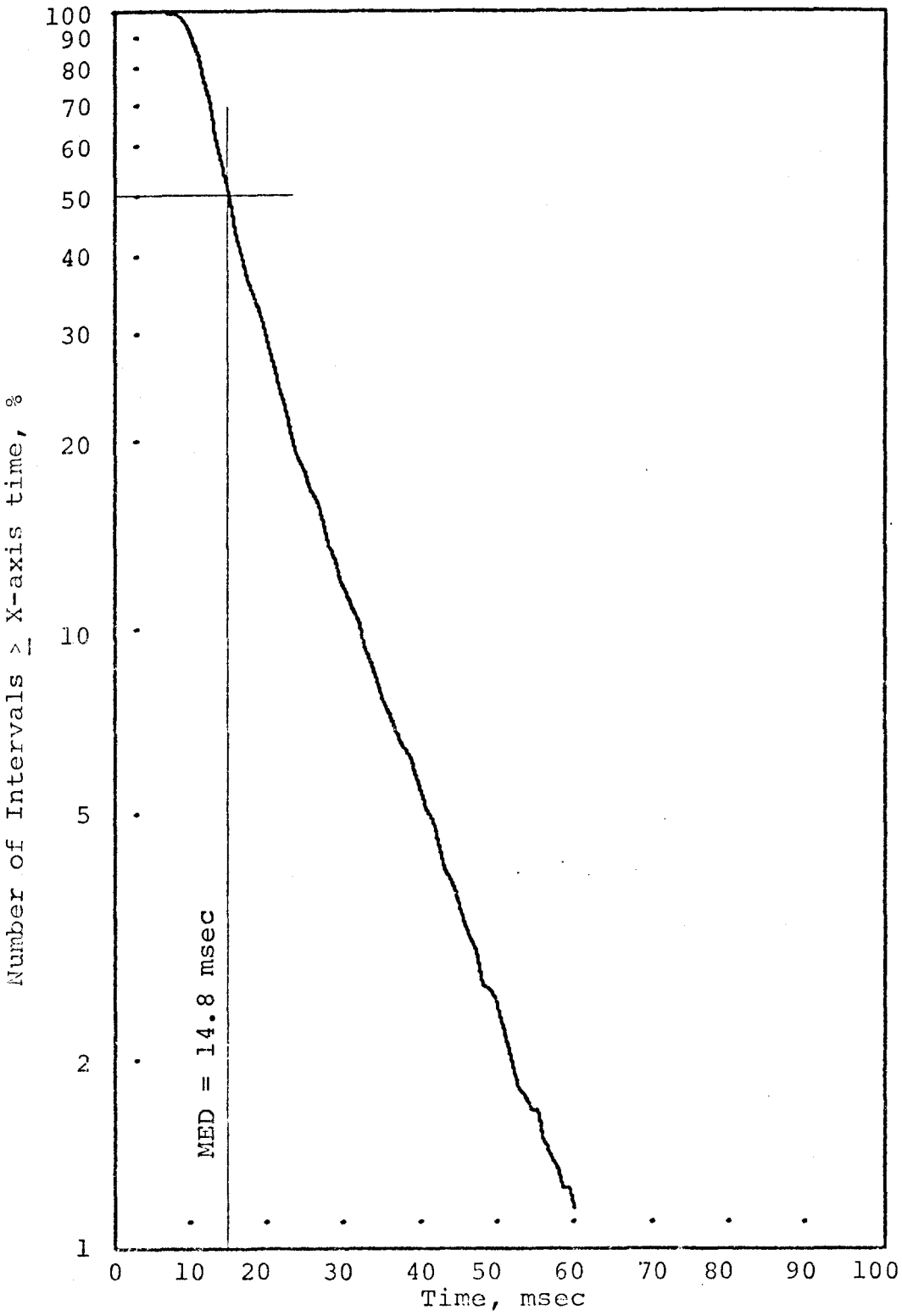

Figure 7. Ogive curve derived from histogram in Figure 6. Median (MED) interval time interpolated from 50% level.

statistical parameters such as the mean, median, mode and standard deviation (119). As reviewed in the Literature, however, respiratory discharges undergo characteristic frequency increase, plateauing and frequency decrease during their "on" phase. For this reason, accessment of respiratory cell output must involve description of sequential interval ordering, information that cannot be extracted from histogram interval distributions. Cohen (40) and Bertrand and Hugelin (24) approached this problem by using phase-triggered time histograms and cycle-triggered spike-density histograms for analysis of respiratory discharges, respectively. Although qualitative accessment was achieved, these methods failed to quantitate dynamic changes in the interspike interval during respiratory cell discharge.

To study dynamic changes in the interspike interval during respiratory burst activity, a new statistical averaging technique was devised as diagrammed in Figure 8 with hypothetical data. Intervals were numbered consecutively (Figure 8A) and corresponding intervals were averaged to construct an idealized respiratory train (Figure 8B). Plotting the sequential interspike intervals of the idealized train as a function of time resulted in a smooth "U"-shaped interspike interval modulation curve (Figure 8C).

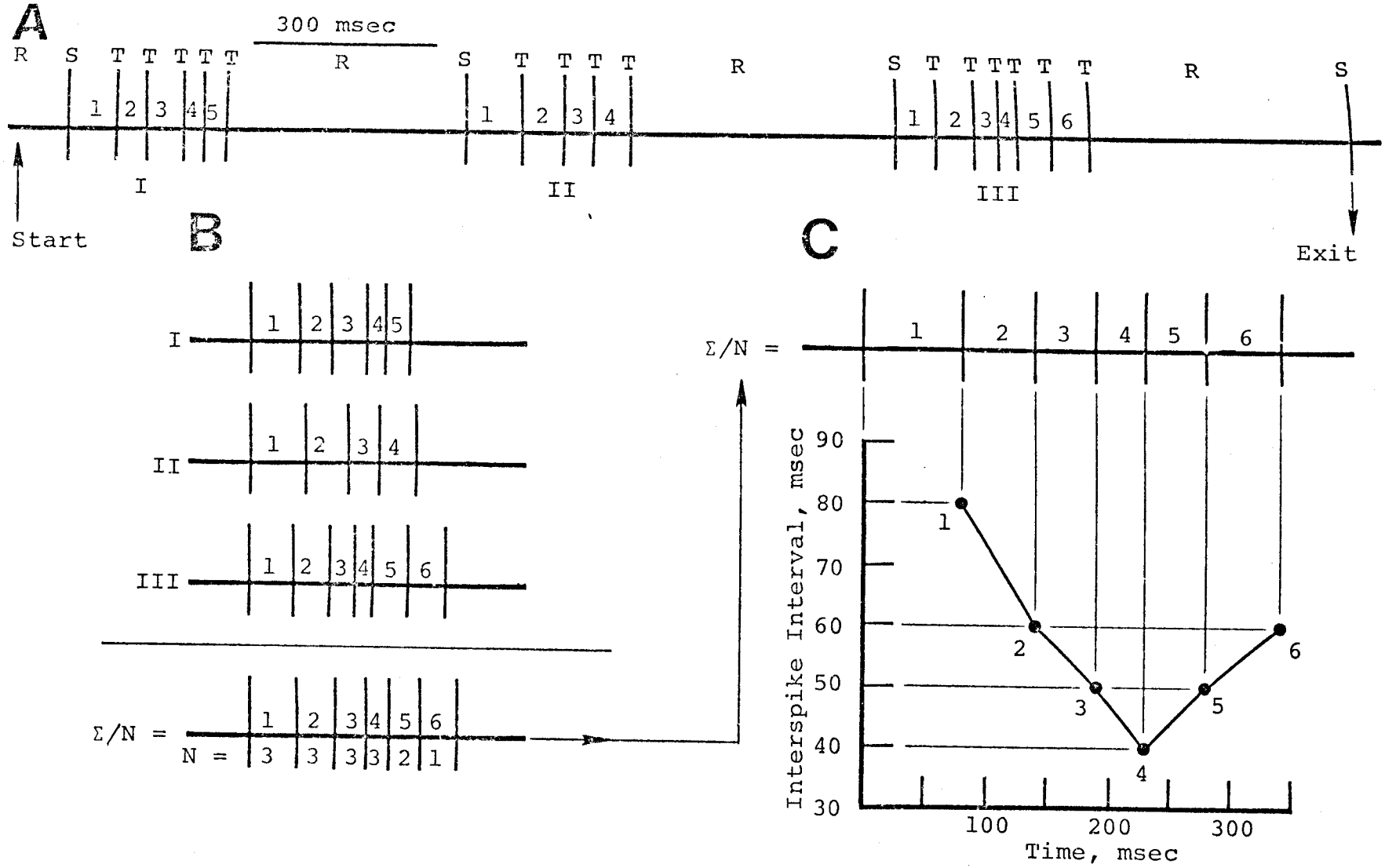

Figure 8. Generation of idealized interspike interval modulation curve from raw data: A. analog data; B. interval averaging; C. graphic display of averaged intervals. See text for details.

In Figure 9, similar plots for cell C29UI7R(2) are presented. For a single burst discharge (NT=1) a very rough curve was described reflecting non-smooth transition between consecutive interspike intervals as the train progressed (Figure 9A). An average of 44 sequential burst discharges (NT=44) eliminated the variability between adjacent intervals and resulted in a smooth interspike interval modulation curve (Figure 9B), readily accessible for mathematical analysis. This mathematical method differed from standard signal averaging techniques (164) which depend on external time references to recover repetitive waveforms from random noise. The analysis worked for both inspiratory and expiratory discharges (Figure 4) and was independent of cycle cues from peripheral respiratory parameters.

The computer techniques employed to generate interspike interval modulation curves can best be understood by paralleling the "S" (start of train), "T" (trigger on successive action potentials) and "R" (reset) designations over the action potentials in Figure 8A with the display "S", display "T" and display "R" commands of loop B in Figure 3. For example, loop B logic was manually entered from either loop A or loop C during the quiescent period of the respiratory discharge (interburst interval). This

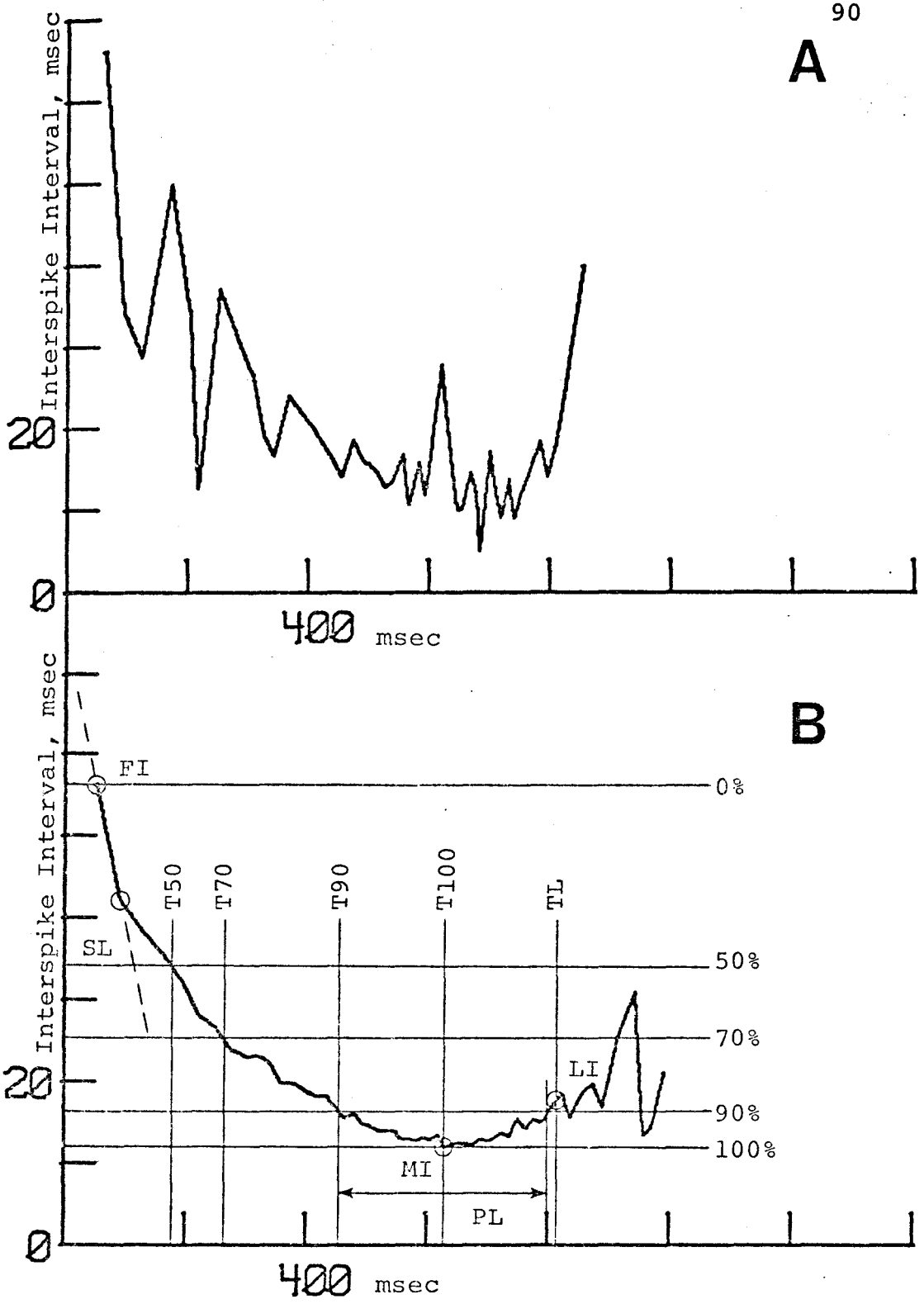

Figure 9. Interspike interval modulation curves derived from inspiratory cell C29UI7R(2) in Figure 4A: A. single train; B. average of 44 trains. Derivation of parameters shown in B are described in text, pages 99-106.

caused an "R" to be flashed on the CRT indicating that appropriate addresses had been reset. Program flow was then delayed in the first trigger loop (TL1) until the first action potential was detected. At this time, an "S" was flashed on the CRT and program flow was then delayed in the second trigger loop (TL2). Starting with the second action potential, all the remaining action potentials in the train caused a "T" to be displayed on the CRT. In conjunction with the clock logic (CL), each of these successive action potentials defined an interspike interval which was stored in an incremental address. Thus, consecutive intervals were stored in consecutive addresses. When a predetermined amount of time (maximum of 4095 msec scaled time) elapsed without any action potentials being detected, it was assumed that the train discharge was terminated for that breath and reset procedures were automatically initiated as revealed by CRT display of the "R". The sequence started all over again when the first action potential (display "S") of the next burst discharge was detected.

By this iterative technique, the PDP-12 memory accumulated the sum of the first intervals, the sum of the second intervals and so forth. To handle large sums, double precision arithmetic was used. That is, two 12-bit registers were daisy-chained together to form a 24-bit register

(maximum value accepted = 2^{23} = 8,388,608). The idealized train was recovered after exit from loop B by dividing each accumulated interval sum by the number of intervals that contributed to that sum. Since the divisor N was variable, the analysis was not limited by the shortest train, a problem described by other workers (24, 40). However, commencing with the first interval after the shortest train and continuing until the last interval of the longest train, the divisor N decreased as fewer and fewer trains contributed to the idealized interspike interval average (Figure 8B). For this reason, a breakdown in the statistical averaging and hence poor curve smoothing was observed towards the end of the train (Figure 9B).

In addition to histogram and interspike interval modulation curve genesis, loop B also stored consecutive cycle times and first interval times during the complete analysis. Cycle time (CT) was defined as the time between first action potentials of consecutive burst discharges. The first interval (FI) was defined as the time between the first two action potentials of each train. This parameter is circled in Figure 9B at the beginning of the train.

Exit from loop B was under both manual and automatic control. During trial runs, output procedures could be initiated by sense switch selection. Also, if more than 510

burst discharges were accumulated, automatic transfer to loop C was performed. For final runs, however, exit from loop B occurred after the histogram N had been filled. If the histogram was filled during the middle of a burst discharge, intervals were still calculated to complete the interspike interval modulation curve for that burst, but the intervals were deleted from histogram construction. Exit proceeded with the first action potential of the very next train (Figure 8A). This permitted accurate measurement of the last cycle time.

Between loops B and C, a series of calculation (CALC) steps were performed (Figure 3). As already discussed, mean interspike intervals were recovered to generate the idealized train. Individual instantaneous respiratory rates were calculated from the reciprocal of each cycle time measurement and these rates were averaged to give a mean respiratory rate (RR) for the analysis period. Mean rates calculated in this manner were slightly higher than averages taken by dividing the number of respiratory cycles observed by the total analysis period. This was due to the hyperbolic relationship between the period and the reciprocal of the period. High and low rates were isolated to reveal the degree of steady-stateness of instantaneous frequencies.

The number of intervals in each train were calculated and the mean spikes per train (ST) were found by adding one to the mean number of intervals per train. By examination of each idealized interval, the minimum interval (MI) in the respiratory train was localized by a search technique. The minimum interval (MI) is circled in Figure 9B. Also, the mean (MEN) interval time was calculated from the idealized train taking into account the variable divisor N, for each interval. The mode (MOD) and median (MED) interval times were extracted from the histogram data and the number of intervals in the bin at the mode (MON) was found. The mean (MEN), median (MED), mode (MOD) and number of intervals at the mode (MON) are diagrammed in the histogram data of cell C29UI7R(2) in Figure 6B.

Finally, the following eleven values were stored in a specific portion of core memory to facilitate transfer to LINC magnetic tape: mean respiration rate (RR), number of trains averaged (NT), spikes per train (ST), first interval time (FI), minimum interval time (MI), number of intervals in the interspike interval modulation curve (FMN), number of intervals in the histogram (HSN), mean (MEN), median (MED) and mode (MOD) interval times, and number of intervals at the mode (MON).

After completion of the calculation procedures,

program flow proceeded to loop C instructions. Loop C (Figure 3) was an output loop responsible for retrieving calculated data. The CRT was used to continuously display the histogram or interspike interval modulation curve (sense switch selection) along with axes and appropriate scaling integers. Titles could be placed on the CRT from the Decwriter keyboard for photographic purposes.

Selection of sense switch W (write) caused the Decwriter to print a hard copy list of digitilized values stored in core memory. Table I is the output from cell C29UI7R(2). In A, the mean, high and low respiration rates (breaths/10 minutes) and instantaneous rates for each breath are given. The number of breaths averaged (N=NT) was 44. In B, the mean spikes per train and the number of intervals for each individual train are given. Concerning the latter, one train was 37 intervals long, six trains were 43 intervals long, five trains were 48 intervals long, etc. The N is repeated as an internal program check. In C, the individual first interval times for each breath are printed to nearest 0.1 millisecond and in D, the digitilized values for the idealized interspike interval curve are listed to nearest 0.1 millisecond in sequential order (e.g. first interval, second interval, etc.). An average of data in C equals the first value in D. Also in D, the mean (MEN),

Table I. Program DATA computer printout derived from inspiratory cell C29UI7R(2) in Figure 4A.

C29UI7R(2)

A R RATE. M 0301 H 0317 L 0287 N 0044

0295	0304	0298	0300	0288	0304	0303	0301	0303	0301
0294	0304	0317	0309	0304	0304	0287	0306	0303	0315
0297	0306	0312	0300	0294	0292	0314	0310	0297	0310
0292	0291	0298	0312	0310	0309	0303	0301	0298	0303
0288	0294	0301	0307						

B TRAINS INT ST 0467 N 0044

0001	0037
0001	0039
0002	0040
0003	0041
0001	0042
0006	0043
0003	0044
0003	0045
0006	0046
0003	0047
0005	0048
0003	0049
0002	0050
0002	0051
0002	0052
0001	0055

C FIRST INT

0607	0806	0496	0414	0524	0482	0581	0574	0598	0661
0615	0528	0531	0479	0424	0709	0520	0578	0637	0615
0645	0519	0460	0763	0423	0632	0616	0614	0606	0612
0507	0528	0611	0450	0557	0123	0562	0487	0630	0648
0701	0459	0505	0657						

D M INTERVALS MEN 0188 MI 0120 N 2011

0561	0419	0381	0354	0319	0280	0265	0239	0229	0231
0221	0198	0197	0190	0181	0183	0169	0155	0162	0148
0145	0140	0140	0140	0129	0129	0128	0131	0127	0136
0120	0123	0126	0123	0121	0129	0127	0129	0137	0131
0155	0141	0154	0149	0167	0185	0155	0186	0197	0168
0254	0309	0134	0143	0211					

E ISIH MOD 0132 MON 0161 MED 0148 N 2000

0000	0000	0001	0004	0001	0006	0003	0004	0011	0014
0029	0061	0086	0112	0140	0131	0161	0147	0117	0098
0076	0067	0049	0054	0047	0045	0046	0038	0035	0039
0023	0019	0016	0021	0027	0018	0017	0012	0012	0011
0015	0013	0013	0010	0007	0008	0007	0006	0007	0009
0006	0003	0009	0008	0004	0005	0006	0003	0003	0007
0001	0002	0003	0005	0003	0003	0001	0002	0000	0003
0002	0001	0002	0000	0002	0005	0005	0000	0002	0001
0002	0001	0002	0001	0000	0000	0000	0001	0001	0000
0000	0000	0000	0000	0001	0000	0000	0000	0000	0000
0001	0000	0000	0000	0000	0000	0000	0000	0000	0000
0000	0000	0000	0000	0000	0000	0000	0000	0000	0000
0000	0000	0000	0000	0000					

minimum interval (MI) and number of intervals contributing to interspike interval modulation curve (N=FMN) are retrieved. Finally, in E, the contents of each of the 125 - 0.8 millisecond bins of the histogram are printed. The mode (MOD), number of intervals at the mode (MON), median (MED) and number of intervals in the histogram (N=HSN) are also given. It can be seen that the 17th bin contains the largest number of counts (MON=161). This by definition is the mode (e.g. 17 bins x 0.8 msec per bin = 13.6 msec or to place the peak at center of 0.8 msec bin, MOD = 13.6 msec - 0.4 msec = 13.2 msec). The reader should be able to correlate the digitalized values of Table 1-D with Figure 9B and Table 1-E with Figure 6.

Selection of sense switch P (plot) caused the Calcomp X-Y digital plotter to plot the histogram and interspike interval modulation data on paper from Table 1-E and 1-D data, respectively. These plots along with axes and scalings were identical to the CRT displays of the same data. Figures 6 and 9 are computer plots for cell C29UI7R(2) obtained from this output procedure.

Finally, selection of sense switch A (address) transfered data in core memory to a specified address of the LINC magnetic tape. Included in this transfer were the individual number of intervals per train and individual first

intervals, histogram and interspike interval modulation data, and the eleven constants mentioned previously (RR, NT, ST, FI, MI, FMN, HSN, MEN, MED, MOD, MON). A CRT display of "F" indicated that the tape contents at the selected address were full. This prohibited overwriting of stored data by mistake, although contents could be replaced if so desired. The tape-stored data were accessed via FOCAL programs for advanced mathematical analysis. In addition, other machine language programs could be run to replot histogram and interspike interval modulation data from the magnetic tape.

Exit from loop C (sense switch control) cleared the core memory and initiated loop B procedures (Figure 3). To examine the single cell input signal it was necessary to manually halt program flow and restart the program at *20.

3. REPLT

Program REPLT permitted replotting of either 100 or 50 millisecond histogram and interspike interval modulation data from the LINC magnetic tape. Data from several steady state observations on the same cell or different cells could be superimposed for visual comparison. Since this program was a modification of the plot routine in program DATA, it is not listed in the Appendix.

C. FOCAL-12 Programs

1. $CALC1

Data stored on the LINC magnetic tape were accessed, manipulated and restored in columnar arrangement by this first calculation program. The following new eleven parameters were derived and added to the list of eleven parameters previously calculated by program DATA. The data from cell C29UI7R(2) found in Table I are used for all examples, which can be substantiated via hand calculations. This program along with all other FOCAL-12 programs are listed in the Appendix.

The train length (TL) was determined to the nearest millisecond by summing consecutive intervals of the idealized interspike interval modulation curve data until the mean number of intervals per train was reached. Mathematically,

$$n = \text{integer}(ST) - 1$$

$$f = ST - 1 - n$$

$$TL(\text{msec}) = \left[\sum_{i=1}^{n} int_i\right] + f[int_{n+1}]$$

where ST is the mean spikes per train; int_n is the last whole interval of the intervals contributing to the train length (TL) and "f" corrects for the fractional contribution from the very next interval, int_{n+1}, for trains terminating

between intervals int_n and int_{n+1}. For cell C29UI7R(2), n = 45, "f" = 0.7 and TL = 845.9 + 0.7(18.5) = 859 milliseconds. A vertical train length (TL) line has been drawn on the interspike interval modulation curve in Figure 9B corresponding to the above measurement for cell C29UI7R(2). It can be observed that the mean train length (TL) was reached before the curve lost the smooth transitions between intervals toward the end of the train. No measurements or interpolations were made past the mean train length (TL). This cutoff was observed for most cells.

The mean cycle time (CT) was calculated to the nearest 10 milliseconds by computing the reciprocal of the mean respiratory rate (RR), That is,

$$CT(msec) = 10 \cdot integer[(RR^{-1} \cdot 60000\ msec/min)/10]$$

For cell C29UI7R(2), CT = 10 · integer(6000/30.1) = 1990 milliseconds.

From program DATA, the number of intervals per individual train and individual first interval times contributing to single steady state averages were stored on LINC magnetic tape. These values were retrieved by program $CALC1 for calculation of the standard deviation (SD) and standard error (SE) for each. These standard statistical measurements were made as follows:

$$SD = \sqrt{[\Sigma X^2 - (\Sigma X)^2/N]/[N - 1]}$$

$$SE = SD/\sqrt{N}$$

where X represents the individual intervals for either case and N is the number of respiratory bursts averaged. For cell C29UI7R(2), N = 44 and SD_{ST} = 3.9, SE_{ST} = 0.58, SD_{FI} = 11.1 and SE_{FI} = 1.68 milliseconds.

The plateau level (PL), defined as the length of time the interspike interval modulation curve was within 10% of the minimum interval (FI - MI difference = 100%), was measured to the nearest millisecond. That is,

$$n = \text{integer}(ST) - 1$$

$$K = 0.10(FI - MI) + MI$$

$$PL(\text{msec}) = \left[\sum_{i=1}^{n} int_i < K\right]$$

where ST is the mean spikes per train, FI is the first interval, MI is the minimum interval and int_n is the last whole interval of the intervals contributing to the mean train length. The plateau level (PL) is drawn in Figure 9B as a horizontal line extending between two vertical lines which intercept the experimental interspike interval modulation curve at the 90% level. Intervals meeting the requirements, but falling after the mean train length (TL), were disregarded. The plateau level (PL) for cell

C29UI7R(2) was 368 milliseconds.

The last interval (LI) was defined as the interspike interval time of the experimental curve at the end of the measured mean train length. This parameter was calculated to the nearest 0.1 millisecond and is circled in Figure 9B at the end of the train. Mathematically,

$$n = \text{integer}(ST) - 1$$

$$f = ST - 1 - n$$

$$LI(0.1 \text{ msec}) = f[int_{n+1} - int_n] + int_n$$

where ST is the mean spikes per train, int_n is the last whole interval of the intervals contributing to the mean train length (TL) and int_{n+1} is the very next interval. The "f" measurement computes a linearly interpolated last interval (LI) correction for train lengths (TL) terminating between intervals int_n and int_{n+1}. For cell C29UI7R(2), LI(0.1 msec) = 0.7(18.5 - 16.7) + 16.7 = 18.0 milliseconds with the train terminating between the 45th and 46th intervals.

The slope (SL) was a measure of the initial rate of change in the interval time of the interspike interval modulation curve. The slope was defined as

$$SL = (SI - FI)/SI$$

where FI is the first interval and SI is the second interval. The slope of the dashed lined connecting the first

two circled intervals in Figure 9B corresponds to this measurement. For cell C29UI7R(2), SL = (41.9 - 56.1)/ 41.9 = -0.34.

The plateau level percent (PLP) was defined as the ratio of the plateau level (PL) to the mean train length (TL). For example,

PLP(%) = (PL/TL)100

This parameter was a normalized measure of the fraction of the cell's "on" time occupied by intervals within 10% of the minimum interval (MI). For cell C29UI7R(2), PLP = (368/859)100 = 42.8%.

The last measurement made by program $CALC1 was the train legnth percent (TLP). This parameter was defined as the ratio of the mean train length (TL) to the cycle time (CT) or

TLP(%) = (TL/CT)100

This measurement normalized the fraction of the respiratory cycle occupied by respiratory cell activity (e.g. percent "on" time). For cell C29UI7R(2), TLP = (859/1990) 100 = 43.2%.

2. $CALC2

Similar to program $CALC1, this second calculation program derived the final twelve parameters from the LINC magnetic tape. These parameters were added to the columnar

data previously calculated, thus completing the number of parameters measured for each steady state observation to thirty-four. The following new parameters were calculated. All examples are taken from cell C29UI7R(2) data listed in Table I permitting verification via hand calculations.

As illustrated by the horizontal lines traversing the interspike interval modulation curve in Figure 9B, the interspike interval times were normalized into percent levels. The range extended from the first interval (FI = 0%) to the minimum interval (MI = 100%) with additional horizontals drawn at the 50, 70 and 90% levels. Where these immaginary lines crossed the experimental curve, vertical lines corresponding to times to reach 50, 70, 90 and 100% levels (T50, T70, T90, T100) were constructed. Measurements of T values were carried out to the nearest millisecond. Linear interpolations were performed in cases where 50, 70, and 90% horizontal levels crossed the curve between two intervals. Associated with these four measurements (T50, T70, T90, T100) were four parameters (N50, N70, N90, N100) representing the number of intervals elapsed before each level was reached. The mathematical expressions used to calculate the T and N values are given below:

$$K = (1 - P/100)(FI - MI) + MI$$

$$T(\text{msec}) = \left[\sum_{i=1}^{n} int_i\right] + \left[\frac{K - int_n}{(int_{n+1} - int_n)/int_{n+1}}\right]$$

$$N = n - (int_n - K)/(int_{n+1} - int_n)$$

where P is the percent level and n is the sequence position of the interval preceeding the first interval less than K. For cell C29UI7R(2),

$$K50 = (1 - 50/100)(56.1 - 12.0) + 12.0 = 34.05$$

$$T50(\text{msec}) = (56.1 + 41.9 + 38.1 + 35.4) + \frac{(34.05 - 35.4)}{(31.9 - 35.4)/31.9} = 184 \text{ msec}$$

$$N50 = 4 - (35.4 - 34.05)/(31.9 - 35.4) =$$

4.4 intervals

Also for cell C29UI7R(2), T70 = 270, T90 = 467 and T100 = 655 milliseconds, and N70 = 7.5, N90 = 17.4 and N100 = 31.0 intervals. From Table 1-D, it can be seen that the minimum interval (MI = 12.0 msec) is the thirty-first interval in the train and corresponds to N100.

Four last parameters were derived by taking the ratio of the T values to the mean train length. That is,

$$T5P(\%) = (T50/TL)100$$

$$T7P(\%) = (T70/TL)100$$

$$T9P(\%) = (T90/TL)100$$

$$T10P(\%) = (T100/TL)100$$

For example, for cell C29UI7R(2), T5P = (184/859)100 = 21.4%. Also, T7P = 31.4%, T9P = 54.4% and T10P = 76.2%.

3. $READ

The thirty-four parameters calculated via programs DATA, $CALC1 and $CALC2 and stored on LINC magnetic tape were retrieved and printed out by program $READ for each steady state respiratory discharge. The computer listing of these parameters for cell C29UI7R(2) is found in Table II. All time measurements (TL, CT, SD_{ST}, SE_{ST}, FI, SD_{FI}, SE_{FI}, MI, MEN, MED, MOD, PL, LI, T50, T70, T90 and T100) are standardized in milliseconds. Parameters that count events (NT, ST, FMN, HSN, MON, N50, N70, N90 and N100) and parameters that are derived from the ratio of time measurements (SL, T5P, T7P, T10P, PLP and TLP) are all dimensionless. The respiratory rate (RR) is given in breaths per minute.

4. $SUM1
5. $SUM2
6. $SUM3
7. $SUM4

Similarly to program $READ, these four programs printed out the thirty-four parameters calculated for each steady state observation, but in a modified format. That is, instead of lising the different parameters in one vertical column as in Table II, parameters were typed out in horizontal rows so that similar measurements from

Table II. Program $READ computer printout derived from inspiratory cell C29UI7R(2) in Figure 4A.

DATA POINT	20
TL	859
CT	1990
RR	30.1
NT	44
ST	46.7
SD	3.9
SE	0.58
FI	56.1
SD	11.1
SE	1.68
MI	12.0
FMN	2011
MSN	2000
MEN	18.8
MED	14.8
MOD	13.2
MON	161
PL	368
LI	18.0
SL	- 0.34
T50	184
T70	270
T90	467
T100	655
N50	4.4
N70	7.5
N90	17.4
N100	31.0
T5P	21.4
T7P	31.4
T9P	54.4
T10P	76.2
PLP	42.8
TLP	43.2

consecutive steady state observations formed vertical columns. For example, parameters listed by programs $SUM1 (RR, NT, ST, SD_{ST}, SE_{ST}, FI, SD_{FI}, SE_{FI}, MI), $SUM2 (FMN, HSN, MEN, MED, MOD, MON, PL, LI), $SUM3 (SL, T50, T70, T90, T100, N50, N70, N90, N100) and $SUM4 (TL, CT, T5P, T7P, T9P, T10P, PLP, TLP) formed four tables of data. By following down any one of the thirty-four columns, alterations in a single parameter for any one cell could be traced and correlated with induced modifications of the breathing pattern.

8. $REORD

The thirty-four parameters associated with any one steady state observation were located in sequential addresses on LINC magentic tape. Since this was an inconvenient format for accessing similar parameter types in certain plotting procedures, program $REORD was used to reorder all the parameters on new LINC magnetic tape. In effect, rows and columns were interchanged which placed similar parameter types in sequential addresses. Two recorded tapes containing inspiratory and expiratory cell data, respectively, were obtained by this procedure.

9. $IVO
10. $IVI
11. $EVO
12. $EVI

The reordered inspiratory and expiratory tapes that

were constructed via program $REORD contained steady state measurements from both vagotomized and vagi-intact preparations. The responsibility of these four programs was to divide vagi-intact (VI) from vagi-out (VO) data points for both inspiratory (I) and expiratory (E) cells. This data manipulation of the two reordered types produced four new LINC tapes including inspiratory vagi-out (I-VO), inspiratory vagi-intact (I-VI), expiratory vagi-out (E-VO) and expiratory vagi-intact (E-VI) data groups. These four tapes were formated as the reordered tapes and were used for statistical computations and regression plotting of raw data.

13. $ROWM

This program calculated the mean, standard deviation (SD), standard error (SE), high and low values and range for each parameter group stored on LINC tapes I-VO, I-VI, E-VO, and E-VI. The standard deviation (SD) and standard error (SE) calculations were identical to those described in program $CALC1. One hundred and thirty-six sets of statistical data (4 tapes · 34 parameters types/ tape) were printed out by program $ROWM.

14. $RLIN
15. $REXP
16. $RLOG
17. $RLLG

Linear and curvilinear regressions were obtained

between groups of similar parameter types taking two groups at a time. Excluding eight groups (SD_{ST}, SE_{ST}, SD_{FI}, SE_{FI}, NT, FMN, HSN and MON), all possible combinations for the remaining twenty-six groups were examined using four different curve fits for each of the four tapes I-VO, I-VI, E-VO and E-VI ($26^2 \cdot 4 \cdot 4 = 10{,}816$ regression comparisons). Coefficients for the four equations,

fit 1 $\quad Y = B + X \cdot M \pm E$ (linear)

fit 2 $\quad Y = EXP(B + X \cdot M \pm E)$ (exponential)

fit 3 $\quad Y = B + \ln(X) \cdot M \pm E$ (logarithmic)

fit 4 $\quad Y = EXP(B + \ln(X) \cdot M \pm E)$ ($\log_e$-$\log_e$)

along with the correlation coefficient "r" and other statistical computations were derived by transforming data for curvilinear regressions,

$Y = \ln(Y)$ for exponential fit

$X = \ln(X)$ for logarithmic fit

$Y = \ln(Y)$ and $X = \ln(X)$ for $\log_e$-$\log_e$ fit

and performing the following linear regression analysis:

$$DX = \Sigma X^2 - (\Sigma X)^2/N$$

$$DY = \Sigma Y^2 - (\Sigma Y)^2/N$$

$$M = [\Sigma XY - (\Sigma X)(\Sigma Y)/N]/DX$$

$$B = [\Sigma Y - (\Sigma X)M]/N$$

$$r = \frac{M \cdot DX}{\sqrt{(DX)(DY)}} = M(SD_X/SD_Y)$$

$$S = DY - M^2 \cdot DX$$

$$E = \sqrt{S/(N - 2)}$$

$$V = r^2$$

where X and Y represent the independent and dependent variables, respectively, of the paired groups, N is the number of parameters in either group, M is the slope, B is the Y intercept, and "r" is the correlation coefficient ($r \leq 1.00$). Note that "r" can be defined as slope (M) times the ratio of X to Y standard deviations. The standard error of estimate (E) defined a range of regression curves including 68% of the individual observations of Y on X. Assuming that the distribution about the regression line was normal and of equal variance, this error term corresponded to one standard deviation unit on either side of the mean regression line. The V value (r^2) described the proportion of the variance of Y that could be attributed to its linear regression on X.

18. $REGSD

The significant difference between two regression slopes (M_1, M_2) was tested by this program. The following calculations applied only to regressions of the same fit (i.e. linear, exponential, logarithmic or log-log):

$$S = (S_1 + S_2)/(N_1 + N_2 - 4)$$

$$DI = \sqrt{S/(DX_1 + DX_2)}$$

$$t = (M_1 - M_2)/DI$$

where S, N, DX and M values were obtained from the regression programs and "t" is the standard Student "t" value with degrees of freedom equal to $(N_1 + N_2 - 4)$. The "t" values were converted into P coefficients in the program, eliminating the use of standard statistical tables.

19. $RSIGD

This program calculated the significant difference between the regression coefficients of two regression equations independent of fit. The following calculations were made:

$$Z_1 = [\ln(1 + r_1) - \ln(1 - r_1)]/2$$

$$Z_2 = [\ln(1 + r_2) - \ln(1 - r_2)]/2$$

$$C = \frac{|Z_1 - Z_2|}{\sqrt{\frac{1}{N_1 - 3} + \frac{1}{N_2 - 3}}}$$

where r_1 and r_2 are the two regression coefficients being compared, N_1 and N_2 are the number of X-Y pairs in fit_1 and fit_2, respectively, and the C value is correlated with P levels of significance from the normal distribution curve (not the "t" distribution). The values for P were computed for the following levels: >0.05, ≤ 0.05, ≤ 0.04,

≤ 0.03, ≤ 0.02 and ≤ 0.01.

20. $PVALR

Correlation coefficients were converted into P levels of significance by first computing Student "t" values.

For example,

$$t = r\sqrt{N - 2}/\sqrt{1 - r^2}$$

where r is the correlation coefficient and N is the number of X-Y pairs correlated. As in program $REGSD, "t" values were converted directly into P coefficients.

21. $STTEST

The standard Student "t" test was programmed to calculate P values for miscellaneous paired or unpaired data. The "t" value was calculated as follows:

$$DM = \sqrt{(SE_1)^2 + (SE_2)^2 - 2r(SE_1)(SE_2)}$$

$$t = |MN_1 - MN_2|/DM$$

$$DF \text{ paired} = (N_1 + N_2 - 2)/2 = N - 1$$

$$DF \text{ unpaired} = N_1 + N_2 - 2$$

where SE_1 and SE_2 are the standard errors of the two sets of data,"r"is the regression coefficient for paired data ($r = 0$ for unpaired data), MN_1 and MN_2 are the means for each data set and N is the number of observations in each set ($N_1 = N_2$ for paired data). The P values were computed automatically from the "t" values.

22. $TIMFOL

This program was designed to compute the time elapsed between two digital tape counter values on the tape recorder. Since the tape counter was driven from the take-up reel, the digital read-out was a non-linear function of time. For this reason, a calibration curve was constructed in which the tape counter value was plotted as a function of time (0 - 100 minutes). This curvilinear plot was broken up into nine linear segments from which accurate time durations could be interpolated from two tape counter values. With this program, the length of time cells were recorded and the time between events could be computed, eliminating the need for hand computations from polygraph records.

D. FOCALPL Programs

1. %PLOT

Groups of data, correlated via regression calculations (programs $RLIN, $REXP, $LOG and $LLG) from LINC magnetic tape data (I-VO, I-VI, E-VO and E-VI), were plotted in scattergram format on the Calcomp digital plotter by program %PLOT. The independent (X) and dependent (Y) variables plotted were under manual selection and scaling factors were determined on the basis of program $ROWM range values for each data set. All regression

plots were transformed to linear coordinates and six plots were placed on each page for space conservation. Program %PLOT is listed in the Appendix along with the other FOCALPL programs.

2. %REGP1

Program %REGP1 superimposed mean regression lines and standard error of estimate lines on the scattergram plots of program %PLOT. For any one plot, scaling factors and type of fit were identical. Coefficients for the linear, exponential, logarithmic and $\log_e$-$\log_e$ equations (fit 1-fit 4) were obtained from the regression data of programs $RLIN, $REXP, $RLOG and $RLLG respectively. All equations were plotted on a linear scale thus rendering exponential, logarithmic and $\log_e$-$\log_e$ fits curvilinear. Because of this, error lines above and below the mean regression line were not always parallel with or symmetrical to the latter as with linear regressions.

3. %REGP2

This program was used to superimpose mean regression lines on the same graph for visual comparison. To avoid confusion, scattergram points of program %PLOT and error lines of program %REGP1 were omitted. Six sets of multiple graphs were condensed to one page. This plotting procedure facilitated data reduction and was useful for

data summarization.

4. %LINEP

Induced changes in single unit parameters followed digitally by programs $SUM1, $SUM2, $SUM3 and $SUM4 were plotted in time sequence by program %LINEP (line plot) for each respiratory cell that was examined for more than one steady state period. With the exception of cycle time (CT), the twenty-five parameters from the regression analysis (T50, T70, T90, T100, PL, TL, FI, MI, LI, MEN, MED, MOD, RR, N50, N70, N90, N100, ST, SL, T5P, T7P, T9P, T10P, PLP and TLP) were plotted on nine graphs (three pages) for each cell. The X scaling was proportioned according to the number of different steady state observations made for each cell and was a non-linear function of time.

CHAPTER V

RESULTS

A. Data Presentation

Single cell studies on the neural control of respiration have been organized into three categories which are presented in the following order. First, parameter measurements from similar cell types have been grouped from many cells for regression analysis. This was an attempt to describe general population characteristics of discharge patterns at different respiratory rates and depths. Second, changes in single unit parameters have been followed during induced modification of the spontaneous breathing pattern. Comparison of these single cell data with population regression data revealed the degree of discharge pattern heterogeneity among similar cell types. Third, the correlation between high barbiturate levels and apneusis has been examined at the single cell level. These data were important for interpretation of population and single cell data obtained after barbiturate

modification of the spontaneous breathing pattern.

B. Population Data

The general statistics of the single cell recordings attempted in 60 out of 85 cats used in this study are summarized in Table III. On the average, approximately three respiratory cells were recorded from each cat in a ratio of two inspiratory cells to one expiratory cell. Of these recorded cells, however, over fifty percent were rejected from final data compilation due to generation of uneven interspike interval modulation curves from poor signal-to-noise ratios or non-uniform breathing patterns.

Steady state computer averages were divided into four categories of inspiratory vagi-intact (I-VI), inspiratory vagi-out (I-VO), expiratory vagi-intact (E-VI) and expiratory vagi-out (E-VO) observations. Cells recorded during unilateral vagotomy were categorized with vagi-intact data, since no significant respiratory rate or depth changes were manifest after removal of one vagus nerve.

Each steady state average was identified by a data point number. There was a total of 333 data points each of which contributed 34 parameter measurements (333 X 34 = 11322 parameters) for regression analysis. An average of four data points (range = 1-17) was obtained from each

Table III. General statistics of respiratory cells analyzed by computer techniques.

Cell Type	# Cells Recorded	# Cells Analyzed	State of Vagi	# Data Points		Analysis Time (Min)		# Trains (NT)		# Intervals (FMN)	
				Total	Mean	Total	Mean	Total	Mean	Total	Mean
I	125	57	VI	175	3.4	188.7	1.1	6079	34.7	256111	1463
			VO	50	5.0	78.0	1.6	1159	23.2	61329	1227
E	57	26	VI	105	4.6	107.7	1.0	3776	36.0	119825	1141
			VO	3	1.0	3.5	1.2	64	21.3	2543	848
Sum Total	182	83		333		377.9		11078		439808	
Grand Mean					4.0		1.1		33.3		1321

respiratory cell. Respiratory cells were recorded for a period of time ranging from 30 seconds to three hours. Steady state averages were derived from mean breathing segments of 1.1 minutes. For all the cells, this analysis time represented more than six hours of spontaneous breathing or more than 25 hours of computer time taking into account the time scaling factor of 4. Derivation of the 333 data points involved over eleven thousand individual breaths and close to one half million interspike intervals. Average interspike interval modulation curves were generated from 33 burst discharges and more than thirteen hundred intervals.

As described in Data Analysis, similar parameter types were grouped together and all possible regression comparisons taking two groups at a time were performed. Interest centered around two regression types in which respiration rate (RR) and mode (MOD) parameters were selected as the independent variables. The respiration rate (RR) parameter, derived from the reciprocal of the cycle time, was a direct measurement of the spontaneous breathing frequency.

The mode (MOD) parameter reflected changes in respiratory depth (or tidal volume assuming constant airflow resistance) as illustrated in Figure 10 for an inspiratory

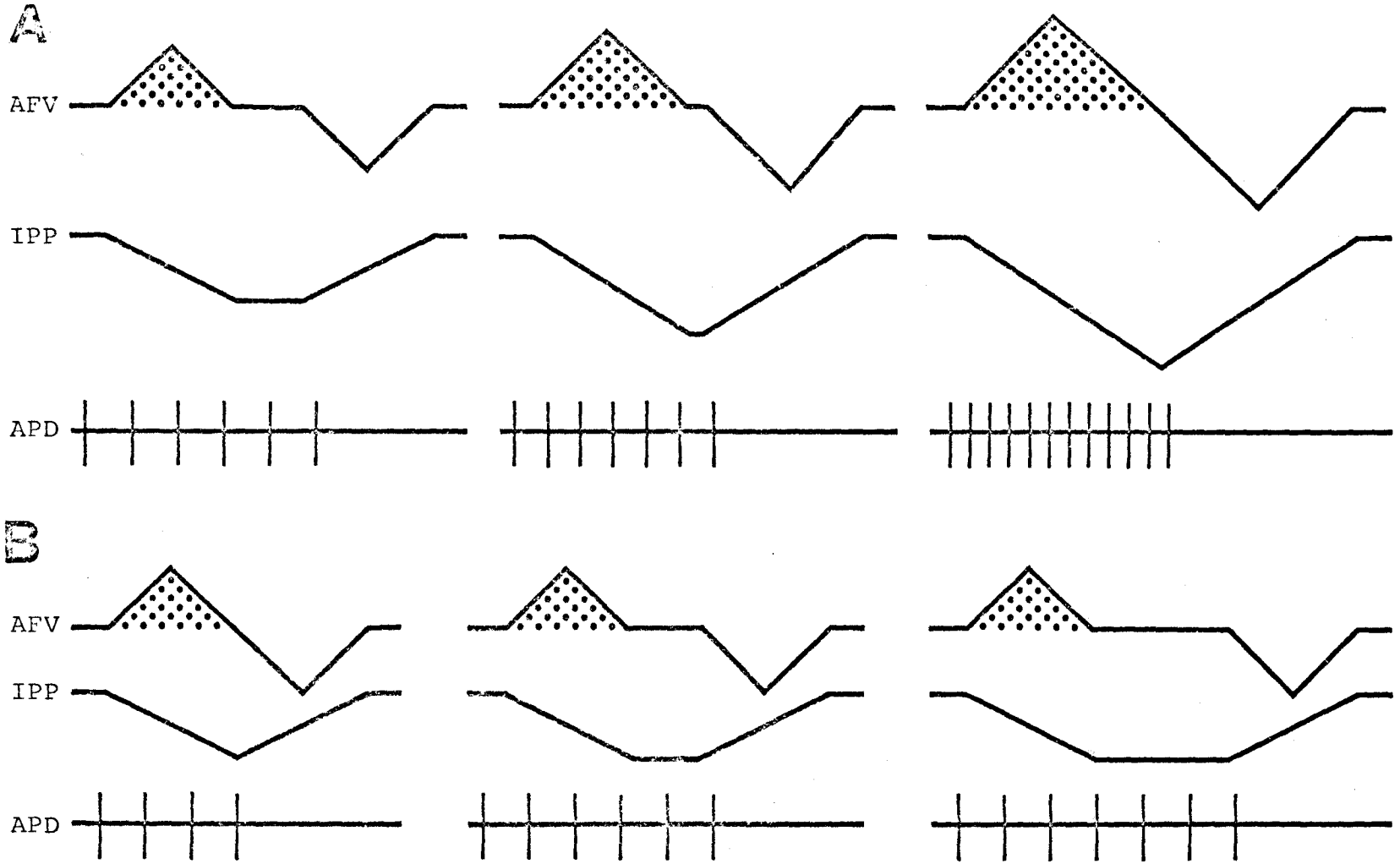

Figure 10. Idealized representation of airflow velocity (AFV), intrapleural pressure (IPP) and action potential discharge (APD) during: A. constant respiratory rate, increasing depth; B. constant depth, decreasing respiratory rate.

cell. In Figure 10A, for example, a decrease in mode (MOD) time is associated with an increased intrapleural pressure and increased tidal volume (shaded area under airflow curve) with no change in respiratory rate (RR = k). Figure 10B diagrams a hypothetical situation where a rate (RR) change is observed in the absence of any depth or tidal volume change. In such a case, the mode (MOD) parameter can be shown to be independent of rate (RR) changes.

This reciprocal relationship between mode (MOD) time and depth or tidal volume (TV $\propto$ 1/MOD) is not unusual since it has been established for both phrenic (39, 50, 53, 58) and central inspiratory cells (72, 129), but does make the assumption that no recruitment of units takes place, at least at the central level. Nesland et al. (129) deny that respiratory neurons are recruited, but this can be debated. The mode (MOD) time was selected over the mean (MEN) or median (MED) times since the former falls within the 100 millisecond segment of the phrenic traffic coincident with the peak of inspiration, integration of which yields the best neural correlate of tidal volume (53). The mode (MOD) is also by definition the most common or frequent interval in the average respiratory train.

For expiratory cells, the reciprocal relationship

between mode (MOD) and tidal volume is more involved. Nevertheless, higher frequency discharges (lower mode times) are expected to be found at larger tidal volumes due to elevated afferent feedback, increased active expiratory movements and postulated higher inhibitory thresholds on inspiratory neurons.

The thirty four parameters defined and measured in this study successfully quantitated all phases of a respiratory neuronal spike discharge. The respiratory train or interspike interval modulation curve (Figure 9B) was segmented into initial (frequency increase), middle (frequency plateau) and terminal phases (frequency decrease). Examination of parameter changes during induced alterations in the spontaneous breathing pattern revealed selective modification of certain phases over others. For example, changes in SL, FI, T50, T70, N50, N70, T5P and T7P reflected changes in the initial phase. Changes in MI, T90, T100, N90, N100, T9P, T10P, PL and PLP reflected changes in the middle phase. Changes in LI, TL and TLP reflected changes in the terminal phase of spike activity. The reader should keep the parameters in this type of perspective when following parameter modification at different spontaneous respiratory rates (RR) and depths (1/MOD). The thirty four parameters have been

tabulated in Table IV for convenient reader reference. Both code identification and definition as used throughout the dissertation are listed for each parameter.

Regression plots of 25 dependent variables (* Table IV) on respiration rate (RR) and mode (MOD) are presented in Figures 11-22 and Figures 23-34 respectively. Three plots for two dependent variables are organized from left to right in each figure for inspiratory vari-out (I-VO), inspiratory vagi-intact (I-VI) and expiratory vagi-intact (E-VI) data respectively. Expiratory vagi-out data (E-VO) have been deleted since only three data points from three expiratory cells were located in vagotomized preparations (cf. Table III). All scaling factors are given for X and Y axes which extend from border to border. The respiration rate (RR) scaling of Figures 11-22 and the mode (MOD) scaling of Figures 23-34 are consistent from plot to plot (X-axis). For any one figure, the scalings of dependent variables (Y-axis) are identical for each of the six plots. Exceptions are found in Figures 19, 28, and 31 where the different dependent parameters have different scaling factors. In these cases, the I-VO, I-VI and E-VI scalings are the same for any one parameter, however. Each axis is labeled with parameter type and appropriate dimension

Table IV. List of parameter abbreviations.

1	CT	Cycle Time
2	T50*	Time to 50%
3	T70*	Time to 70%
4	T90*	Time to 90%
5	T100*	Time to 100%
6	PL*	Plateau Level
7	TL*	Train Length
8	RR*	Respiration Rate
9	ST*	Spikes per Train
10	FI*	First Interval
11	MI*	Minimum Interval
12	LI*	Last Interval
13	MEN*	Mean
14	MED*	Median
15	MOD*	Mode
16	N50*	# of Intervals to 50%
17	N70*	# of Intervals to 70%
18	N90*	# of Intervals to 90%
19	N100*	# of Intervals to 100%
20	T5P*	T50 Percent
21	T7P*	T70 Percent
22	T9P*	T90 Percent
23	T10P*	T100 Percent
24	PLP*	Plateau Level Percent
25	TLP*	Train Length Percent
26	SL*	Slope
27	SE_{ST}	Standard Error (ST)
28	SE_{FI}	Standard Error (FI)
29	SD_{ST}	Standard Deviation (ST)
30	SD_{FI}	Standard Deviation (FI)
31	NT	# of Trains
32	FMN	# of Intervals in Interspike Interval Modulation Curve
33	HSN	# of Intervals in Histogram
34	MON	# of Intervals at Mode

*Parameter plotted in Figures 11-43.

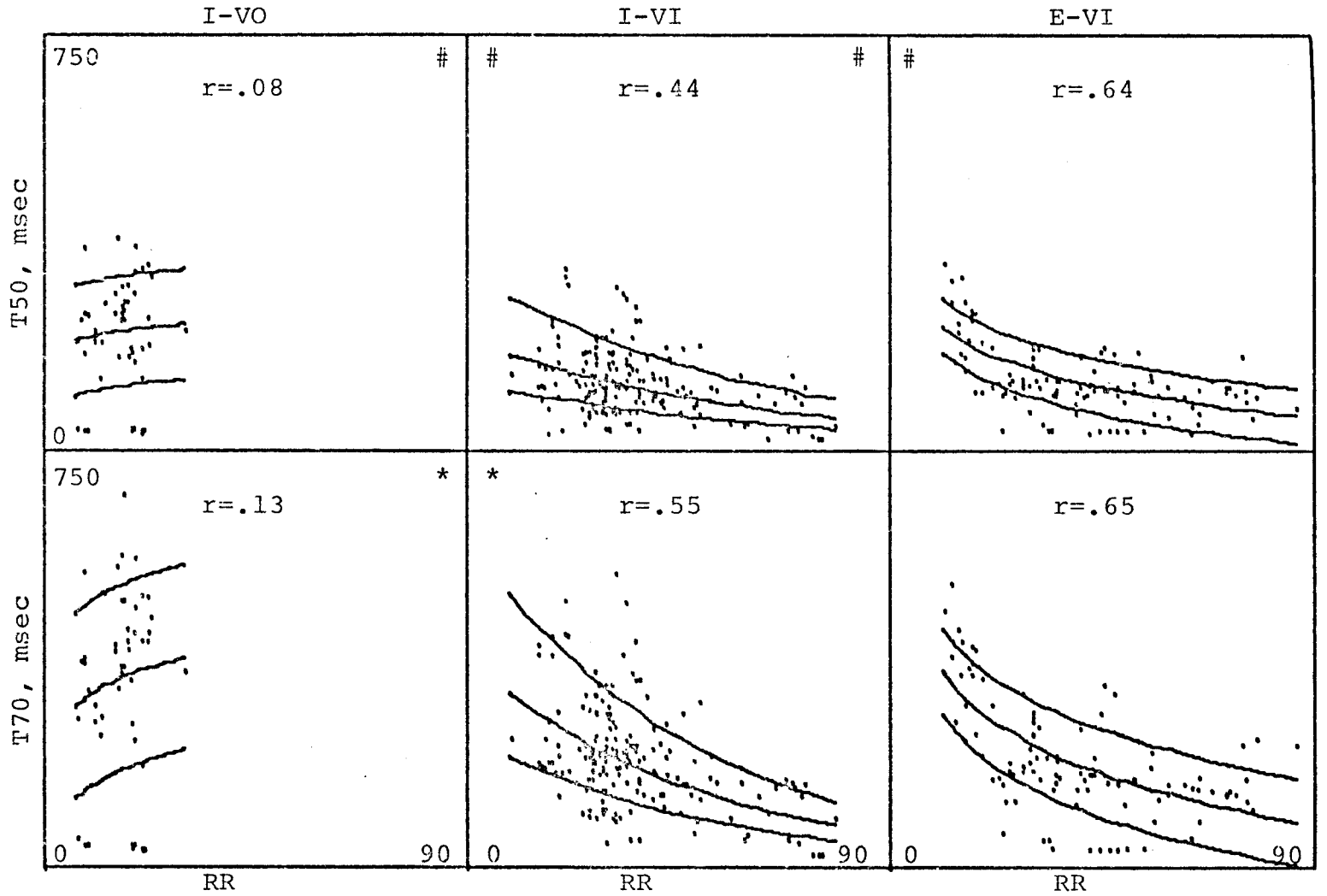

Figure 11. Regression of T50 and T70 on RR for I-VO, I-VI and E-VI cells.

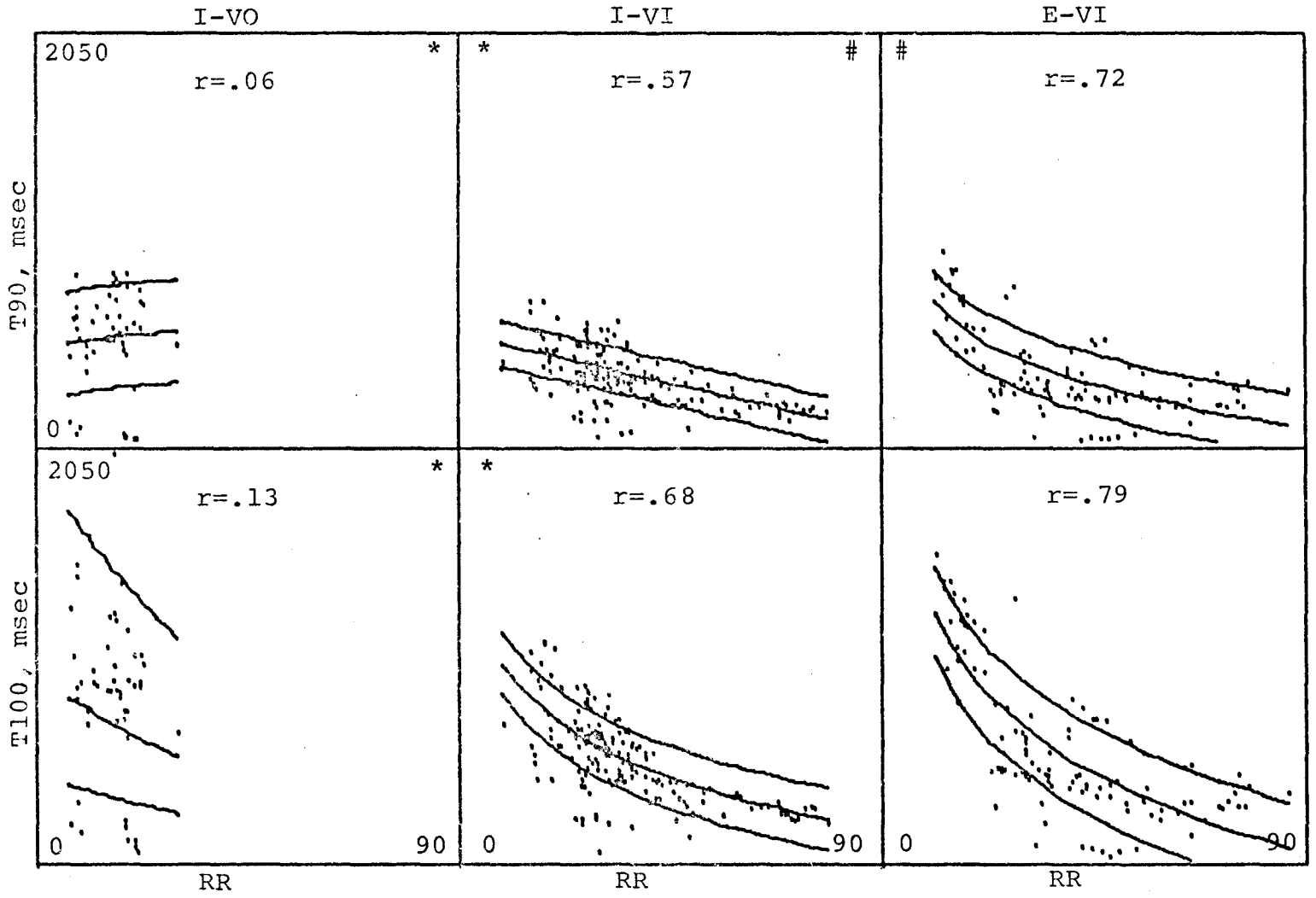

Figure 12. Regression of T90 and T100 on RR for I-VO, I-VI and E-VI cells.

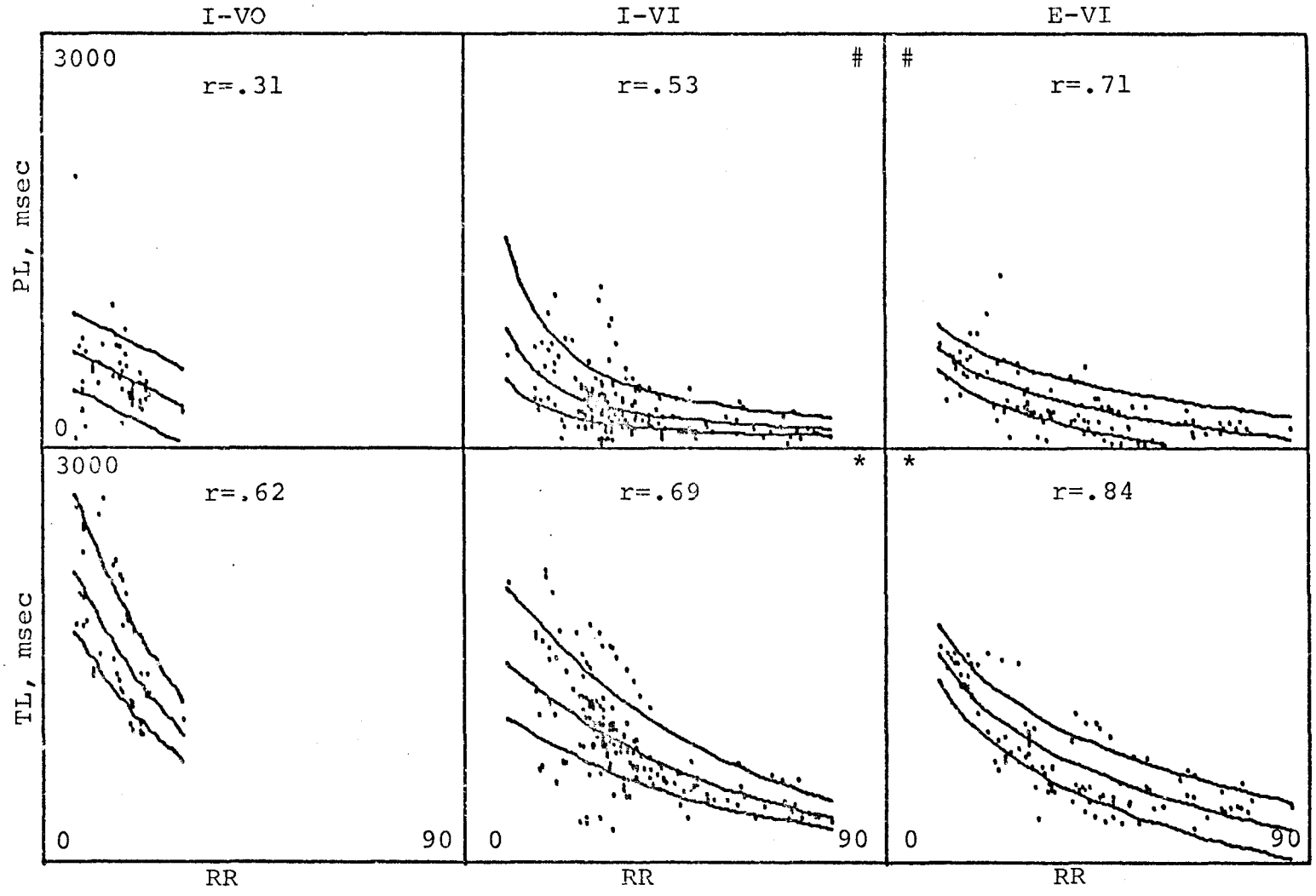

Figure 13. Regression of PL and TL on RR for I-VO, I-VI and E-VI cells.

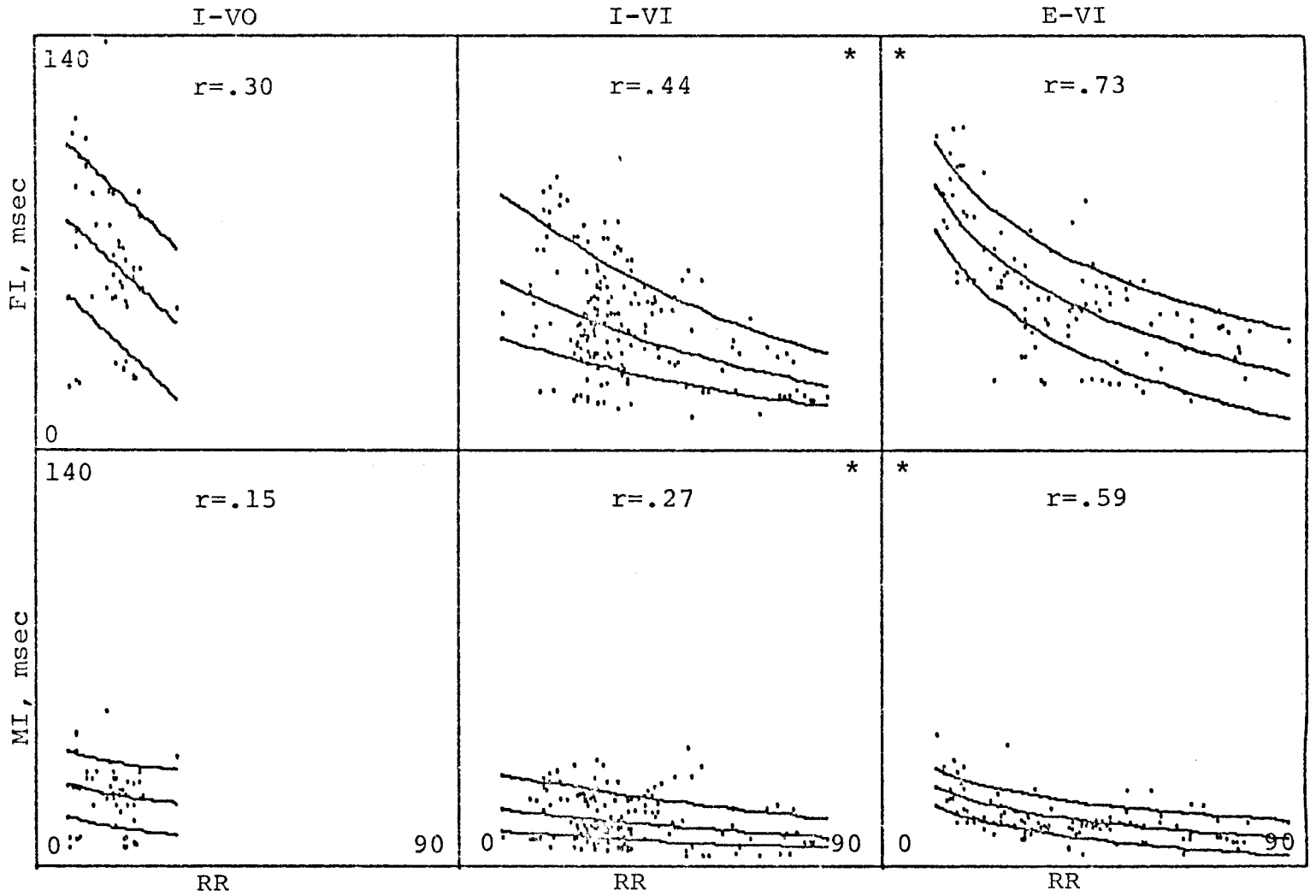

Figure 14. Regression of FI and MI on RR for I-VO, I-VI and E-VI cells.

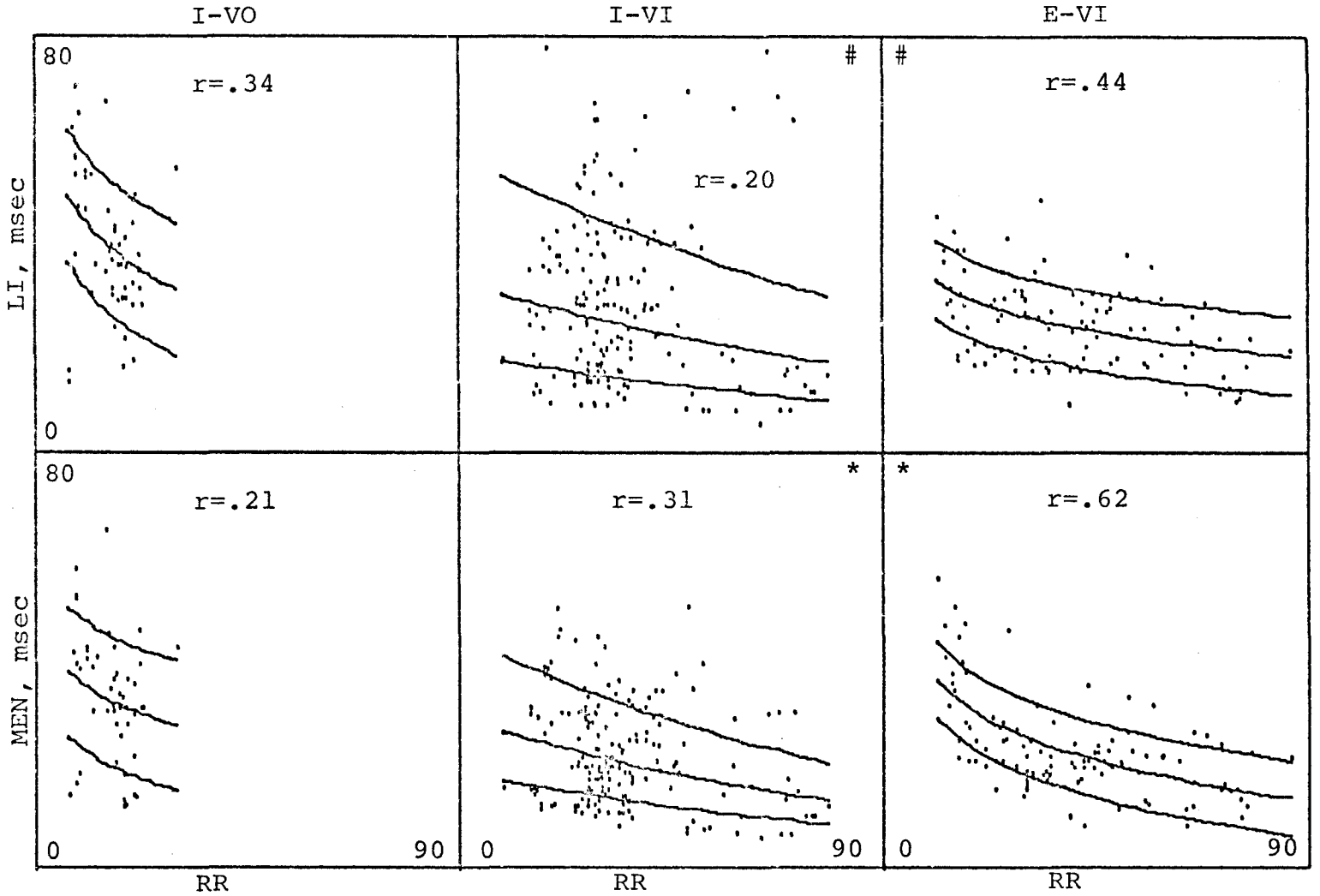

Figure 15. Regression of LI and MEN on RR for I-VO, I-VI and E-VI cells.

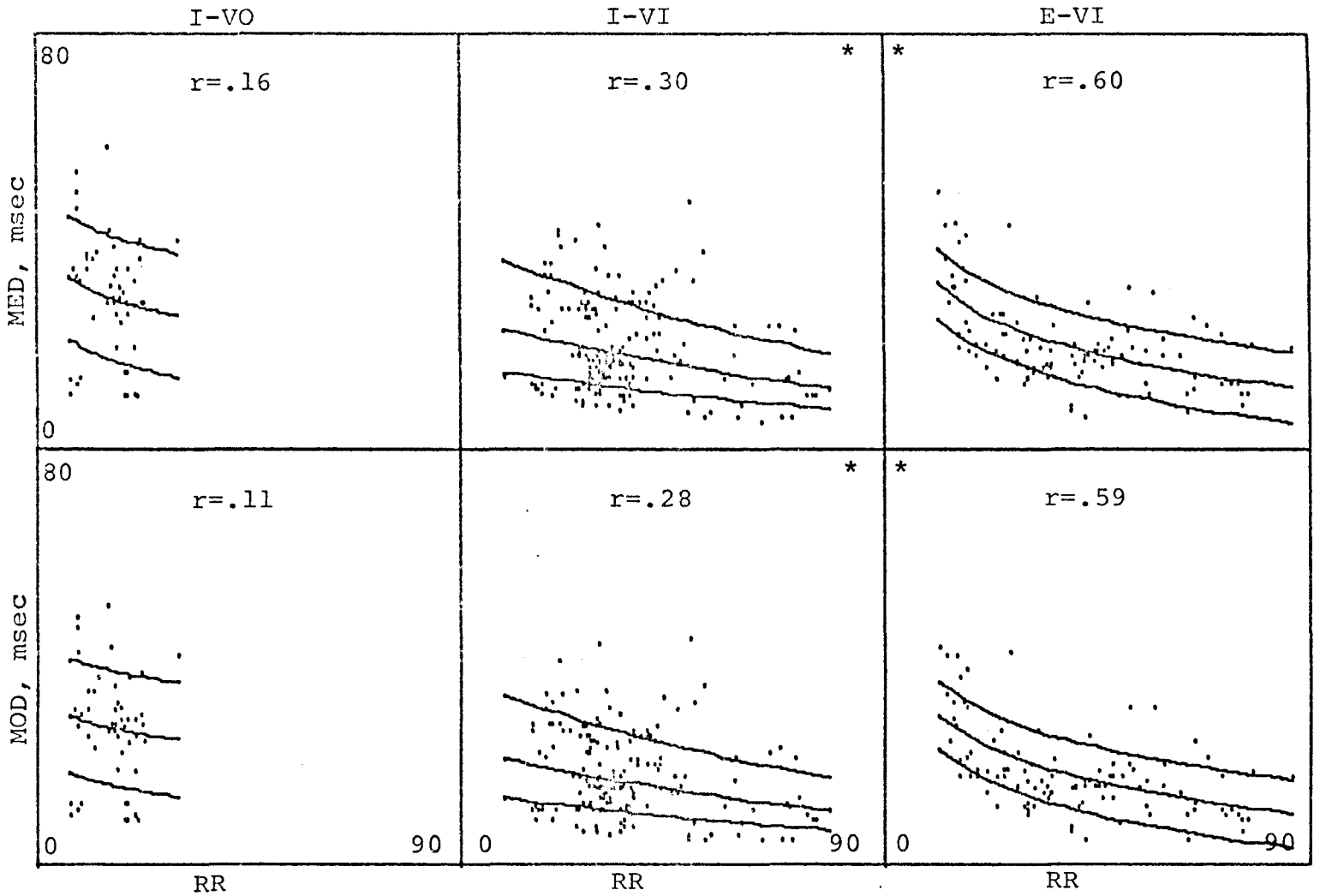

Figure 16. Regression of MED and MOD on RR for I-VO, I-VI and E-VI cells.

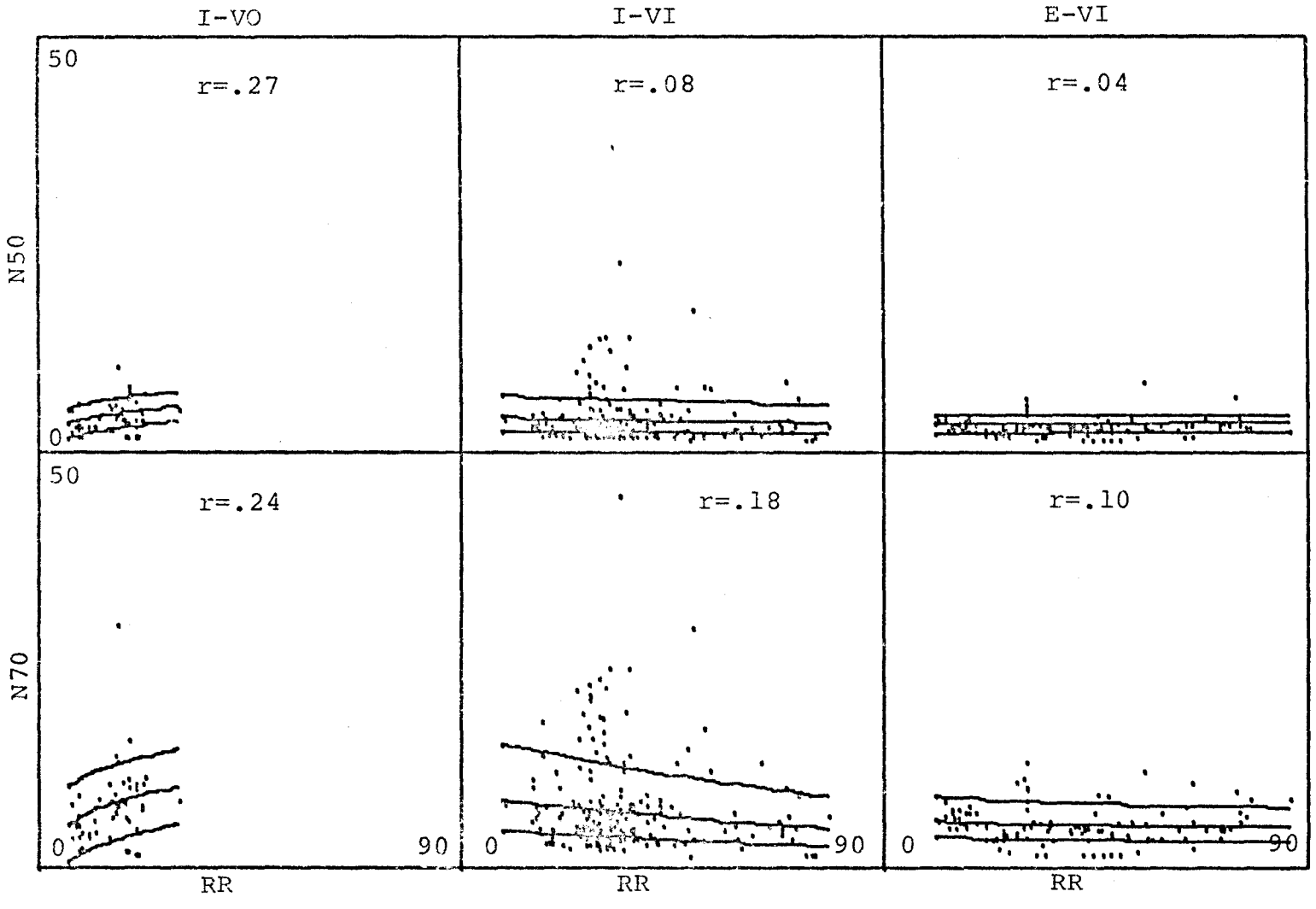

Figure 17. Regression of N50 and N70 on RR for I-VO, I-VI and E-VI cells.

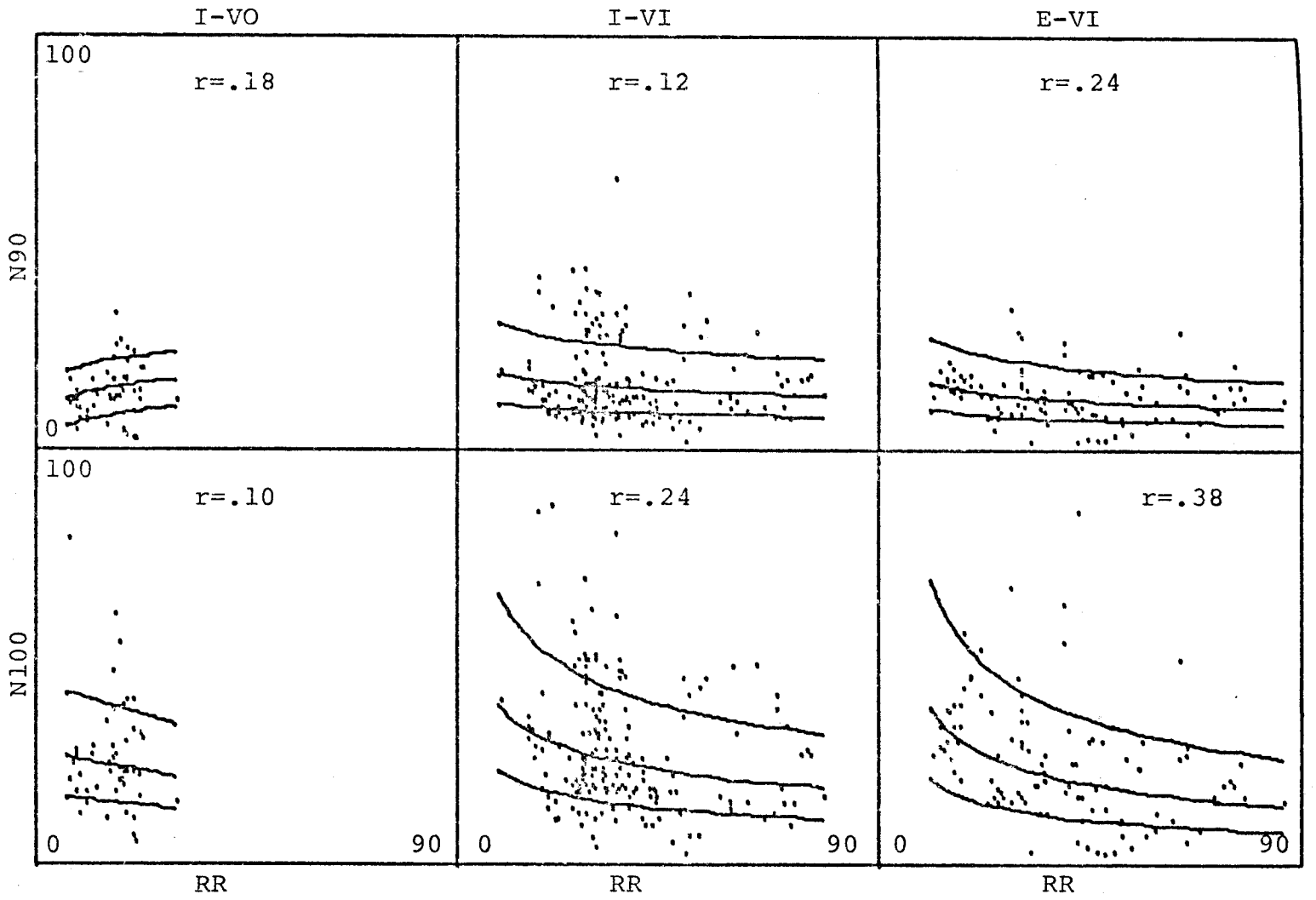

Figure 18. Regression of N90 and N100 on RR for I-VO, I-VI and E-VI cells.

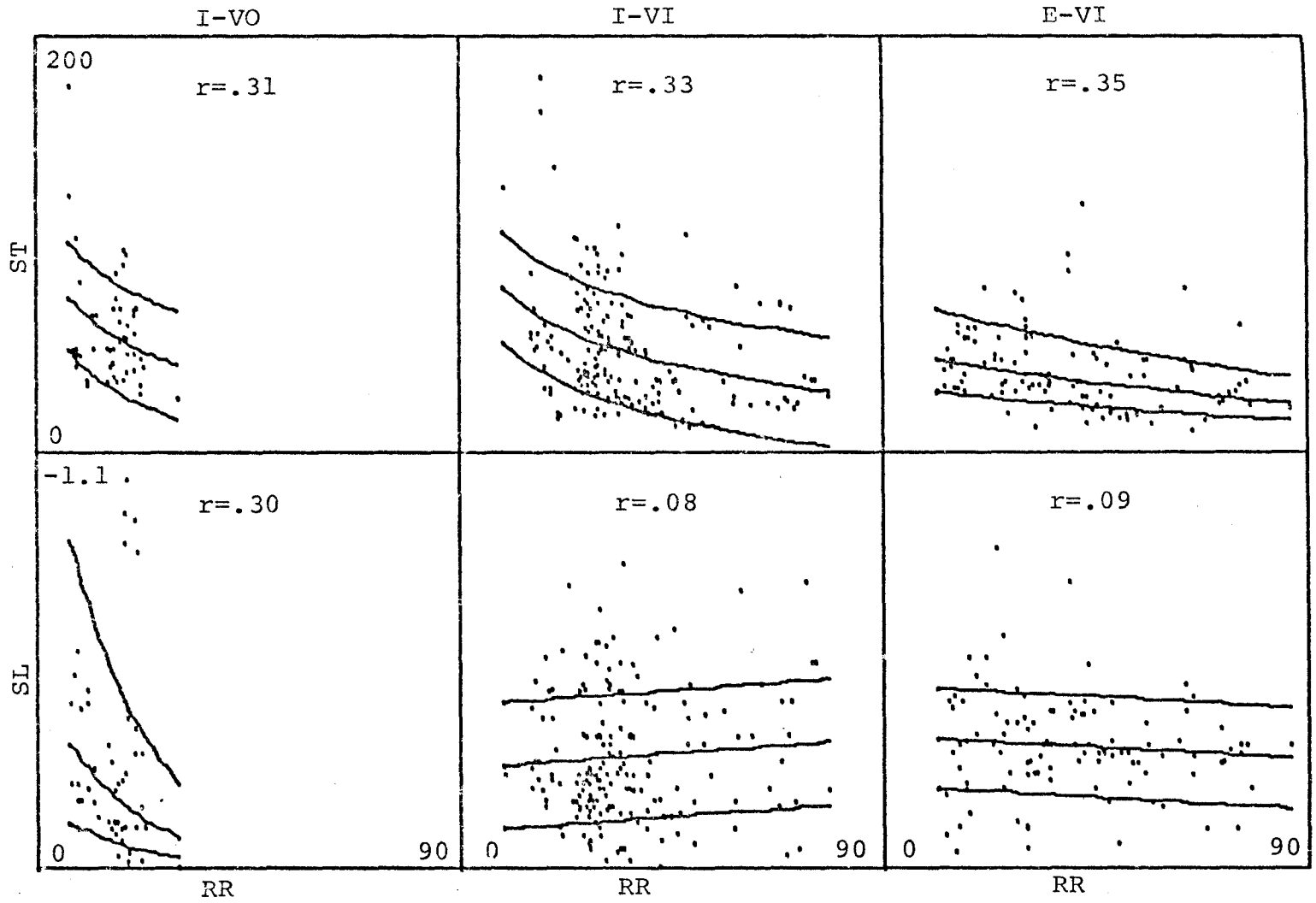

Figure 19. Regression of ST and SL on RR for I-VO, I-VI and E-VI cells.

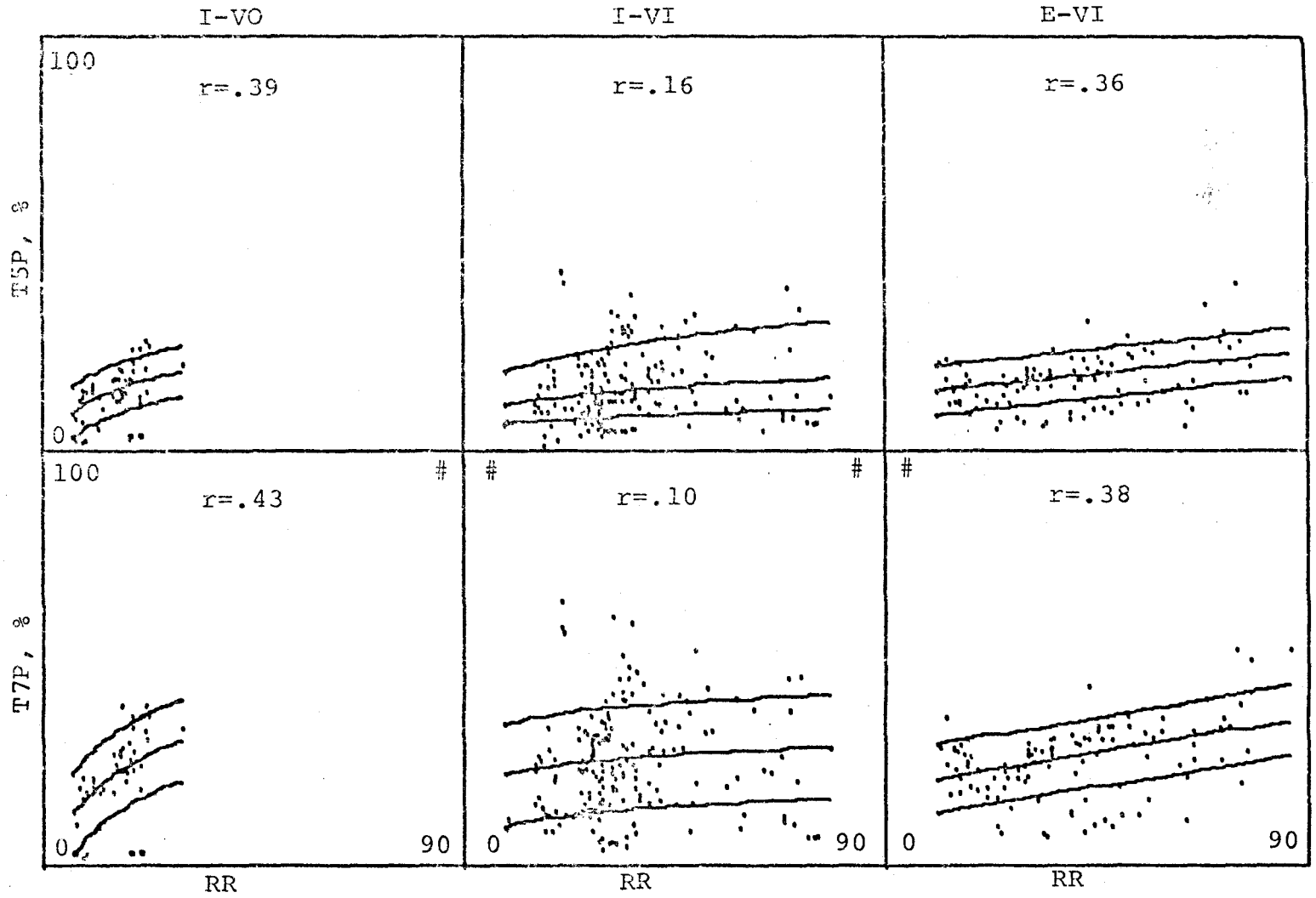

Figure 20. Regression of T5P and T7P on RR for I-VO, I-VI and E-VI cells.

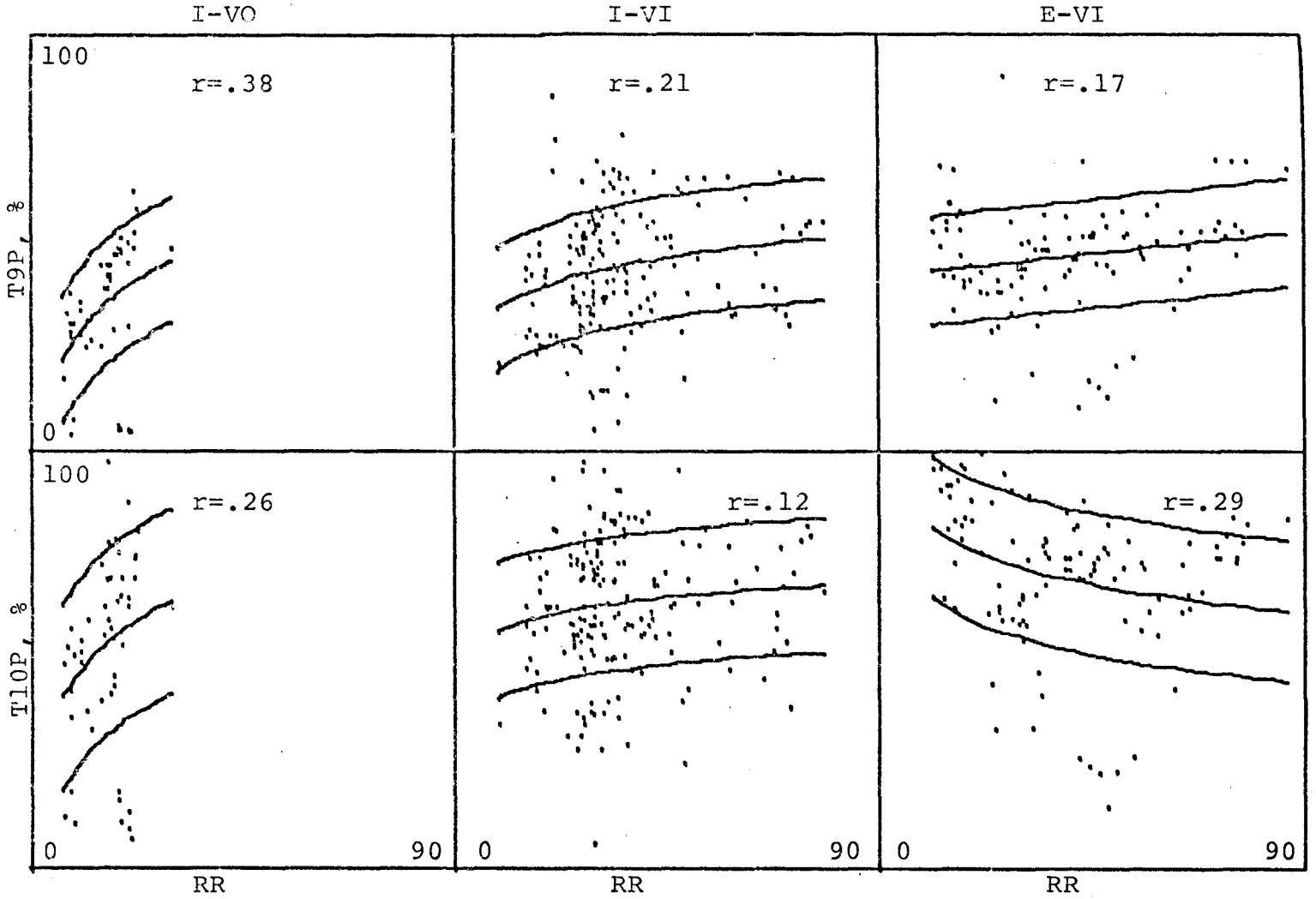

Figure 21. Regression of T9P and T10P on RR for I-VO, I-VI and E-VI cells.

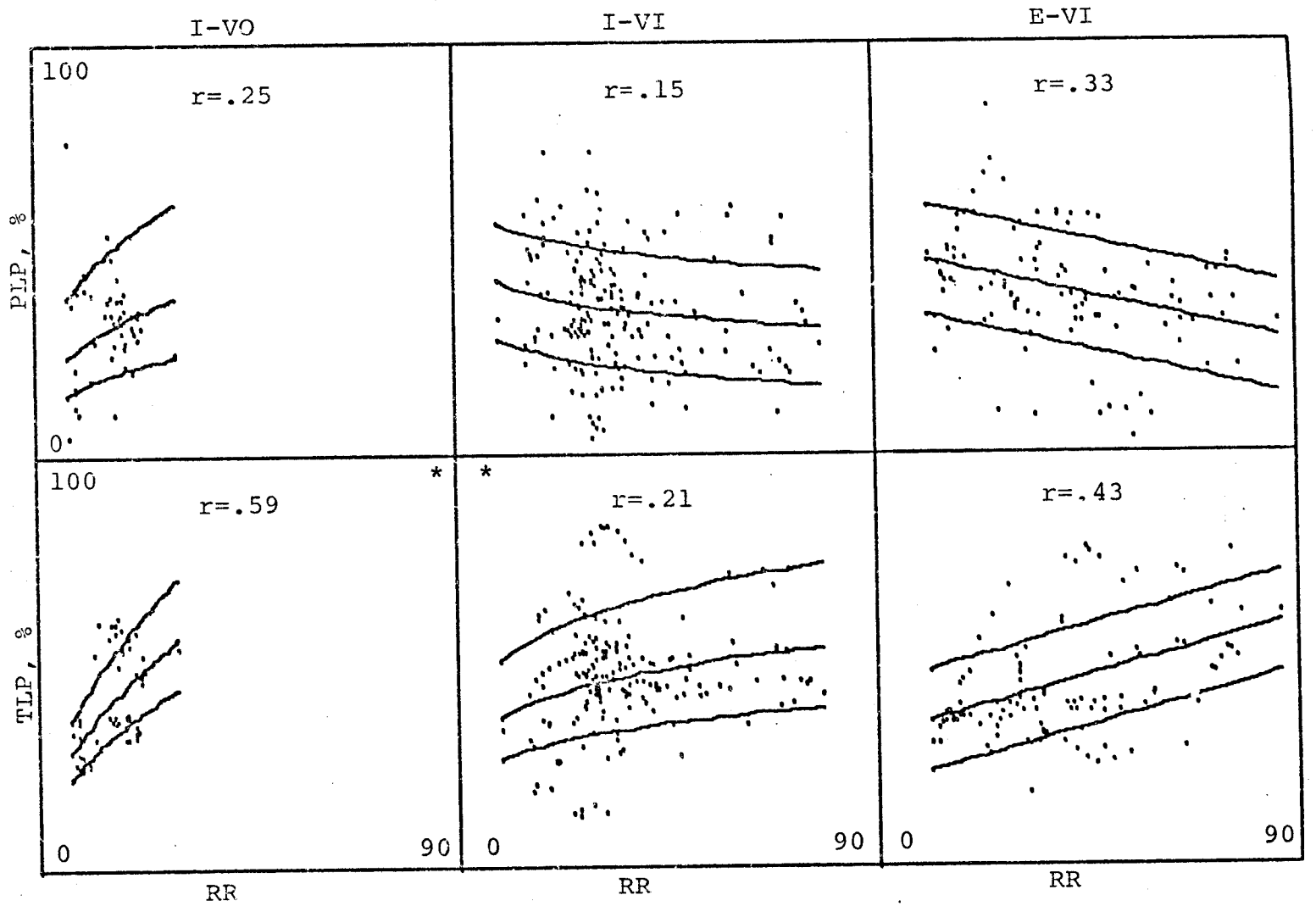

Figure 22. Regression of PLP and TLP on RR for I-VO, I-VI and E-VI cells.

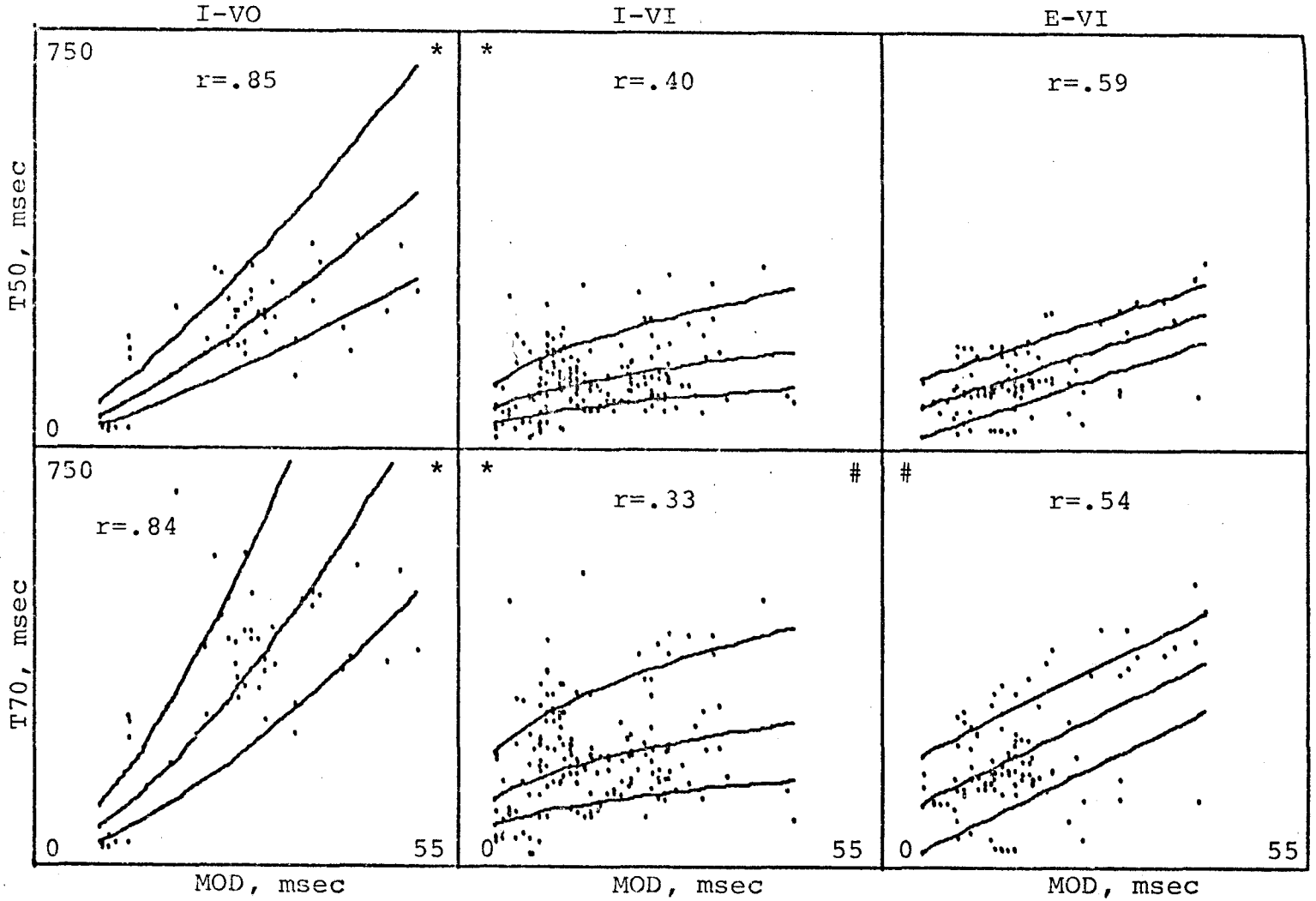

Figure 23. Regression of T50 and T70 on MOD for I-VO, I-VI and E-VI cells.

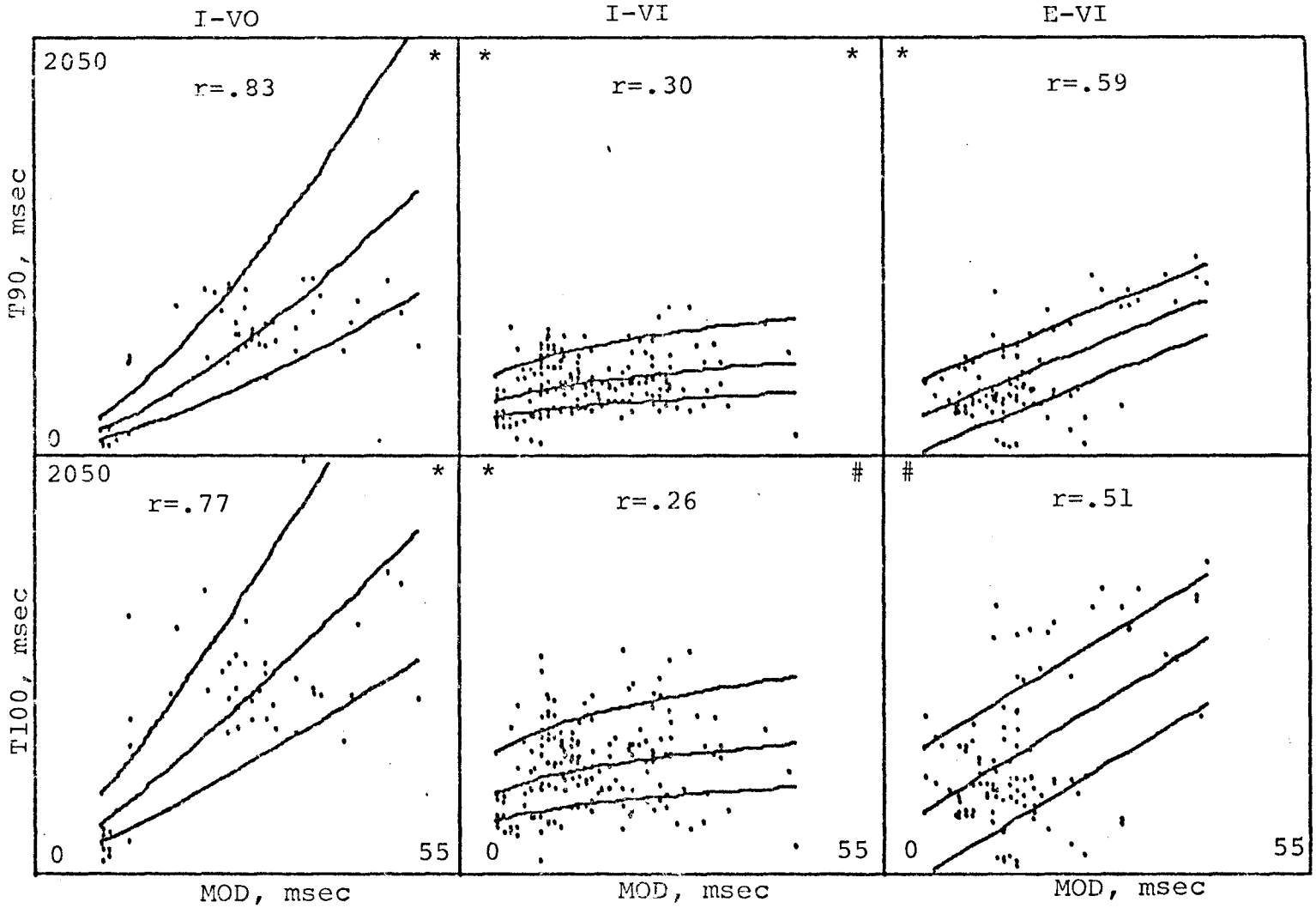

Figure 24. Regression of T90 and T100 on MOD for I-VO, I-VI and E-VI cells.

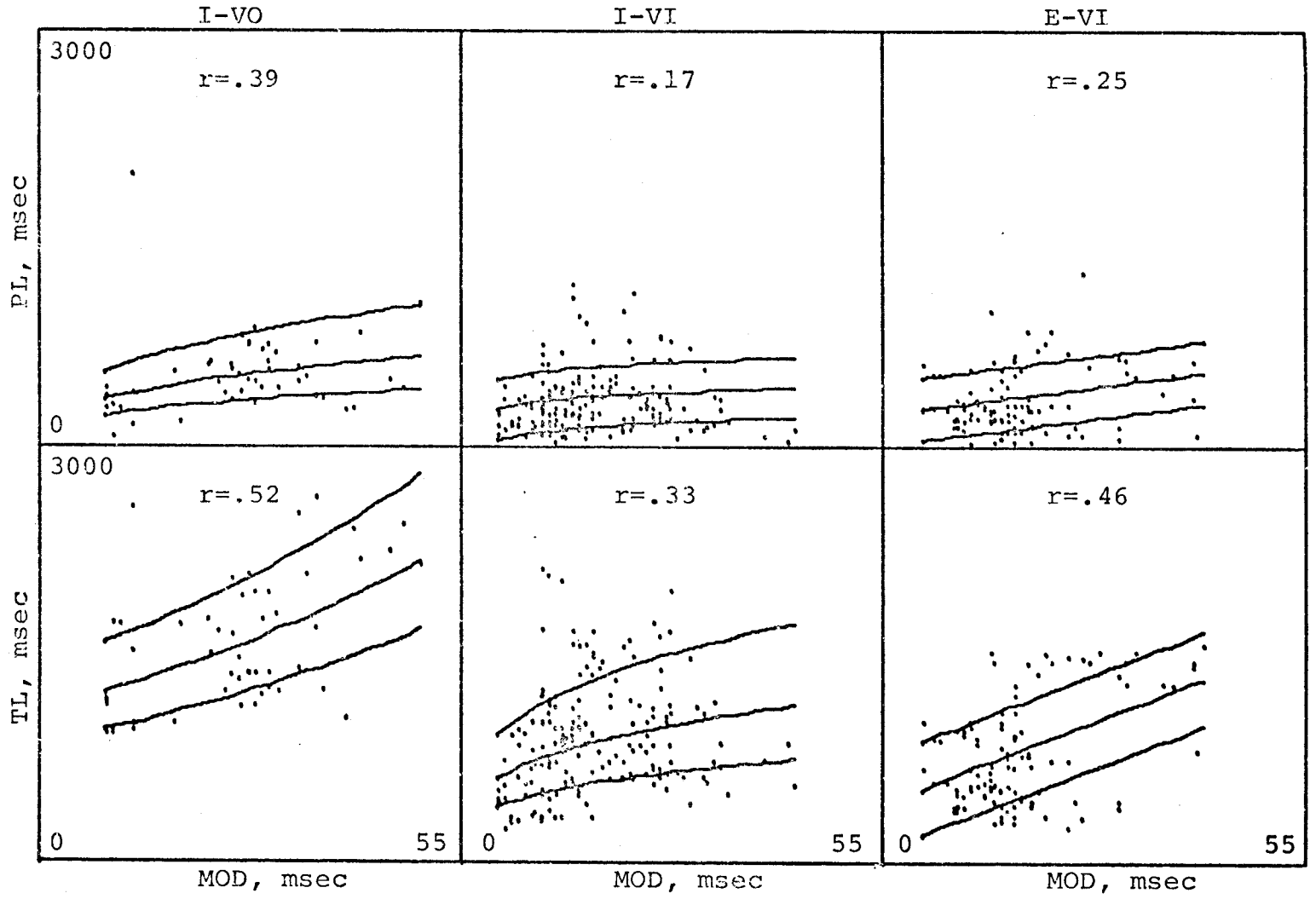

Figure 25. Regression of PL and TL on MOD for I-VO, I-VI and E-VI cells.

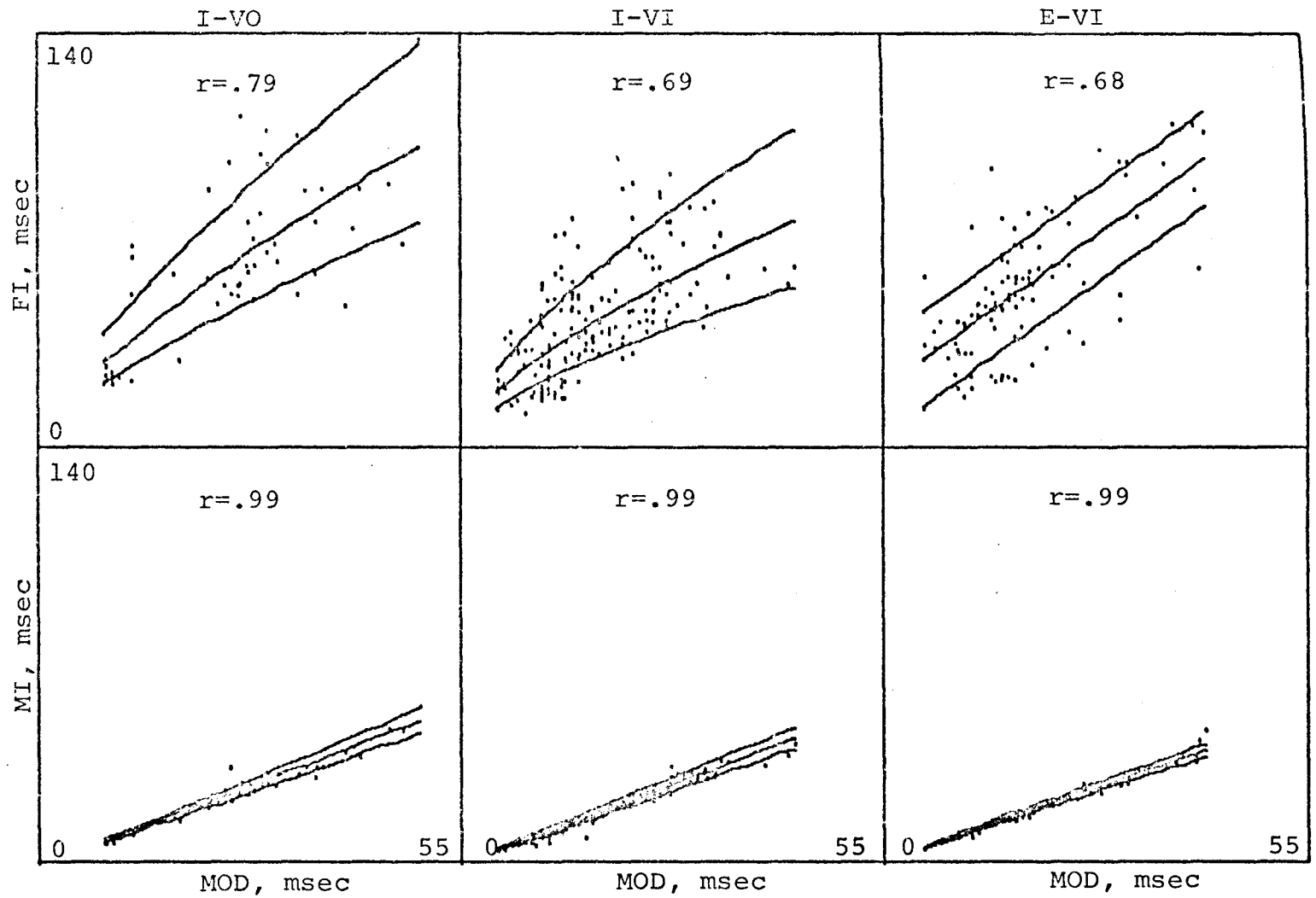

Figure 26. Regression of FI and MI on MOD for I-VO, I-VI and E-VI cells.

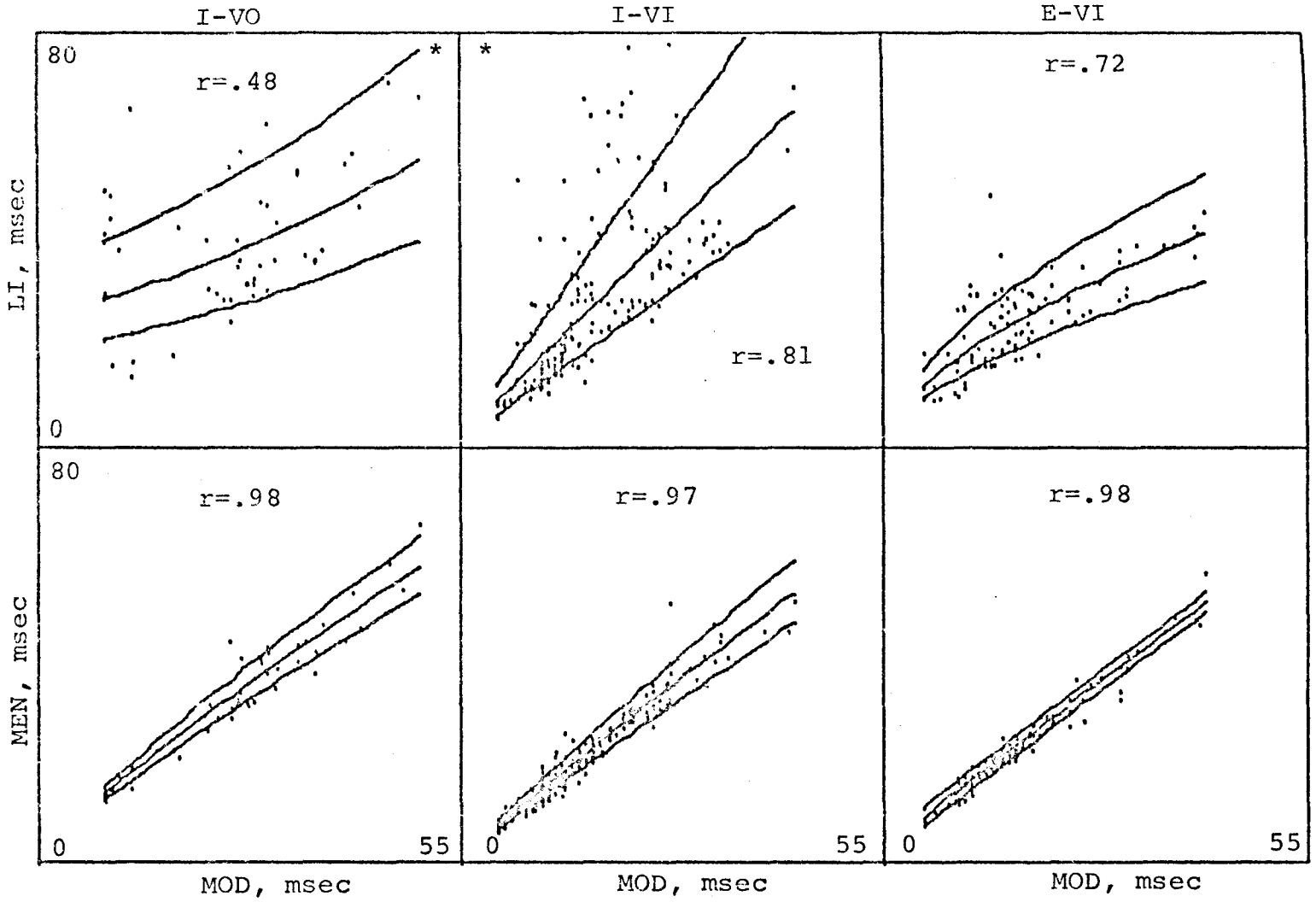

Figure 27. Regression of LI and MEN on MOD for I-VO, I-VI and E-VI cells.

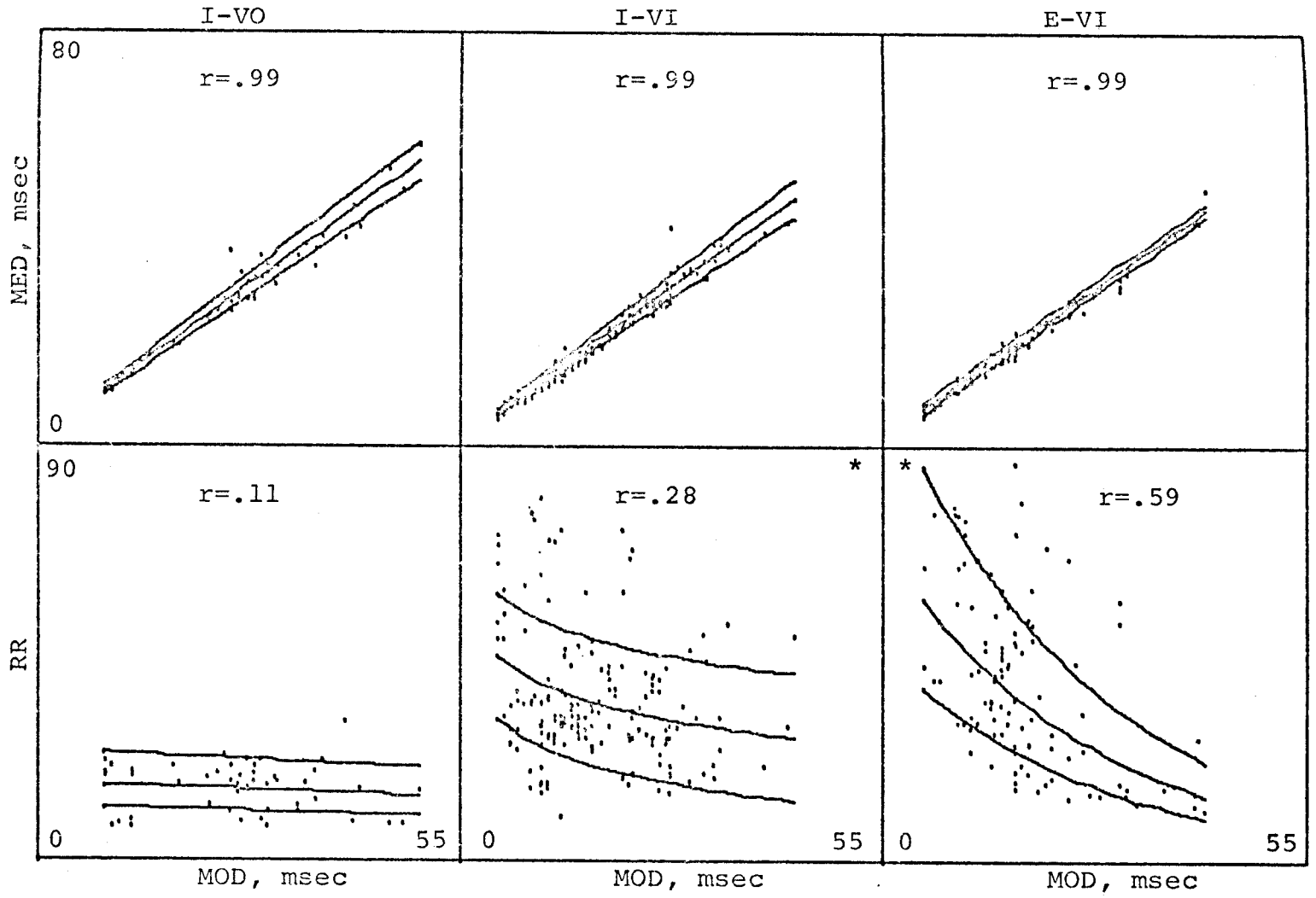

Figure 28. Regression of MED and RR on MOD for I-VO, I-VI and E-VI cells.

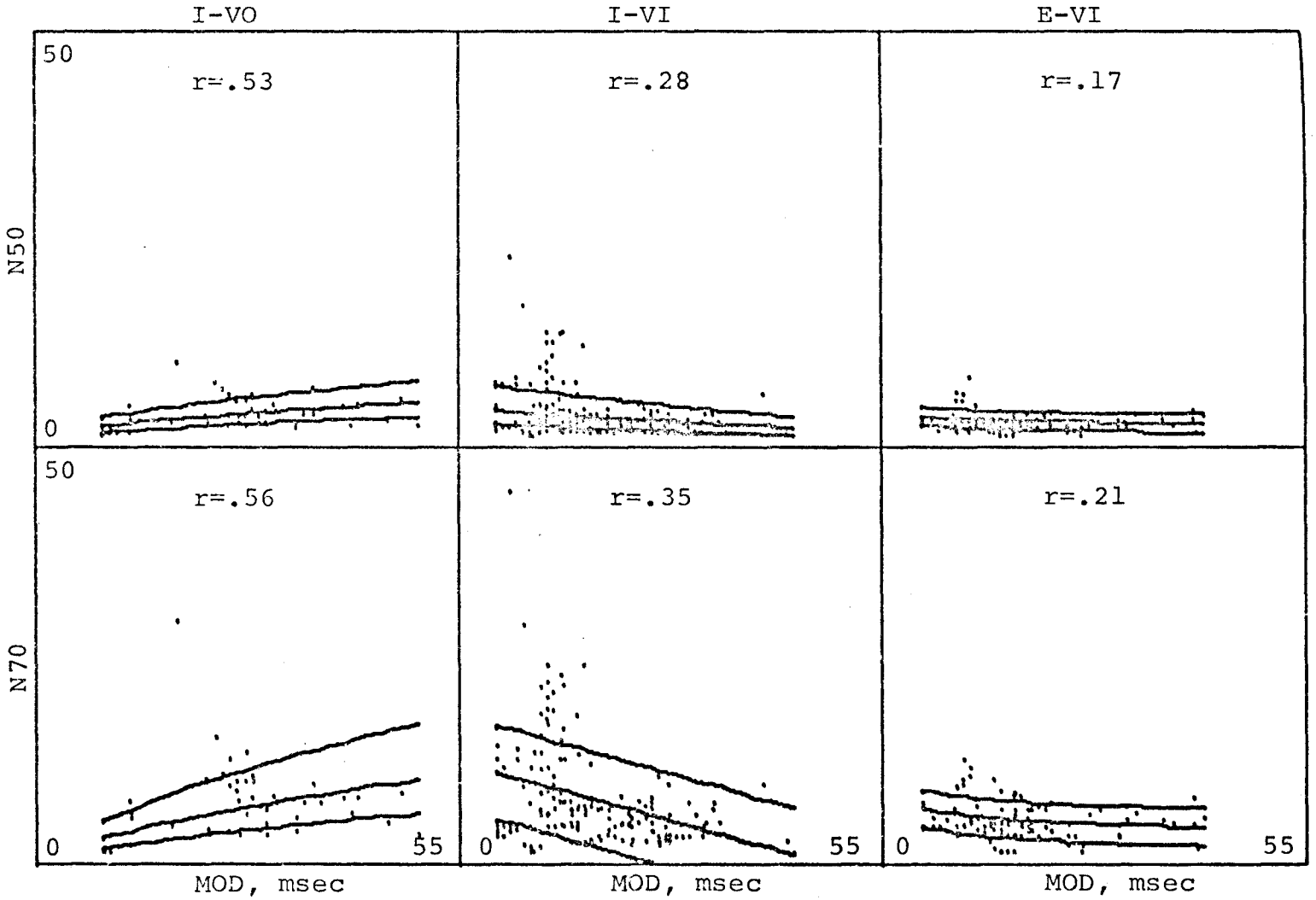

Figure 29. Regression of N50 and N70 on MOD for I-VO, I-VI and E-VI cells.

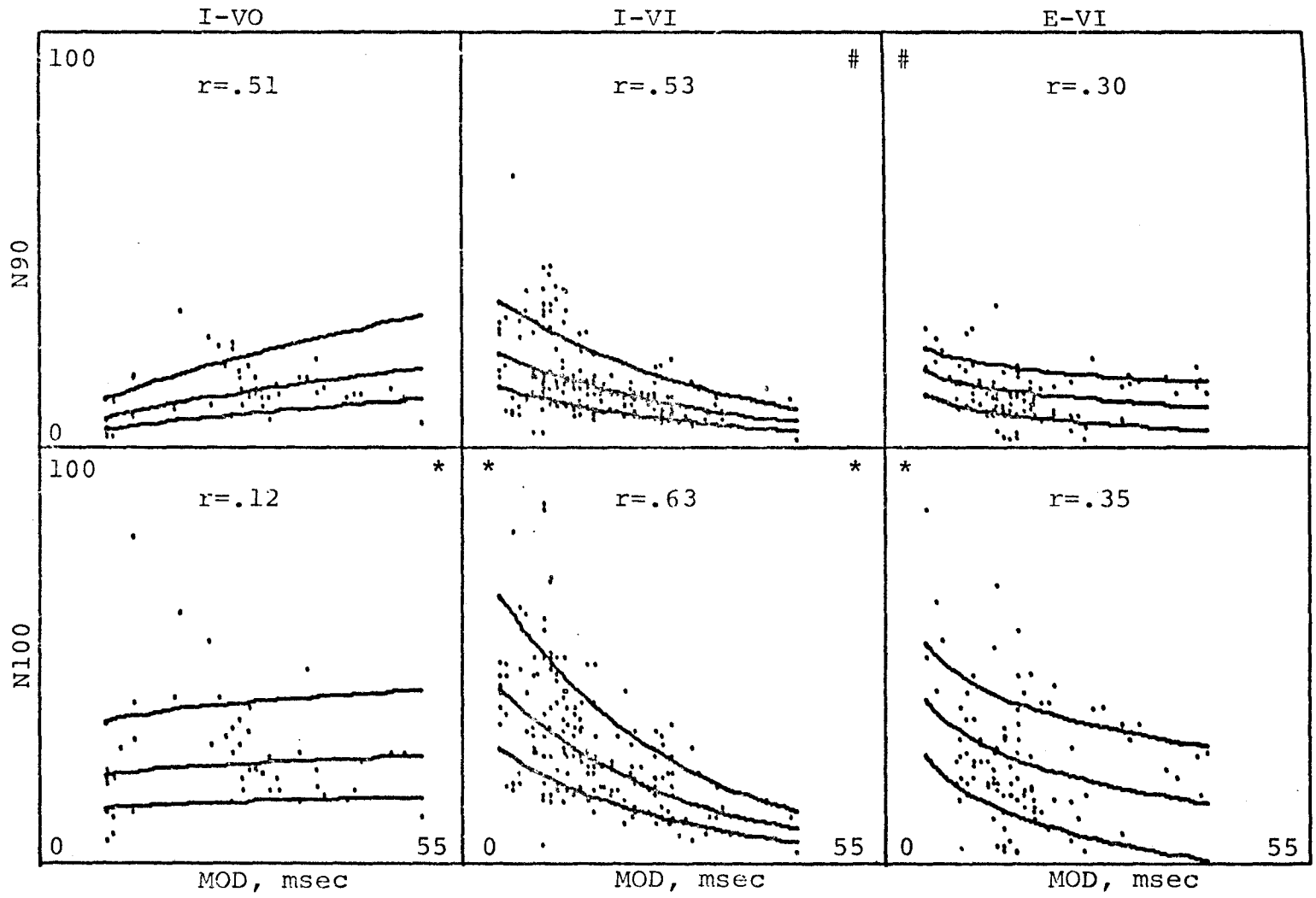

Figure 30. Regression of N90 and N100 on MOD for I-VO, I-VI and E-VI cells.

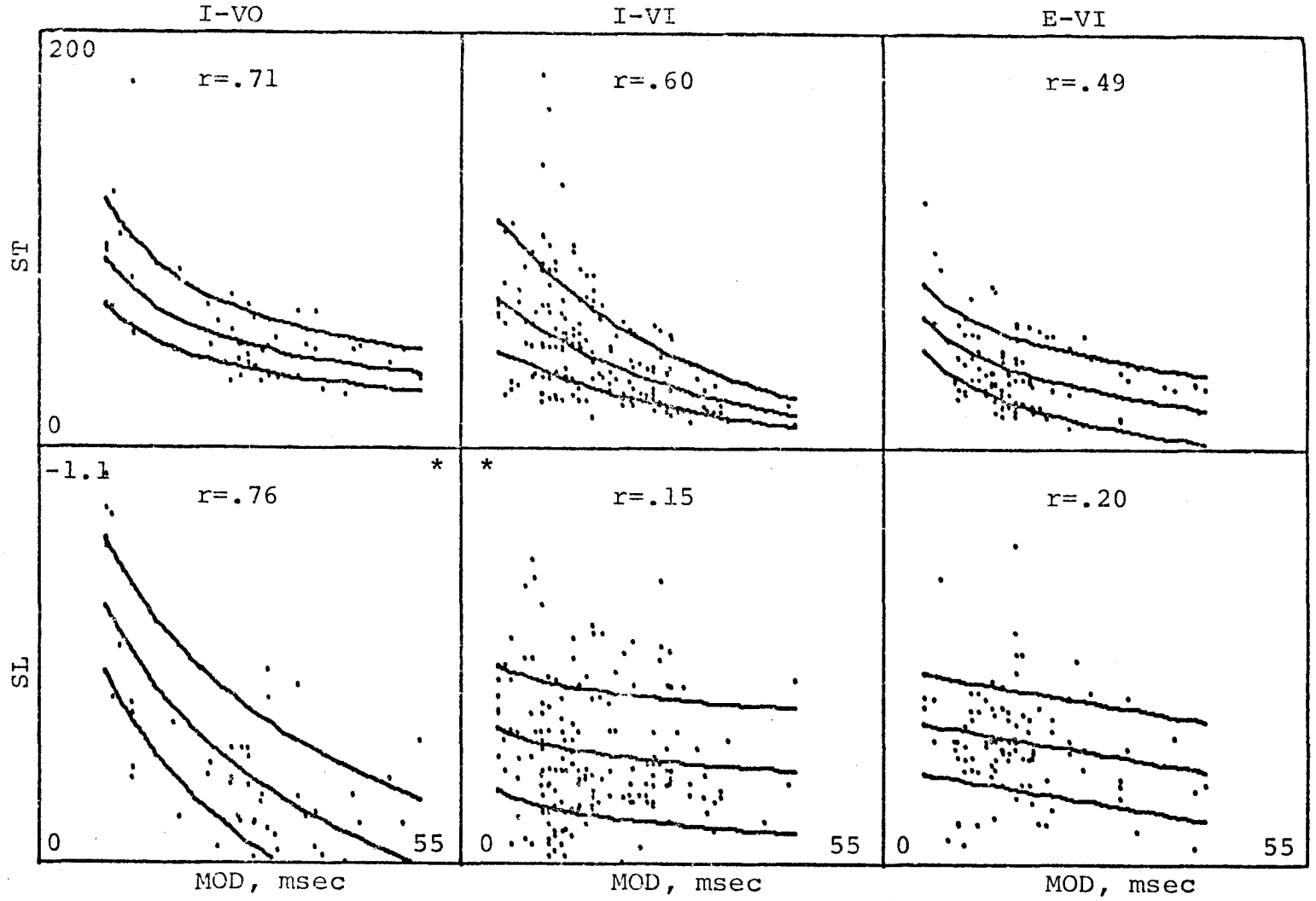

Figure 31. Regression of ST and SL on MOD for I-VO, I-VI and E-VI cells.

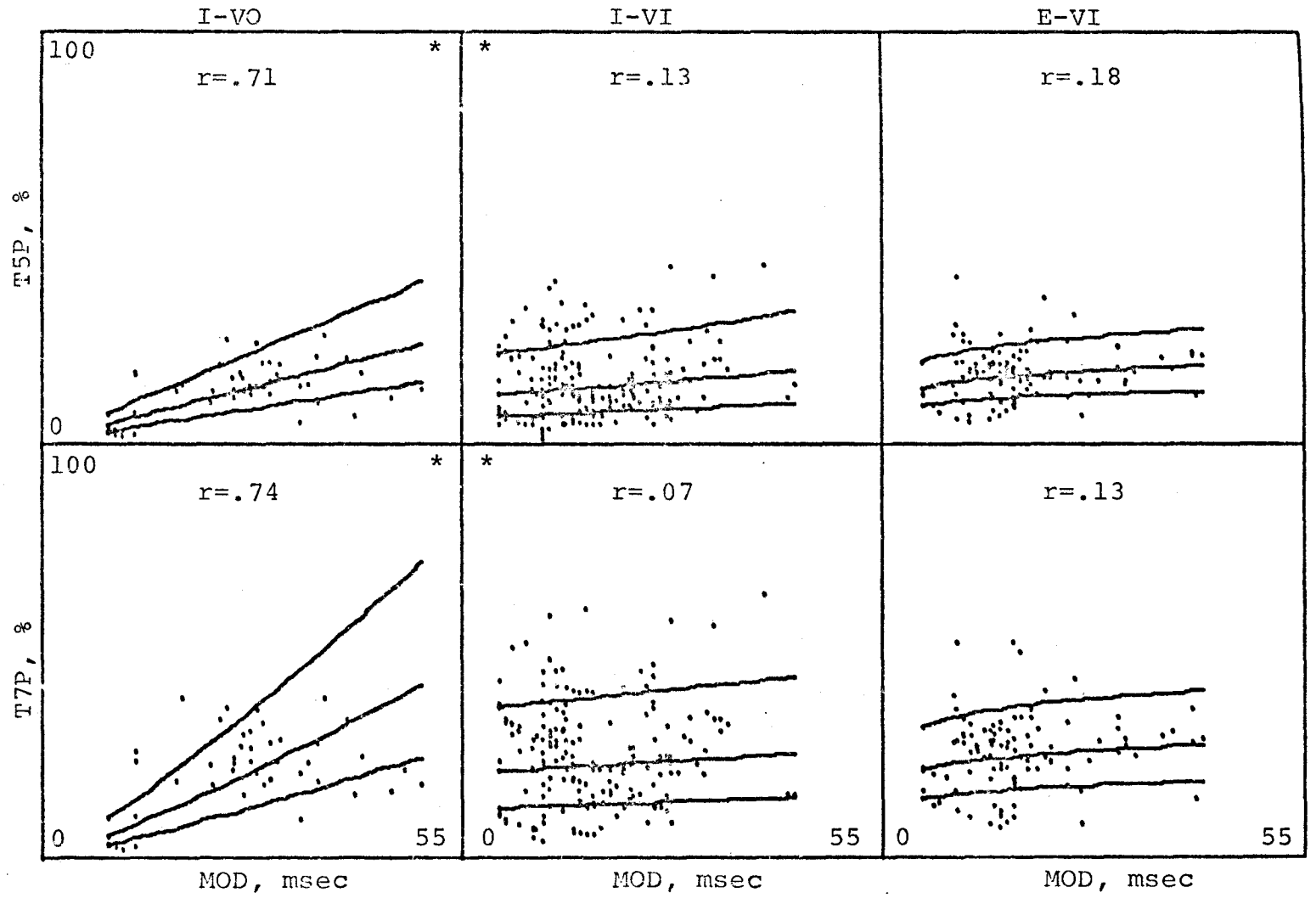

Figure 32. Regression of T5P and T7P on MOD for I-VO, I-VI and E-VI cells.

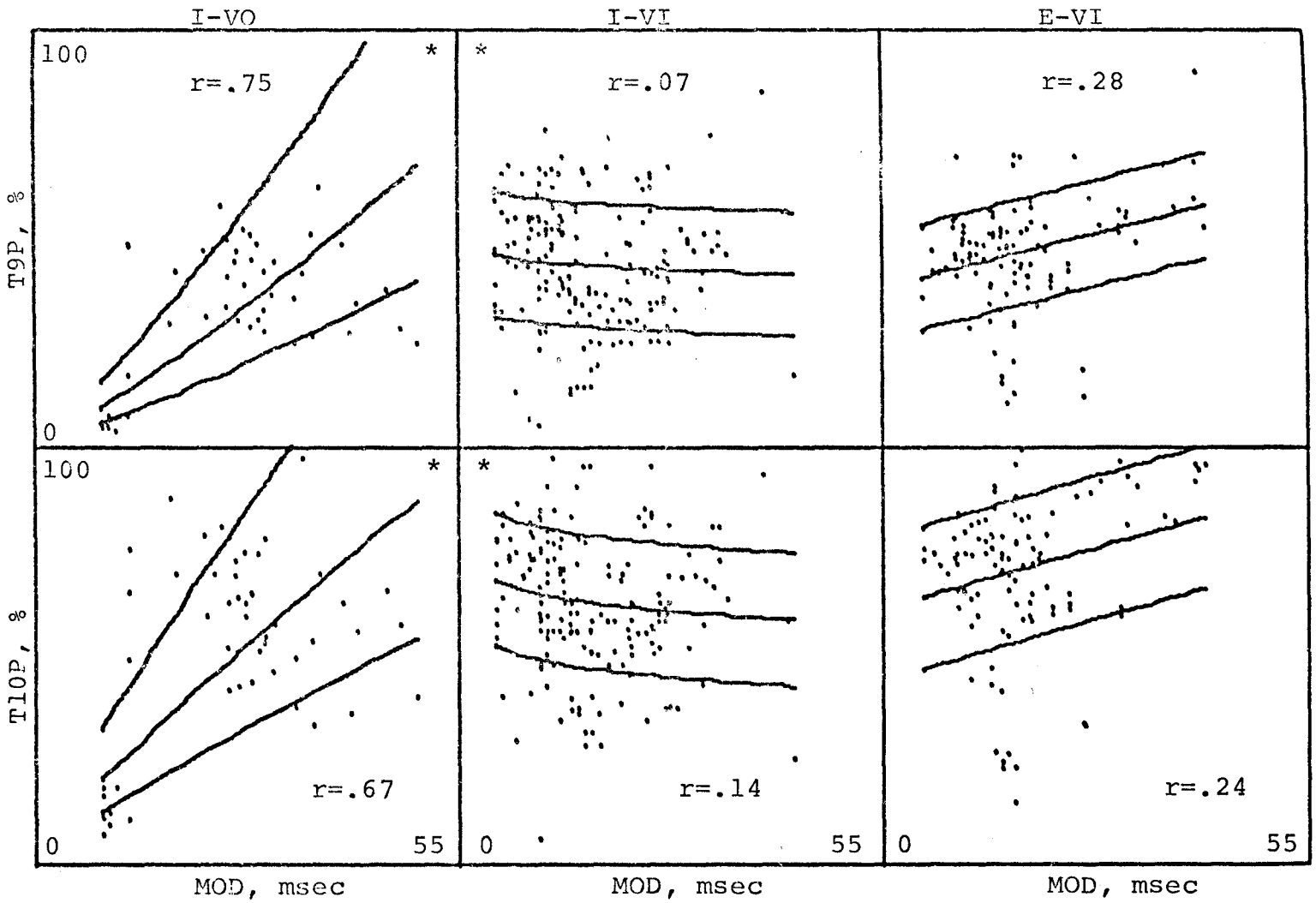

Figure 33. Regression of T9P and T10P on MOD for I-VO, I-VI and E-VI cells.

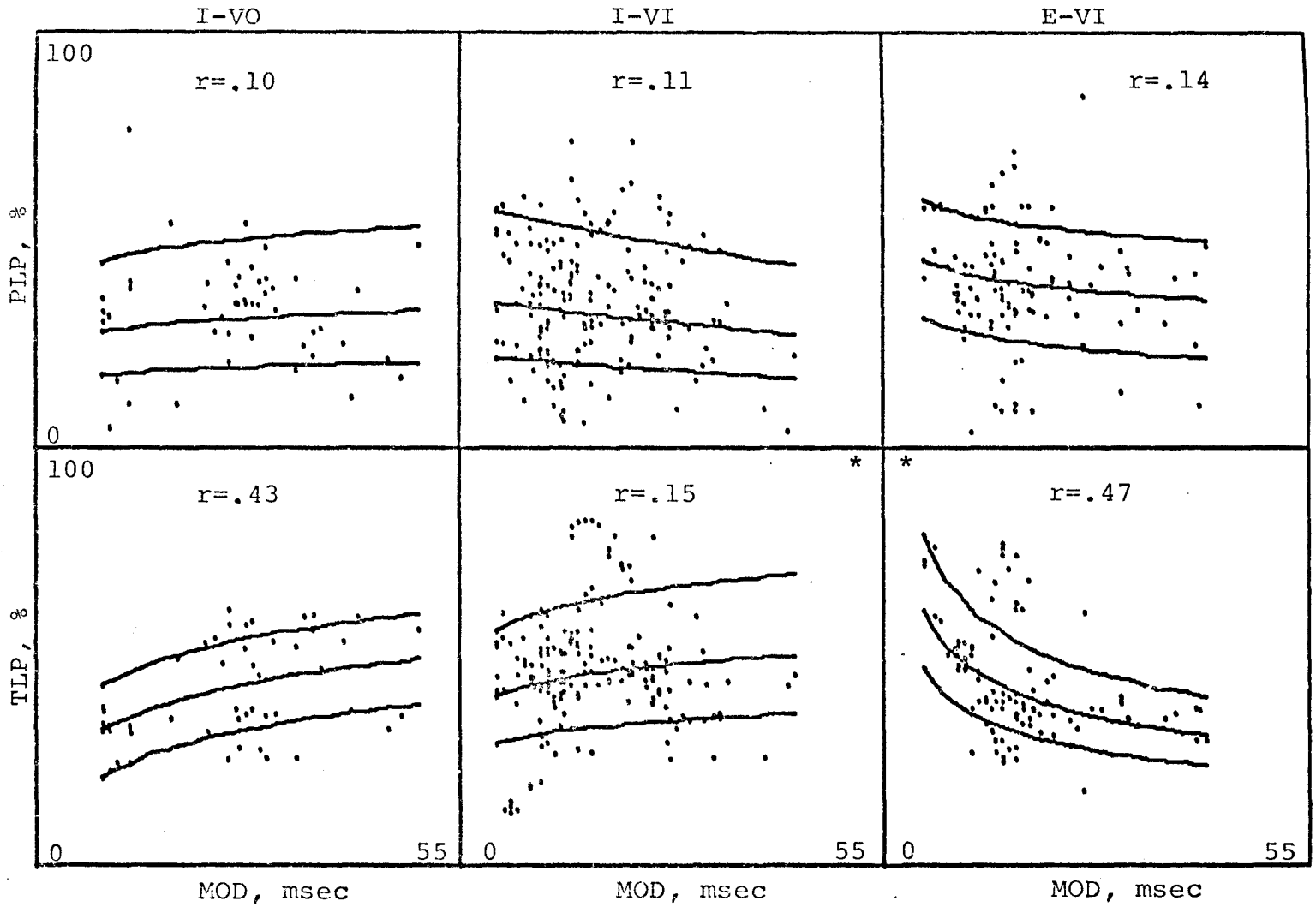

Figure 34. Regression of PLP and TLP on MOD for I-VO, I-VI and E-VI cells.

where applicable. Respiration rate (RR) is understood to be in breaths per minute.

The raw data points for each regression plot are placed in scattergram format. From Table III data, all I-VO plots contain 50 data points from 10 cells, all I-VI plots contain 175 data points from 51 cells and all E-VI plots contain 105 data points from 26 cells. In the regression analysis, each data point was considered as a new observation. No weighting factors were introduced to balance unequal data point contributions from various cells. The three lines drawn in each graph represent the mean regression line and error lines on either side of the mean for the best regression fit. The best fit was defined as that fit (linear, exponential, logarithmic or log-log) possessing the highest correlation coefficient for each set of data. The mean regression and error lines extend from low to high values of the independent variable which includes the entire rate or mode range observed for each case (I-VO, I-VI, E-VI) in this study. All plots are on a linear scale which renders curvilinear fits non-linear. Transformation of curvilinear regressions back to linear coordinates also distorts the symmetry of error lines on either side of the mean regression line. Still, the error lines include

68% of the raw data points or one standard deviation on either side of the mean regression line. The equations for all regression plots in Figures 11-34 are listed in the Appendix (Tables VIII-XIII). These equations can be used for accurate interpolation of dependent variables from independent variables. The type of fit (linear, exponential, logarithmic or log-log) used to correlate X and Y data for each regression plot are also listed in the Appendix (Table XIV).

Correlation coefficients or "r" values ranged from 0.04 to 0.99 and are given for each regression plot. Steep slopes and/or narrow error bands are associated with large "r" values and good fits. Flat slopes and/or wide error bands are associated with low "r" values and poor fits. The significant difference between "r" values of adjacent horizontal panels is designated by a number sign (#) for $P<0.05$ or an asterisk (*) for $P<0.01$. Blank panels indicate that the correlation coefficients between I-VO and I-VI or I-VI and E-VI plots are not significantly different at the 0.05 level.

In Figure 11, T50 is plotted as a function of RR. For I-VI and E-VI populations, T50 decreases as rates increase from 9.9 to 78.7 and 11.5 to 86.6 breaths per minute respectively. This indicates that at higher

breathing frequencies it takes less time on the average for inspiratory and expiratory trains to reach interspike intervals which are one half the difference between the first interval (FI) and minimum interval (MI). Comparison of I-VI and E-VI plots indicates that expiratory T50's are slightly longer in time than inspiratory T50's for equivalent respiratory rates. The expiratory regression has less scatter and a slightly greater slope as indicated by the significantly higher "r" value at the 0.05 level. For the I-VO population, respiration rate ranges from 7.9 to 30.9 breaths per minute. This decrease in rate response to drug stimulation or depression after vagotomy implicates the vagus in control of respiratory rate. For the T50 parameter, vagotomy significantly decreases the "r" value at the 0.05 level. That is, the correlation between T50 and RR is lost by cutting both vagus nerves (low slope, wide scatter). A similar analysis can be done by the reader for the remaining respiration rate regressions in Figures 11-22.

In Figure 23, T50 is plotted as a function of MOD. Mode ranges are approximately the same for I-VO, I-VI and E-VI populations and extend from 9.2 to 50.0, 5.2 to 43.6 and 5.2 to 42.0 milliseconds respectively. The plots show that T50 is directly related to the mode for

all populations. That is, as the mode decreases (increasing depth or tidal volume) it takes less time for respiratory trains to be activated. The inspiratory and expiratory populations are approximately the same and do not have significantly different "r" values at the 0.05 level. The relationship of T50 versus MOD is by far the best in the I-VO panel (highest "r" value) indicating that vagotomy significantly increases the correlation between T50 and MOD for inspiratory cells at the 0.01 level. Similar comparisons can be made by the reader for the remaining regressions in Figures 23-34.

Correlation coefficients ("r") are placed in rank order for the regression of I-VO, I-VI and E-VI cell discharge parameters on respiration rate and mode in Tables V and VI respectively. Correlations of inspiratory (I-VI) and expiratory (E-VI) parameters as a function of respiratory rate in Table V appear to parallel each other in rank order while vagotomy (I-VO) tends to invert the ordering for inspiratory (I-VI) cells. These same general relationships tend to hold for parameters plotted as a function of the mode in Table VI, but the I-VI - E-VI pairings and the I-VI - I-VO reciprocity are not as well defined. Comparison of respiration rate (Table V) and mode (Table VI) rankings for similar cell types reveals poor order

Table V. Rank ordering of correlation coefficients for the regression of 24 parameters on respiratory rate for I-VO, I-VI and E-VI cell types.

Rank Order	I-VO Parameter	"r"	I-VI Parameter	"r"	E-VI Parameter	"r"
1	TL	.62	TL	.69	TL	.84
2	TLP	.59	T100	.68	T100	.79
3	T7P	.43	T90	.57	FI	.73
4	T5P	.39	T70	.55	T90	.72
5	T9P	.38	PL	.53	PL	.71
6	LI	.34	T50	.44	T70	.65
7	ST	.31	FI	.44	T50	.64
8	PL	.31	ST	.33	MEN	.62
9	SL	.30	MEN	.31	MED	.60
10	FI	.30	MED	.30	MOD	.59
11	N50	.27	MOD	.28	MI	.59
12	T10P	.26	MI	.27	LI	.44
13	PLP	.25	N100	.24	TLP	.43
14	N70	.24	T9P	.21	T7P	.38
15	MEN	.21	TLP	.21	N100	.38
16	N90	.18	LI	.20	T5P	.36
17	MED	.16	N70	.18	ST	.35
18	MI	.15	T5P	.16	PLP	.33
19	T70	.13	PLP	.15	T10P	.29
20	T100	.13	T10P	.12	N90	.24
21	MOD	.11	N90	.12	T9P	.17
22	N100	.10	T7P	.10	N70	.10
23	T50	.08	N50	.08	SL	.09
24	T90	.06	SL	.08	N50	.04

Table VI. Rank ordering of correlation coefficients for the regression of 24 parameters on mode for I-VO, I-VI and E-VI cell types.

Rank Order	I-VO Parameter	"r"	I-VI Parameter	"r"	E-VI Parameter	"r"
1	MED	.99	MED	.99	MED	.99
2	MI	.99	MI	.99	MI	.99
3	MEN	.98	MEN	.97	MEN	.98
4	T50	.85	LI	.81	LI	.72
5	T70	.84	FI	.69	FI	.68
6	T90	.83	N100	.63	RR	.59
7	FI	.79	ST	.60	T90	.59
8	T100	.77	N90	.53	T50	.59
9	SL	.76	T50	.40	T70	.54
10	T9P	.75	N70	.35	T100	.51
11	T7P	.74	TL	.33	ST	.49
12	T5P	.71	T70	.33	TLP	.47
13	ST	.71	T90	.30	TL	.46
14	T10P	.67	RR	.28	N100	.35
15	N70	.56	N50	.28	N90	.30
16	N50	.53	T100	.26	T9P	.28
17	TL	.52	PL	.17	PL	.25
18	N90	.51	SL	.15	T10P	.24
19	LI	.48	TLP	.15	N70	.21
20	TLP	.43	T10P	.14	SL	.20
21	PL	.39	T5P	.13	T5P	.18
22	N100	.12	PLP	.11	N50	.17
23	RR	.11	T9P	.07	PLP	.14
24	PLP	.10	T7P	.07	T7P	.13

correlations which may even approach randomization. The reader can use Tables V and VI as references relating to those parameters which are correlated best with either respiration rate (RR) or mode (MOD) for each cell type studied (I-VO, I-VI, E-VI).

The numerous regression plots presented in Figures 11-34 are condensed in Figures 35-43 for reader convenience. In these latter plots, cells are still separated into I-VO, I-VI and E-VI types, but different parameters are superimposed in individual plots. Only the mean regression lines are plotted to avoid confusion from overlapping error lines and raw data points. In each figure, the same parameters are plotted both as a function of respiration rate (RR) and mode (MOD) for easy comparison. The respiration rate (RR) and mode (MOD) scalings are identical to those used in Figures 11-34 and the data ranges are the same. The dependent variable scalings are equivalent for both rate and mode plots for any one figure and correspond to values selected in Figures 11-34 with a few appropriate exceptions. Each axis is labeled with time or percent scales where applicable. Respiration rate (RR) is given in breaths per minute.

In Figure 35, T50, T70, T90 and T100 are plotted

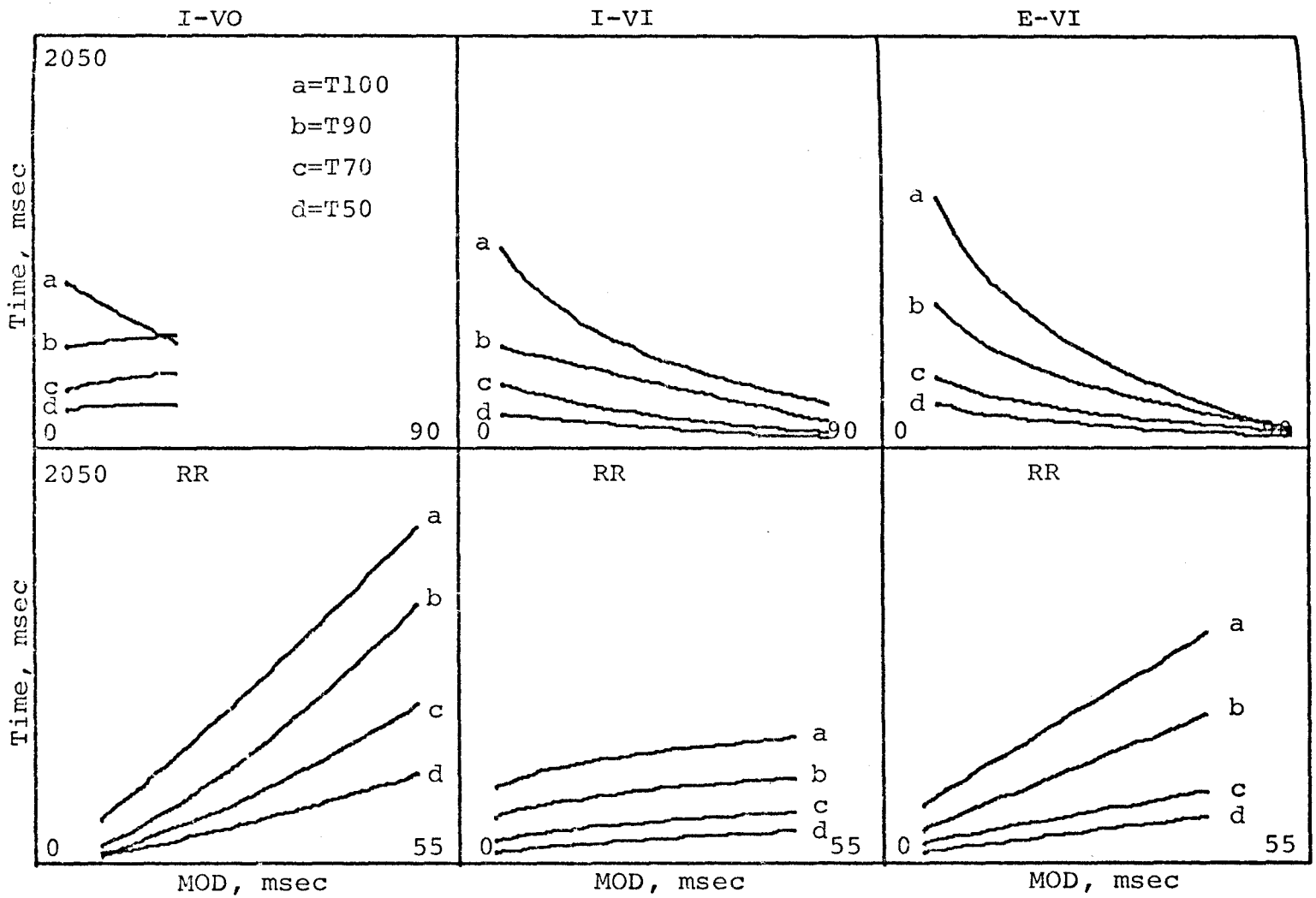

Figure 35. Regression of T100, T90, T70 and T50 on RR and MOD for I-VO, I-VI and E-VI cells.

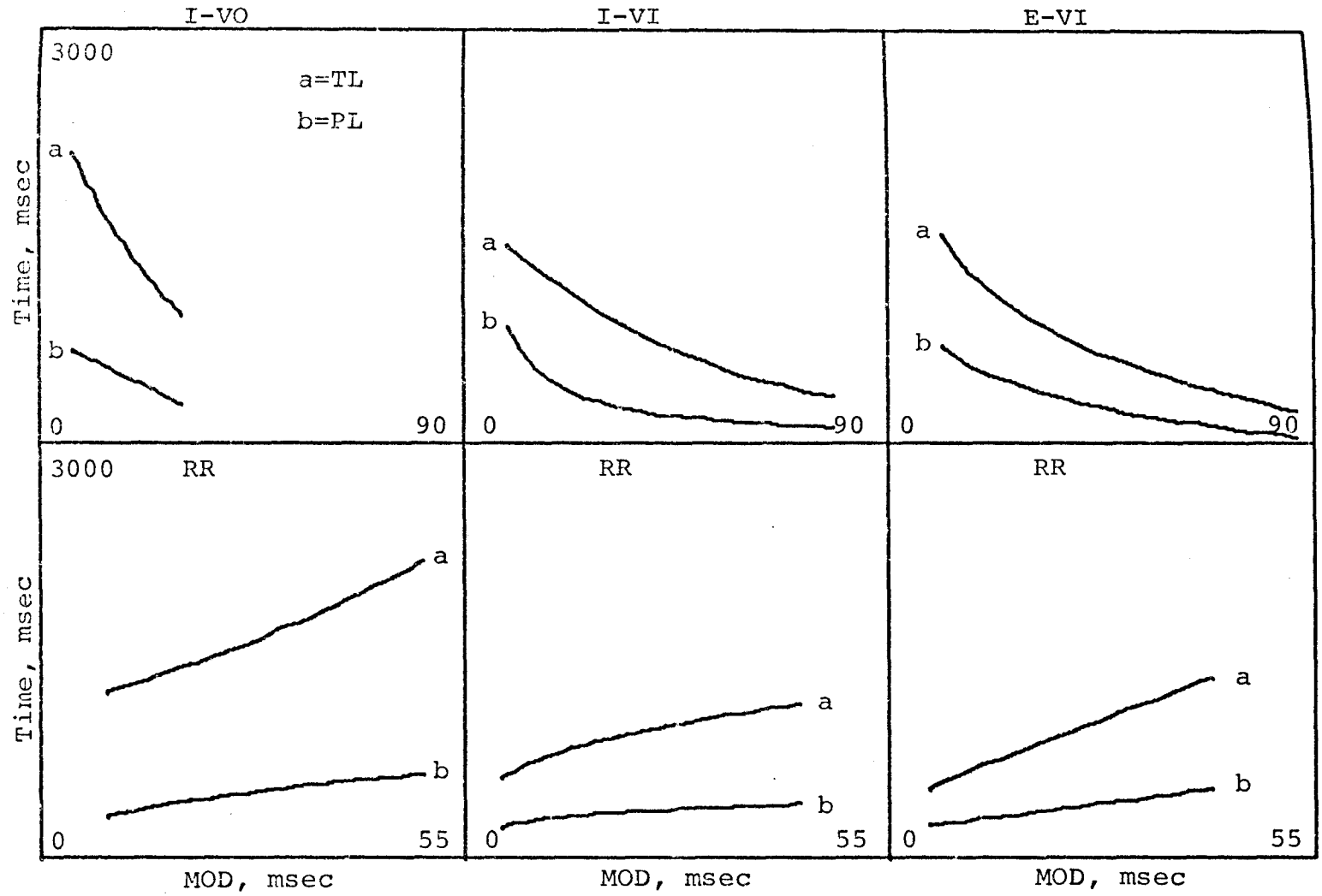

Figure 36. Regression of TL and PL on RR and MOD for I-VO, I-VI and E-VI cells.

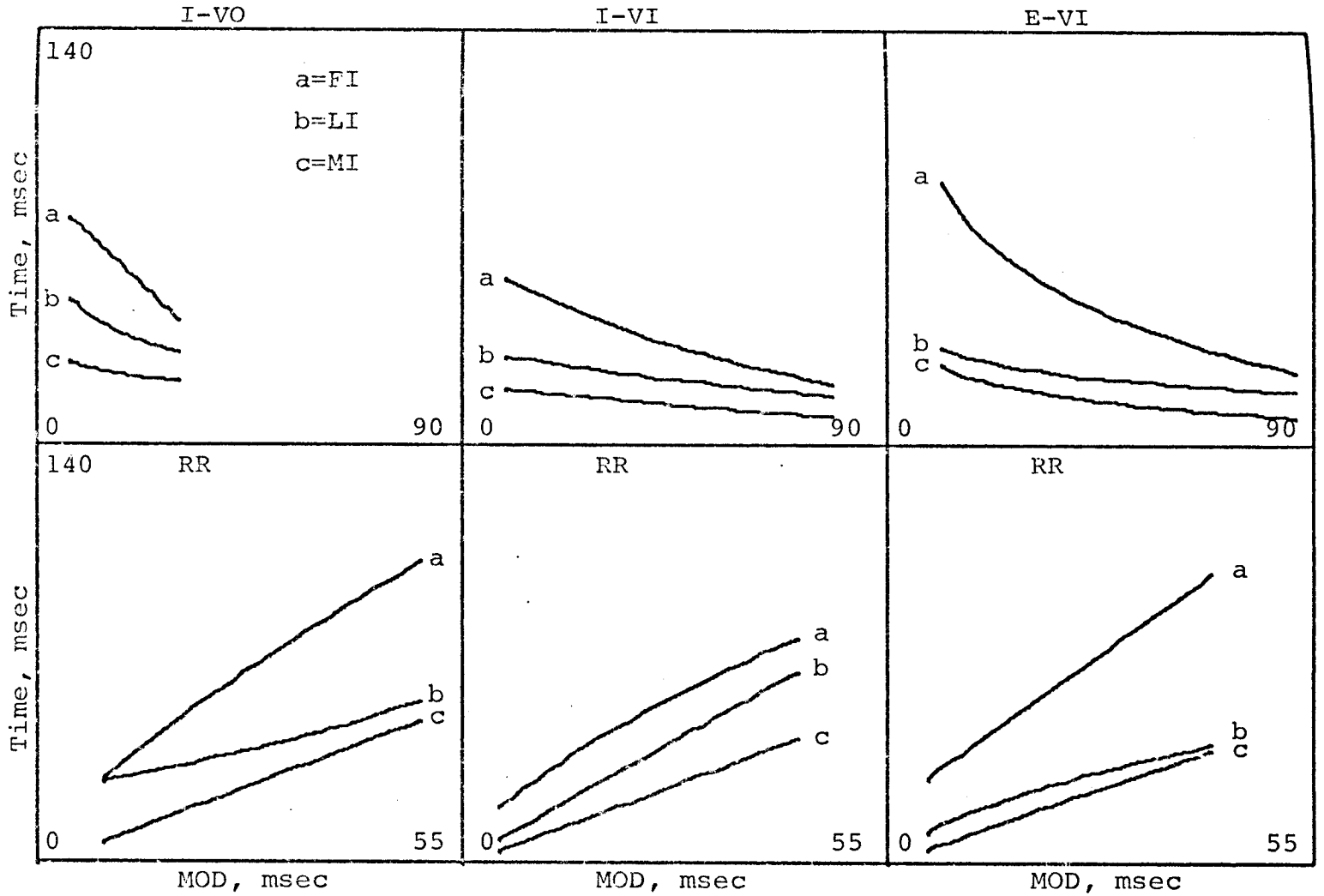

Figure 37. Regression of FI, LI and MI on RR and MOD for I-VO, I-VI and E-VI cells.

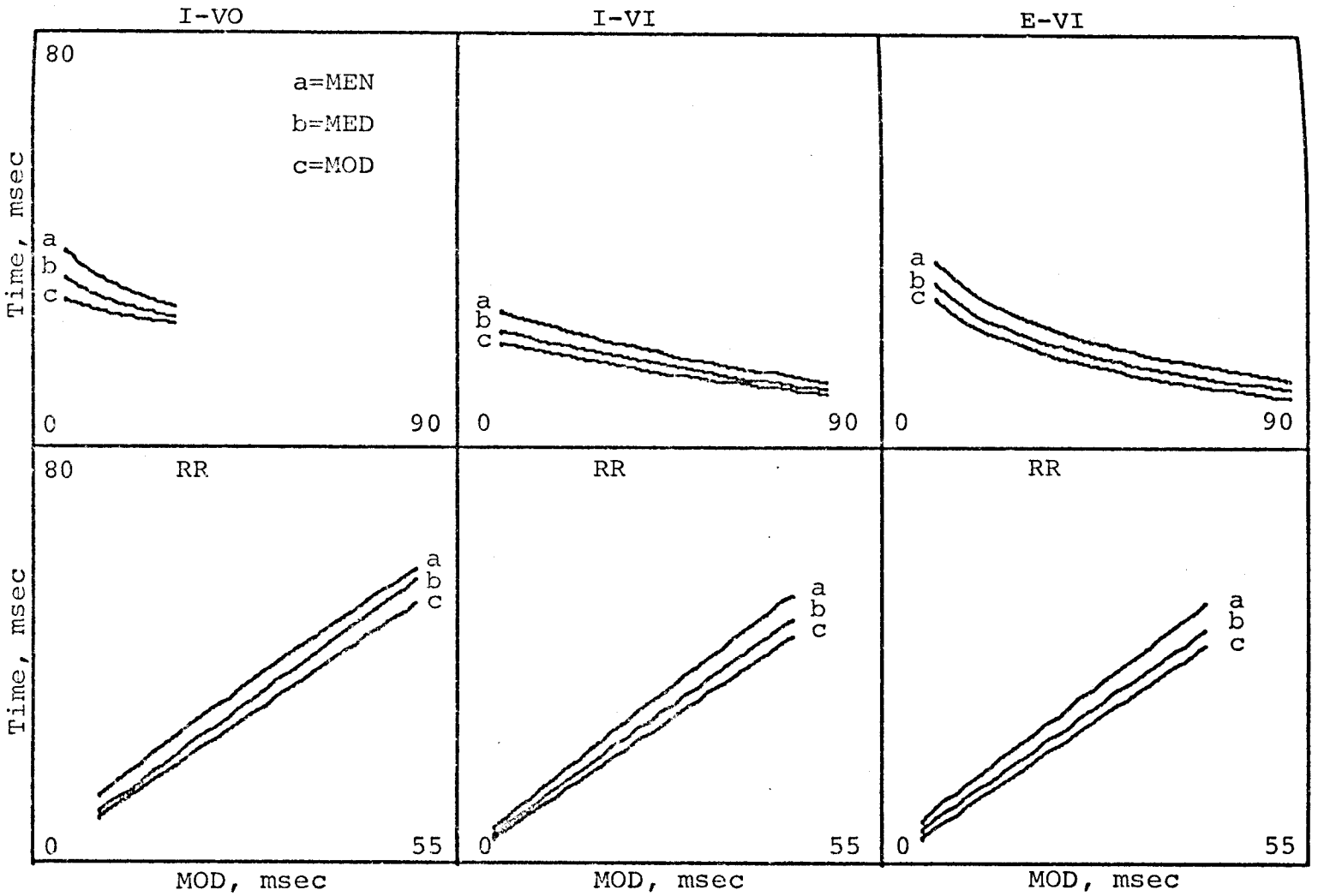

Figure 38. Regression of MEN, MED and MOD on RR and MOD for I-VO, I-VI and E-VI cells.

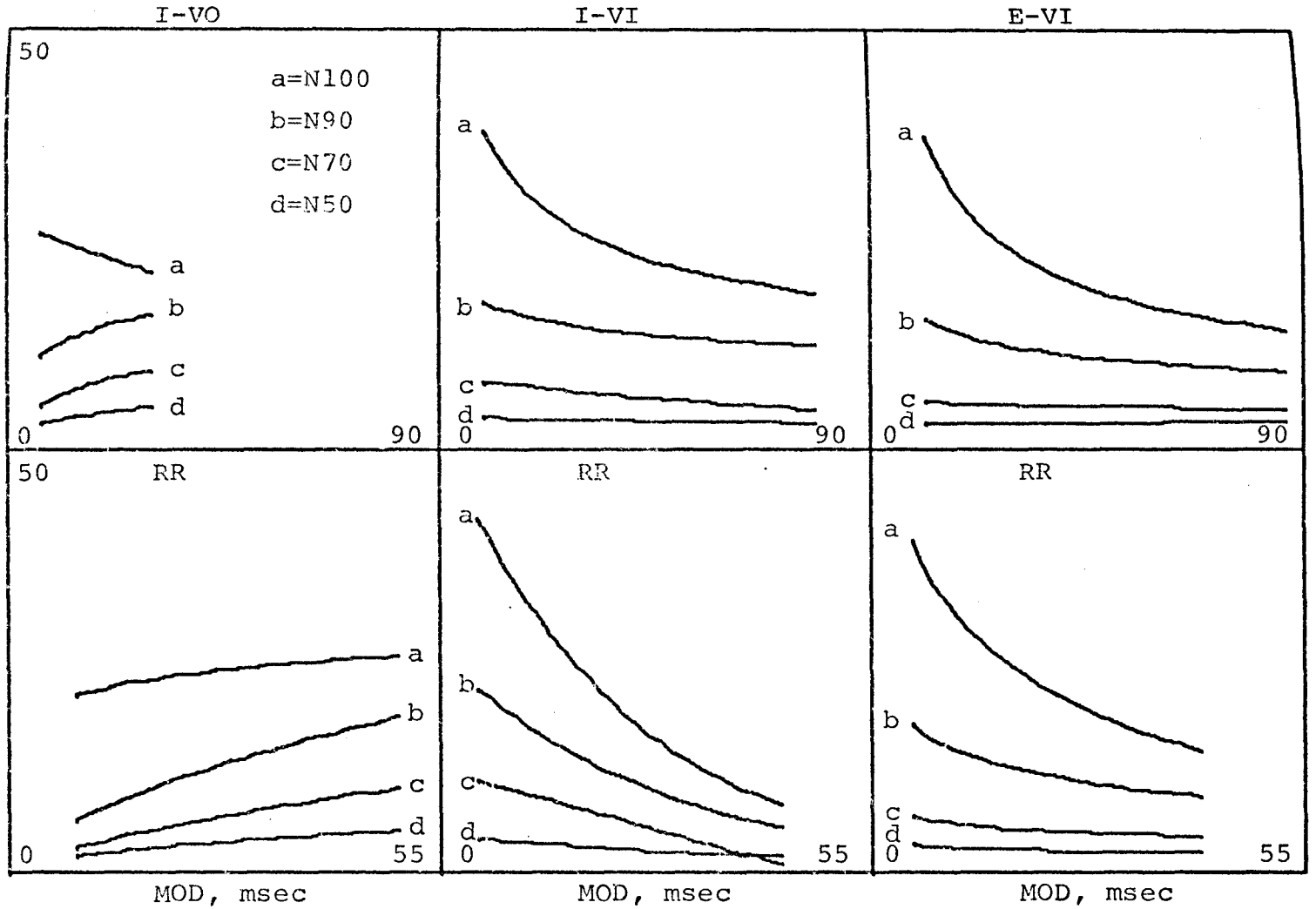

Figure 39. Regression of N100, N90, N70 and N50 on RR and MOD for I-VO, I-VI and E-VI cells.

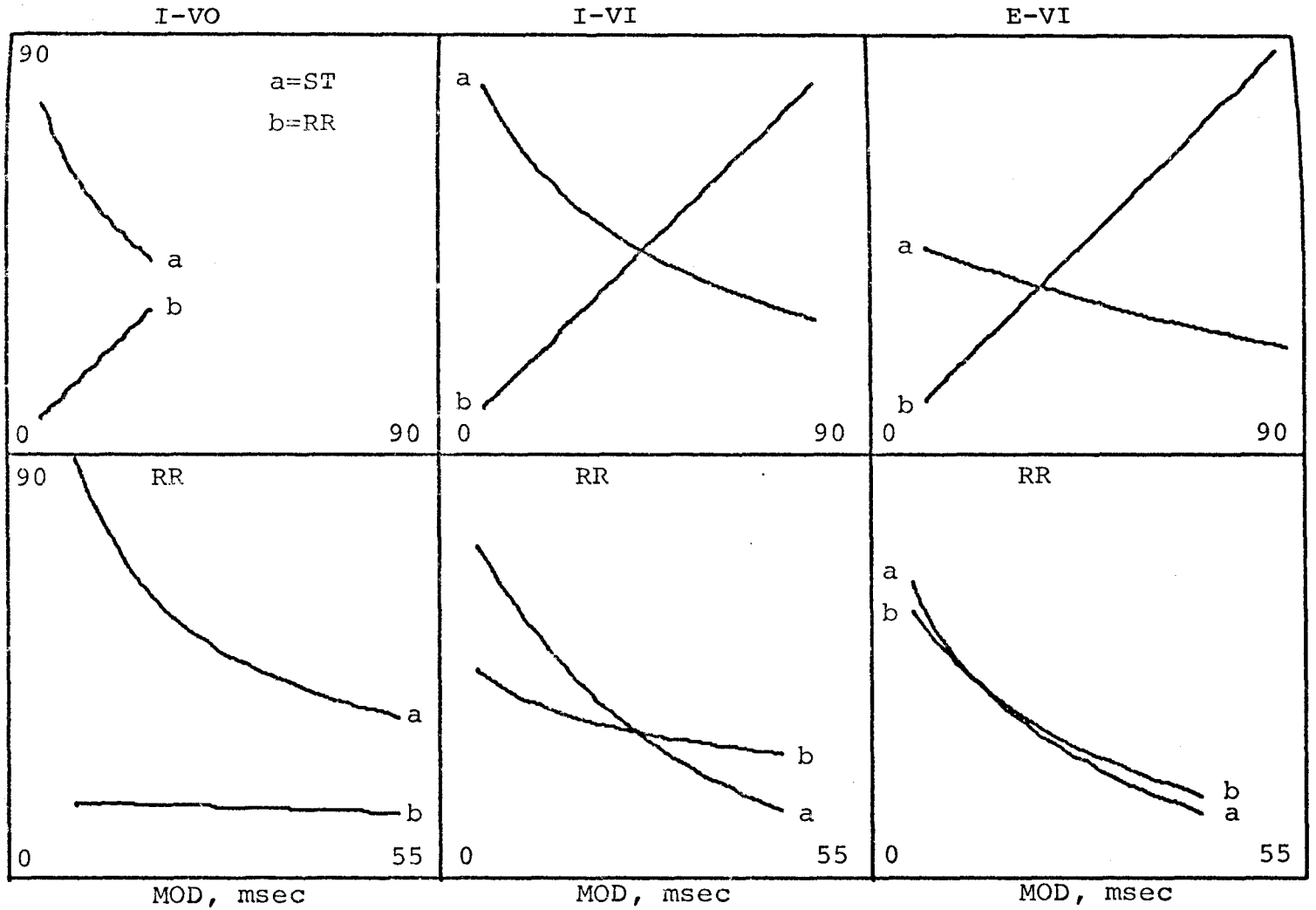

Figure 40. Regression of ST and RR on RR and MOD for I-VO, I-VI and E-VI cells.

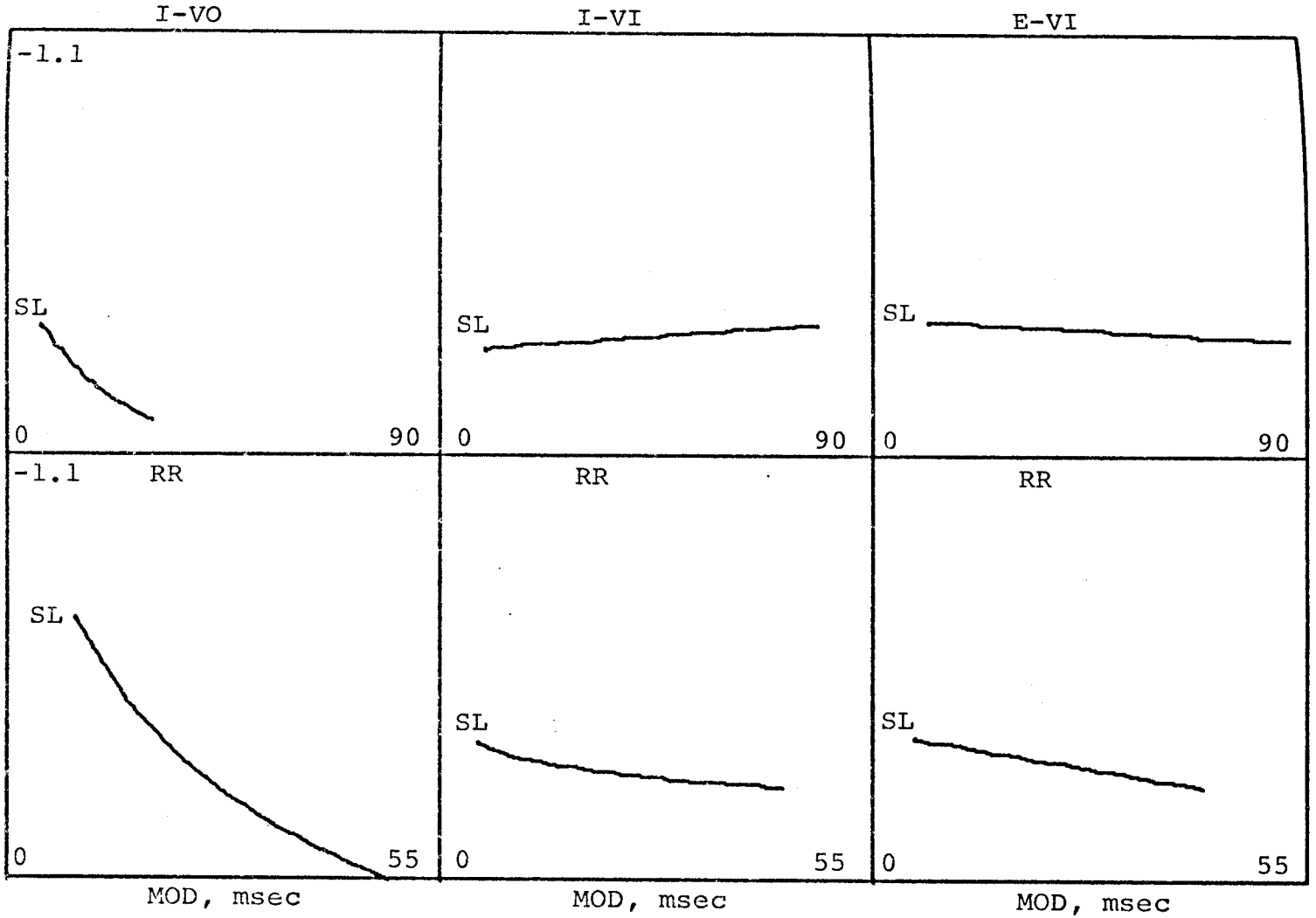

Figure 41. Regression of SL on RR and MOD for I-VO, I-VI and E-VI cells.

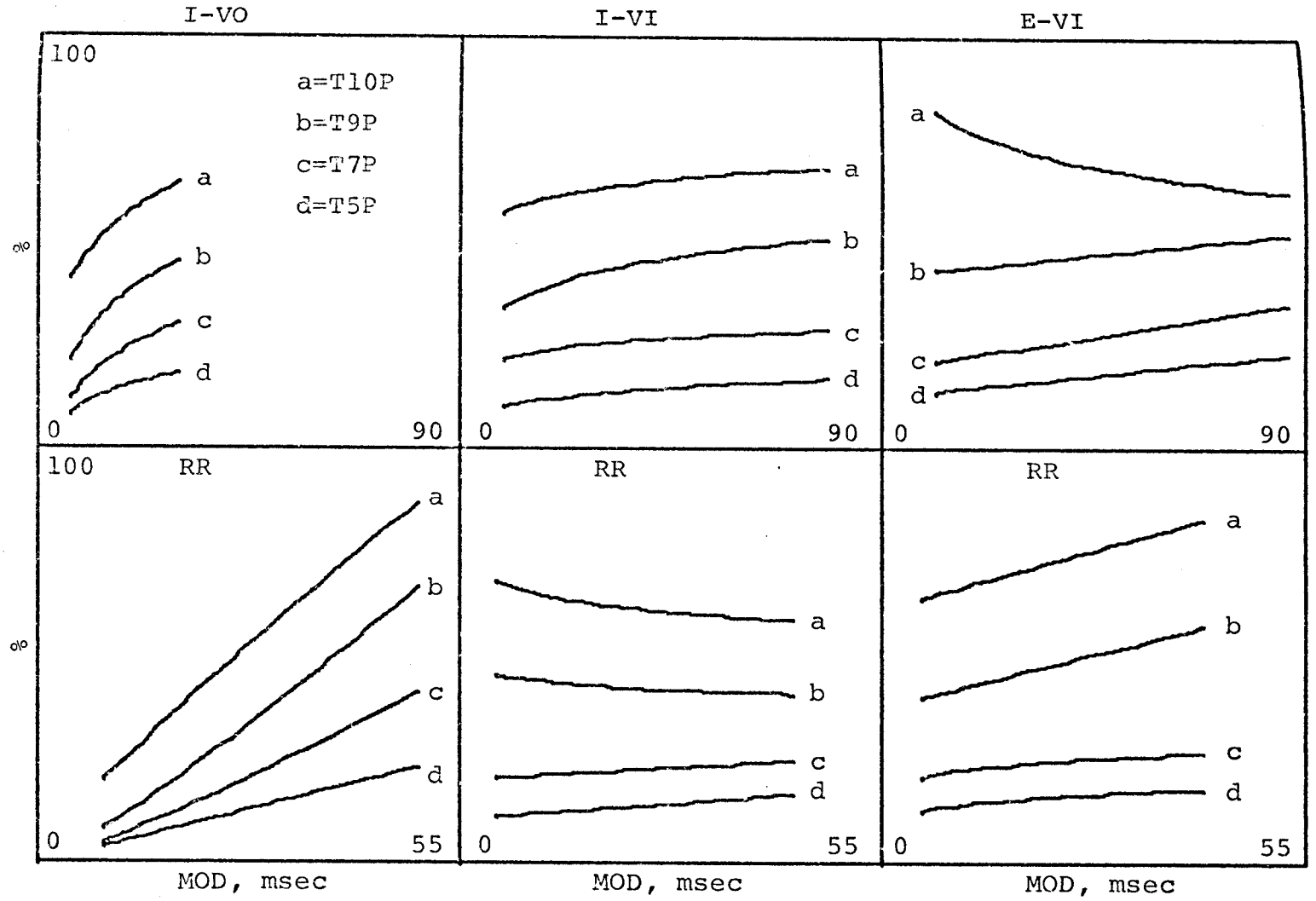

Figure 42. Regression of T10P, T9P, T7P and T5P on RR and MOD for I-VO, I-VI and E-VI cells.

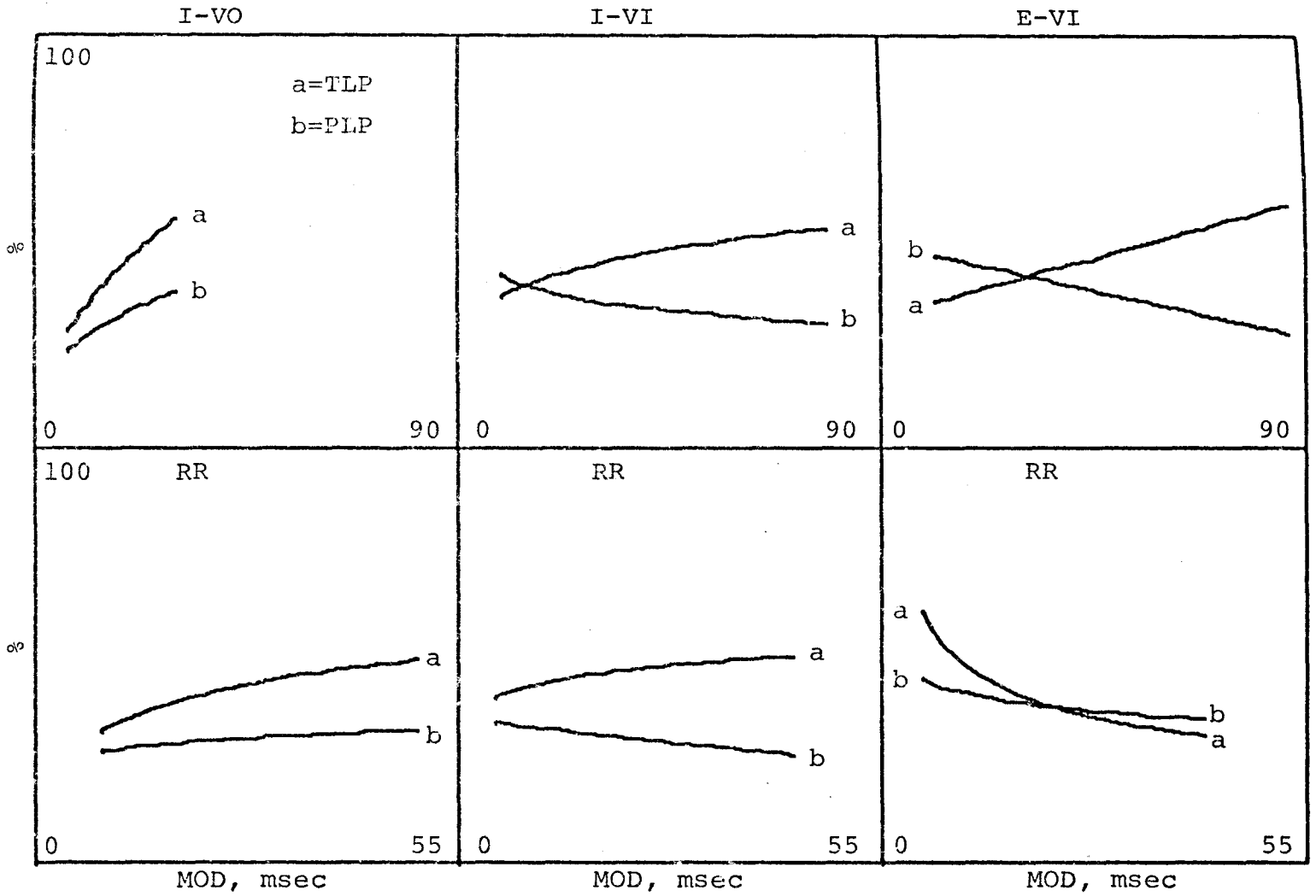

Figure 43. Regression of TLP and PLP on RR and MOD for I-VO, I-VI and E-VI cells.

as a function of both respiration rate (RR) and mode (MOD) for I-VO, I-VI and E-VI cells. In accordance with the definition of each parameter, T50 < T70 < T90 < T100 for each of the six plots. Seven comparisons can be made between the six panels (e.g., I-VI to I-VO and I-VI to E-VI for RR and MOD plots and RR to MOD for I-VO, I-VI and E-VI plots). For example, the following observations can be made by comparing adjacent panels in the horizontal plane. Times to reach fractions of the way to the minimum interval (T50, T70, T90, T100) decrease as the respiration rate (RR) increases for both inspiratory and expiratory cells. Vagotomy abolishes this relationship for inspiratory cells. For inspiratory cells, T parameters are almost independent of changes in the mode (MOD) when the vagi are intact (I-VI), but become positively correlated when the vagal influence is removed (I-VO). For expiratory cells, T parameters follow changes in the mode (MOD).

Comparison of adjacent panels in the vertical plane reveals that T50, T70, T90 and T100 parameters for expiratory cells (E-VI) correlate with either respiration rate (RR) or mode (MOD), but parameter correlations for inspiratory cells (I-VI, I-VO) depend on the state of vagal innervation. That is, when the vagi are intact (I-VI),

T parameters correlate best with the respiration rate (RR). When the vagi are cut, the T parameters correlate best with the mode (MOD). This reversal is of importance to consider when comparing rate and depth outputs of the respiratory system. The reader can make similar comparisons between other cell and parameter types from the rest of the superimposed regression plots in Figures 36-43. Major findings from the population data will be elaborated in the Discussion.

C. Single Cell Data

From the 83 cells (Table III) contributing to the I-VO, I-VI and E-VI population data (Figures 11-43), 14 cells have been selected to illustrate single unit responses to induced or spontaneous changes in respiratory rate and/or depth. The reader should make careful comparisons between the single cell data presented and the population plots of Figures 35-43.

One of the important questions to consider in this study is how well do mode (MOD) interval times of single cells correlate with the depth of respiration. The theoretical reasoning diagrammed in Figure 10 predicts that for any one inspiratory cell, the mode (MOD) should be reciprocally related to the depth of respiration and independent of changes in spontaneous respiratory rate.

Examples from six inspiratory cells (I-VI) are presented to qualitatively establish the mode-depth relationship, point out quantitative cell-to-cell differences and suggest that mode interval times can fluctuate with the spontaneous respiratory rate in some circumstances. For each example, the depth of respiration is defined in relative terms as the average end inspiratory to end expiratory intrapleural pressure difference (ΔIPP).

Three histograms and interspike interval modulation curves for inspiratory cell C32UI1R are superimposed in Figure 44A and B respectively. The curves are numbered consecutively, denoting a chronological data point acquisition sequence. Corresponding absolute and percent changes in the respiratory rate (RR), mode (MOD) and respiratory depth (ΔIPP) measurements are listed for each data point in tabular format. In this series, there was a substantial spontaneous increase in the depth of respiration (73.1%) with only a small rate decrease (11.9%). The single unit response was one of activation. That is, the histogram interval distribution was shifted to the left (Figure 44A) resulting in a decreased mode time (34.5%) and the interspike interval modulation curve was shifted downward in a parallel fashion (Figure 44B). Rate and mode interaction, if any, cannot be ascertained

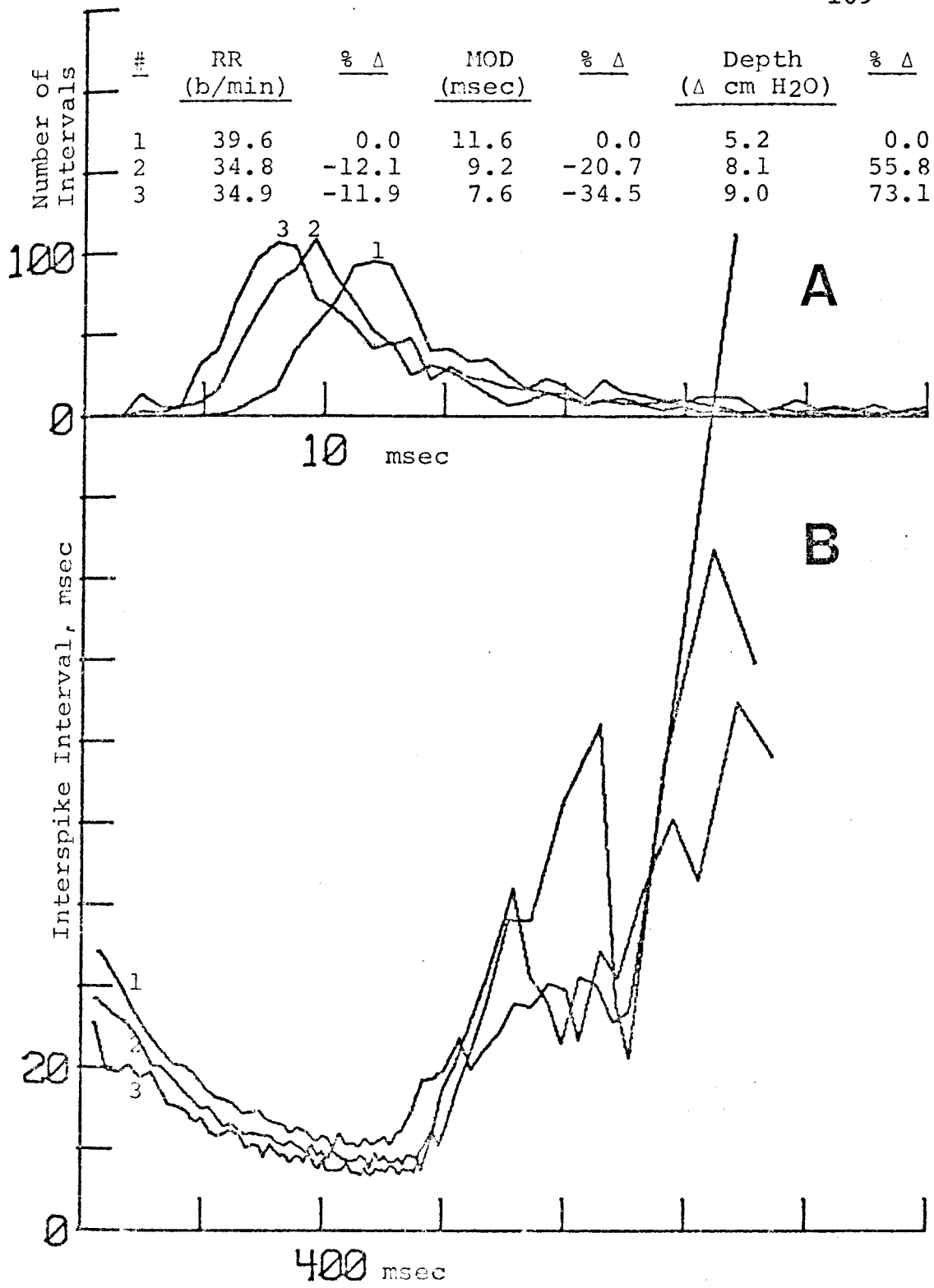

Figure 44. C32UI1R. Effect of spontaneous increase in respiratory depth on histogram (A) and interspike interval modulation curve (B). Data points numbered in time sequence. Vagi intact.

from these data. If one assumes that this cell possesses characteristics similar to the population data of Figure 16 where mode and rate are reciprocally related, the rate slowing observed in Figure 44 may limit the mode decrease during an increase in respiratory depth. From the data presented in Figure 44 it is reasonable to conclude that mode time and respiratory depth have a reciprocal relationship.

Figure 45 shows single cell data for cell C80UI1R obtained during a spontaneous decrease in respiratory depth (ΔIPP). In this case, the depth decreases proportionately more than the rate increases (28.0% versus 13.8% respectively) suggesting that the mode increase (54.5%) is associated with the former. The cell displays a typical deactivation pattern in which the histogram interval distribution shifts to the right and the interspike interval modulation curve is shifted upward. In another cell, not pictured, C29UI7R, the increase in the mode from 10.8 to 13.2 milliseconds (22.2%) was associated with a depth change from 4.4 to 3.7 centimeters of water (-15.9%). The rate change was minimal from 30.7 to 29.7 breaths per minute (-3.3%). These single cell examples suggest that mode time and respiratory depth are reciprocally related.

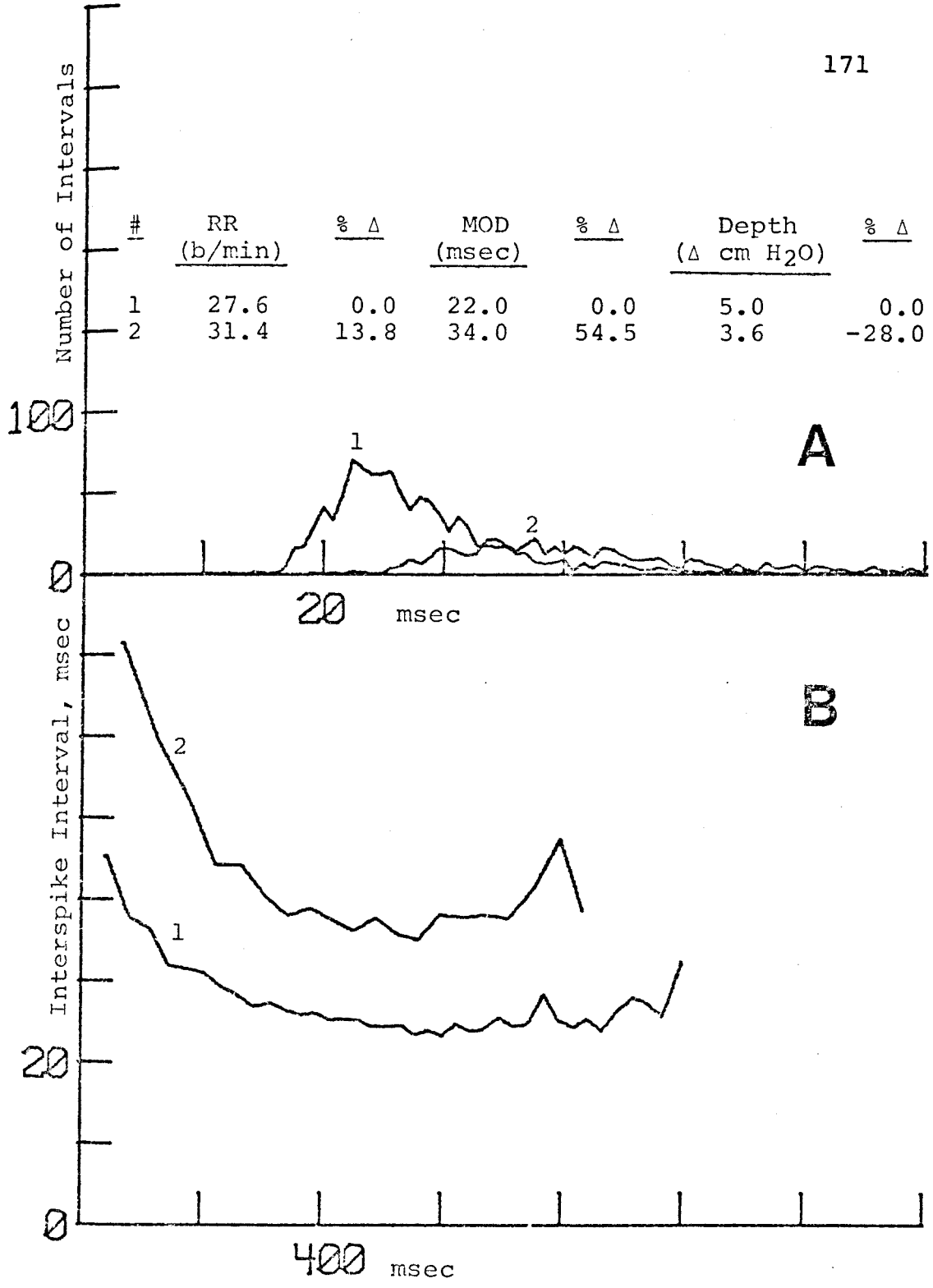

Figure 45. C80UI1R. Effect of spontaneous decrease in respiratory depth on histogram (A) and interspike interval modulation curve (B). Vagi intact.

Careful inspection of tabular data in Figures 44 and 45 shows that an absolute depth (ΔIPP) of about 5.2 to 5.0 centimeters of water is paralleled by mode times of 11.6 and 22.0 milliseconds respectively. These differences in single cell firing frequencies at equivalent depths can be explained in two ways. First, the two cats may have had different (and unknown) compliances. Mode time may be directly related to compliance for any given volume or depth. Second, the difference may be attributed to characteristic variations among central inspiratory neurons. Both phenomena are probably operative in the respiratory control system, but the following experiment was addressed to the latter point.

In one cat breathing spontaneously, two inspiratory cells were recorded simultaneously with two separate microelectrodes inserted on opposite sides of the medulla. As shown in Figure 46A, the left cell (I2L) had a higher discharge frequency than the right cell (I3R). The histogram plots and frequency modulation curves of Figure 46B and C, respectively, show firing pattern differences between the fast (I2L) and slow (I3R) cells. Since both cells were recorded at the same time in the same animal, differences in mode time cannot be attributed to variations in mechanical or chemical

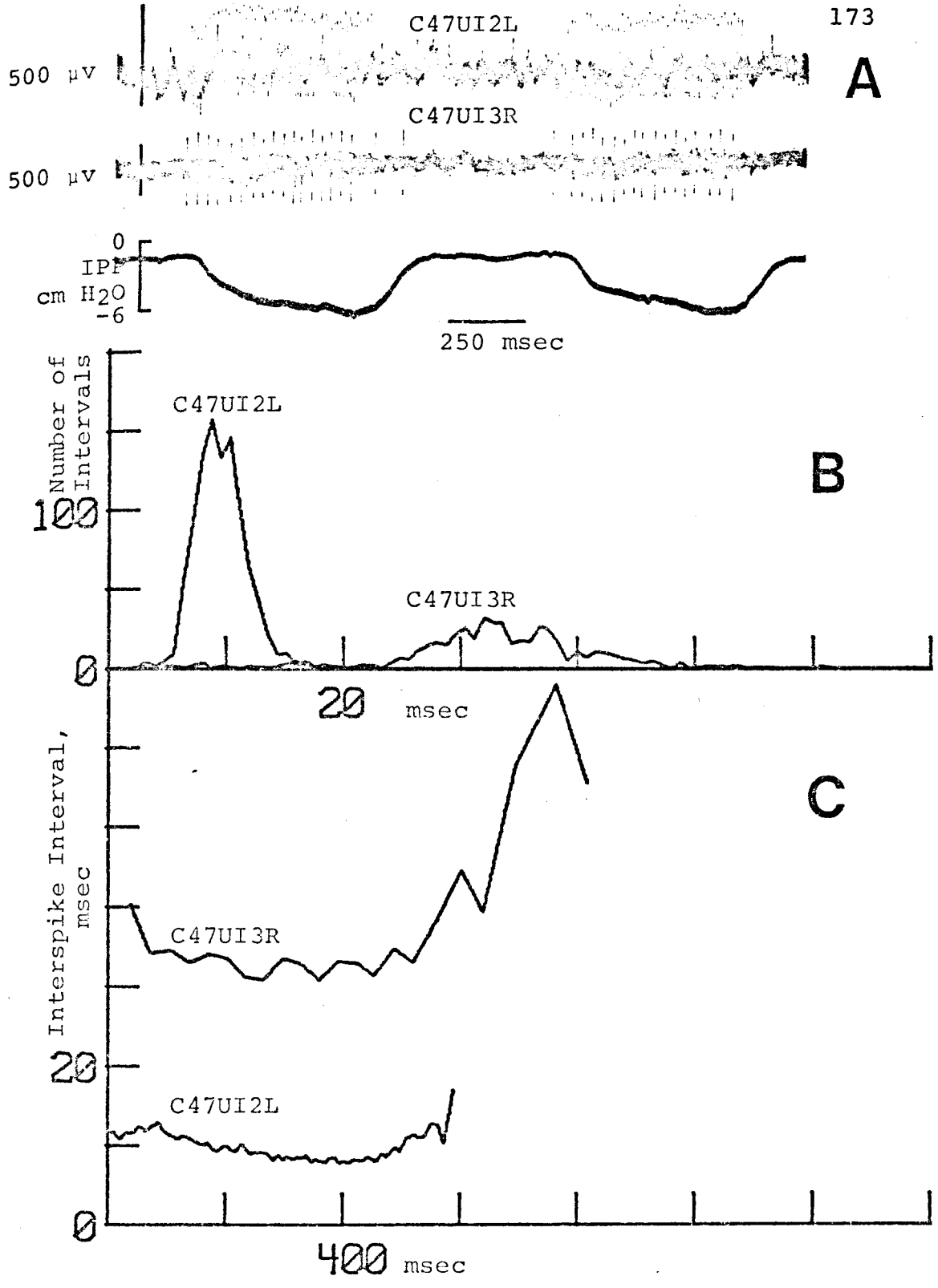

Figure 46. Two simultaneously recorded inspiratory cells from right and left medulla (A), their histograms (B) and interspike interval modulation curves (C). Vagi intact.

factors. Rather, it is suggested that inherent variability exists at the cellular level presumably due to differences in cell size, membrane characteristics and interneurone connections. This reasoning explains the scatter of mode (MOD) values plotted as a function of respiratory rate (RR) in Figure 16 and probably is a factor causing scatter of data points in all the regression plots (Figures 11-34). Because of these cell-to-cell differences, quantitation of parameter interactions (e.g., MOD versus 1/depth) cannot be done at the single cell level. That is, quantitation of one cell's characteristics represents a specific individual case. Quantitation of the whole population requires sufficient sampling of all representative cell types in the respiratory complex and statistical averaging of cell discharges in time and space. The latter is probably handled physiologically at several synaptic levels in the efferent pathway.

Although Figures 44 and 45 suggest that mode changes are associated with modifications in respiratory depth, Figure 47 presents evidence that this is not always the case. Here, a spontaneous increase in the respiratory rate occurs (40.8%) which is accompanied by an increase in the mode (MOD) interval time (31.6%). Since the maximal change in respiratory depth is at best

#	RR (b/min)	% Δ	MOD (msec)	% Δ	Depth (Δ cm H_2O)	% Δ
1	33.1	0.0	22.8	0.0	6.8	0.0
2	37.0	11.8	26.0	14.0	7.0	2.9
3	39.6	19.6	26.0	14.0	6.8	0.0
4	40.8	23.3	25.2	10.5	7.0	2.9
5	42.2	27.5	26.8	17.5	7.0	2.9
6	46.6	40.8	30.0	31.6	6.8	0.0

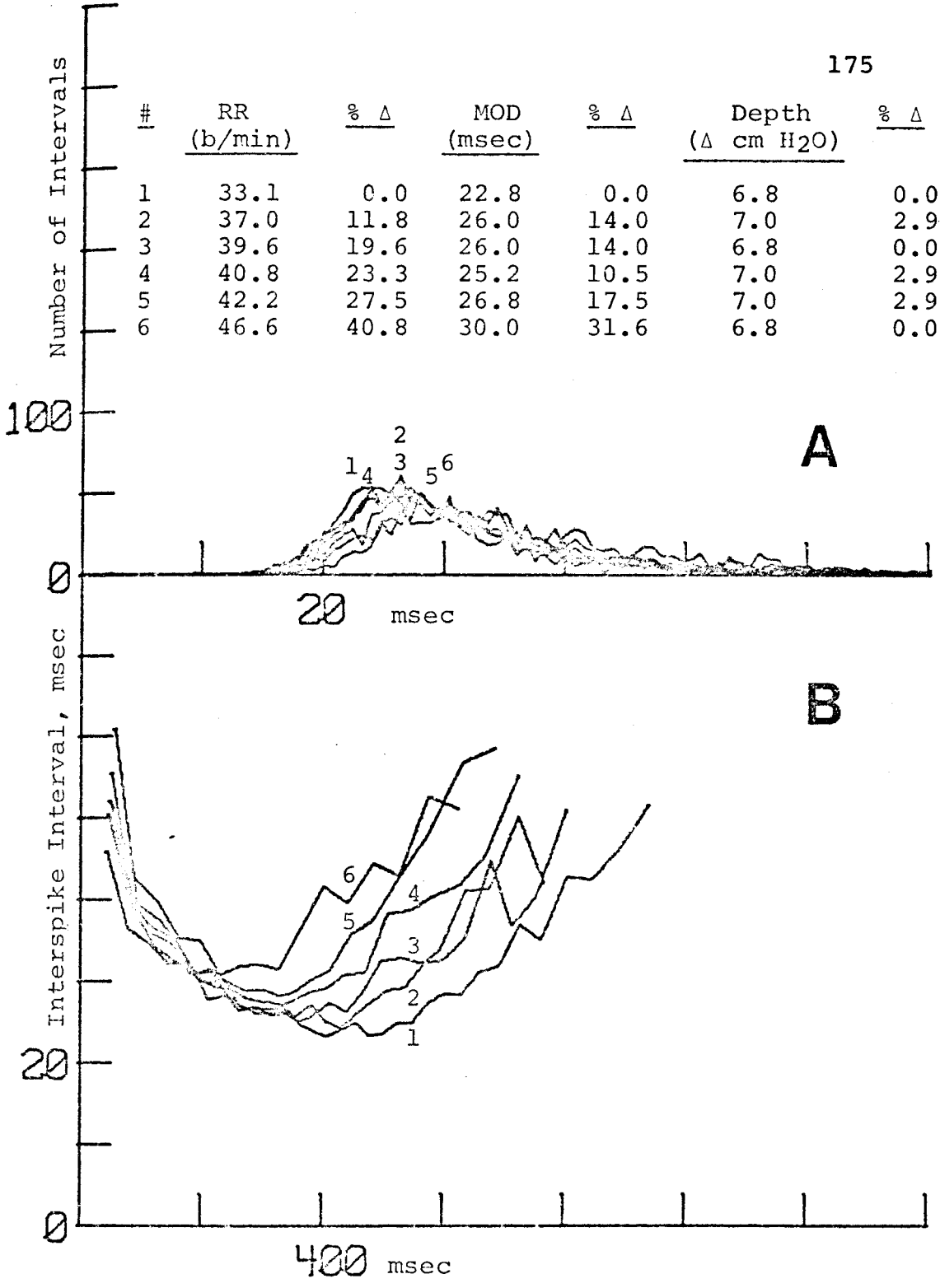

Figure 47. C28UI5. Effect of spontaneous increase in respiratory rate on histogram (A) and interspike interval modulation curve (B). Vagi intact.

only minimal (2.9%), the cellular depression must have been due to other factors. It is interesting to note that the histogram shift to the right (Figure 47A) is not a smooth transition as seen for the rate elevation. Also, the interspike interval modulation curve shift is not parallel (Figure 47B) as observed for other inspiratory cells (Figures 44-45). That is, the latter part of the train is affected to a larger extent than the initial phase of unit activity. These variations may explain the abnormal mode modification during spontaneous changes in breathing patterns involving rate, but not depth.

Seven cells have been selected to demonstrate the effects of certain drugs on discharge patterns. The pharmacologic agents (pentobarbital sodium, thiopental sodium, doxapram hydrochloride and morphine sulphate) were chosen because of their known effects on gross respiratory function. For example, Figures 48 and 49 illustrate the quantitative responses of cell C62UI3R to two injections of doxapram. Before discussing the physiological responses, however, the format of Figure 49 is described to facilitate reader comprehension of the data presentation. The data from the six remaining cells in this section have identical formats.

In Figure 49, the twenty five parameters examined

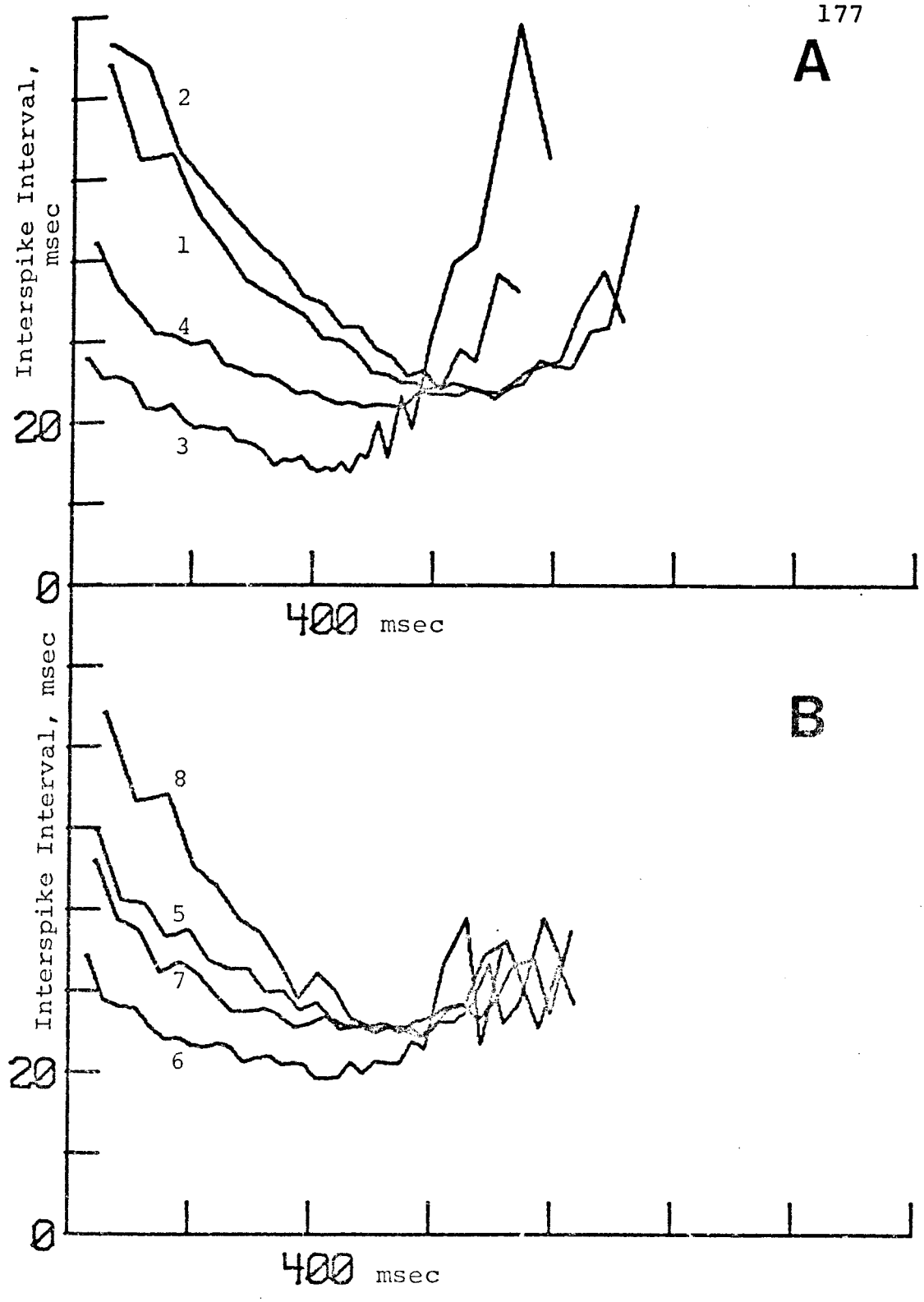

Figure 48. C62UI3R. Effect of doxapram on interspike interval modulation curve: A. 1.6 mg/Kg doxapram given between Curves 2 and 3; B. 1.6 mg/Kg doxapram given between Curves 5 and 6. Vagi intact.

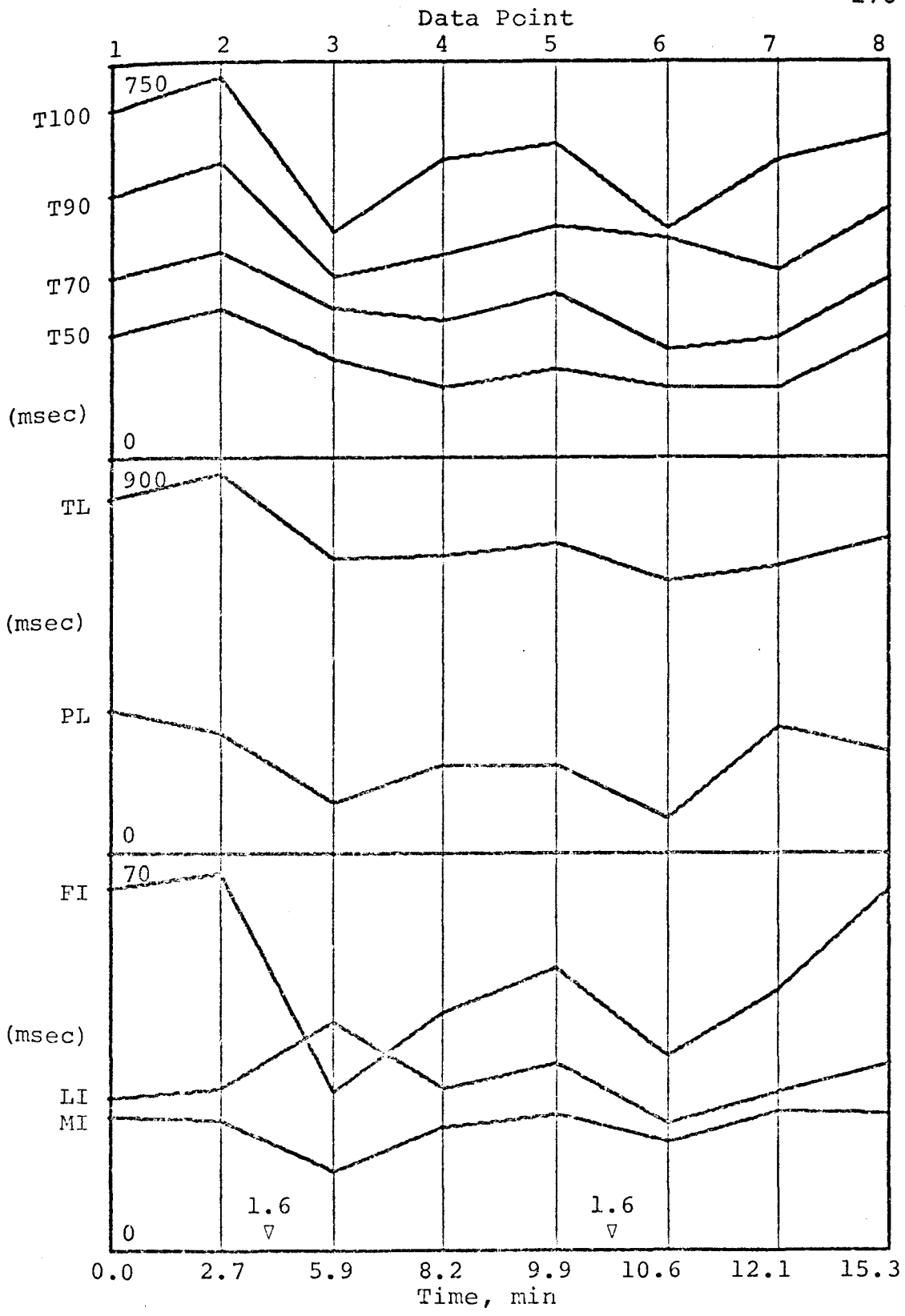

Figure 49A. C62UI3R. Effect of doxapram on parameters of inspiratory cell discharge. See text for details.

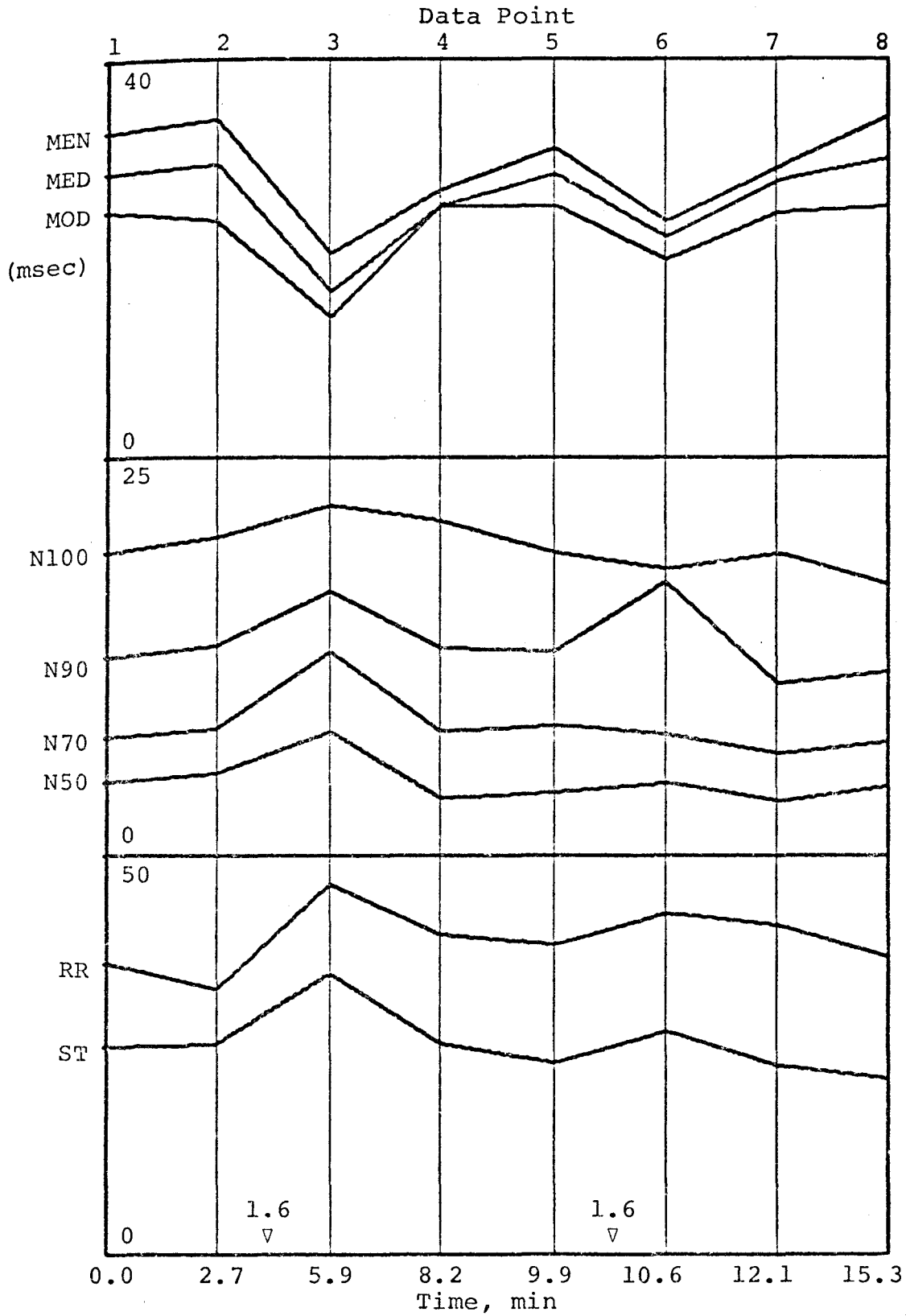

Figure 49B. C62UI3R. Effect of doxapram on parameters of inspiratory cell discharge. See text for details.

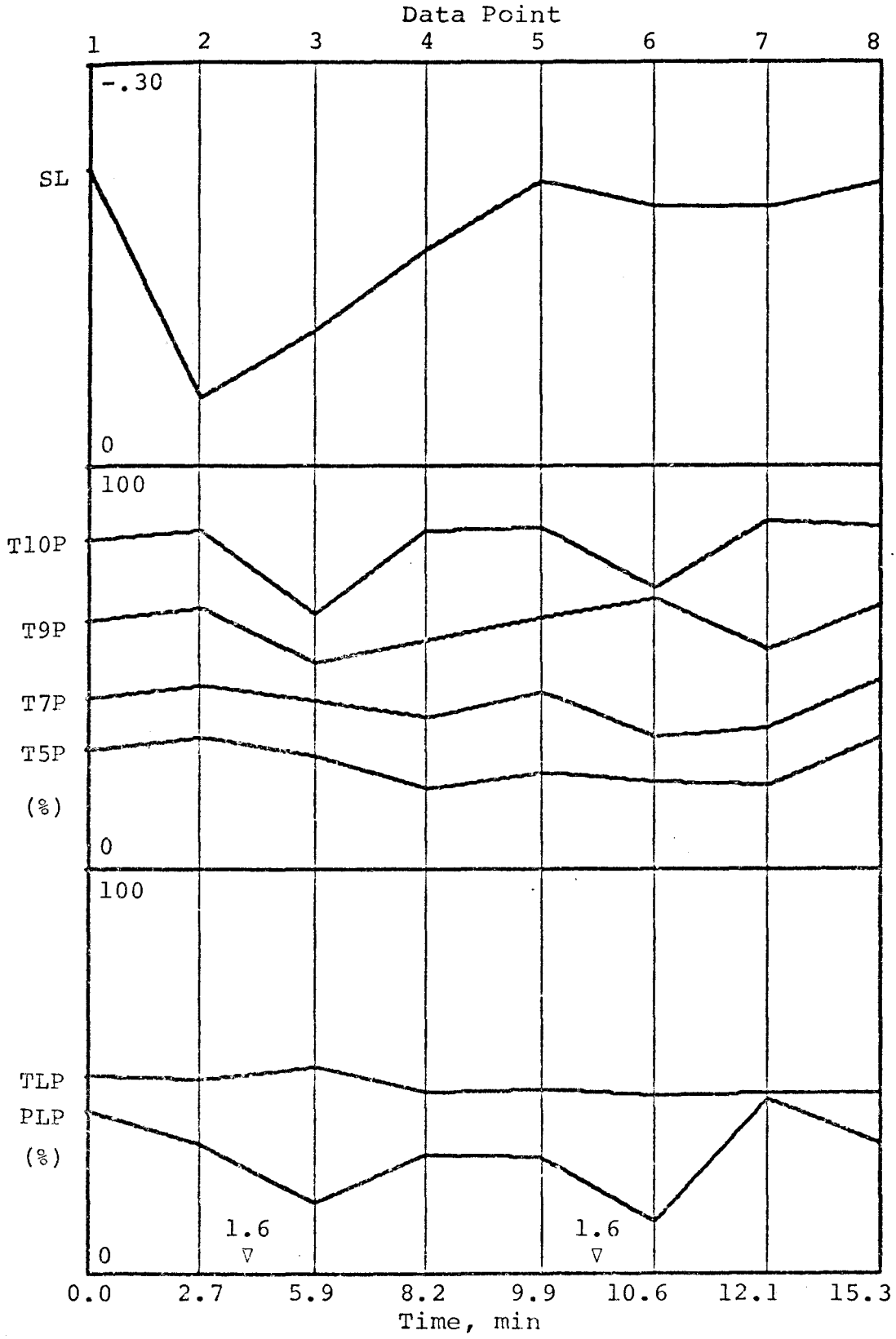

Figure 49C. C62UI3R. Effect of doxapram on parameters of inspiratory cell discharge. See text for details.

by regression analysis (Figures 11-43) are plotted as a function of time in nine panels on three pages. All parameters are identified according to the abbreviations listed in Table IV. By examination of mode and respiration rate trends in the upper and lower panels of Figure 49B, respectively, comparison of single cell characteristics with the mean population data is possible.

Each steady state measurement is marked off by a vertical line which is identified by a data point number at the top and a time measurement to the nearest tenth of a minute at the bottom. The uniformly spaced data points form a non-linear time function on the X-axis. Scaling of dependent variables is given for each group of parameters and appropriate dimensions are supplied. Respiration rate is in breaths per minute. Timings of doxapram injections are identified by inverted triangles with superscript numbers denoting drug dose in milligrams per kilogram (e.g. $\overset{1.6}{\nabla}$).

Changes in interspike interval modulation curves for inspiratory cell C62UI3R following two separate injections of doxapram are shown in Figure 48A and B respectively. Superimposed Curves 1 and 2 in Figure 48A are pre-injection controls. Curve 3 represents the discharge pattern change shortly after injection of doxapram

(1.6 mg/kg) and Curve 4 shows partial recovery from drug activation. In Figure 48B, the series is continued using Curve 5 as the new control. The second doxapram injection (1.6 mg/kg) caused a pattern shift to Curve 6, but this activation level was not as high as in Curve 3, possibly due to tachyphylaxis. Curves 7 and 8 are recovery patterns.

Doxapram effects on the individual parameters for cell C62UI3R are shown in Figure 49. Doxapram accelerates the respiration rate (RR) and decreases the mode (MOD) interval time. Corresponding decreases in the first interval (FI), minimal interval (MI), times to reach portions of the way to the minimal interval (T50, T70, T90, T100), plateau level (PL), train length (TL), mean (MEN) and median (MED) times all parallel predicted parameter responses to increased rates and decreased modes from the mean population data (Figures 35-43). The last interval (LI) has an inconsistent biphasic response while the N50, N70, N90, N100 and ST parameters follow predicted changes in the mode but not the rate. The spikes per train response indicates that the mode time is decreasing faster than the train length. The slope (SL) has a very unpredictable pattern which must be associated with the poor correlation coefficients for

regressions of slope on rate (Figure 19, I-VI) and slope on mode (Figure 31, I-VI). Variable responses are seen for the normalized parameters (T5P, T7P, T9P, T10P, PLP) while the percent time the cell fires during the respiratory cycle (TLP) appears to be independent of rate and mode changes induced by doxapram.

Variations occur in the characteristics of single unit patterns in response to barbiturate administration. These are illustrated in the following two sets of data derived from two different cells. The vagus nerves were intact in each case which permits comparison of these single cell data with the mean I-VI population data in Figures 35-43. Data from the first inspiratory cell, C63UI4R, are presented in Figures 50 and 51. Identical doses of pentobarbital (1.5 mg/kg) were injected between each data point. With increasing accumulated dosage of pentobarbital it can be seen that respiration rate decreases from 44.7 to 24.0 breaths per minute (Figure 51B). The mode (MOD) time, however, only slightly increases from 14.0 to 13.8 milliseconds as illustrated in Figure 50A, where histogram distributions fall in overlapping populations. In contrast to the response of cell C62UI3R (Figure 49B) where both spikes per train (ST) and respiration rate (RR) showed parallel increases after doxapram

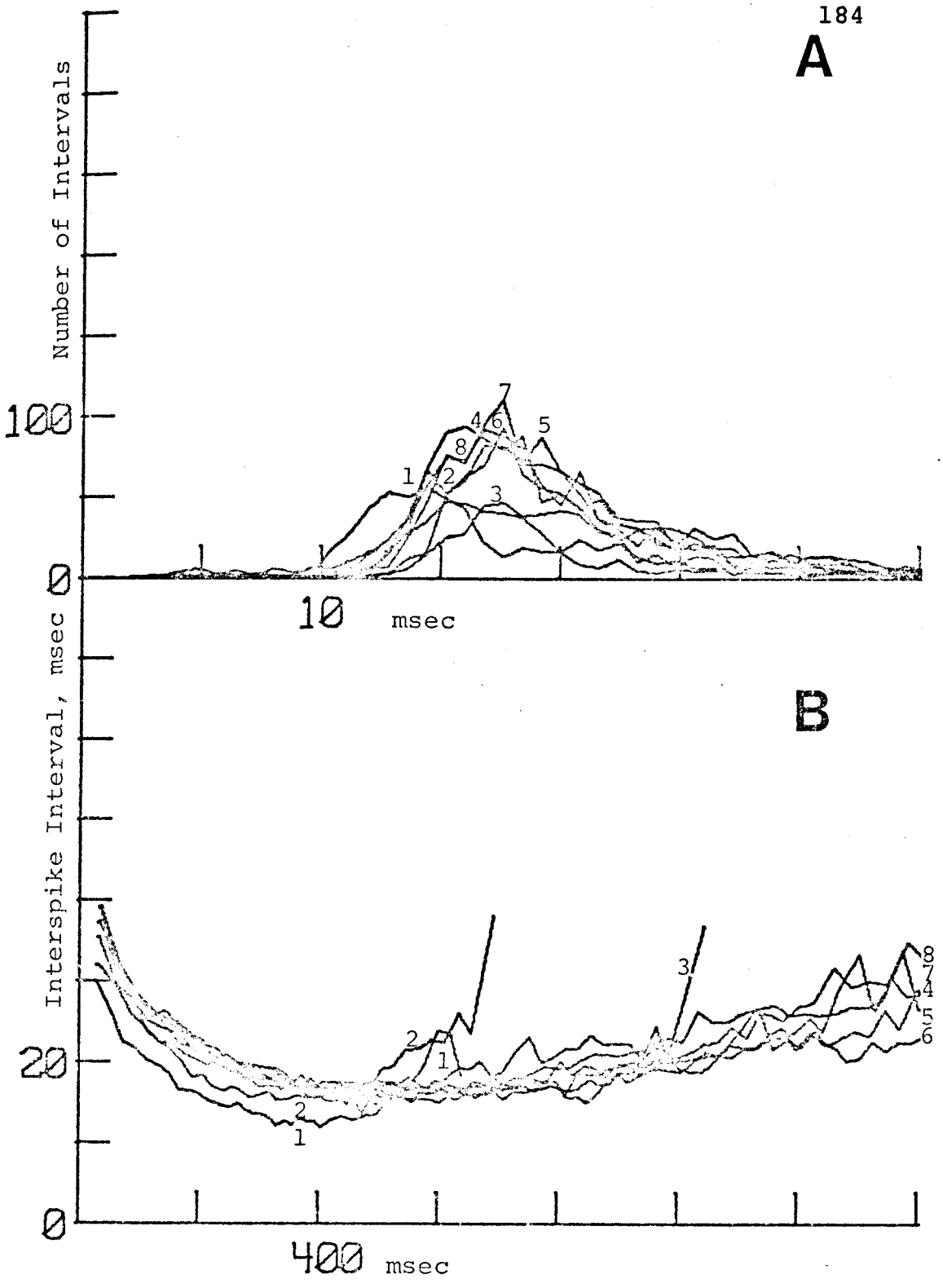

Figure 50. C63UI4R. Effect of cumulative doses of pentobarbital on histogram (A) and interspike interval modulation curve (B). Vagi intact.

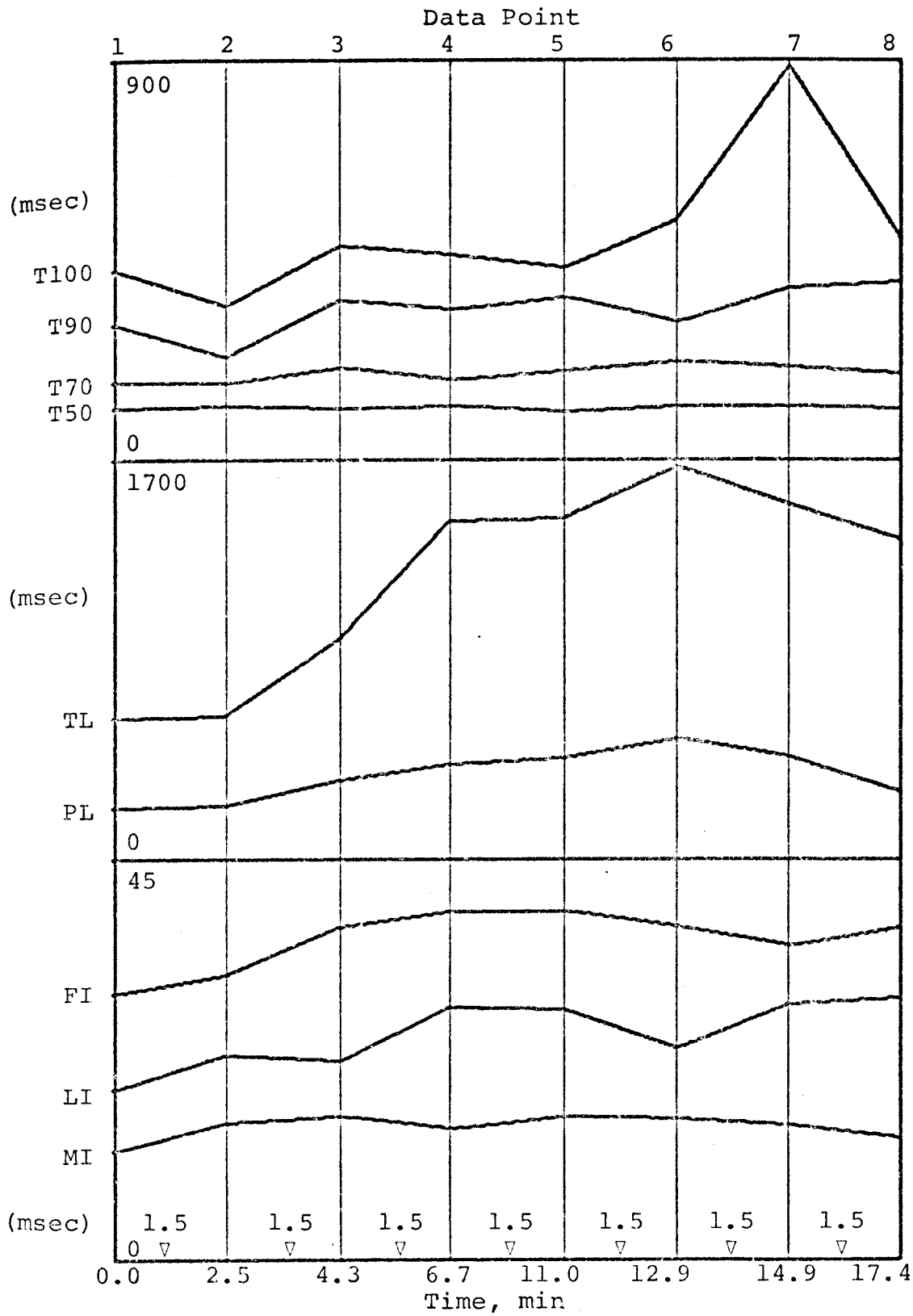

Figure 51A. C63UI4R. Effect of pentobarbital on parameters of inspiratory cell discharge. See text for details.

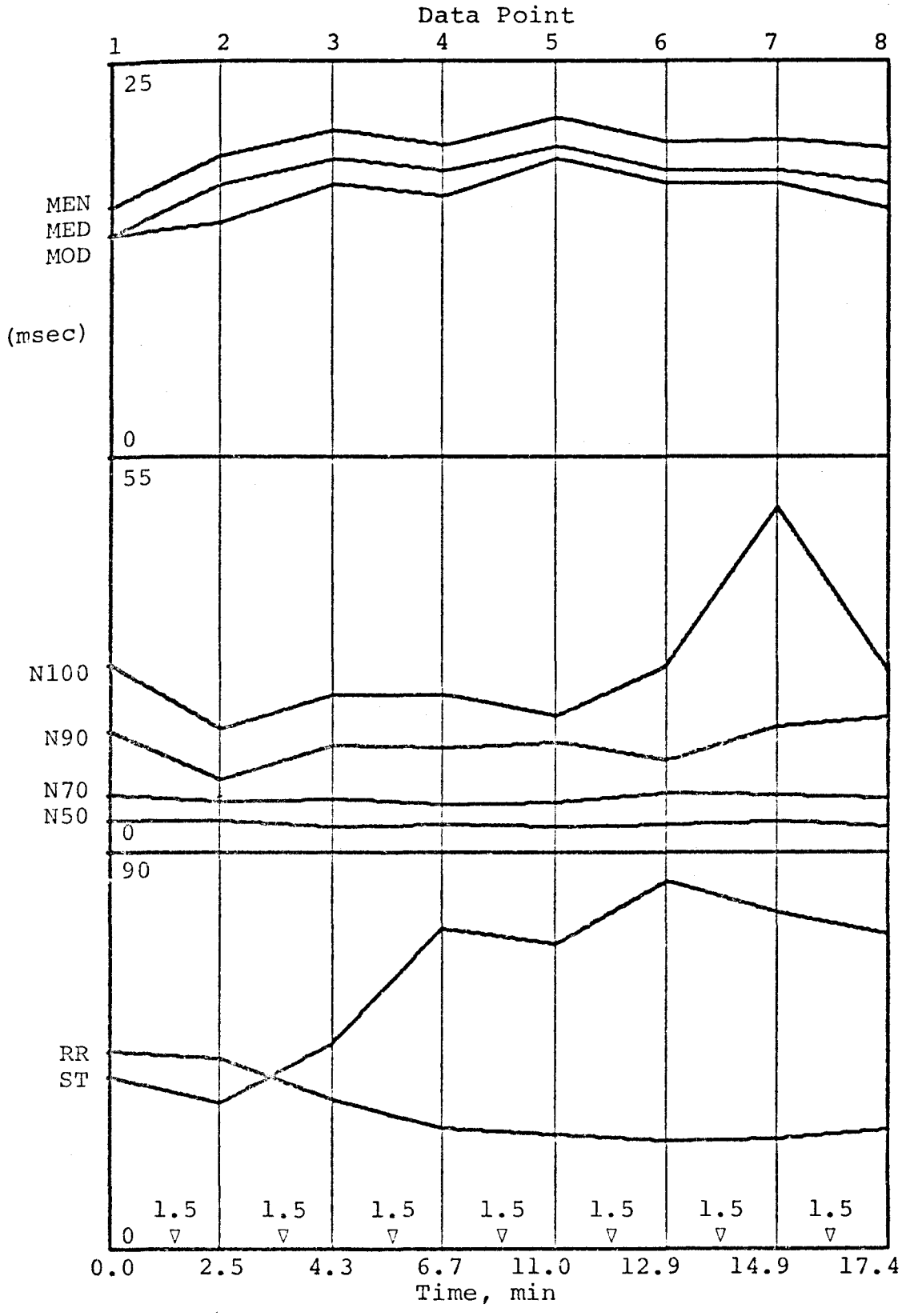

Figure 51B. C63UI4R. Effect of pentobarbital on parameters of inspiratory cell discharge. See text for details.

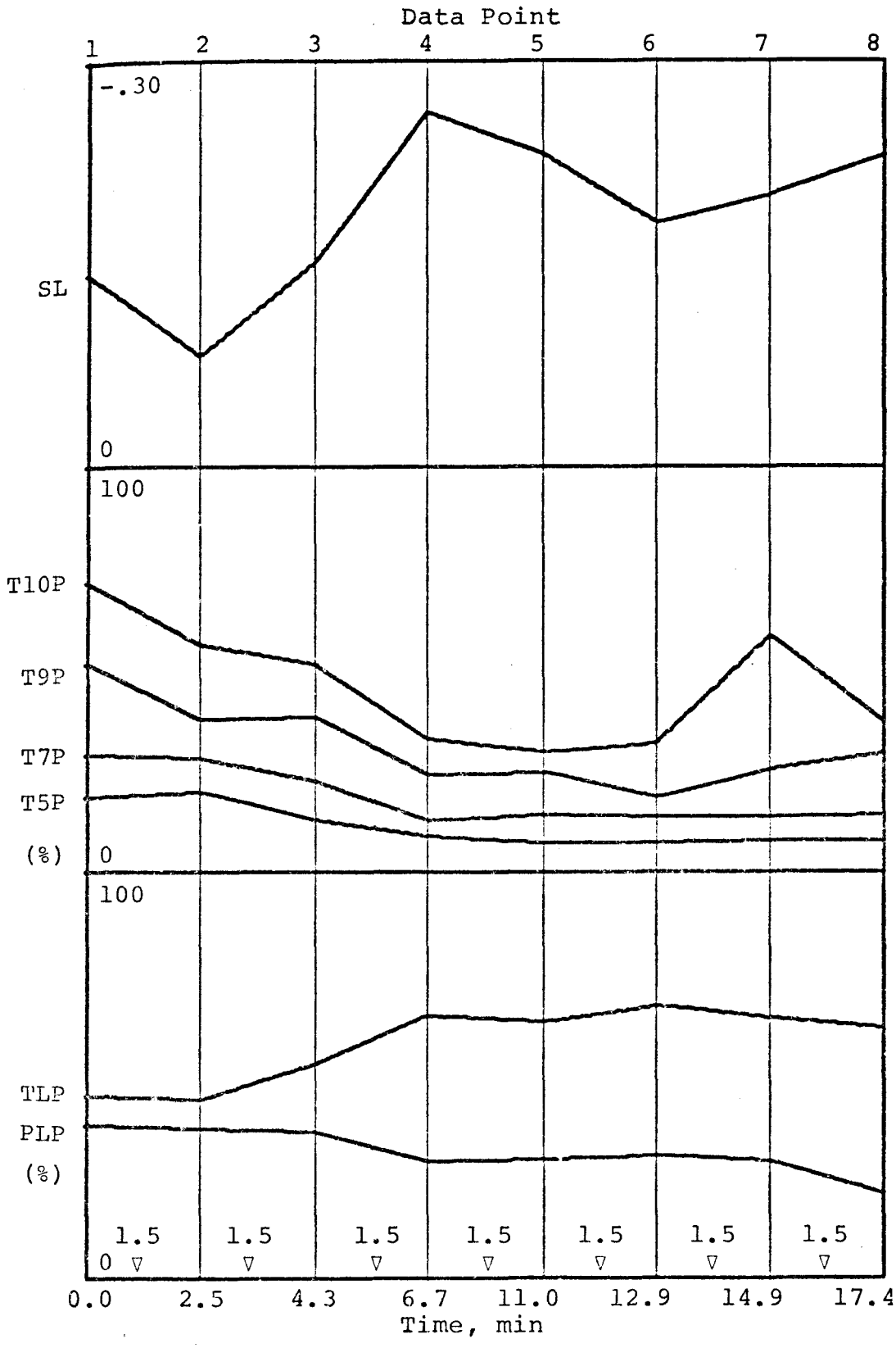

Figure 51C. C63UI4R. Effect of pentobarbital on parameters of inspiratory cell discharge. See text for details.

injections, ST and RR for cell C63UI4R change in opposite directions during barbiturate depression. This is due to the dramatic increase in train length (TL) following respiratory rate slowing with only a small decrease in the discharge frequency (Figure 50B). Parameters T50, T70, T90, T100 and PL show little change except for T100, which increases abruptly after the sixth injection of pentobarbital (Figure 51A). These observations, coupled with the longer train lengths, explain the decrease in the T5P, T7P, T9P, T10P and PLP measurements (Figure 51C). Vertical shifts of the interspike interval modulation curves are small as shown by the relatively small changes in first interval (FI), minimum interval (MI) and last interval (LI) during drug depression (Figure 51A). Similarly, N50, N70, N90 and N100 parameters show little change until high nembutal levels are reached (Figure 51B). In general, the slope (SL) tends to increase as a function of drug depression, but individual directional changes are not predictable. Finally, pentobarbital causes inspiratory train discharge to occupy more of the respiratory cycle time as indicated by the increase in TLP (Figure 51C). This is due to a greater increase in train length than in cycle time during the slowing of respiratory rate. Most of these pattern changes are consistent

with those predicted from the mean population data (Figures 35-43).

Data from the second inspiratory cell, C83UI1L, are presented in Figures 52 and 53. In this case, consecutive equal doses of pentobarbital (1.7 mg/kg) decreases both respiration rate from 71.8 to 29.9 breaths per minute and mode interval time from 21.2 to 14.8 milliseconds. The latter is illustrated in Figure 52A by a significant shift of the histogram interval distributions to the left. This mode response, which is quite different from that for cell C63UI4R (Figures 50 and 51), is indicative of unit activation (increased firing frequency). This presents an apparent paradox in which increased unit activity occurs during depression of respiratory rate. Data bearing specifically on this problem will be presented in the last part of Results. Similar to cell C63UI4R, the train length of cell C83UI1L was greatly increased by pentobarbital as shown in Figure 52B. The increasing train length and decreasing mode both contribute to an increase in spikes per train, and again the mode is inversely related to respiration rate. While the T50, T70, T90, T100 and PL parameters show predicted responses, an interesting inversion of first and last interval times is seen. That is, with accumulating doses

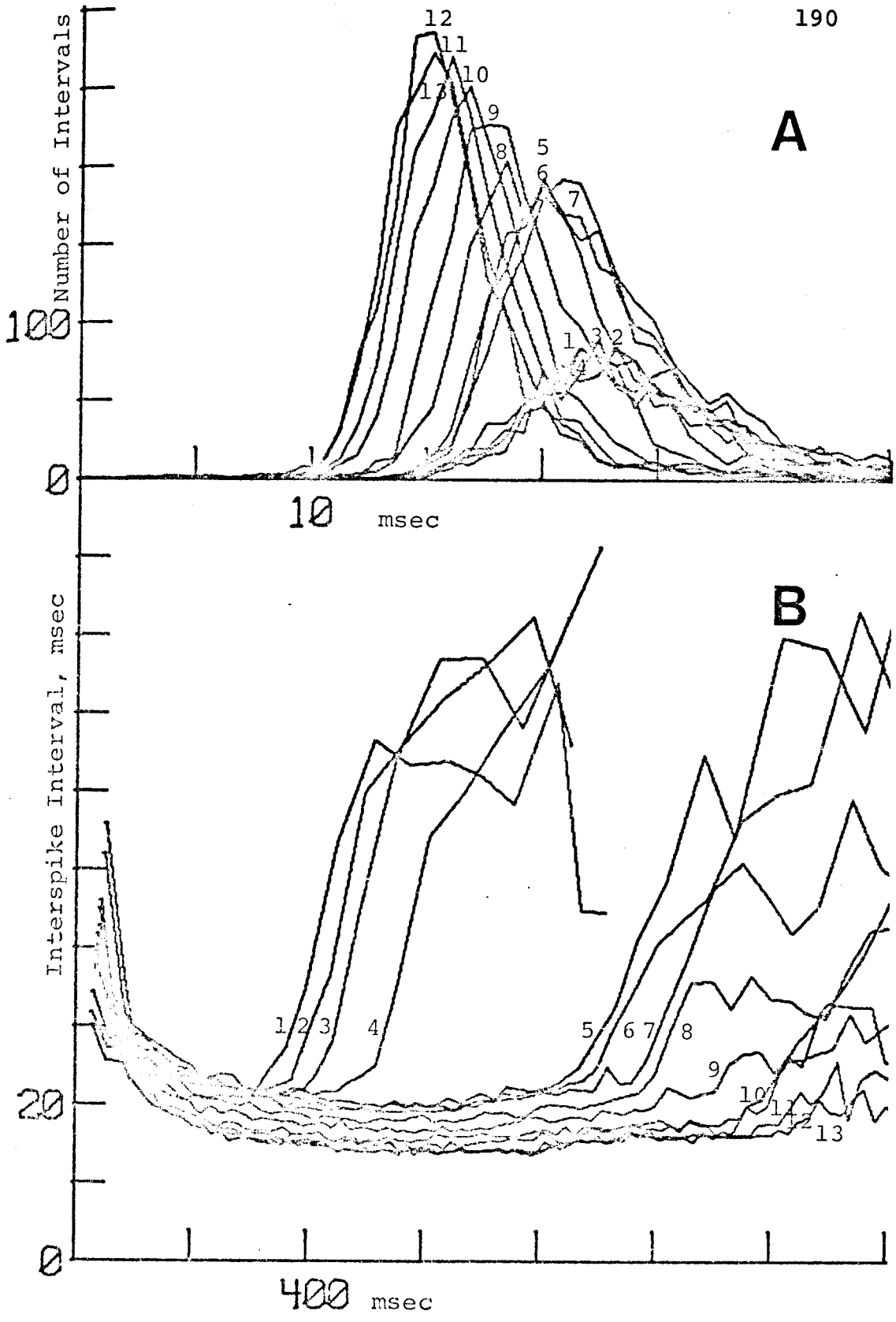

Figure 52. C83UIlL. Effect of cumulative doses of pentobarbital on histogram (A) and interspike interval modulation curve (B). Vagi intact.

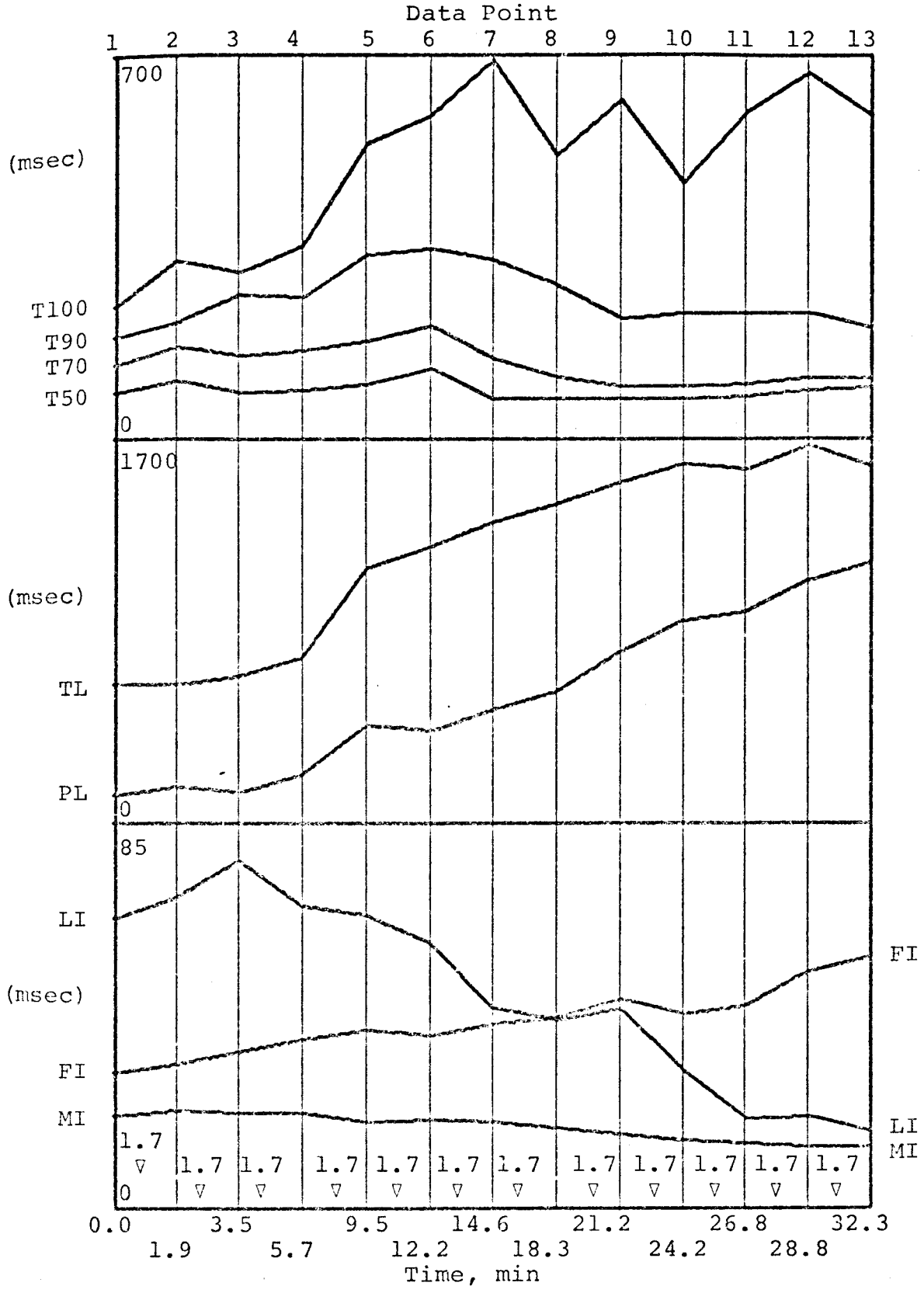

Figure 53A. C83UI1L. Effect of pentobarbital on parameters of inspiratory cell discharge. See text for details.

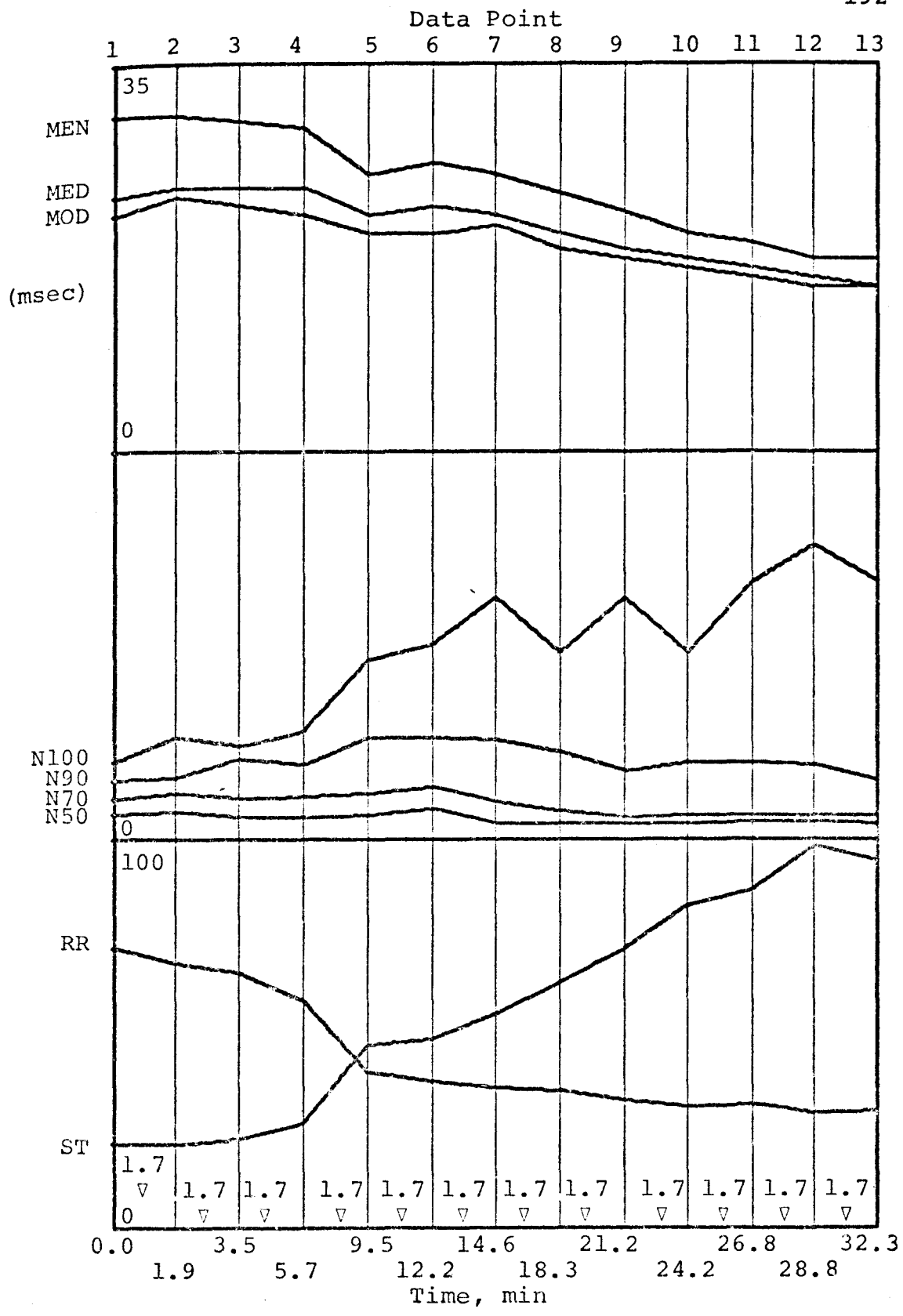

Figure 53B. C83UI11. Effect of pentobarbital on parameters of inspiratory cell discharge. See text for details.

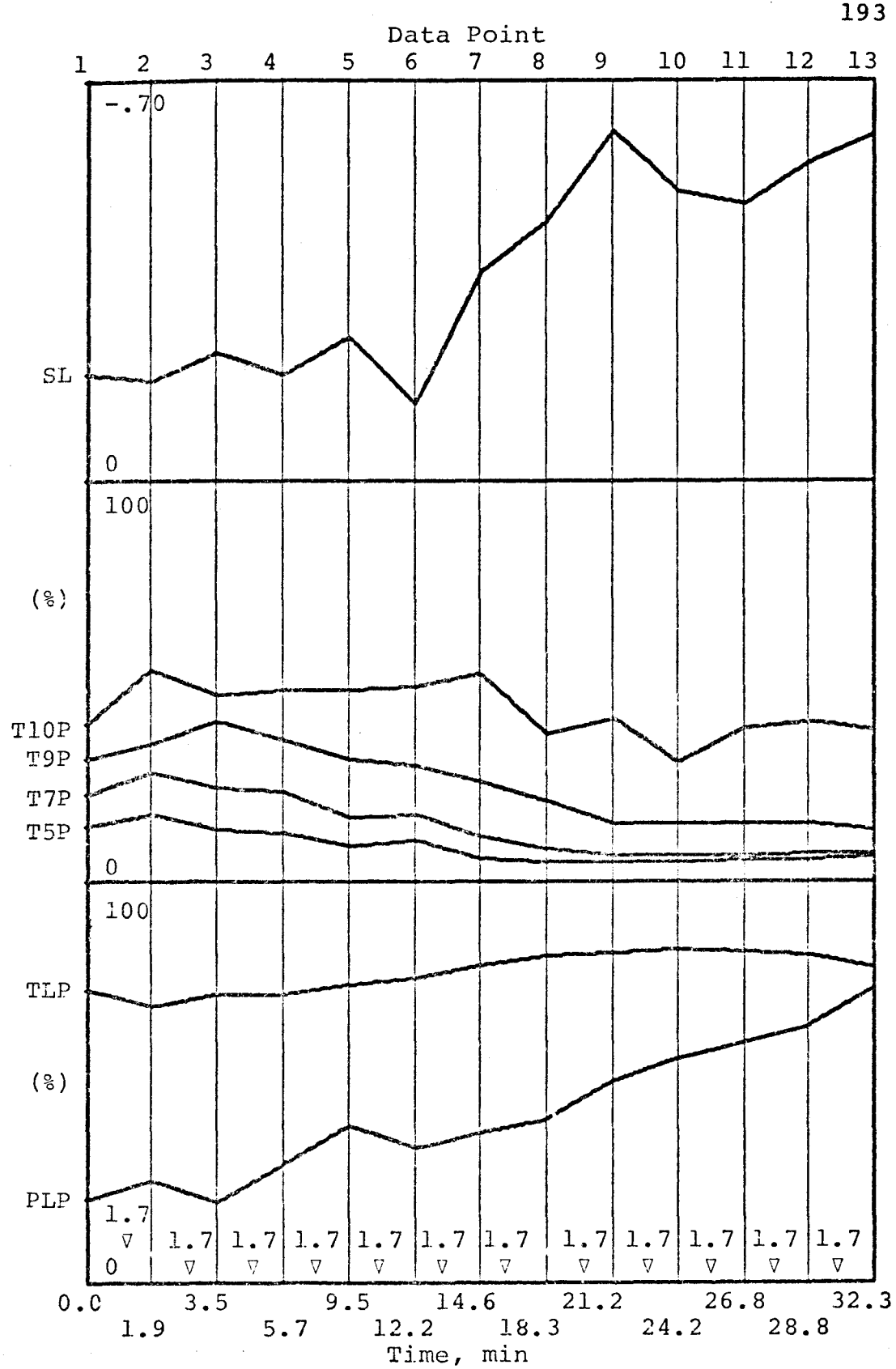

Figure 53C. C83UI1L. Effect of pentobarbital on parameters of inspiratory cell discharge. See text for details.

of pentobarbital, the first interval and the last interval change in opposite directions (Figures 52B and 53A). The slope again shows tendencies to increase at higher barbiturate doses. This is due mainly to first interval lengthening. Finally, the TLP remains independent of either rate or mode changes induced by pentobarbital depression. Single cell data and mean population data (Figures 35-43) are generally consistent for all parameters plotted as a function of rate, but not as a function of mode. The two significant exceptions are the regression of mode and last interval on respiratory rate.

The next inspiratory cell, C81UI5L, was selected to show single unit response to barbiturate depression in the absence of vagal afferent feedback. The data are shown in Figures 54 and 55 which can be correlated with the mean I-VO population data trends in Figures 35-43. Data point 1 represents a prevagotomy control. Data points 2 and 3 show parameter responses to section of the left ($\overset{LV}{\nabla}$) and right ($\overset{RV}{\nabla}$) vagus nerves respectively. Most parameter responses appear independent of unilateral vagotomy and become evident only after section of the second vagus nerve. The immediate effect of severing the left vagus on firing frequency is most likely related to the fact that this unit was located in the left medulla.

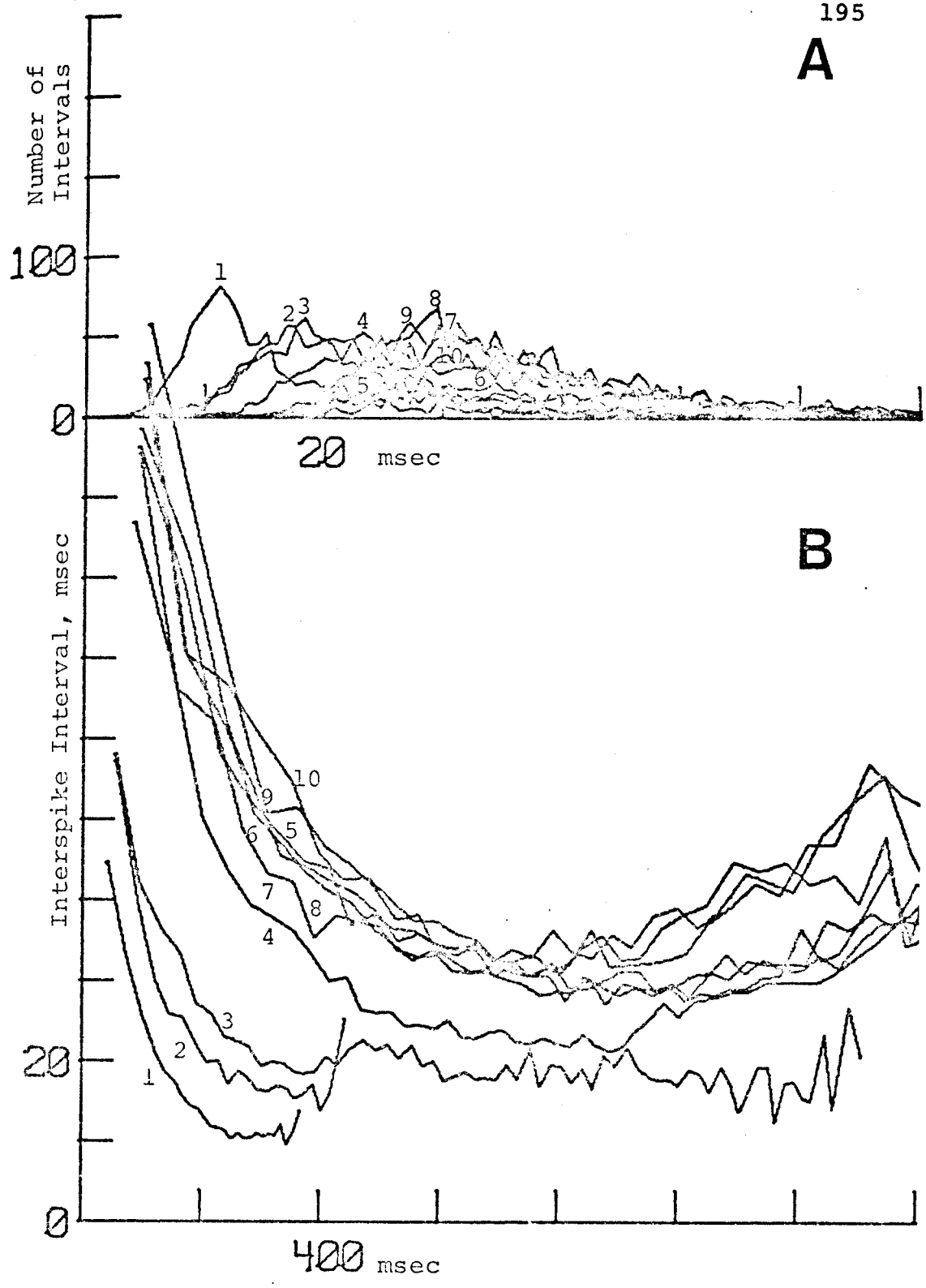

Figure 54. C81UI5L. Effect of cumulative doses of pentobarbital on histogram (A) and interspike interval modulation curve (B). Left vagus sectioned after #1; right vagus sectioned after #2.

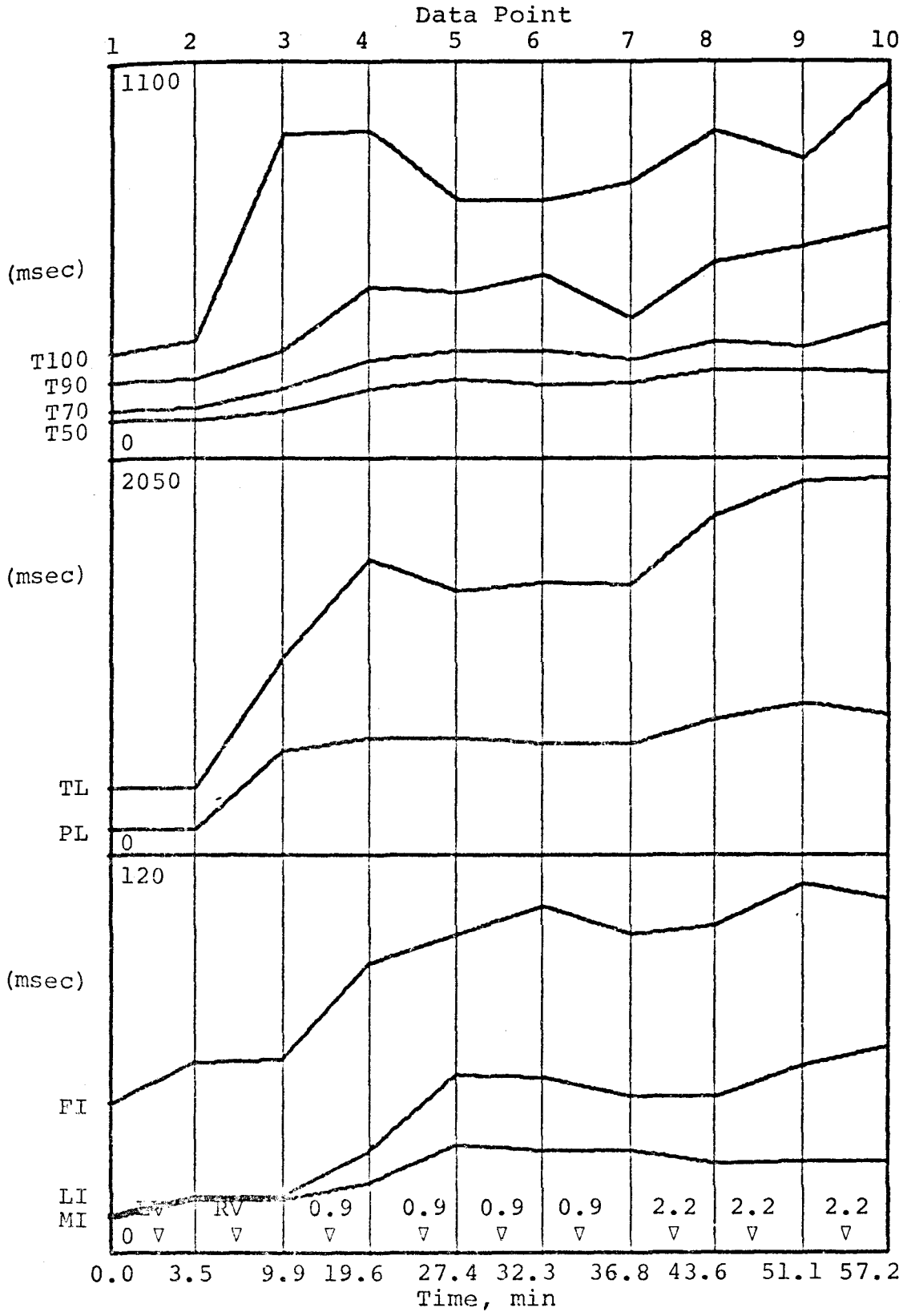

Figure 55A. C81UI5L. Effect of pentobarbital on parameters of inspiratory cell discharge. See text for details.

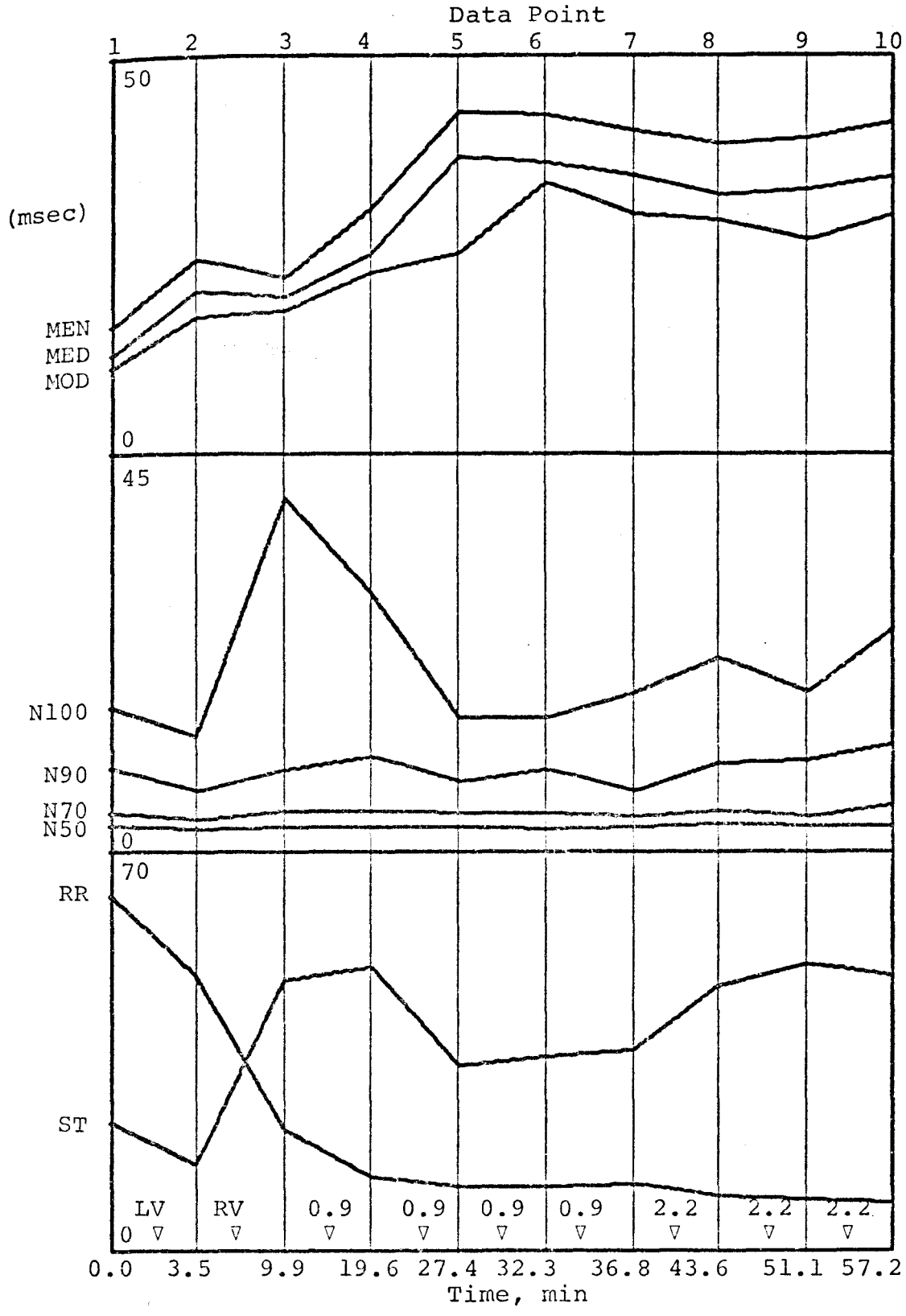

Figure 55B. C81UI5L. Effect of pentobarbital on parameters of inspiratory cell discharge. See text for details.

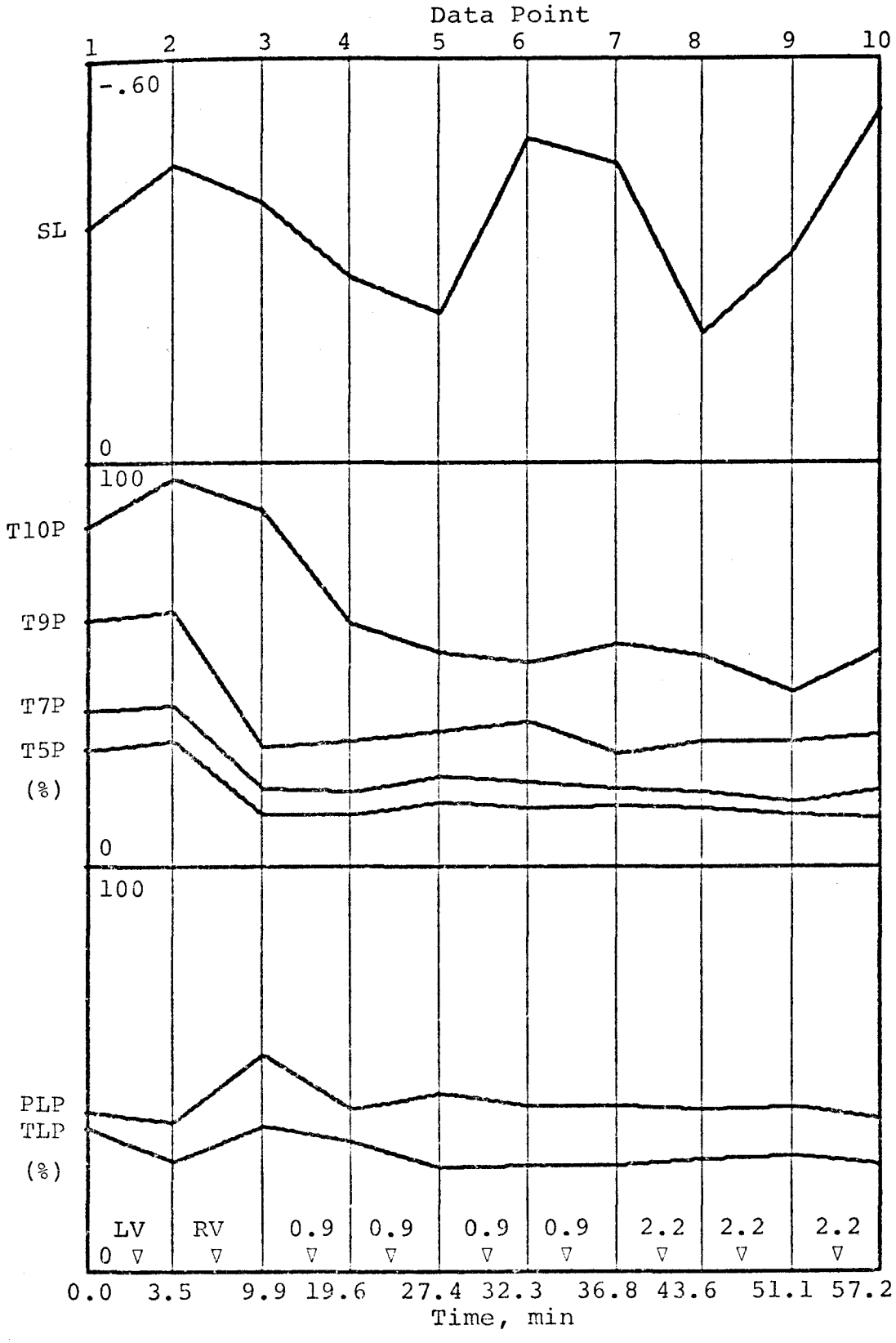

Figure 55C. C81UI5L. Effect of pentobarbital on parameters of inspiratory cell discharge. See text for details.

Starting with data point 3 as the vagotomized control, the parameters are plotted as a function of pentobarbital dose in Figure 55. Respiration rate decreases from 21.1 to 8.1 breaths per minute and mode time increases from 18.0 to 30.0 milliseconds. This is a typical depression response with the characteristic shift in the histogram to the right (Figure 54A) and an upward shift of the interspike interval modulation curve (Figure 54B). The train length increases, but due to the depression in firing frequency, the spikes per train remains relatively constant. The reciprocal relationship between ST and RR seems to be lost when the vagi are cut, at least for this cell. All other parameters follow predicted directional changes during rate and firing frequency depression when compared to the mean population data (Figures 35-43). It can be noted that the slope data are very unpredictable.

The responses of two expiratory cells during barbiturate accumulation are presented to show not only individual characteristics, but to reveal pattern similarities to inspiratory cells already discussed. The vagi are intact for each expiratory cell, which allows comparisons to be made with the mean E-VI population data in Figures 35-43. The data from the first expiratory

cell, C64UE4R, are plotted in Figures 56 and 57. Respiration rate decreases from 86.6 to 40.5 breaths per minute during pentobarbital depression while the mode shows little change except for a significant decrease from 17.2 to 12.4 milliseconds at data point 4. This single shift in the histogram can be seen in Figure 56A. As with inspiratory cells, the train length greatly increases (Figures 56B and 57A) which causes an increase in the spikes per train. An inverse relationship between ST and RR is thus established. A small increase in the plateau level is also observed. The T50, T70, T90 and T100 parameters tend to increase indicating that pentobarbital modifies the expiratory discharge pattern such that it takes more time to reach portions of the way to the minimum interval. These increases parallel train length increase since T5P, T7P, T9P and T10P measurements remain approximately constant for most of the drug range. The first, last and minimum intervals increase significantly, slightly and not at all as a function of accumulated drug respectively. The N parameters appear to be independent of drug modification except for N100 which increases after three pentobarbital injections. The slope response appears randomized as in other cells. Finally, TLP remains relatively constant indicating that this expiratory cell always fires

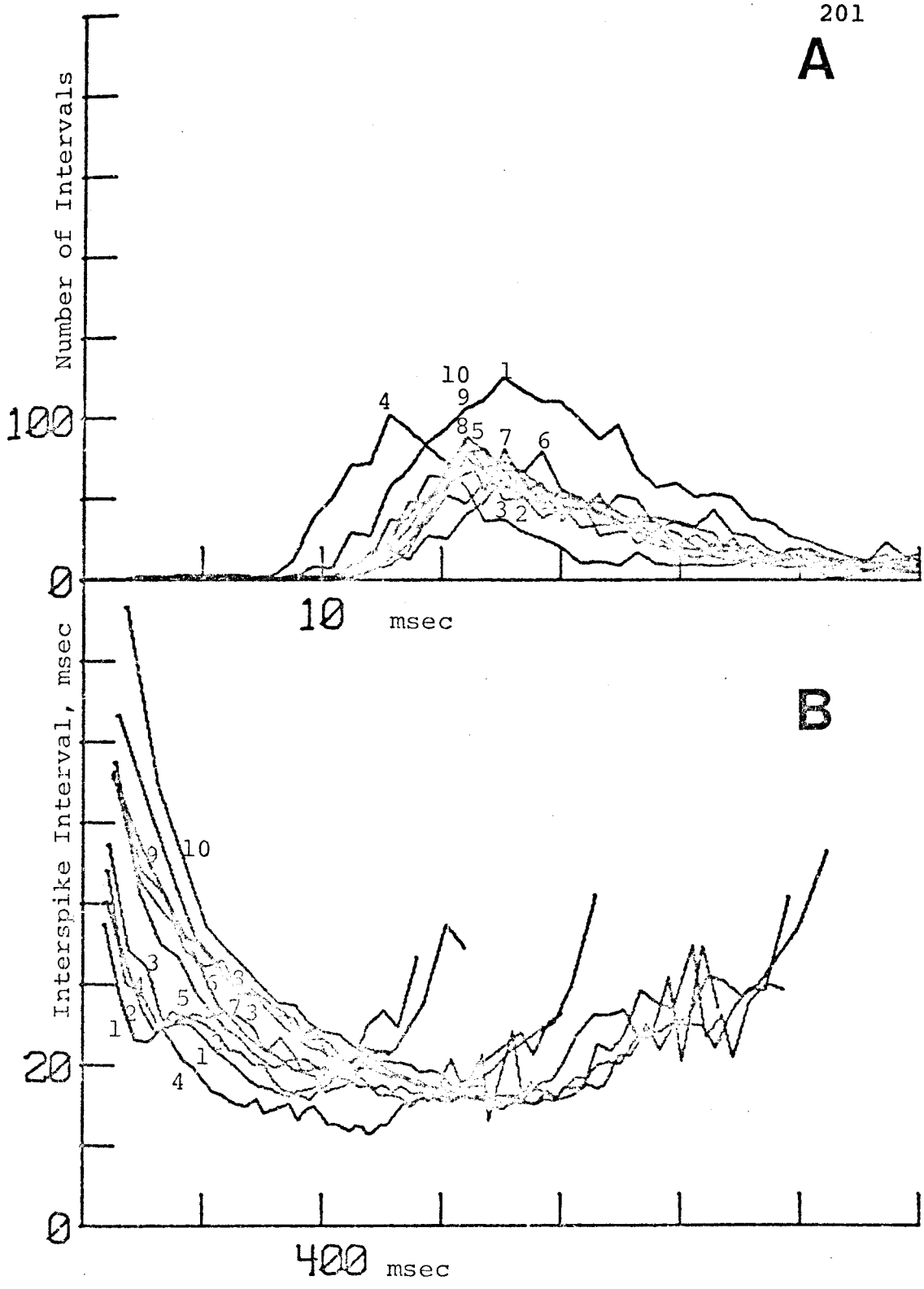

Figure 56. C64UE4R. Effect of cumulative doses of pentobarbital on histogram (A) and interspike interval modulation curve (B). Vagi intact.

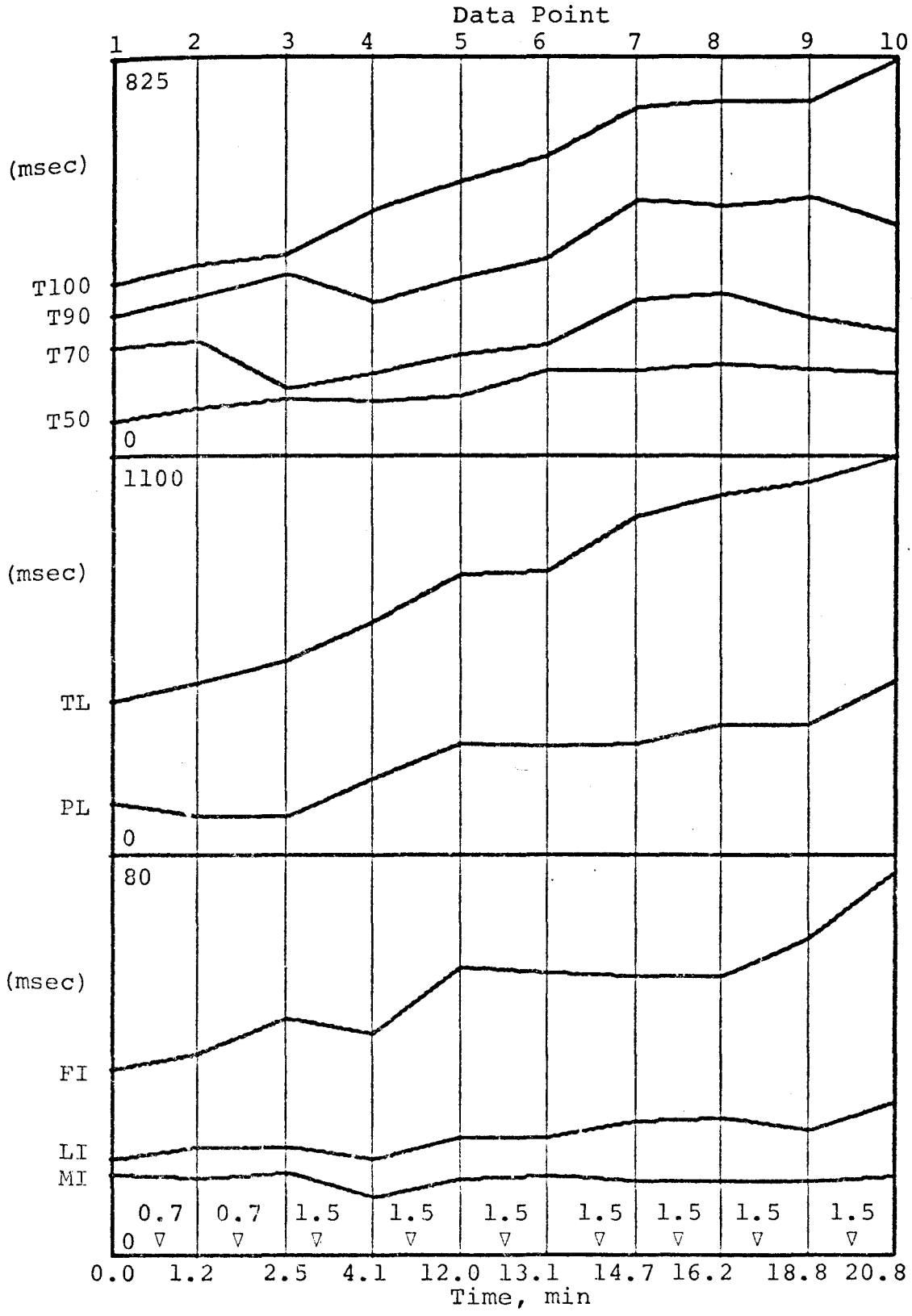

Figure 57A. C64UE4R. Effect of pentobarbital on parameters of expiratory cell discharge. See text for details.

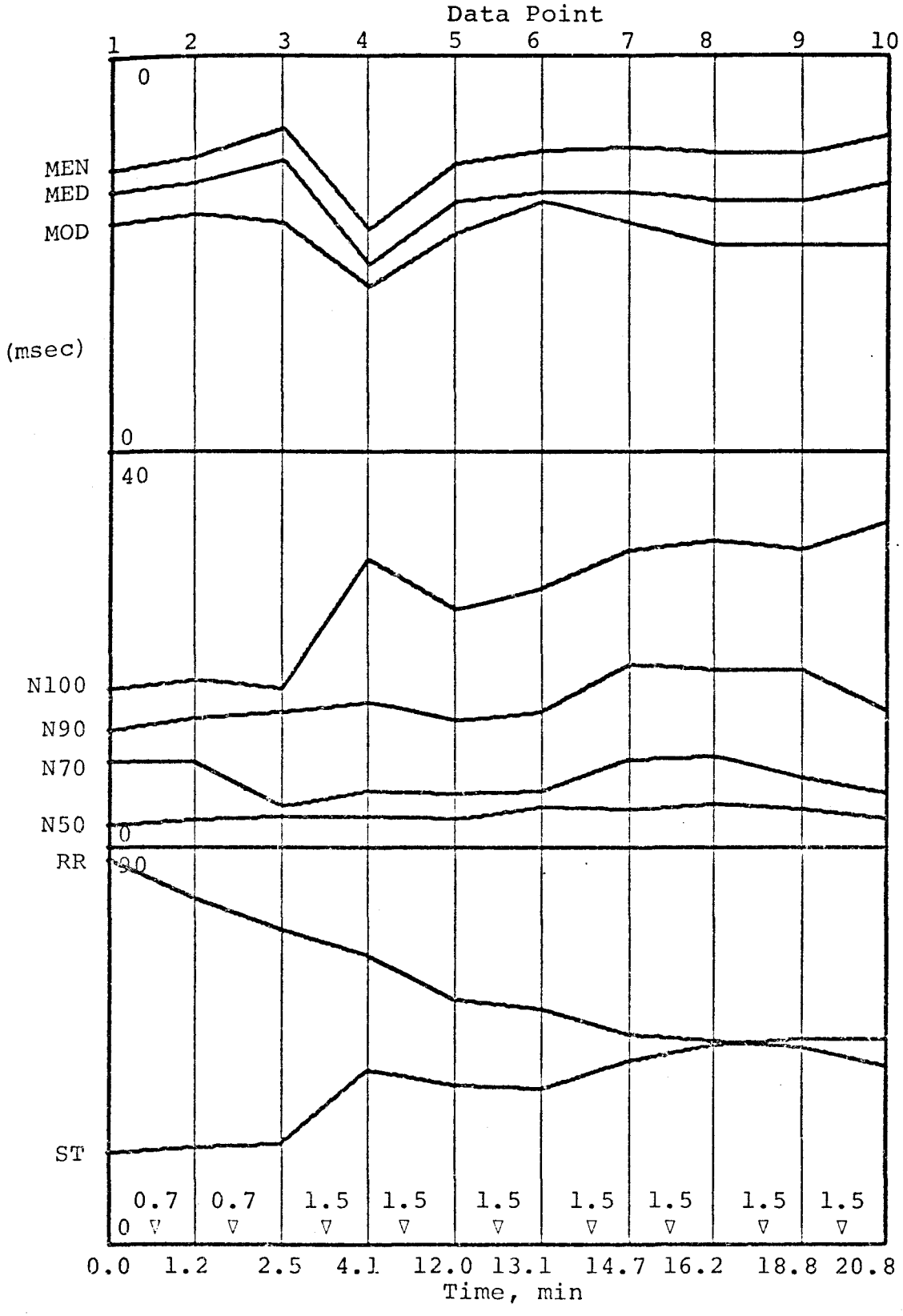

Figure 57B. C64UE4R. Effect of pentobarbital on parameters of expiratory cell discharge. See text for details.

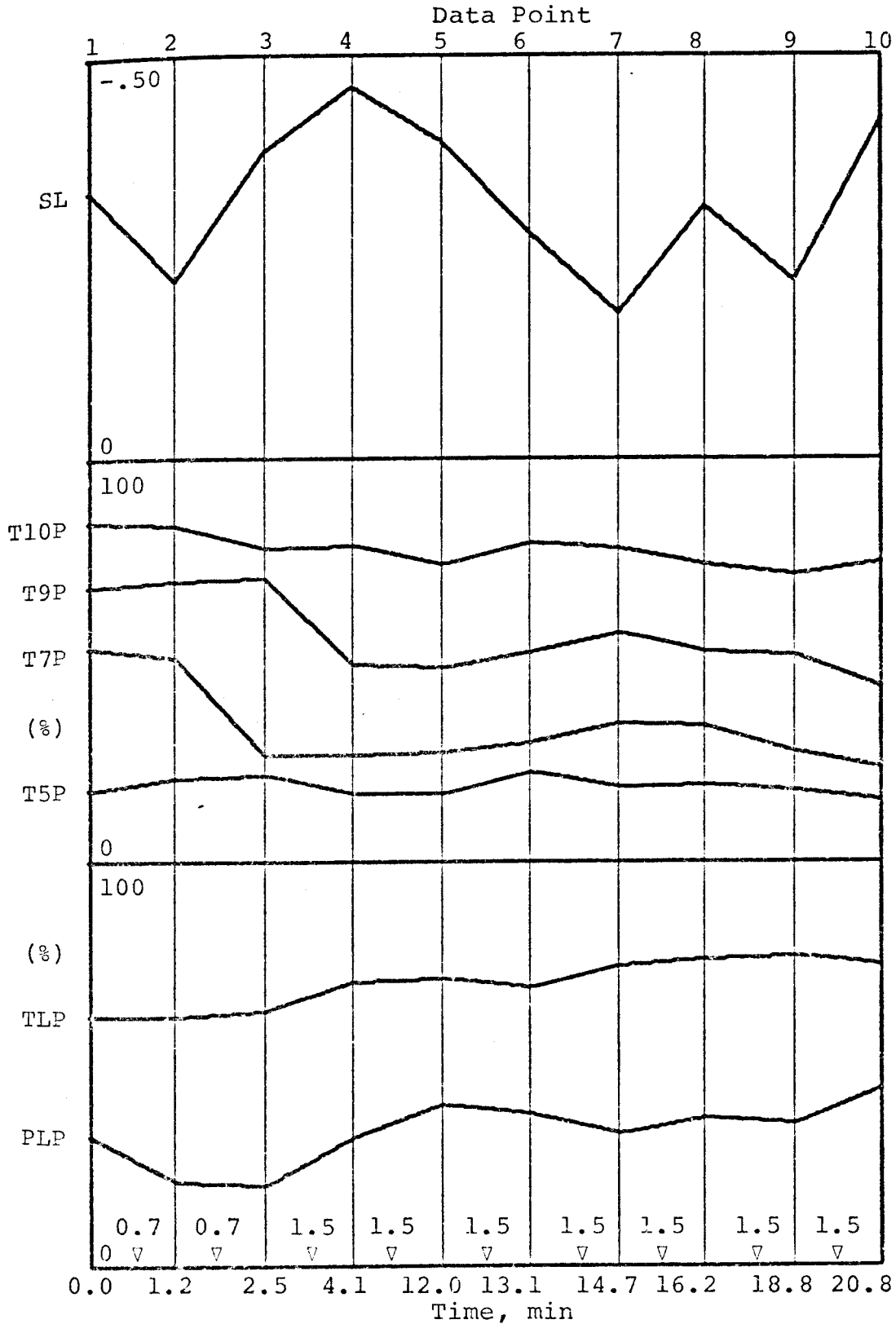

Figure 57C. C64UE4R. Effect of pentobarbital on parameters of expiratory cell discharge. See text for details.

for the same fraction of the respiratory cycle, regardless of the respiratory rate. All of these single cell observations on expiratory cell C64UE4R follow the mean E-VI population trends in Figures 35-43. It is significant that no outstanding differences between expiratory and inspiratory single cell responses to barbiturate depression can be observed.

Data from the second expiratory cell, C71UE2R, are presented in Figures 58 and 59. Successive barbiturate injections depressed the respiratory rate from 21.6 to 11.5 breaths per minute, but produced a triphasic shift in the mode. The mode first increased from 14.0 to 40.4 milliseconds, then decreased to 26.8 milliseconds and finally increased to 42.0 milliseconds. This can be seen as an inflection in the mode, median and mean curves between data points 9 and 12 in Figure 59B. Every other data point is plotted in Figure 58 to clarify histogram and interspike interval modulation curve shifts. This effect is best seen in Figure 58B. Increasing dosage of pentobarbital first causes an upward shift in the interspike interval modulation curve (data points 1, 3, 5, 7, 9), then a downward shift occurs (data point 11) followed by a final upward shift (data point 13). This pattern resembles the activation of

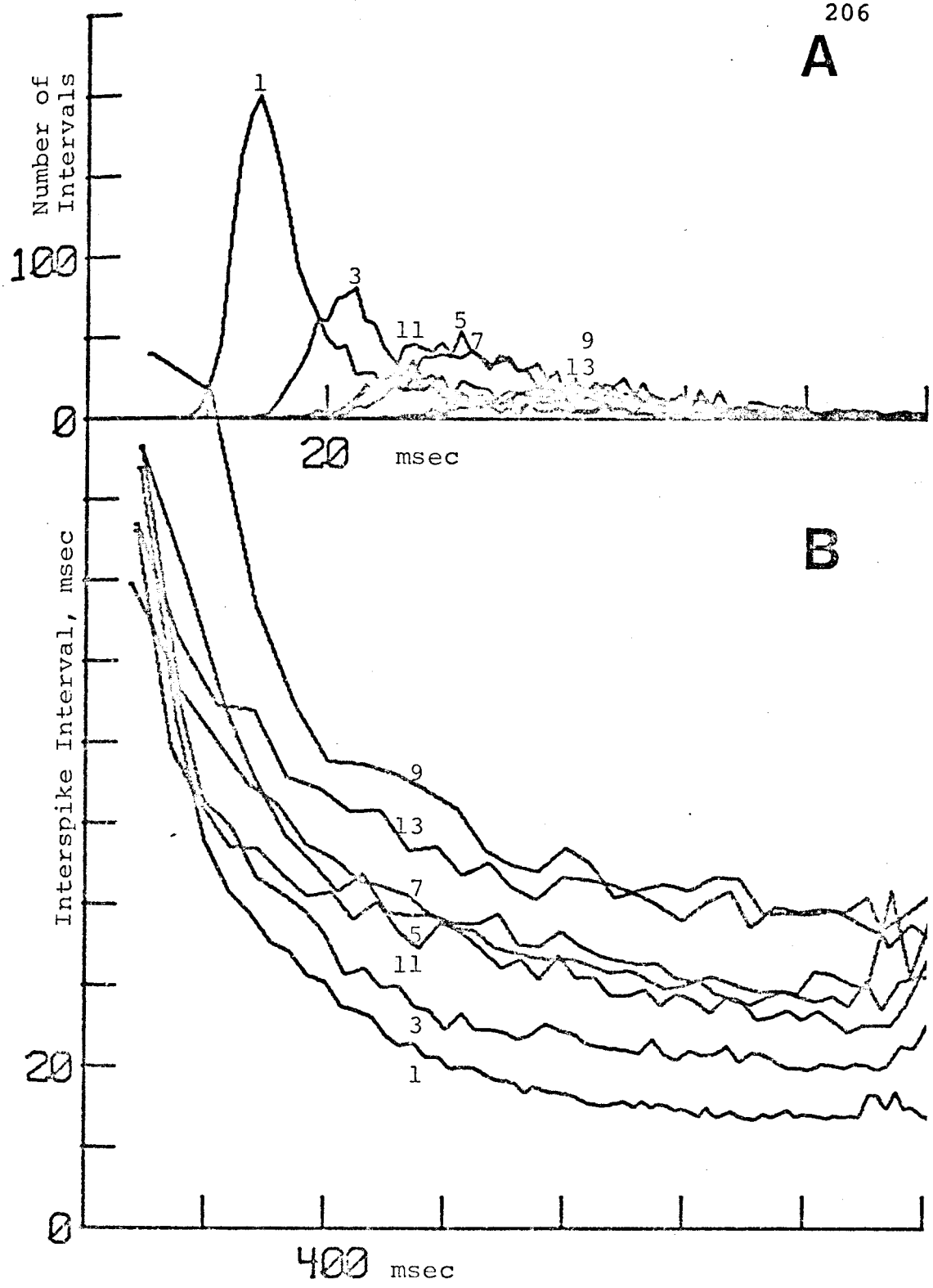

Figure 58. C71UE2R. Effect of cumulative doses of pentobarbital on histogram (A) and interspike interval modulation curve (B). Vagi intact.

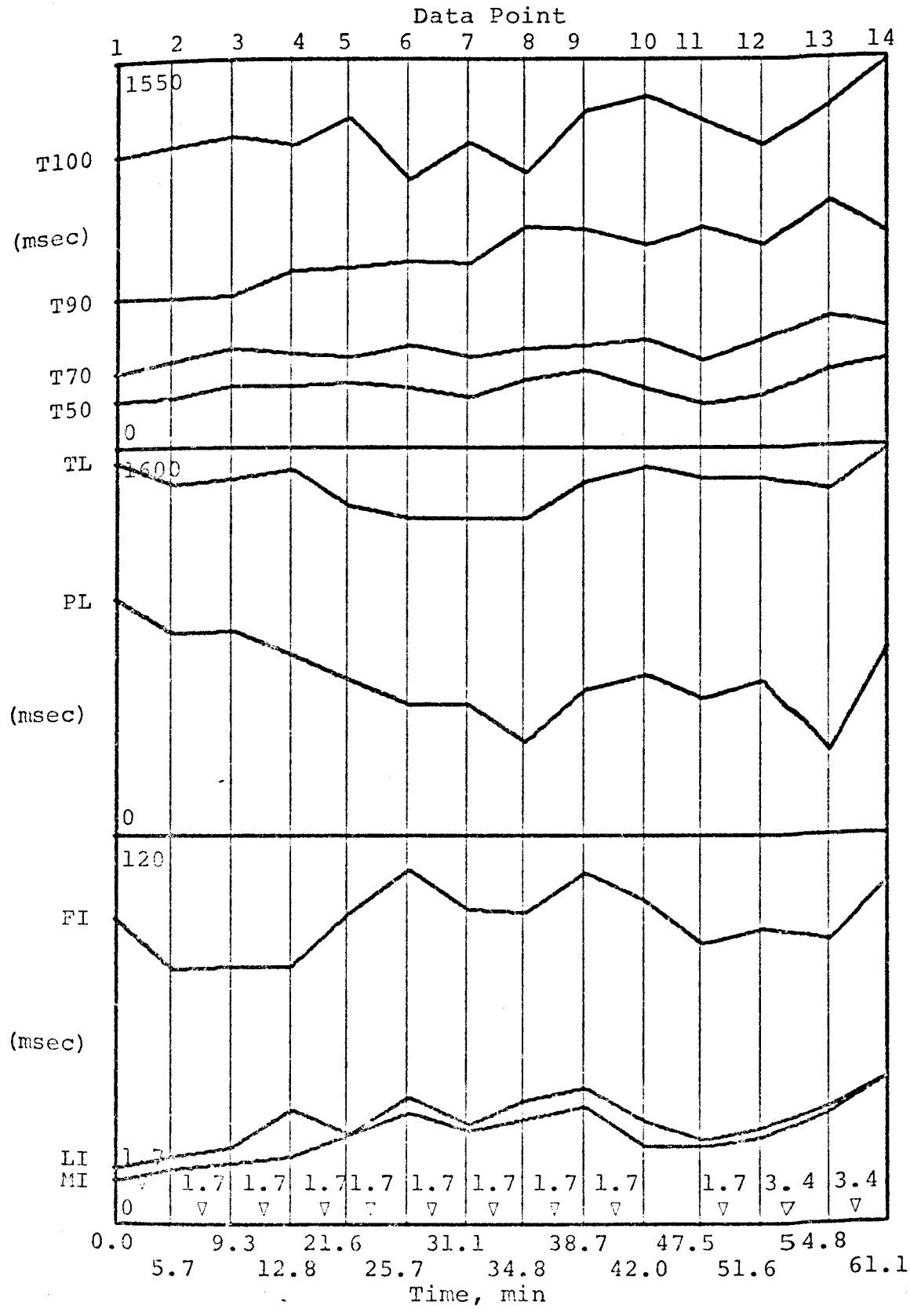

Figure 59A. C71UE2R. Effect of pentobarbital on parameters of expiratory cell discharge. See text for details.

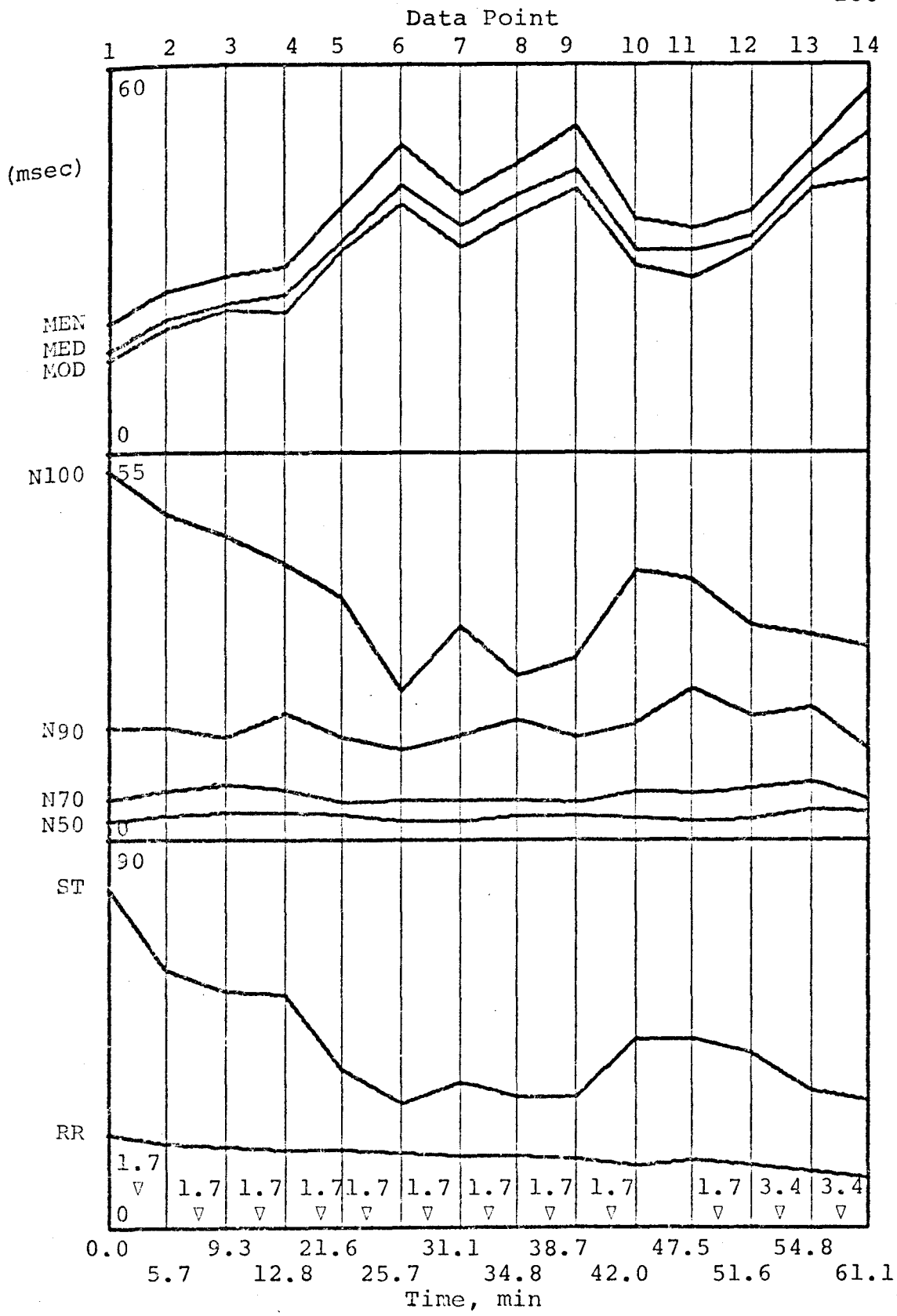

Figure 59B. C71UE2R. Effect of pentobarbital on parameters of expiratory cell discharge. See text for details.

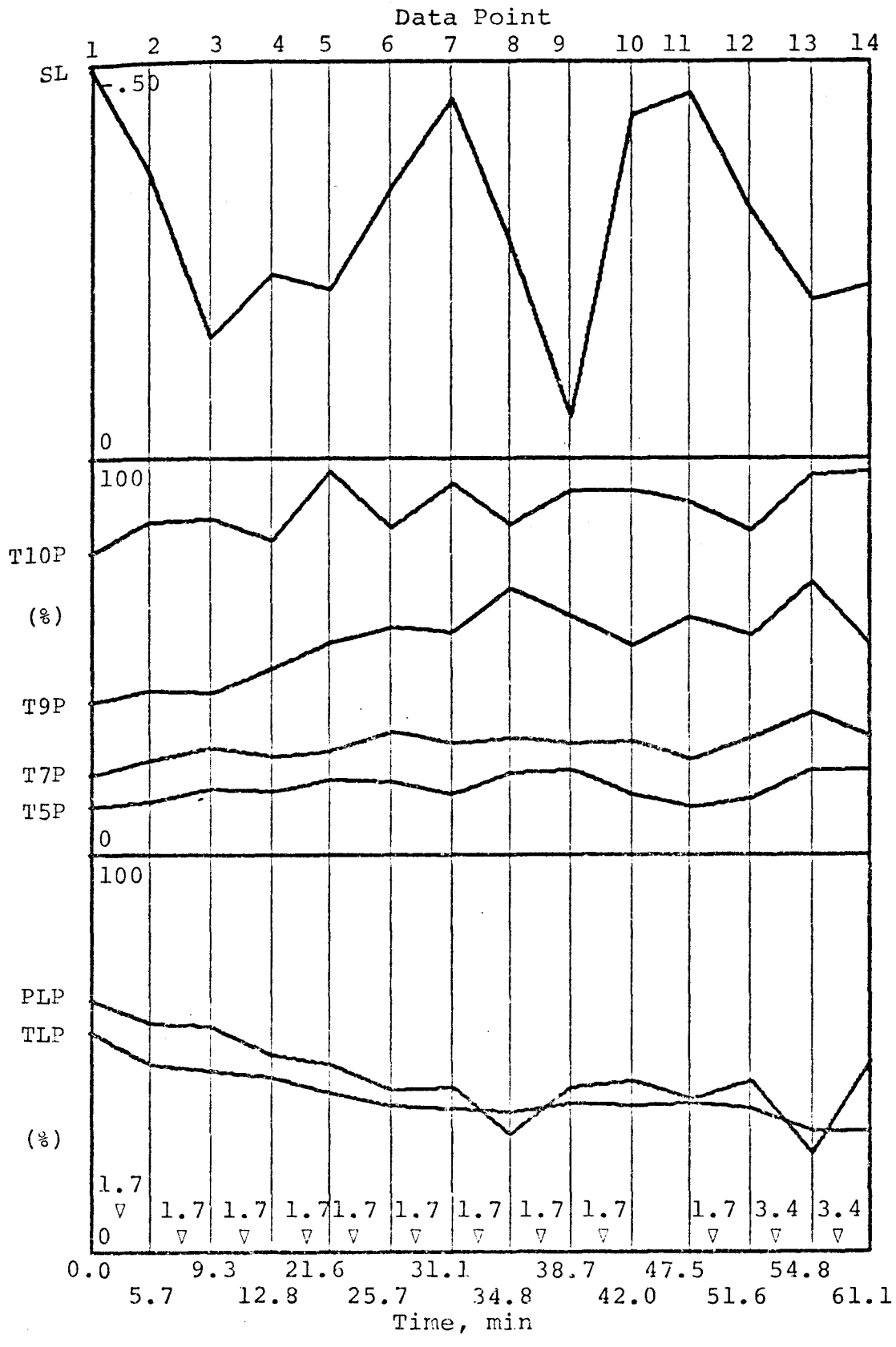

Figure 59C. C71UE2R. Effect of pentobarbital on parameters of expiratory cell discharge. See text for details.

inspiratory cell C83UI1L (Figures 50 and 51) during barbiturate administration and will be examined later.

Expiratory cell C71UE2R exhibits several atypical parameter responses during barbiturate depression. For example, pentobarbital has no effect on modifying the train length, a response which was observed consistently for other cells. For this reason, spikes per train mirror changes in the mode and the inverse relationship with respiratory rate is lost. Also, for the first time, the plateau level is seen to decrease as a function of barbiturate dose. Since the train length is not changing, PLP parallels the plateau level decrease and TLP decreases due to a lengthening of the respiratory cycle. The first, minimum and last intervals show variable fluctuations while N50, N70 and N90 parameters appear to be independent of pentobarbital effects. The N100 measurement, however, parallels the spikes per train and generally decreases at higher drug levels. A similar directional change for N100 is observed for inspiratory cell, C81UI5L (Figures 54 and 55) recorded when vagal afferents were removed. The slope pattern for this expiratory cell is very irregular and yields no useful information. Comparison of these parameter responses to the mean population data in Figures 35-43 reveals many

individual differences.

Another expiratory cell, C82UE3R, was examined during morphine administration as shown in Figures 60 and 61. Pattern shifts induced with morphine were considerably different from those seen in expiratory cells during barbiturate administration (Figures 56-59). After a small decrease in respiration rate from 29.4 to 24.0 breaths per minute, the rate was facilitated up to 53.8 with cumulative doses of morphine. This unexpected species-specific result may be attributed to sensitization of pulmonary receptors. A true depression of the discharge frequency is observed as shown by the shift to the right in the histogram distribution (Figure 60A) and the increased mean, median and mode times (Figure 61B). Figure 61 shows that most parameters are decreased by morphine. These effects are in direct opposition to those seen during pentobarbital depression of expiratory cells, but strict comparisons must be avoided since respiration rate alterations with each drug are going in reverse directions. These data indirectly demonstrate that morphine and pentobarbital probably act via different mechanisms. This is a significant observation worthy of further exploration.

Finally, the quantitative effects of vagotomy on

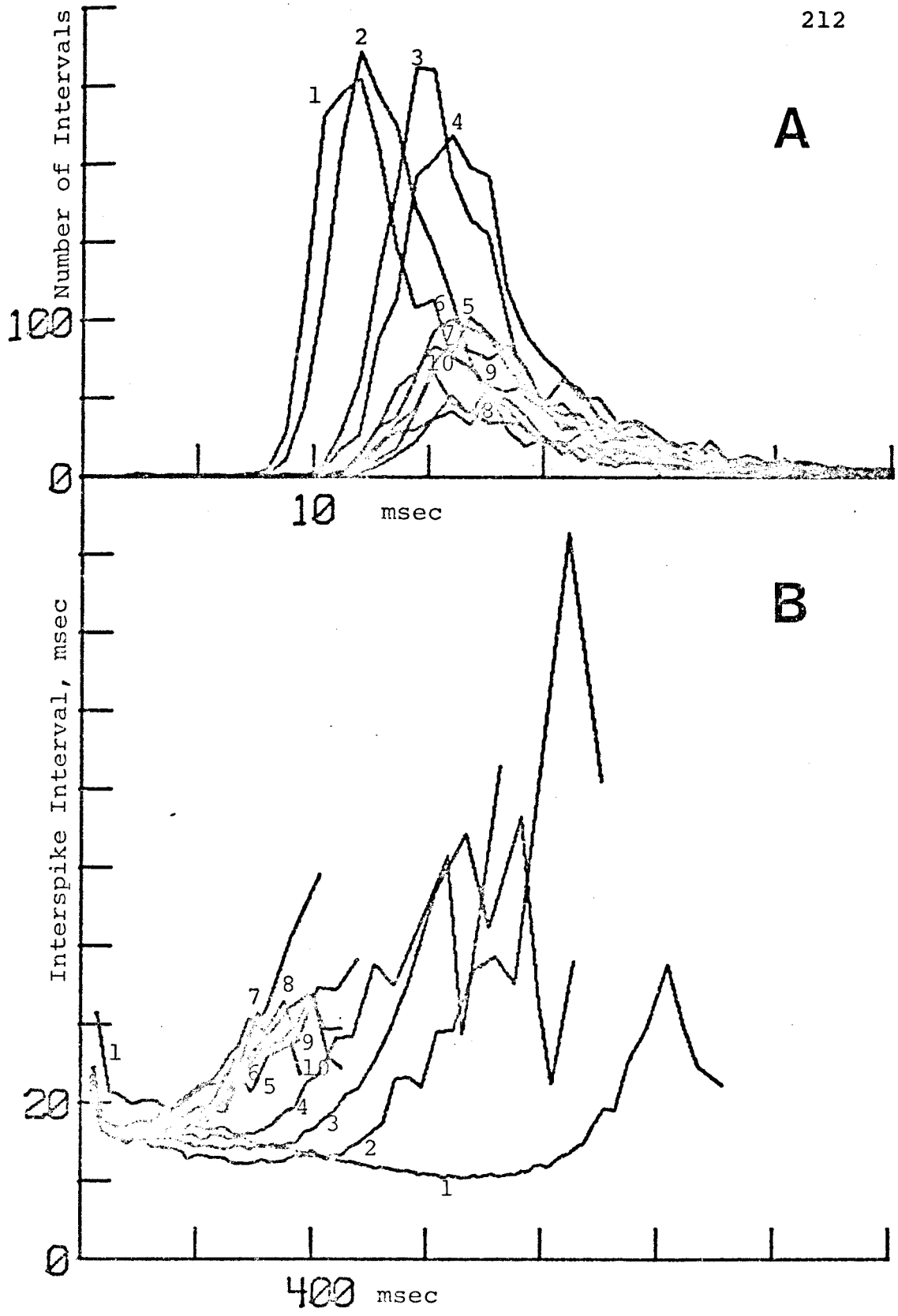

Figure 60. C82UE3R. Effect of cumulative doses of morphine sulphate on histogram (A) and interspike interval modulation curve (B). Vagi intact.

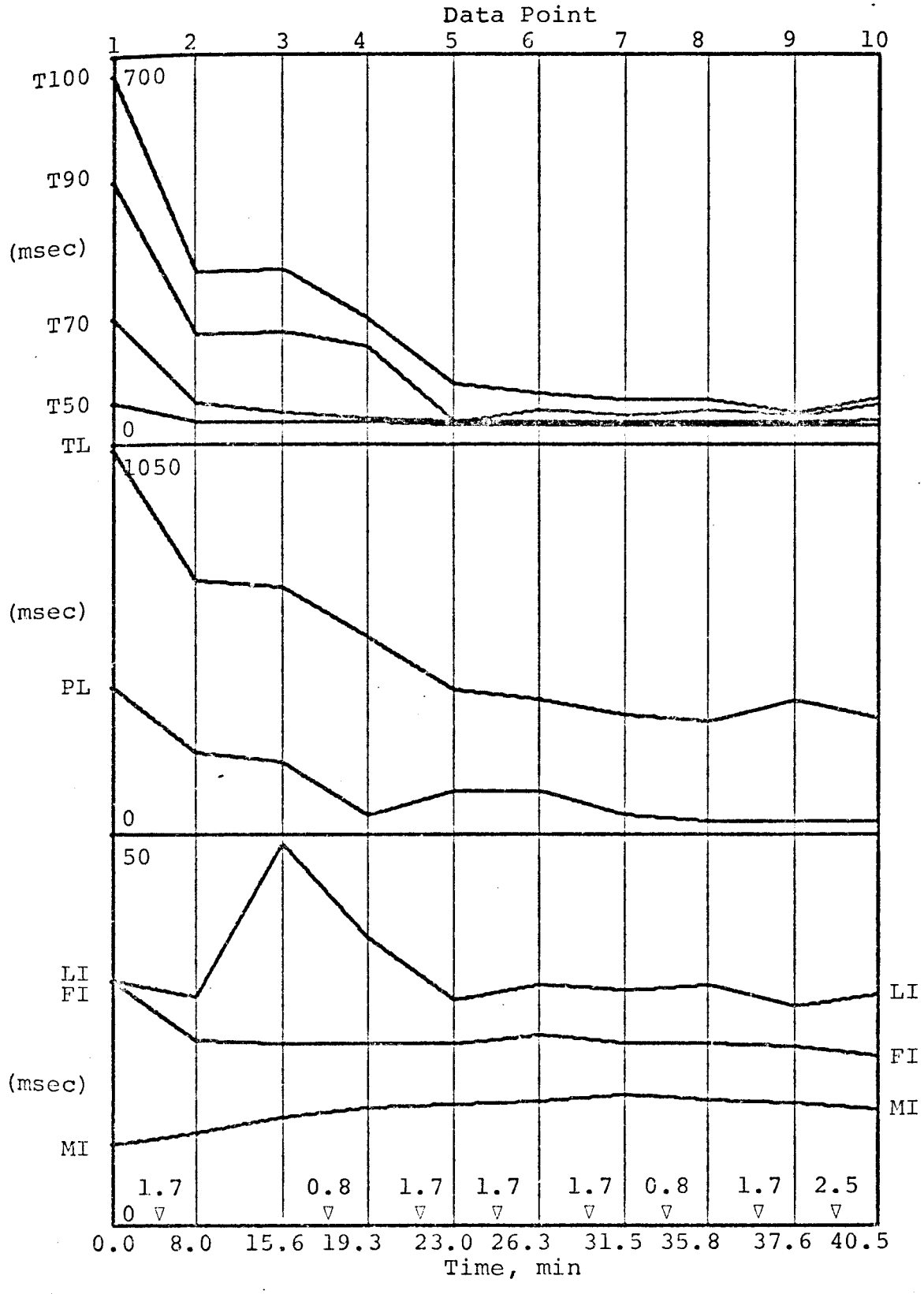

Figure 61A. C82UE3R. Effect of morphine on parameters of expiratory cell discharge. See text for details.

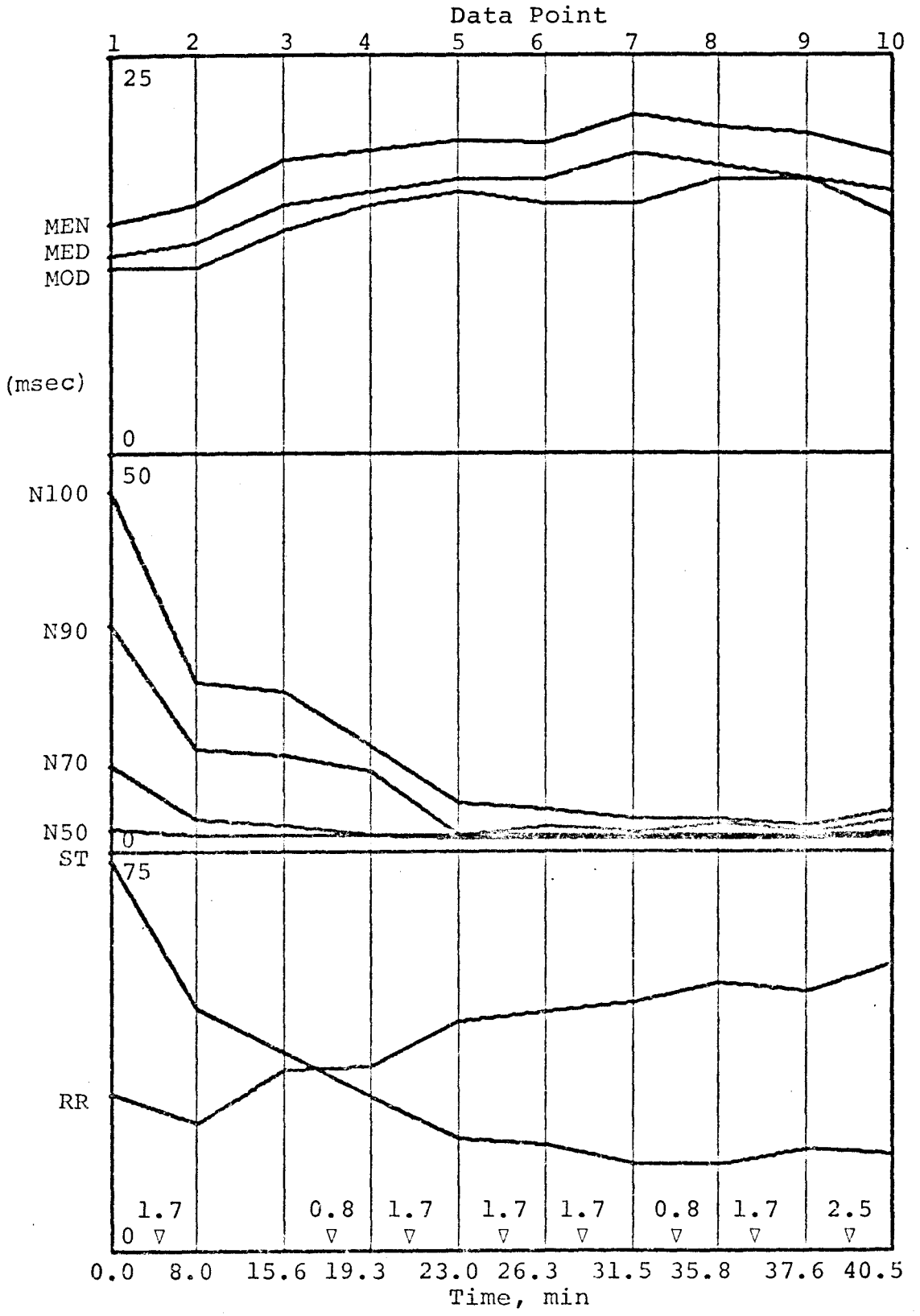

Figure 61B. C82UE3R. Effect of morphine on parameters of expiratory cell discharge. See text for details.

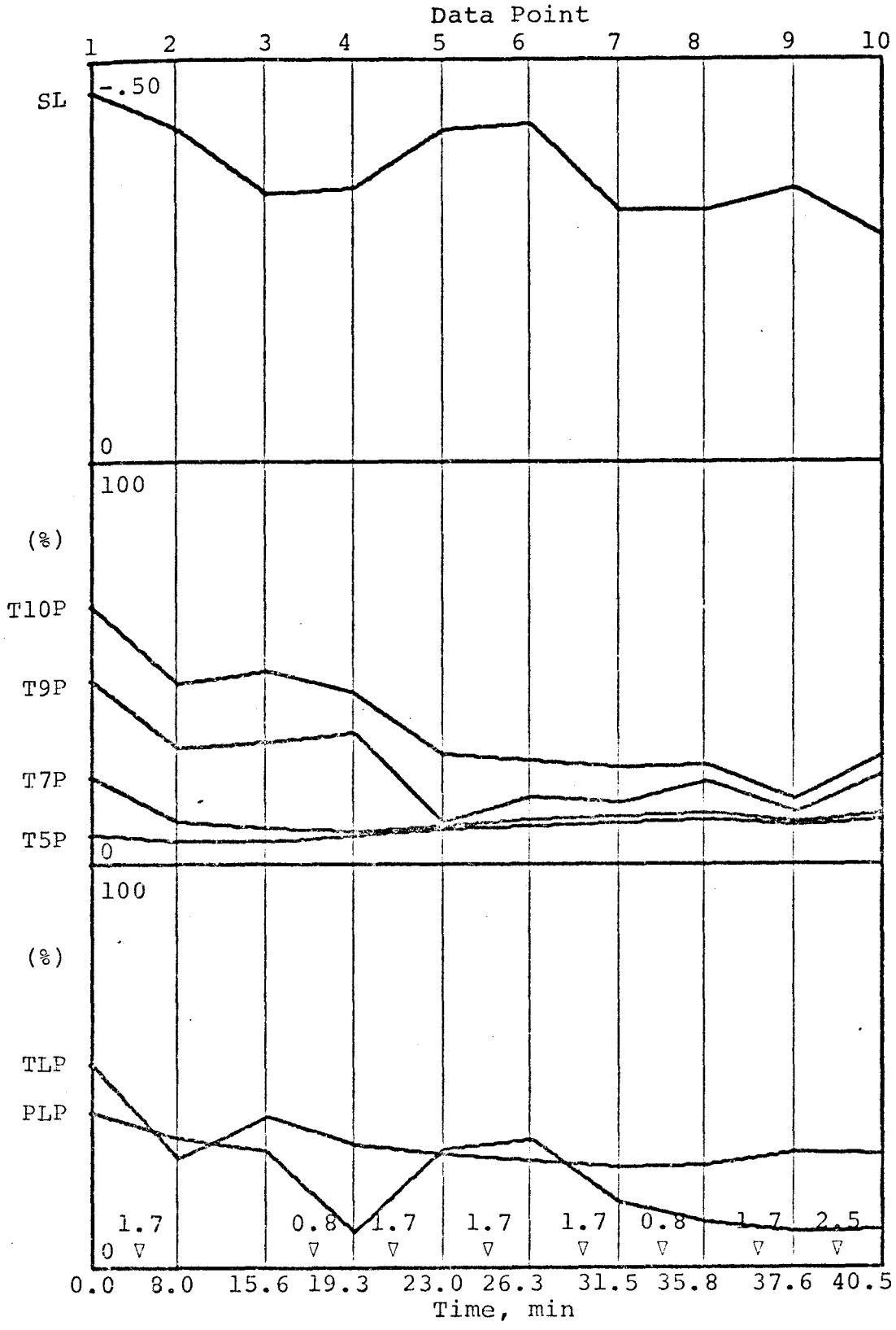

Figure 61C. C82UE3R. Effect of morphine on parameters of expiratory cell discharge. See text for details.

expiratory cell C68UE6R are shown in Figure 62. The first steady state measurement (Curve 1) is a prevagotomized control. One half a minute after cutting the left vagus nerve, a new steady state discharge was attained. The histogram was shifted to the right (Figure 62A) and the modulation curve shifted upward (Curve 2). After an additional 1.7 minutes, the curves assumed position 3. These shifts corresponded to an increase in the mode time from 10.8 to 19.6 to 30.8 milliseconds. This was associated with small respiratory rate decreases from 65.3 to 59.4 to 57.0 breaths per minute. The discharge pattern was analyzed up to 4.8 minutes after the initial unilateral vagotomy, but did not differ significantly from Curve 3. However, subsequent sectioning of the right vagus immediately terminated the expiratory discharge. Since the cell was anatomically located in the right medulla, it is postulated that the right vagal afferents were responsible for the activation of this expiratory unit. Removal of these afferents inhibited unit discharge. These vagotomy effects on an expiratory cell can be compared to the response of inspiratory cell C81UI5L in Figures 54 and 55 subjected to similar procedures.

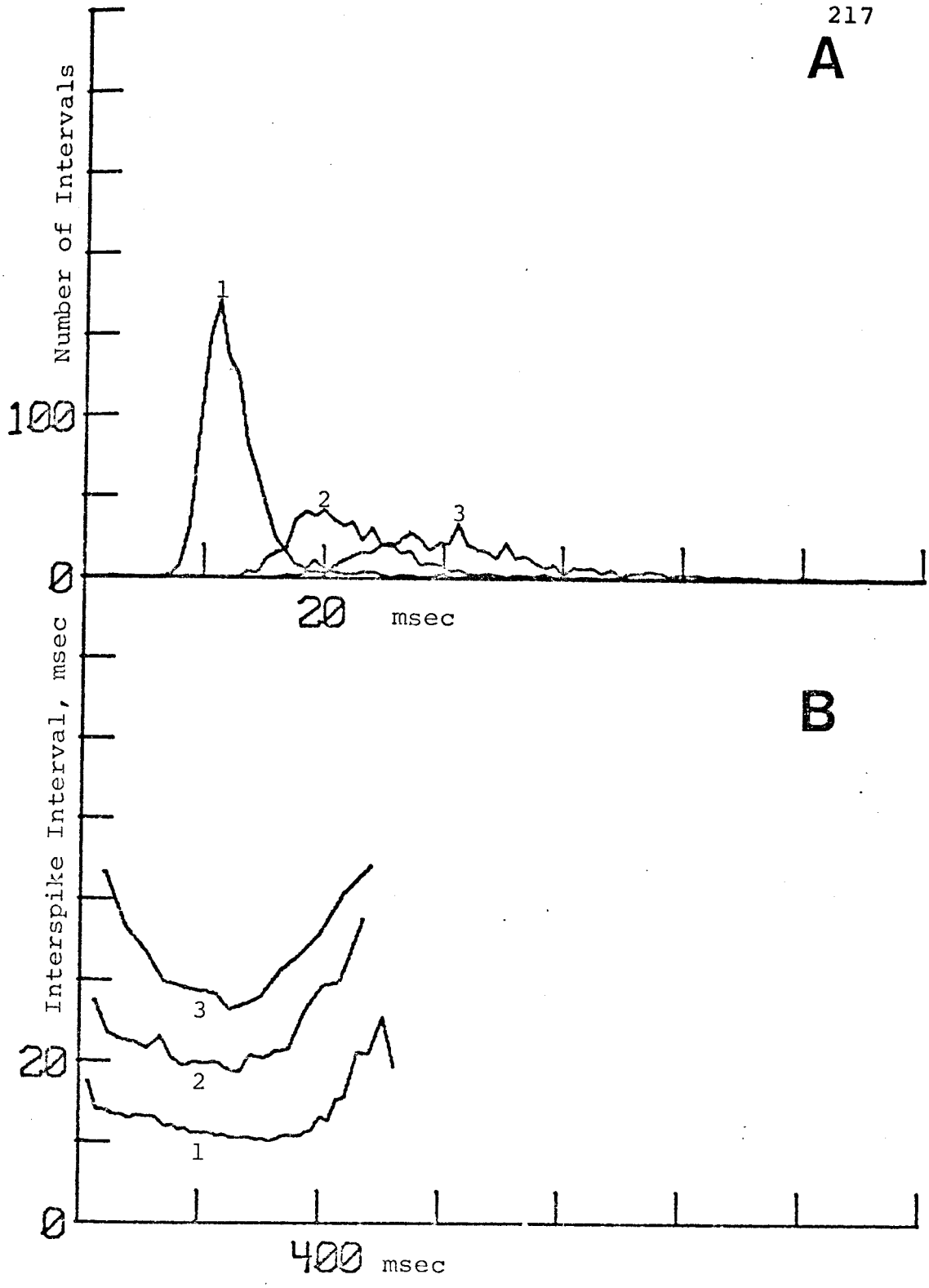

Figure 62. C68UE6R. Histogram (A) and interspike interval modulation curves (B) before (Curve 1) and after (Curves 2 and 3) unilateral left vagotomy.

D. Barbiturate Apneusis

During single cell depression studies, it was frequently observed that apneustic breathing patterns could be induced after summation of several serial injections of a barbiturate (pentobarbital or thiopental sodium). This well documented phenomenon (cf. Literature Review) was further investigated to facilitate interpretation of the mean population regressions (Figures 11-43) and single cell data (Figures 50-59) previously presented.

Classically, apneusis in the cat can be produced by surgical removal of the rostral pons (pneumotaxic area) coupled with bilateral vagotomy. This is illustrated in Figure 63. Previous to this record, the cerebellum of cat 12 was removed and the brainstem was transected at the level of the inferior colliculi. The cat continued to breathe rhythmically at about five breaths per minute and this breathing pattern was not altered significantly by unilateral vagotomy on the left side. Subsequent section of the right vagus nerve, however, initiated a sustained inspiratory effort as seen in the intrapleural pressure tracing (IPP). Clearly, pneumotaxic and vagal mechanisms play important roles in the maintenance of eupneic respiration. The literature also implicates the cerebellum as an additional source of inspiratory inhibition.

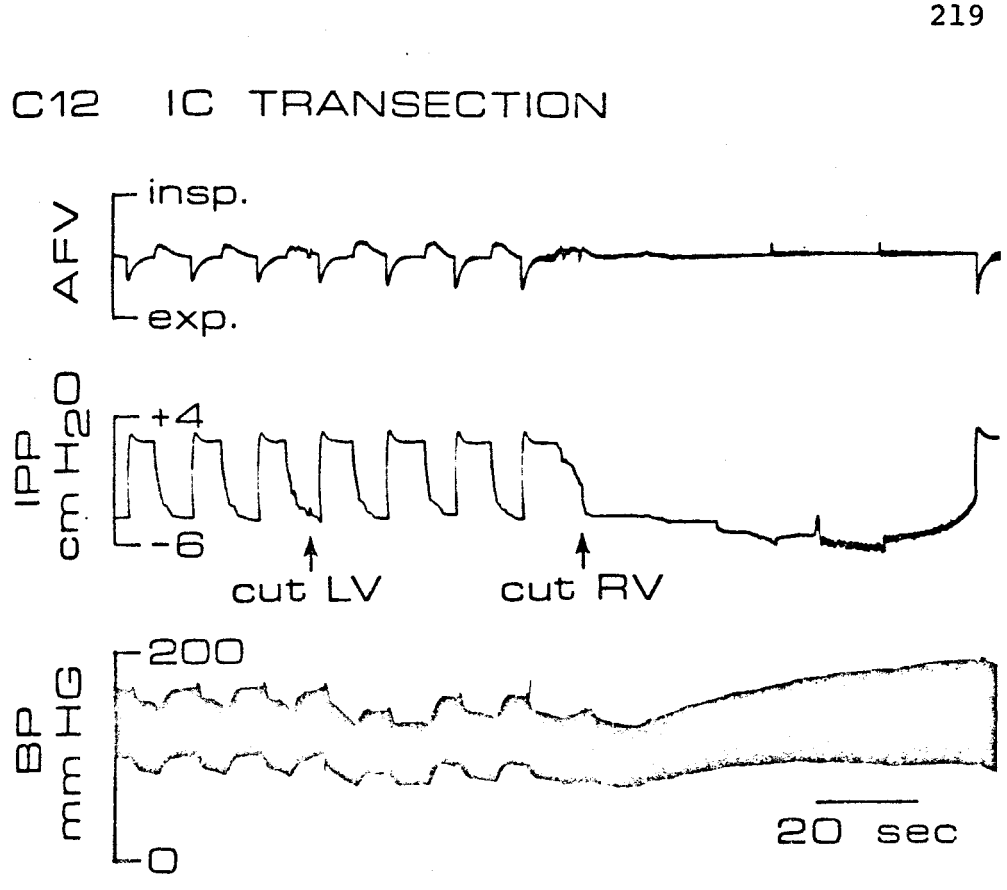

Figure 63. Genesis of classical apneusis in the cat. Prior to the beginning of record an inferior collicular transection was made. The left (LV) and right (RV) vagus nerves were sectioned at times indicated by arrows. Tracings top to bottom: air flow velocity (AFV), intrapleural pressure (IPP) and systemic blood pressure (BP).

Figure 64 shows a representative example of barbiturate induced apneusis in a cat with intact brainstem, cerebellum and vagi. At the arrow, 3.4 mg/kg pentobarbital was injected intravenously, raising the total dosage of barbiturate to 57.6 mg/kg, including the initial anesthetic dose of 30.0 mg/kg. After a short circulation delay, a prolonged inspiratory hold of more than 30 seconds was observed. A normal respiratory pattern then emerged, but the system was operating at a higher end-expiratory % CO_2 level. It is possible that this elevated CO_2 drive was responsible for the return to cyclicity. This example illustrates that pentobarbital can in some way block pneumotaxic, vagal and cerebellar inhibitions on inspiratory drive with the resultant genesis of apneusis. Similar results were found using thiopental.

Supportive evidence that the cerebellum is inhibitory to inspiration is given in Figure 65. The control respiratory pattern in panel A was obtained from cat 49 which had brainstem, cerebellum and vagi all intact. Between panels A and B the cerebellum was quickly removed by suction with very little blood loss. Immediately after cerebellectomy the eupneic respiration was transformed into one of apneusis with elevated end-expiratory % CO_2 values (panel B). Eight minutes later (panel C) the

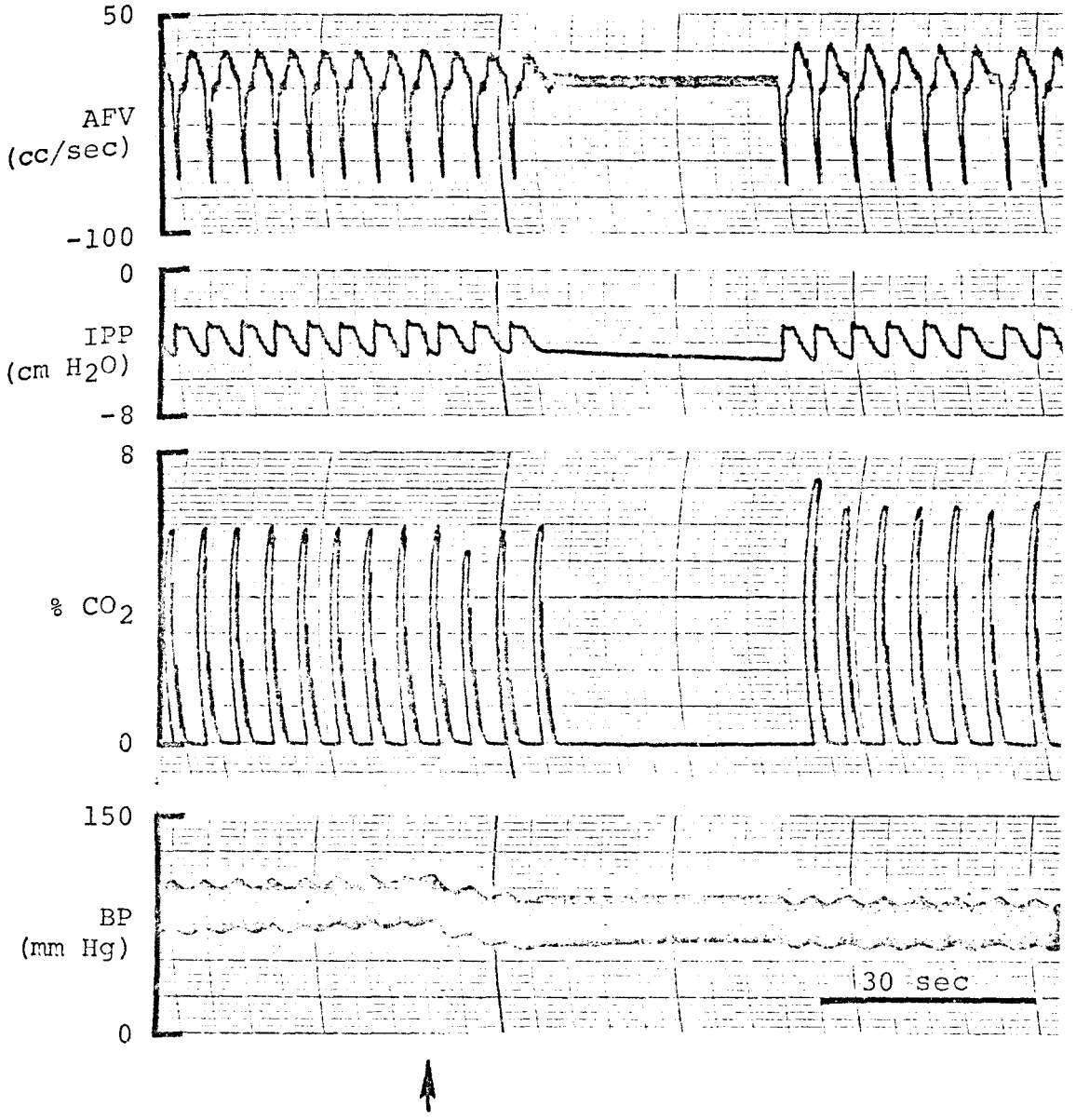

Figure 64. Pentobarbital apneusis. Cerebellum and vagi intact. Injection of 3.4 mg/Kg pentobarbital (arrow) induced a prolonged apneustic breath. Tracings as in Figure 63 with the addition of end-expiratory % CO_2 recording in third panel from top.

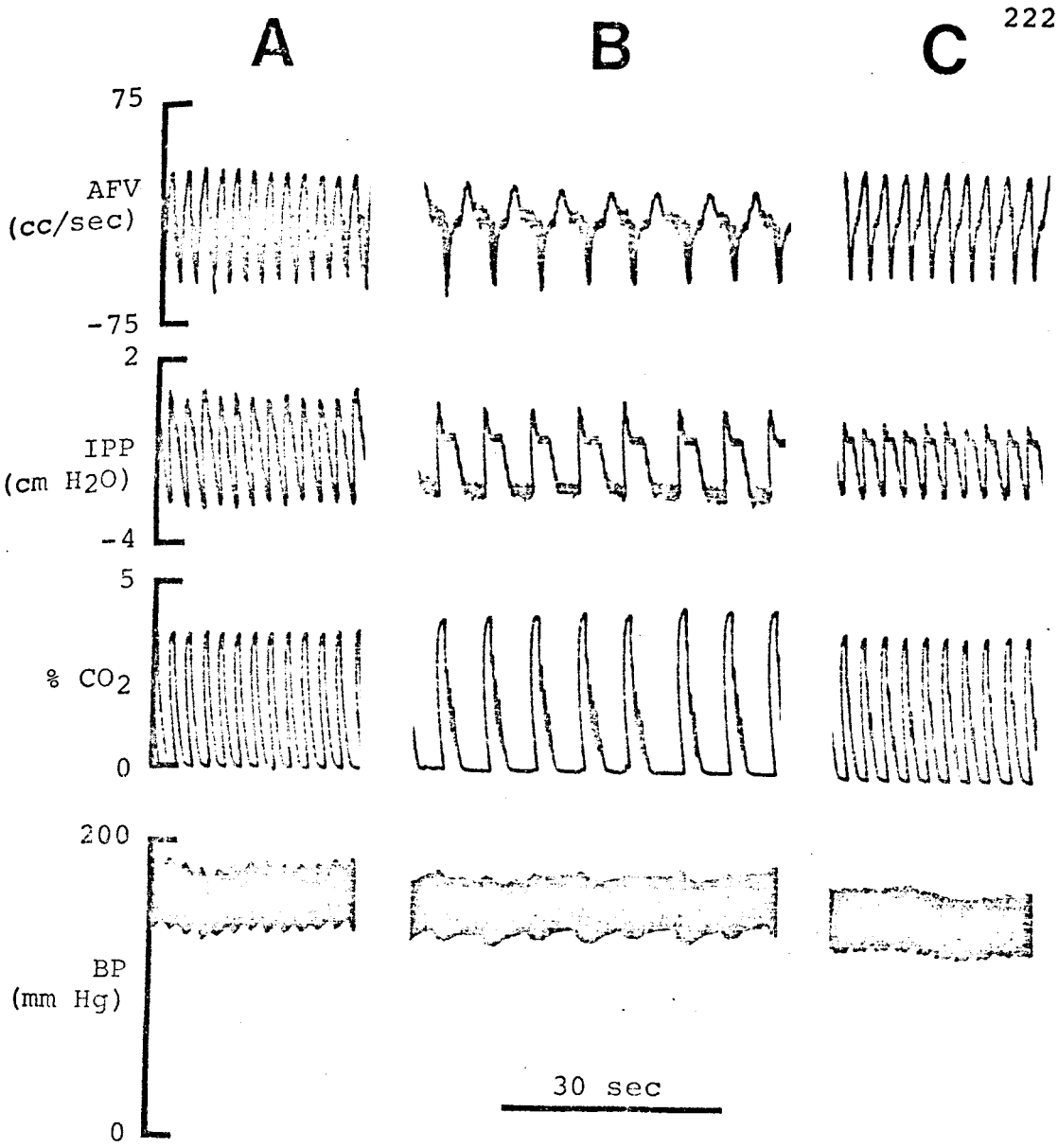

Figure 65. Apneustic pattern produced by acute cerebellectomy: A. control; B. three minutes later after cerebellectomy; C. recovery after eight minutes. Tracings as in Figure 64.

apneustic breaths were replaced by a normal respiratory pattern and the % CO_2 returned to control levels. Evidently the system is capable of readjustment, suggesting that cerebellar inhibition is of secondary importance (76).

Figure 66 summarizes apneustic threshold data for four different procedures. The apneustic threshold was defined as the amount of barbiturate required to induce the first apneustic breath under various experimental conditions. The total accumulated dose was expressed as the incremental amount over and above the initial anesthetic level of 30 mg/kg pentobarbital. For example, successive small increments of thiopental (A) and pentobarbital (B) were administered until the first apneustic breath was produced (cf. Figure 64). Approximately twice the dosage of pentobarbital was required to reach the apneustic threshold in cats with brainstem, cerebellum and vagi intact. The difference between pentobarbital and thiopental threshold doses was significant at the 0.04 level. This was probably due to the fast acting characteristics of thiopental, a short acting barbiturate that is rapidly absorbed.

In C, drug data are pooled for apneustic breaths induced by vagotomy at low pentobarbital levels and from

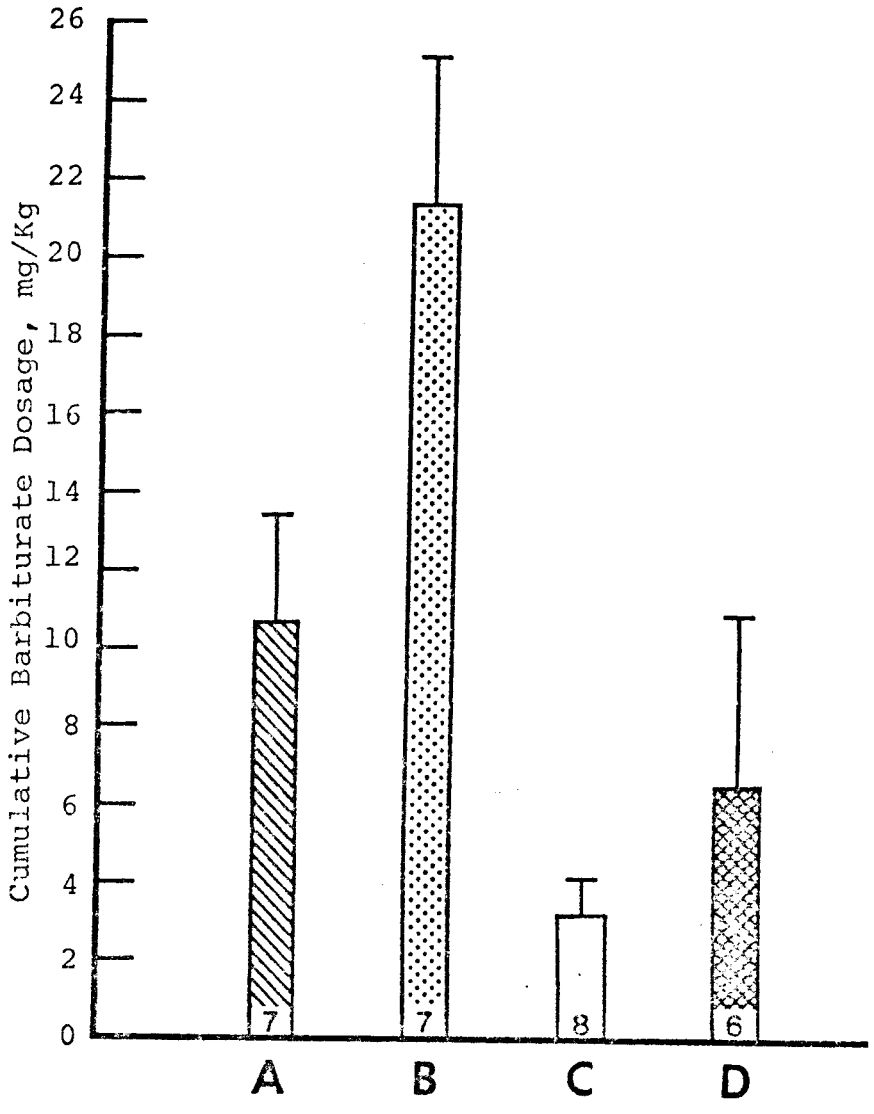

Figure 66. Mean and SEM of barbiturate dosage at apneustic threshold: A. thiopental; B. pentobarbital; C. pentobarbital after vagotomy only; D. pentobarbital after cerebellectomy only. Levels of significance: A vs. B, $P<0.04$; B vs. C, $p<0.0005$; C vs. D, $p>0.4$; B vs. D, $p<0.03$. Ordinate expressed as cumulative dosage over and above initial anesthetic dose of 30 mg/Kg pentobarbital.

pentobarbital titration studies in vagotomized cats failing to show long inspiratory holds following vagal section. In the former group, the apneustic breath observed was not believed to be due to mechanical stimulation of the vagus, since this generally leads to expiratory apnea. Comparison of B and C shows that it was significantly easier ($p<0.0005$) to induce apneusis at lower pentobarbital levels when vagal inhibition was absent.

Finally, the cerebellum was removed in a group of cats with intact brainstem and vagi. The pentobarbital level to induce apneustic breaths (cf. Figure 65) in this group is shown in D. Comparison of B and D shows that cerebellectomy significantly decreased ($p<0.03$) the amount of pentobarbital required to induce sustained inspiratory holds in brainstem and vagi intact cats. Although there is no significant difference ($p>0.4$) between C and D, it cannot be concluded that vagal and cerebellar inhibitions are of equal strength because of the nature of these experiments. That is, apneusis often resulted immediately after vagotomy or cerebellectomy procedures indicating that the apneustic threshold was already exceeded by an unknown amount of barbiturate.

In conclusion, these results show that relatively large doses of barbiturate are required to block major

inhibitions on inspiration before apneusis is produced. However, partial reduction of inhibitory input (vagotomy or cerebellectomy) significantly decreases this barbiturate dose requirement. This implies that apneusis depends on the relative balance between excitatory and inhibitory inputs to the brainstem inspiratory cells.

Figure 67 shows the effect of vagotomy on cat 63 previously subjected to pentobarbital apneusis (17.8 mg/kg incremental dose) and cerebellectomy (22.2 mg/kg pentobarbital level). Thirty minutes after the latter procedure, the cat had recovered to the prevagotomy control pattern in Figure 67. At this point, section of the left vagus immediately prolonged the average inspiratory to expiratory time ratio and subsequent section of the right vagus further increased this ratio. At least two conclusions can be drawn from these results. First, the length of apneustic holds is directly related to the degree of blockade of inspiratory inhibitory systems. Second, a high pentobarbital level may block brainstem interconnections, since the control pattern was lost after unilateral vagotomy on the left side, a response which did not occur at lower pentobarbital levels (Figure 63).

Barbiturate induced apneusis was examined at the

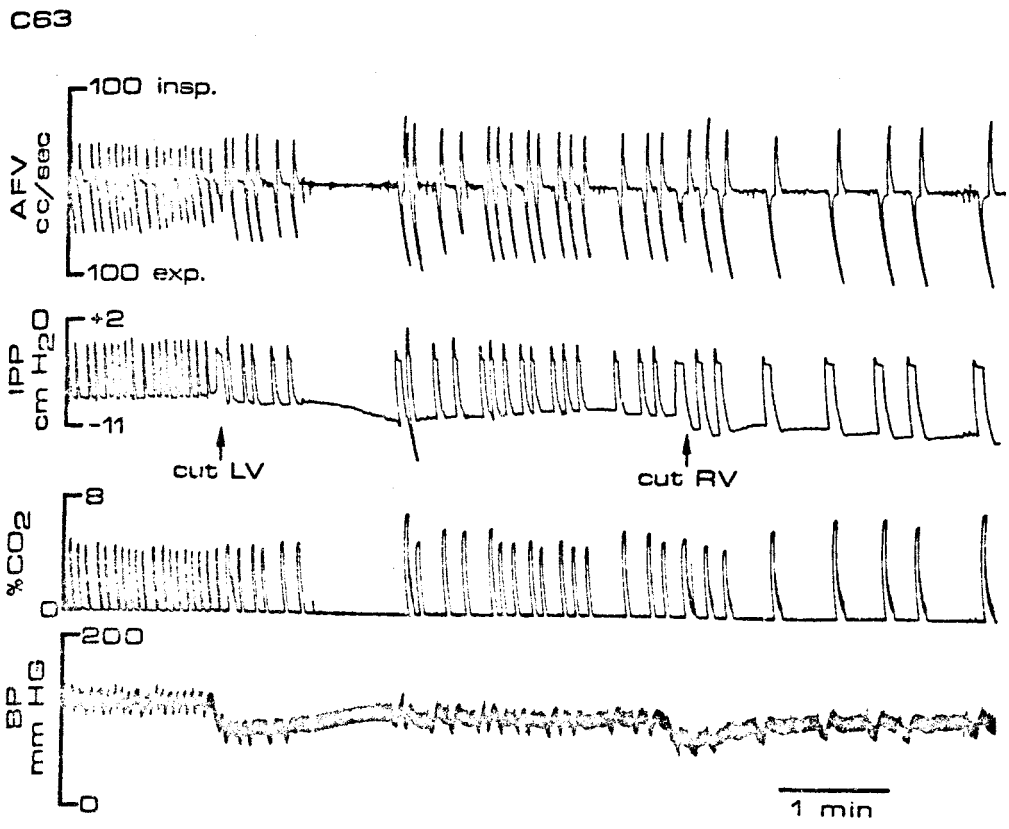

Figure 67. Effect of sequential left (LV) and right (RV) vagotomy on respiratory patterns. Cat previously subjected to cerebellectomy and high doses of pentobarbital. Tracings as in Figure 64.

single cell level. In Figure 68, an inspiratory cell was found to fire continuously during a sustained inspiratory hold induced by pentobarbital administration. An expiratory cell subjected to a similar procedure was inhibited throughout the apneustic breath as shown in Figure 69. These observations support the idea that inspiratory and expiratory cells are reciprocally inhibitory.

In another study, shifts in the histogram interspike interval distribution of a single inspiratory cell were followed after several thiopental injections as shown in Figure 70. In this preparation, which had intact brainstem, cerebellum and vagi, there was a consistent decrease in the respiration rate from 57 to 15 breaths per minute. However, an interesting triphasic shift in the histogram was observed as previously shown for another inspiratory cell during pentobarbital accumulation in Figures 52 and 53. For example, at low incremental thiopental doses (0-4 mg/kg) the histogram was first shifted to the right as the unit was deactivated (Figure 70, top panel). At medium thiopental levels (4-7 mg/kg), the unit became activated causing a shift in the histogram to the left (Figure 70, middle panel). Finally, at high thiopental levels (7-9 mg/kg), the inspiratory cell experienced a second depression

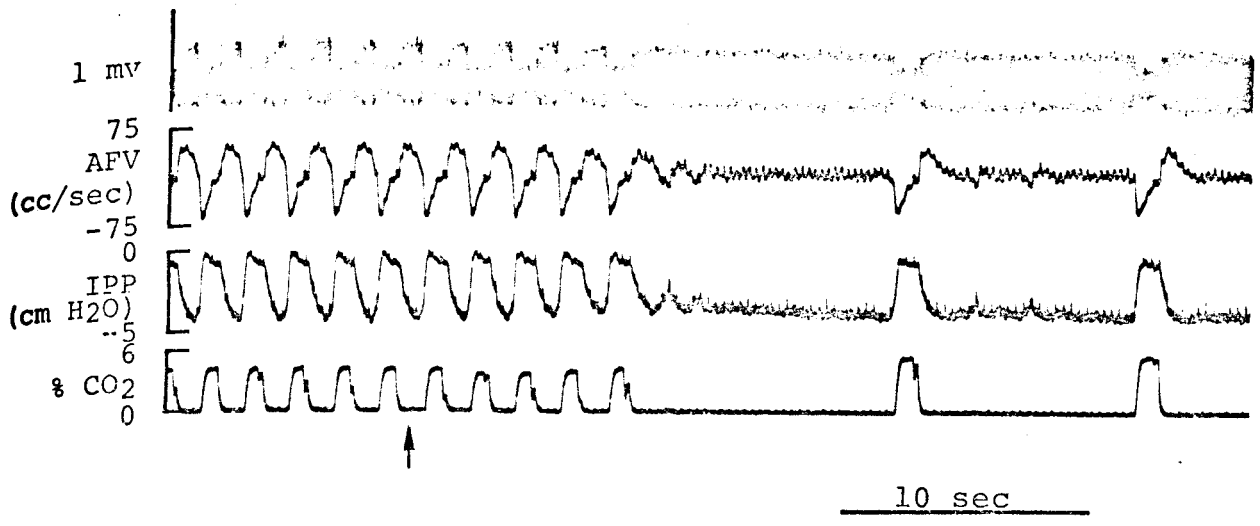

Figure 68. C50UI5R. Single inspiratory cell recording during induction of apneusis after administration of 1.0 mg/Kg pentobarbital (arrow). Tracings top to bottom: unit activity, air flow, intrapleural pressure and end-expiratory % CO_2.

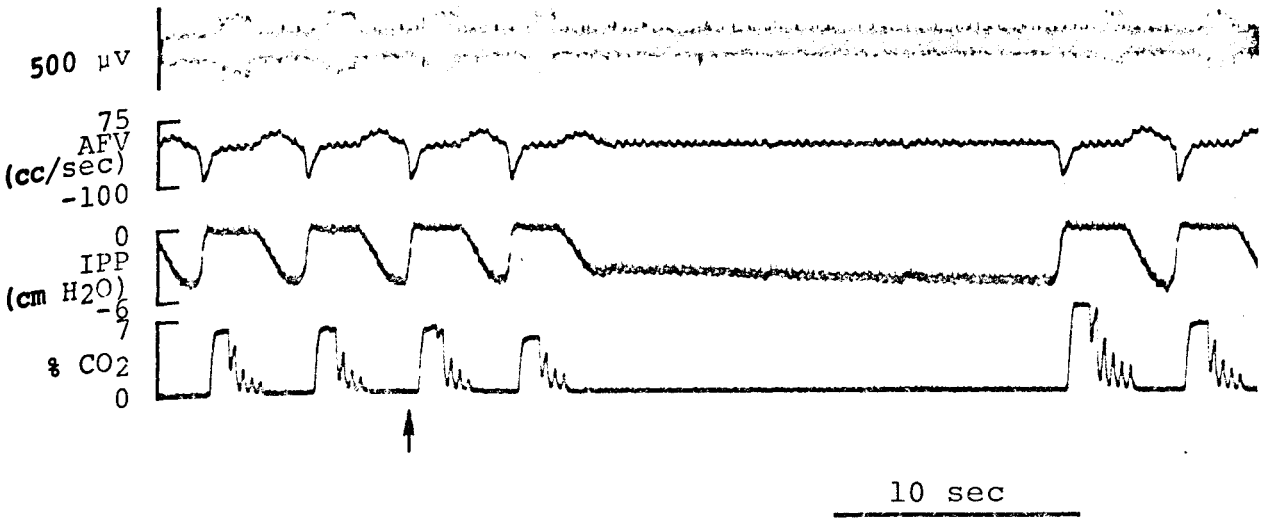

Figure 69. C64UE5R. Single expiratory cell recording during induction of apneusis after administration of 3.0 mg/Kg pentobarbital (arrow). Tracings as in Figure 68.

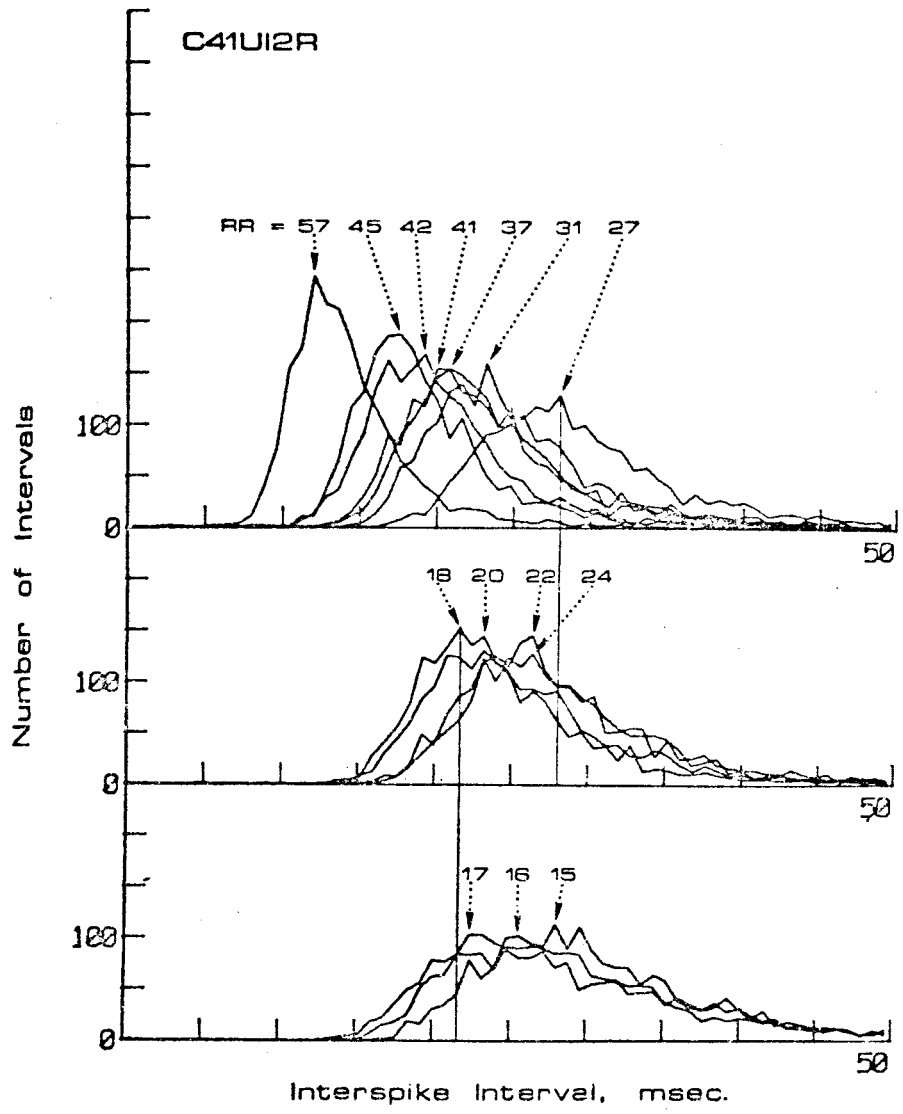

Figure 70. Changes in single inspiratory cell histogram during progressive depression of respiration rate (RR) produced by serial thiopental injections. Corresponding respiration rates and histogram modes are indicated by arrows.

trend and the histogram shifted back to the right (Figure 70, bottom panel). Apneusis was never produced.

Explanation of this response most likely involves differential thiopental depression of inhibitory versus excitatory inputs to the medullary inspiratory mechanism. That is, at medium thiopental levels (4-7 mg/kg), a significant fraction of total inhibition could be sufficiently depressed by the barbiturate, thereby allowing inspiratory unit activation. This would result from pneumotaxic, cerebellar or vagal blockade, or partial depression of each by thiopental.

The mode, median and mean interval times from each histogram distribution in Figure 70 are plotted as a function of thicpental dose and respiration rate in Figure 71A and B respectively. The dose is expressed as the incremental level over the initial anesthetic dose of 30 mg/kg pentobarbital. Similar data from expiratory cell C47UE10R are included for comparison. The triphasic shift in interval times for inspiratory cell C41UI2R are clearly seen in each plot. Qualitatively speaking, a mirror image triphasic shift can also be observed for expiratory cell C47UE10R. This was previously seen for expiratory cell C71UE2R (Figures 58 and 59). For example, when the inspiratory unit was depressed, the expiratory

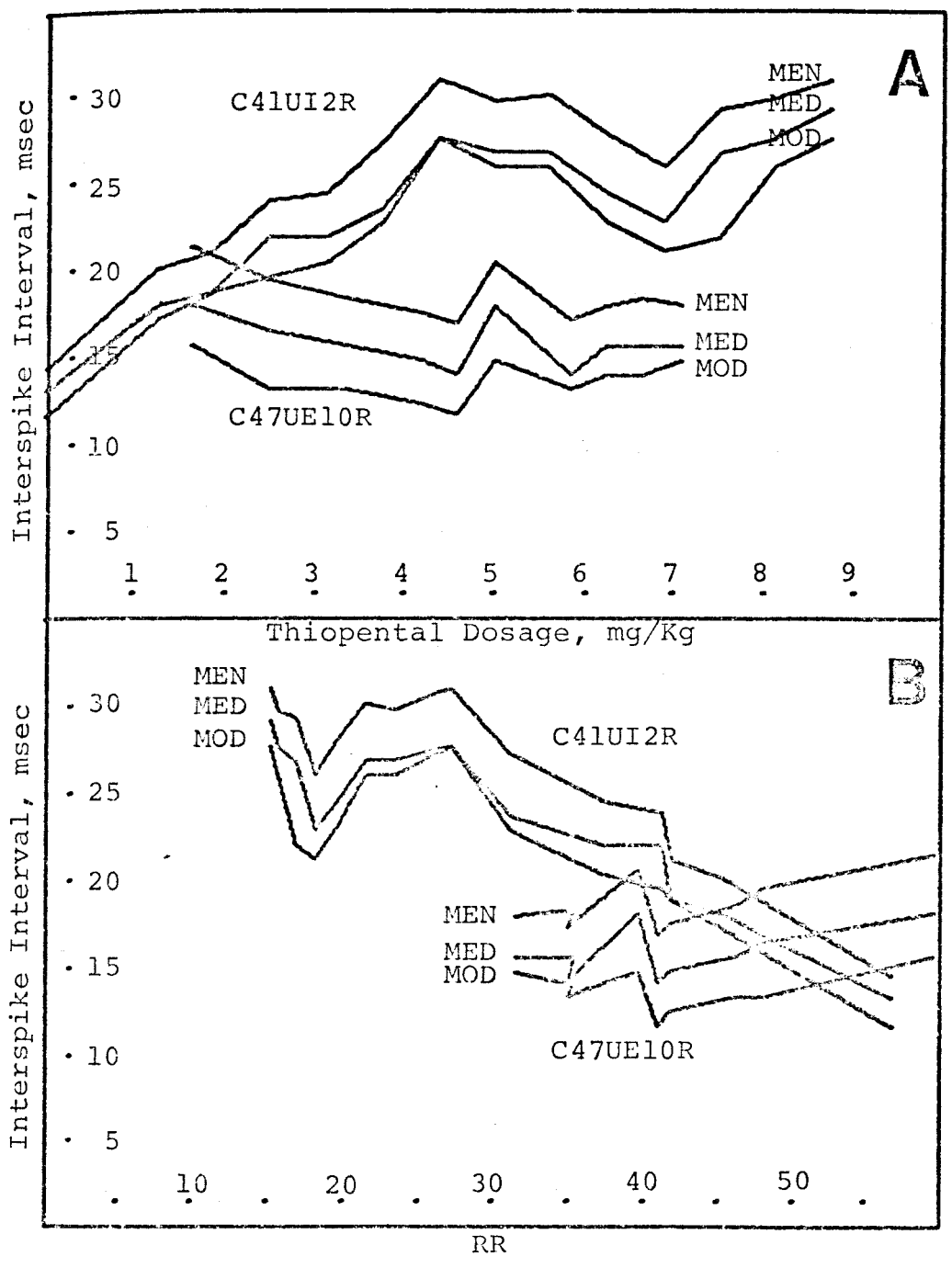

Figure 71. Histogram data for cell C41UI2R (Figure 70) replotted to show changes in mean (MEN), median (MED) and mode (MOD) as a function of thiopental dosage (A) and respiration rate (B). Expiratory cell C47UE10R plotted for comparison.

unit was activated and vice versa. This implies a negative reciprocal relationship between firing frequencies of inspiratory and expiratory cells.

An attempt was made to determine if pentobarbital could differentially block pneumotaxic regions before medullary areas. The cerebellum was removed from cat 65 and an electrode was inserted into the classical pneumotaxic region of the rostral pons. The vagi were intact. Figure 72 shows the frequency discharge response of three constantly firing (non-respiratory) cells plotted as a function of time before and after pentobarbital administration. Cell K1, the first cell found, was completely inhibited by a 2.7 mg/kg injection of pentobarbital which brought the total sum dose over the anesthetic level to 4.0 mg/kg. Another cell, K2 was soon found which had a discharge frequency approximately half that of cell K1. After a 2.7 mg/kg pentobarbital injection, the discharge frequency was sharply inhibited, but rebounded back to the control level in less than a minute. This unit could not be completely inhibited by two additional pentobarbital injections (3.3 and 2.7 mg/kg). Finally, a third constantly firing cell (K3) was located in the upper pons. The firing frequency of this unit was very low presumably due to the high pentobarbital

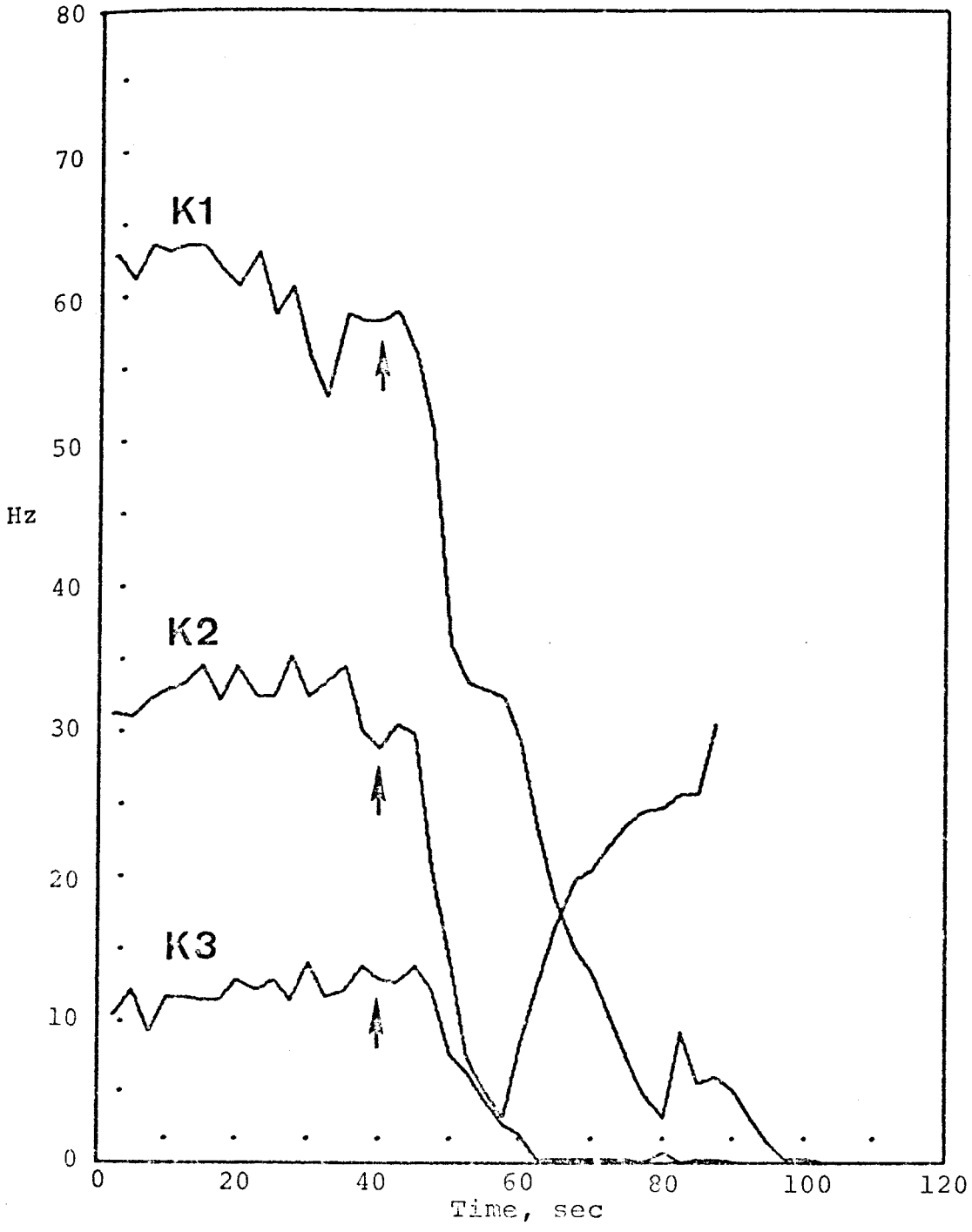

Figure 72. Effect of pentobarbital (arrows) on discharge frequency of three non-respiratory pontine cells. See text for details.

level (12.7 mg/kg). When 3.3 mg/kg pentobarbital was given, this cell was completely inhibited like cell K1 and a tendency toward apneusis was observed. Subsequent searching for non-specific units in the rostral pons was not successful and it was concluded that this region of the brainstem was deeply depressed by the total sum level of pentobarbital present (16.0 mg/kg). Replacement of the same recording electrode in the medullary architecture, however, immediately yielded unit activity. Soon an inspiratory cell was located which correlated with the oscillating peripheral parameters. This demonstrated two points. First, the failure to find single cell discharges in the pons could not be attributed to microelectrode failure. Second, the medulla was not as highly depressed as the rostral pons at an incremental pentobarbital level of 16.0 mg/kg. This information suggests that the inflection of the mode curve for inspiratory cell C41UI2R in Figure 71 may be due to depression of pneumotaxic circuits by pentobarbital.

In final studies, miscellaneous procedures were performed to induce apneusis in the spontaneously breathing cat. Figure 73 illustrates the effect of bilateral carotid occlusion (BCO) on modification of the breathing pattern at different pentobarbital levels. In this

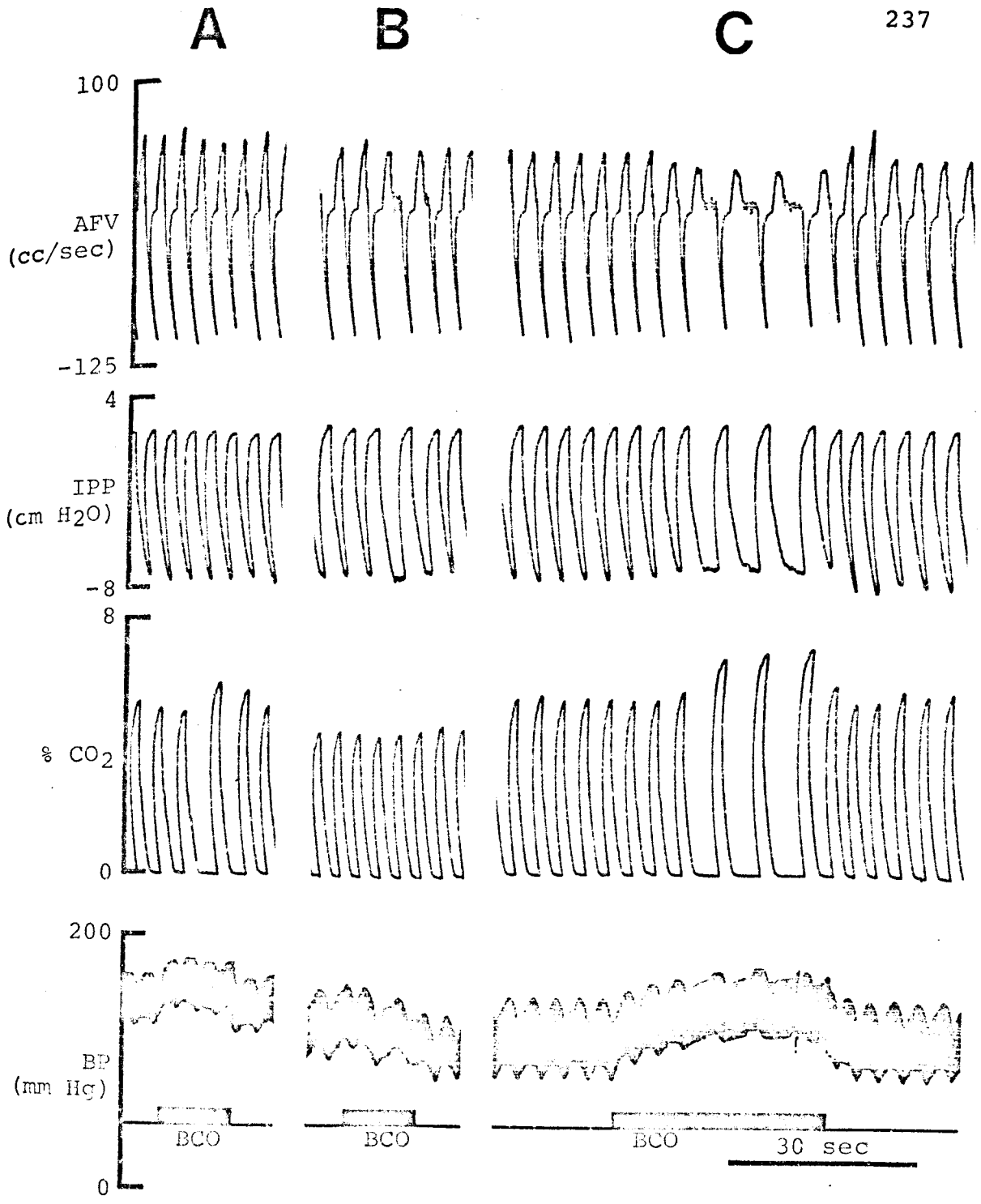

Figure 73. Changes in respiratory patterns during bilateral carotid occlusion (BCO) in a vagotomized cat with increasing pentobarbital dosage: A. after 31.0 mg/Kg; B. after 32.8 mg/Kg; C. after 34.5 mg/Kg. Tracings as in Figure 64.

preparation, vagi were cut but the cerebellum was still intact. As the total barbiturate level was elevated from 31.0 to 32.8 to 34.5 mg/kg in panels A, B and C, respectively, there was an increased tendency toward apneusis during each BCO procedure. This demonstrates that a change in inhibitory input to respiratory centers over carotid sinus afferents (baroreceptor or chemoreceptor) can induce apneusis provided the barbiturate depression is at an appropriate level.

Similar results were found in another cat in which carotid sinus pressure was decreased via intravenous administration of histamine as shown in Figure 74. The vagi were cut and the cerebellum was intact as in Figure 73. The accumulated total dose of thiopental over the initial anesthetic dose of pentobarbital was 34.4 mg/kg. The effective dose was lower, since thiopental injections were given over a five hour period. After histamine injection there was a precipitous fall in systemic blood pressure from about 150 to 85 millimeters mercury due to peripheral vasomotor dilatation. A corresponding modification in the breathing pattern resulted with prolongation of the inspiratory duration resembling apneusis. As the blood pressure returned to a pre-injection control level over the following five

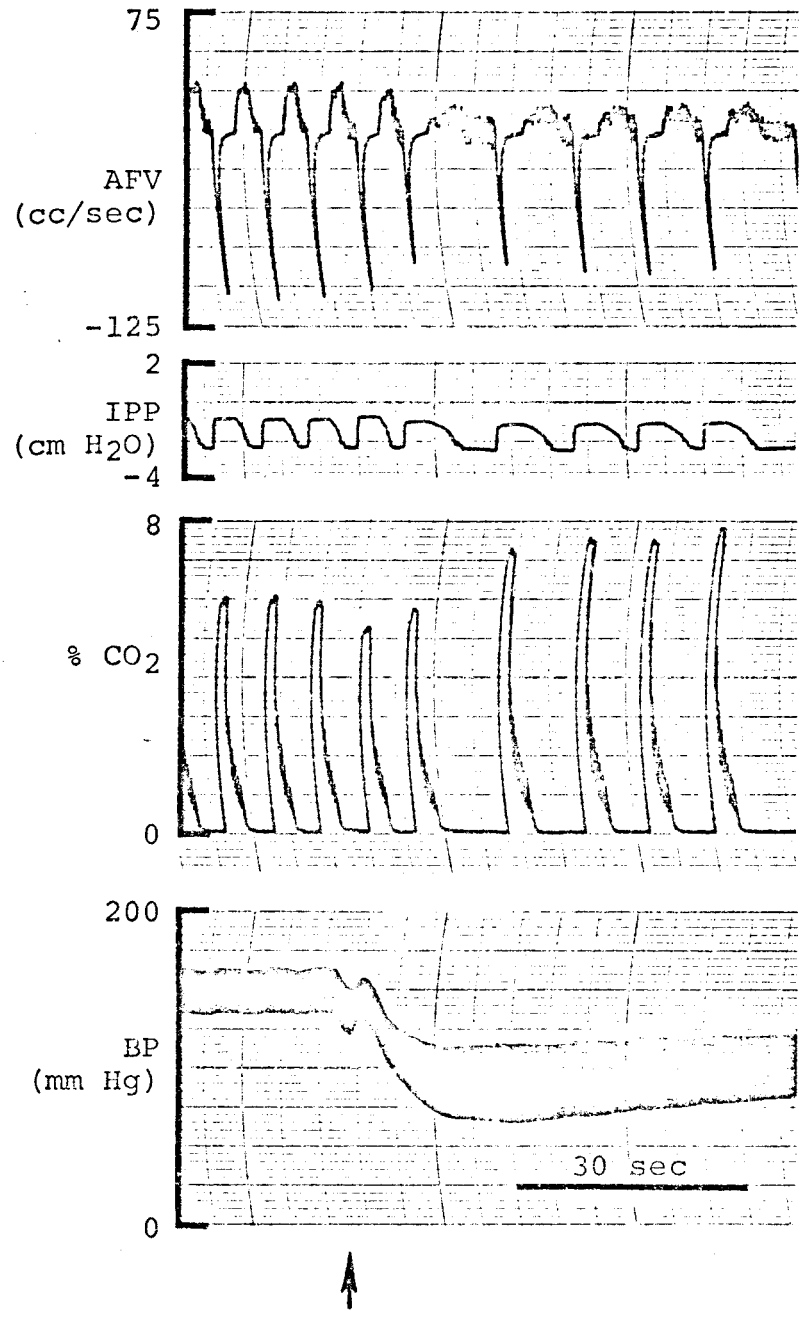

Figure 74. Changes in respiratory pattern produced by 17.0 µgm histamine phosphate (arrow) in a vagotomized cat. Tracings as in Figure 64.

minutes, the respiratory pattern lost its apneustic form. These results substantiate the conclusions made for Figure 73; namely, a decrease in the inhibitions to the inspiratory mechanism can lead to apneusis when other inhibitory systems are partially blocked by barbiturate depression.

A final attempt was made to induce apneusis by facilitating excitatory inputs to the inspiratory complex. In Figure 75, doxapram, a respiratory stimulant, was given intravenously to a cat with severed vagi and intact cerebellum. The pentobarbital level was at 4.4 mg/kg over the initial anesthetic dose. Following a transient dip in the blood pressure, two prolonged apneustic breaths were produced. This response is consistent with the concept that inspiratory duration is a "simple" algebraic summation function of all excitatory and inhibitory inputs impinging on inspiratory cells in the medulla at any given point in time.

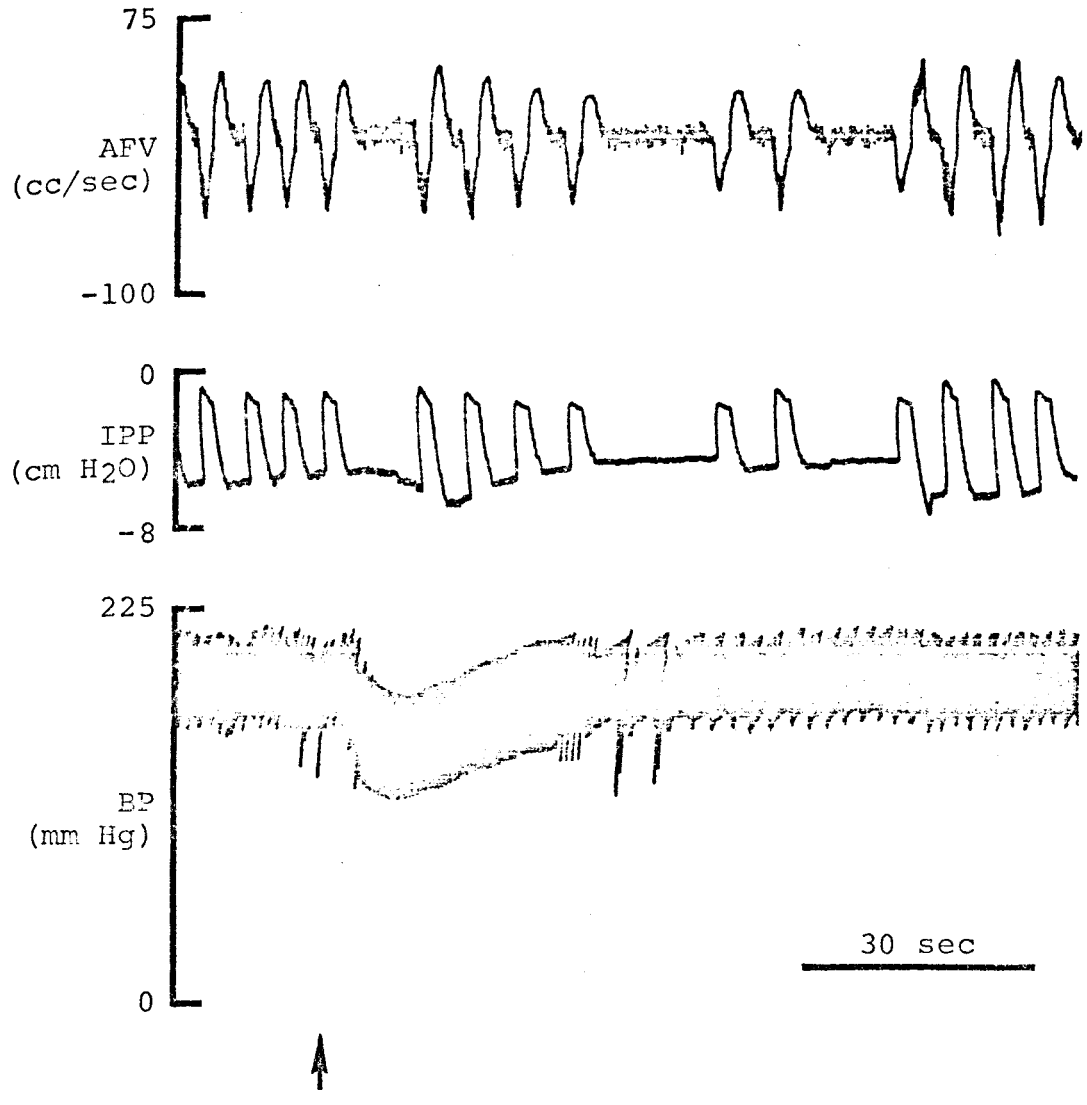

Figure 75. Changes in respiratory pattern produced by 4.4 mg/Kg doxapram (arrow) in a vagotomized cat. Tracings as in Figure 63.

CHAPTER VI

DISCUSSION

A. Population Modeling

In assessing the experimental data presented in this dissertation, two crucial questions arise: first, how are the limits of a cell population determined, and second, how many single cell elements need to be combined to represent physiological response characteristics of the defined population?

Concerning the first question, the assumption must be made that "singular" biological populations possess inherent variability. Population characteristics may follow normal or skewed distributions, but in either case, variations are present. Recognition of this fact is important, since it may prevent establishment of such rigid criteria for a population (minimization of variability) that only a few elements are eligible. This, by necessity, requires the postulation of a number of other so-called populations. Cohen (40, 41, 42, 43, 45) and others (14, 15, 128, 169, 173), in describing no less than eight different

respiratory phasing patterns, may have failed to recognize inherent biological variability. If so, the elaborate theories on rate and depth control proposed by different individuals (15, 42) are highly questionable. Under these conditions, the experimental analysis no longer deals with real biological entities, but with artifactual systems whose parameters are mere functions of the experimental techniques employed.

A second, but less common error, is the tendency to be over-inclusive when defining the limits of a population. In this case, cells rightfully belonging to separate populations are included within the same category. Subsequent averaging of data results in the masking of real and important physiological trends. Obviously, a balance between over and under selectivity should be sought when attempting to assign single cell observations into appropriate groups. As a guideline, it is suggested that population limits be set such that standard deviations of individual elements approach predictable magnitudes as determined from statistical theory.

Assuming that real physiological populations can be defined, the second question posed above seeks realistic means whereby population characteristics can be accurately assessed. Since it is unlikely that all components

in a population can be sampled, functional description of many systems, notably CNS subsystems, must rely on approximation techniques (31, 41, 51, 101, 102, 127, 129). Two powerful techniques stand out in importance. First, Knight (101, 102) has stressed the importance of averaging repetitive observations from a single cell when describing activity in a population of neurons. In his own words (101), "While at present it is not feasible to record individually from a uniform population of neurons, it is possible to do something equivalent: to record from a single member over repeated stimuli." That is, processes spacially distributed over many components, but occurring at the same point in time, can be approximated by temporal summation of a single component's output at one point in space. Second, Nelson (127) has emphasized the importance of grouping characteristics of individual cells for accurate population description. He writes, "Ideally, the electrode records from but a single element in the system; with data from a large number of such elements it is possible to 'resynthesize' the total population and draw conclusions about the location of units having similar temporal patterns of firing." These two mutually interactive techniques can be coupled as follows in population description studies:

Population	Single Cell Discharge Pattern	# Cells	# Cycles
Homogeneous	Smooth	1	1
Homogeneous	Rough	1	N
Heterogeneous	Smooth	N	1
Heterogeneous	Rough	N	N

The number of cells and number of cycles averaged for each cell are listed as either 1 or N (arbitrary large number) in specific combination pairs depending on the type of population and type of single cell discharge pattern. For example, if all the components of a population are identical (homogeneous) and if each discharge is not subject to change fluctuations (smooth), population characteristics can be identified by examination of a single burst discharge from one cell in the population. If all the cells are identical (homogeneous), but are subject to change fluctuations (rough), then it is necessary to average many output cycles from one cell before description of population characteristics is possible. In situations where the population contains a variety of cellular individuality (heterogeneous), it is necessary to sample from a large representative fraction of the population for accurate description. Considering the argument of inherent biological variability presented above, the

first three cases possessing population homogeniety and/or single cell regularity must be rejected as untenable. For the respiratory system, this is confirmed by the rough interspike interval modulation curves for single burst discharges (Figure 9A) and the presence of error lines (standard deviation) in all regression plots (Figures 11-34). This leaves the fourth case which demands that many cycles from single cells and repeated observations on different cells be averaged for population assessment. Description errors are, of course, minimized by maximizing the N values.

In this study, four respiratory neuron populations were defined which subdivided inspiratory and expiratory cell types into vagi-intact and vagotomized groups (I-VO, I-VI, E-VO, E-VI). The limits of each population were inclusive enough to allow for inherent variability, but exclusive enough to avoid masking of important physiological data (determined via range of error lines in Figures 11-34). Data analysis of single cell discharges included generation of common histogram interval distributions (66, 67, 68, 106, 139, 165 and Figure 6) and the new interspike interval modulation curve (Figure 9). The latter quantitatively defined the average interval ordering for a single respiratory cell discharging under

steady state conditions. This technique proved superior to those of Cohen (40) and Bertrand and Hugelin (24) who used modified histogram techniques. From the histogram (Figure 6) and interspike interval modulation curve (Figure 9B), 34 parameters were defined (Table IV) which successfully quantitated all phases of spike activity (initial, middle, terminal). This analysis compares favorably with other work published in the literature in which only a few parameter measurements were made in any one study. For example, the following parameters form an almost complete list of measurements made on single respiratory discharges (listed in decreasing frequency of occurrence - author references not exhaustive): ST (31, 40, 41, 51, 63, 91, 97, 127, 129); TL (31, 41, 51, 63, 91, 97, 127, 129); mean discharge frequency or 1/MEN (31, 40, 51, 69, 72, 91, 97); RR (31, 127, 129); CT (127, 129); peak discharge frequency or 1/MI (40, 97); T100 (97); TLP (129).

Discharge characteristics of the I-VO, I-VI, and E-VI populations were determined by regression analysis of 24 parameter groups on respiration rate and mode (Figures 11-43). The E-VO population data were not reported since only three cells contributed to this group (cf. Table III). Before discussing the parameter trends observed, it is important to consider the degree to which

separate populations have been sampled.

Waldron (174) has estimated that at any one time there are at least 2000 respiratory (inspiratory and expiratory) neurons in the total respiratory complex of the rostral medulla. Assuming this to be a reasonable estimate and assuming an inspiratory to expiratory cell ratio of 2:1 (155), there must be at least 1333 inspiratory and 667 expiratory cells involved in respiratory function (cf. Table III). In this study, only 10 I-VO, 51 I-VI and 23 E-VI cells were analyzed (Table III) which corresponds to 0.8%, 3.8% and 3.4% of each respective population. However, assuming that each burst discharge in time represents one cell in space (101), corrections can be made for the repetitive observations on single cells during curve smoothing procedures. For example, 1159 I-VO, 6079 I-VI and 3776 E-VI trains (Table III) or simulated cell samples contributed 86.9%, 456.0% and 566.1%, respectively, to each population. Within the constraints of these assumptions, the mathematical analysis used in this study has provided an excellent estimate of the inspiratory (I-VO, I-VI) and expiratory (E-VI) populations. Data interpretation should be weighed accordingly.

Parameter regressions plotted in Figures 11-43 represent specific population trends during barbiturate

and doxapram induced modifications in the spontaneous respiration rate and mode interval time. If it can be assumed that mode and tidal volume are reciprocally related as the rationale in Results proposes, specific characteristics in respiratory cell discharge patterns can be correlated with the two major outputs of the respiratory system namely, respiration rate and depth. Both rate and mode curves (Figures 11-43) can be viewed as barbiturate depression curves since pentobarbital or thiopental administration leads to decreased rates and tidal volumes (82, 131). Relatively speaking, the contribution from doxapram-facilitated data points is minimal.

Two series of figures are presented to summarize I-VO, I-VI and E-VI population characteristics. In the first series, Figures 76-80, regression correlation coefficients ("r" values) are plotted in bar graph format for each parameter as a function of either respiration rate or mode. All populations are represented. The "r" value reveals the degree of population homogeniety toward any one parameter. For example, as "r" values range from 0.00 to 1.00, there is a population trend or shift from complete heterogeniety to complete homogeniety. By definition, all parameters fall with these limits. For specific respiration rate or mode plots, different populations

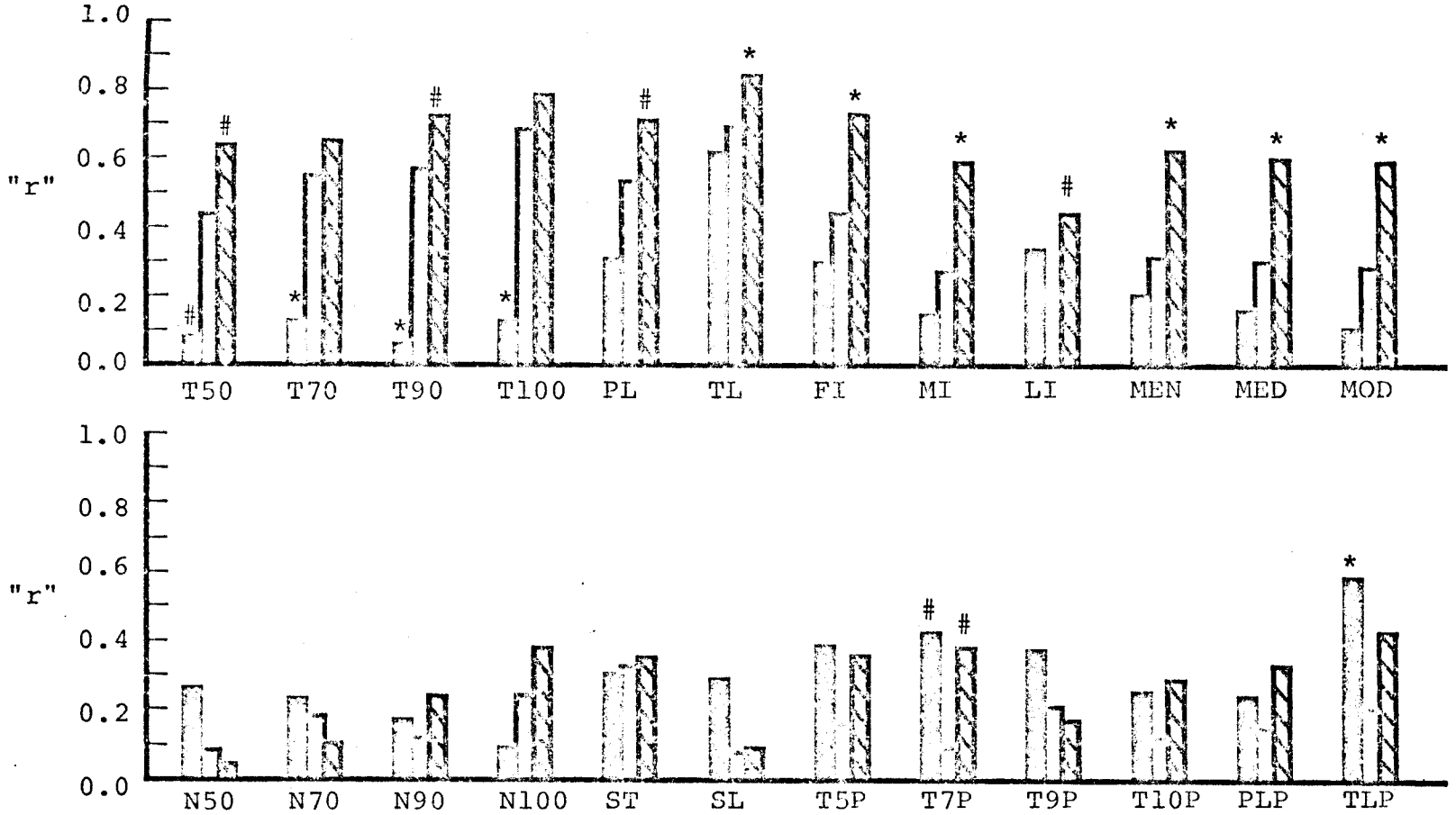

Figure 76. Comparison of correlation coefficients for 24 parameters on respiration rate for I-VO (solid), I-VI (open) and E-VI (striped) cells: # = $P<0.05$; * = $P<0.01$.

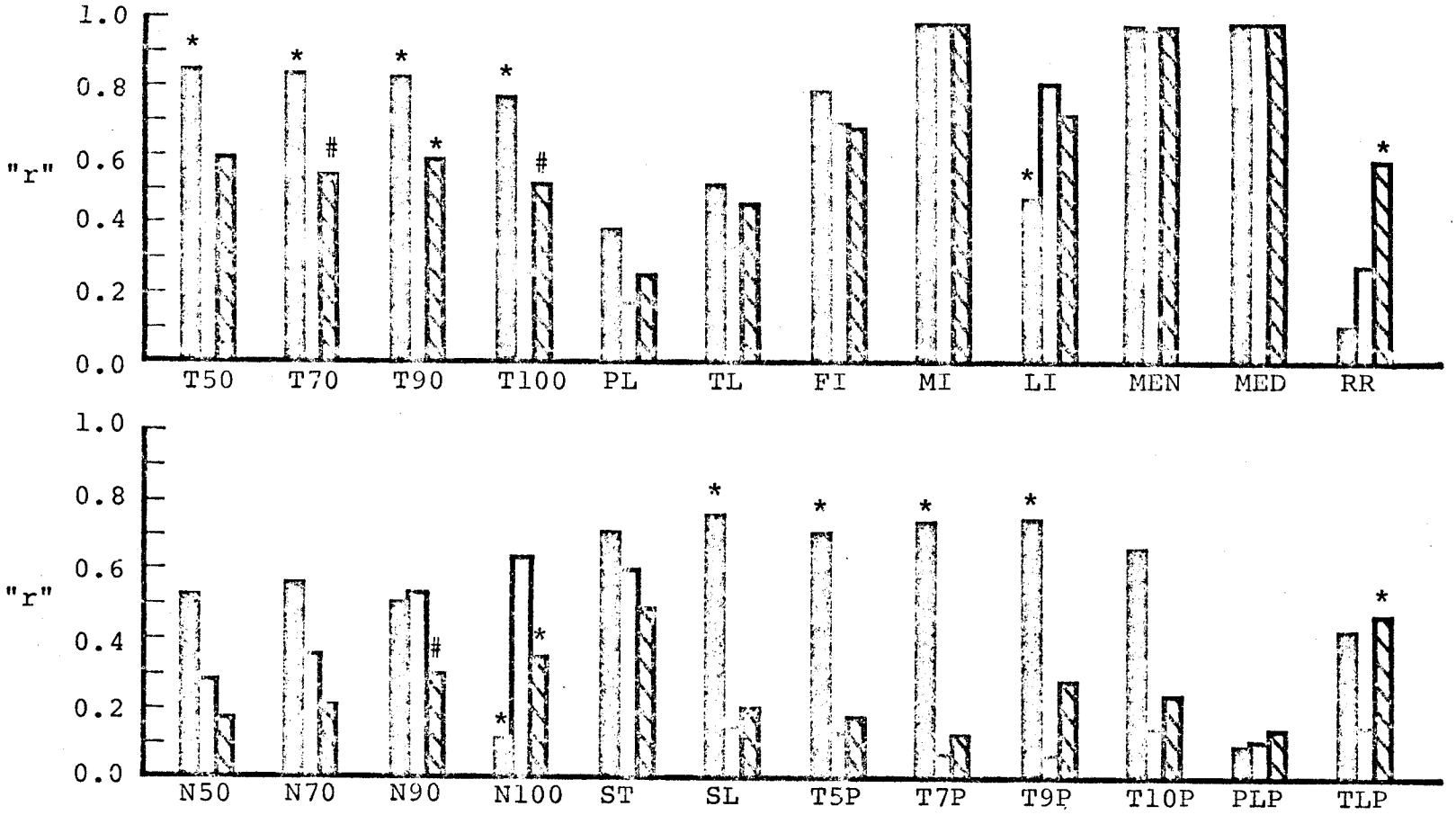

Figure 77. Comparison of correlation coefficients of 24 parameters on mode for I-VO (solid), I-VI (open) and E-VI (striped) cells: # = $P<0.05$; * = $P<0.01$.

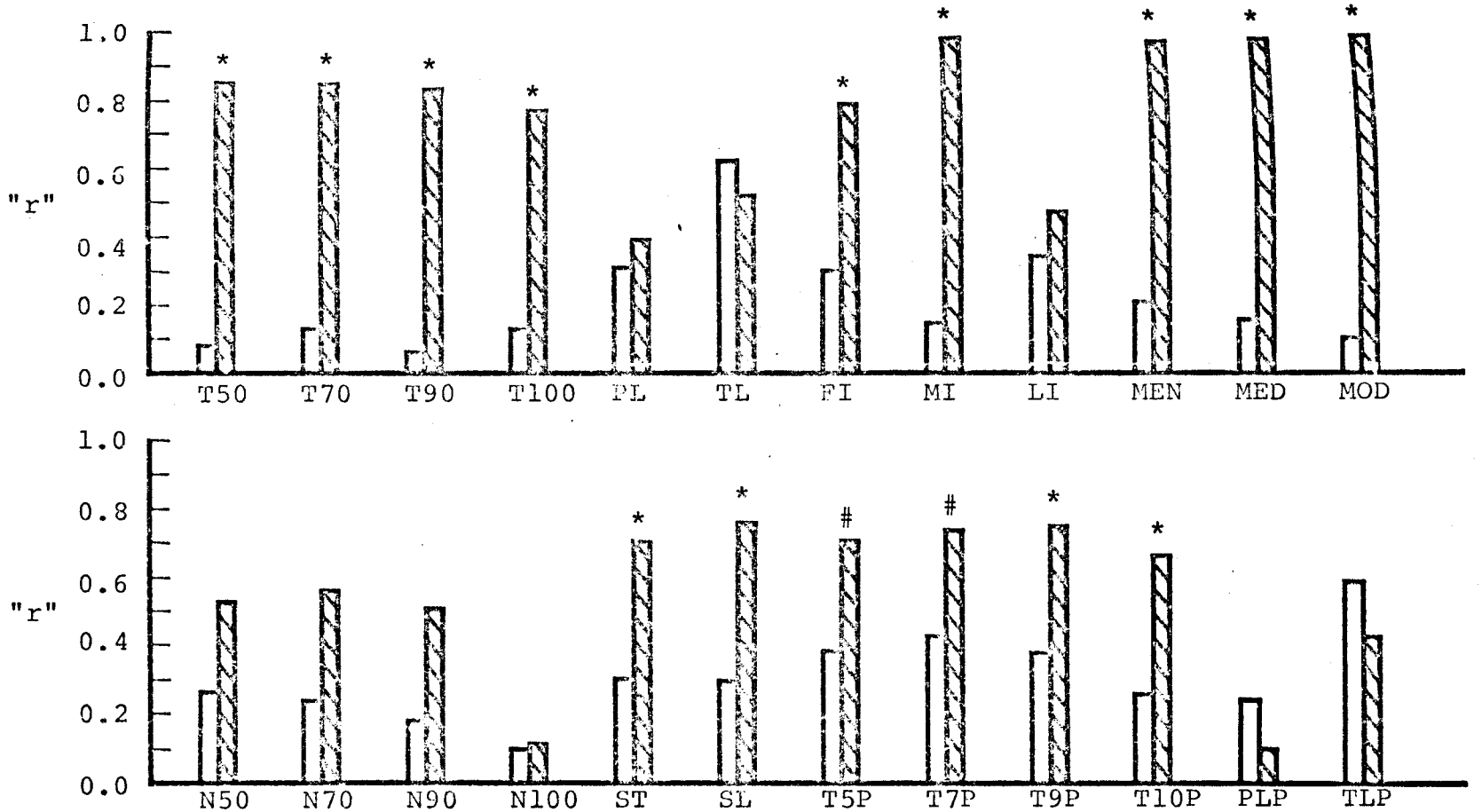

Figure 78. Comparison of correlation coefficients for 24 parameters on respiration rate (open) and mode (striped) for I-VO cells: # = $P<0.05$; * = $P<0.01$.

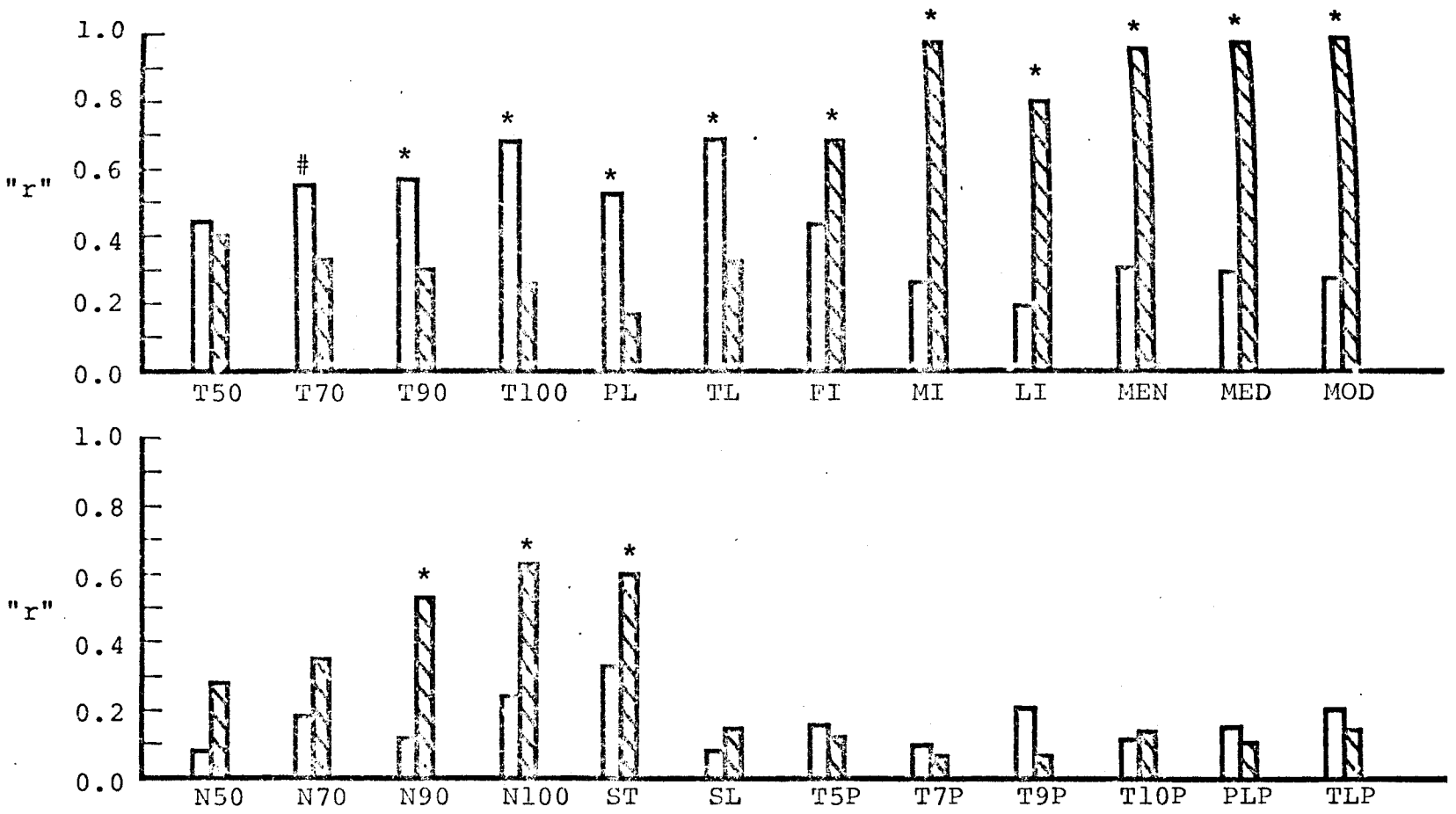

Figure 79. Comparison of correlation coefficients for 24 parameters on respiration rate (open) and mode (striped) for I-VI cells: # = $P<0.05$; * = $P<0.01$.

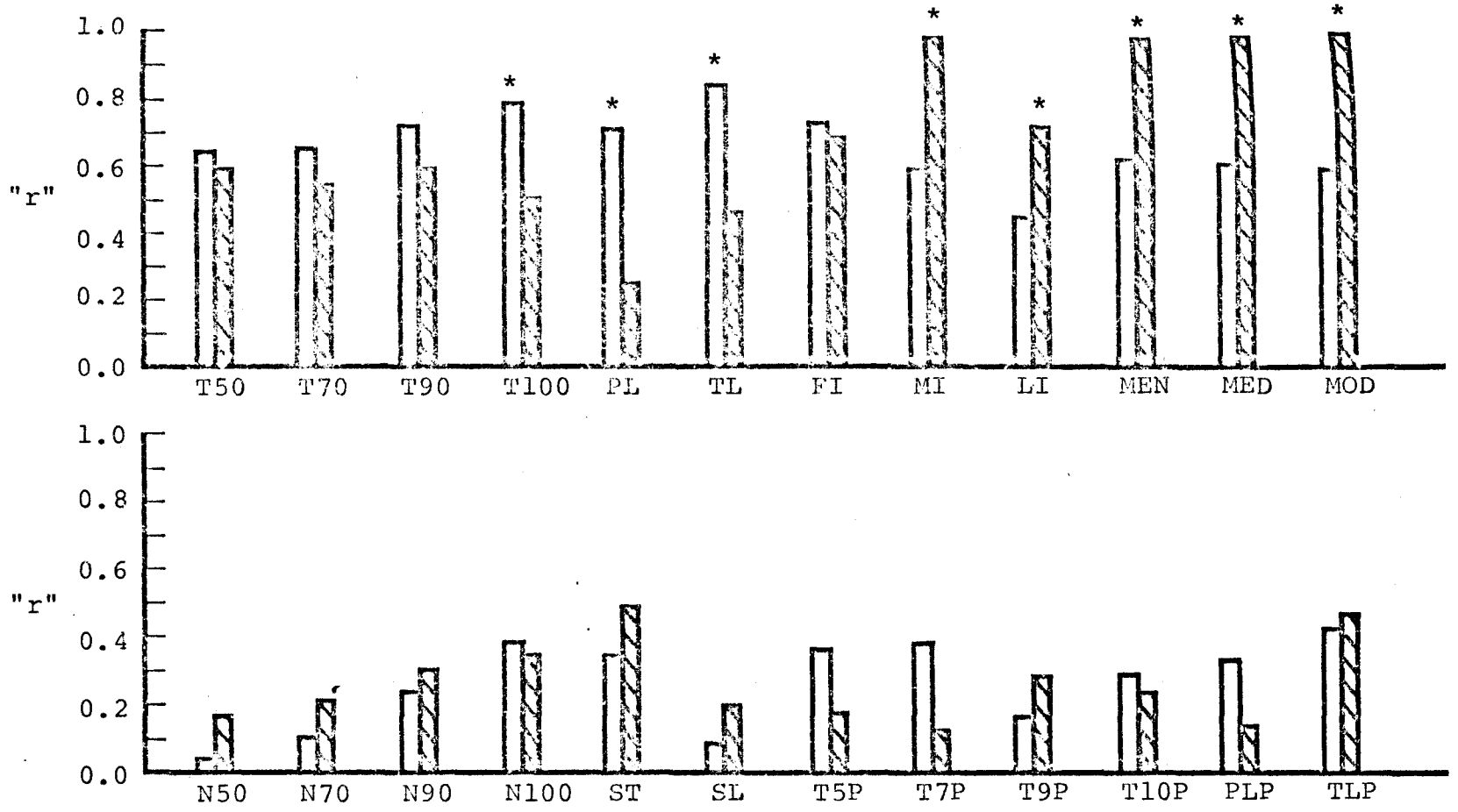

Figure 80. Comparison of correlation coefficients for 24 parameters on respiration rate (open) and mode (striped) for E-VI cells: * = $P<0.01$.

exhibit different "r" values. Also, any one parameter usually correlates better with respiration rate than mode and vice versa. In such cases, the significant difference between "r" values is indicated by a number sign (#) for $P<0.05$ and an asterisk (*) for $P<0.01$. Lack of a symbol designates that "r" values are not significantly different at the 0.05 level.

Figure 76 shows that for the first 12 parameters (T50 - MOD) expiratory cells have a higher degree of correlation with respiration rate than do inspiratory cells. This indicates that for these parameters, the expiratory population possesses less individual cell-to-cell differences and is relatively more homogeneous than either inspiratory population. Comparison of I-VO and I-VI data for the first 12 parameters shows that vagotomy usually decreases the correlation coefficients of inspiratory cell characteristics on rate. This evidence supports the concept that the control of respiratory rate operates through vagal afferent feedback (55, 57, 73, 129, 161, 162, 171). None of the latter 12 parameters (N50 - TLP) for any cell type in Figure 76 display high "r" values, illustrating that these measurements are relatively independent of rate changes.

Figure 77 shows that I-VO parameters usually correlate

best with mode, indicating that vagotomy significantly entrains many inspiratory discharge characteristics with alterations in respiratory depth. The expiratory and I-VI orderings are fairly consistent with rate data (Figure 76), with E-VI cells showing higher correlations on mode than I-VI cells. Also, the last 12 parameters for these two populations correlate very poorly with mode suggesting that, with the exception of I-VO parameters on mode, these parameters are poor indicators of either rate or depth changes.

In Figure 78, I-VO parameter "r" values are presented for both rate and mode regressions. Similar plots are found in Figure 79 for I-VI cells. When the vagi are intact (Figure 79), parameters derived from the summation of intervals (T50 - TL) correlate best with respiration rate, while individual interspike intervals (FI - MOD) correlate best with the mode. Parameters N50 - ST show an increased tendency to correlate with the mode, but the latter parameters (SL - TLP) fail to correlate with either rate or mode for I-VI cells. Sectioning of the vagi (Figure 78) significantly alters the correlation pairing for inspiratory T50 - PL parameters from rate to mode. The significant TL correlation with rate when the vagi are intact is reduced to no significant difference

from the mode regression after cutting both vagi. The FI - MOD parameters retain their strong mode correlations after vagal section. Finally, vagotomy tends to increase all mode correlations for the last 12 parameters (N50 - TLP) in the inspiratory population. These results show that, with the exception of parameters T50 - TL when the vagi are intact, most parameters correlate best with fluctuations in the mode irrespective of the presence or absence of vagal afferents. In general, this indicates that vertical ordering of the interspike interval modulation curve is more sensitive to depth changes, while horizontal interval ordering (Σ intervals) varies with respiration rate changes. The latter reverts to mode correlations after vagal section.

Figure 80 presents similar data for E-VI cells. Expiratory cells tend to show the same qualitative "r" value pattern as I-VI cells for most parameters (compare with Figure 79). This includes a respiratory rate coupling for horizontal time measurements (T50 - TL) and mode coupling for vertical time measurements (LI - MOD) with the exception of FI. As with I-VI cells, the last 12 E-VI parameters (N50 - TLP) show poor correlations with either rate or mode.

It has been indicated previously that correlation

coefficients or "r" values reveal the degree of homogeniety or degree of fit. This concept of correlation also involves the type of fit since population data were represented by the best of four different regression equations; namely, linear, exponential, logarithmic or log-log. The best type of equation fits for all cell type parameters are listed in the Appendix (Table XIV) for both respiration rate and mode regressions. Taking all 24 parameters at a time for each cell type reveals that 16 I-VO, 11 I-VI, and 13 E-VI parameters are fit best with logarithmic, exponential and logarithmic equations, respectively, as a function of respiration rate. For mode regressions, 19 I-VO, 11 I-VI and 12 E-VI parameters fit best with logarithmic and linear equations respectively. The interpretations of these data are highly speculative but they are suggestive of different processes in operation for different cell populations as a function of either rate or mode.

The second series of summarization data for population studies are presented in Figures 81-83. For each cell type, I-VO, I-VI and E-VI, a family of theoretical interspike interval modulation curves were reconstructed by interpolation of parameter values from regression equations in the Appendix (Tables VIII-XIII) at five

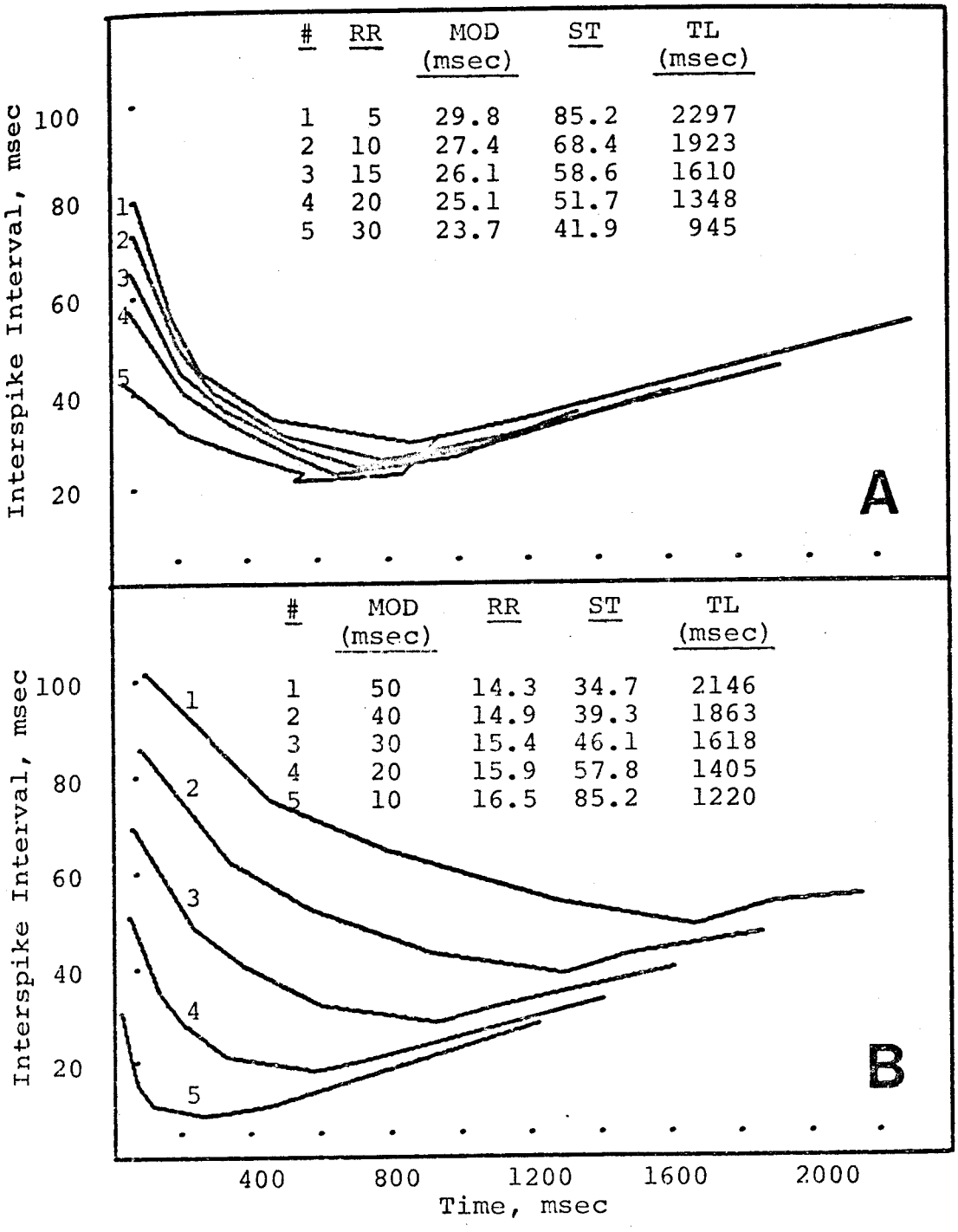

Figure 81. Theoretical reconstruction of interspike interval modulation curves for I-VO cells. Pattern shifts are shown for increasing respiration rate (A) and for decreasing mode (B). Tabular data is given for selected parameters.

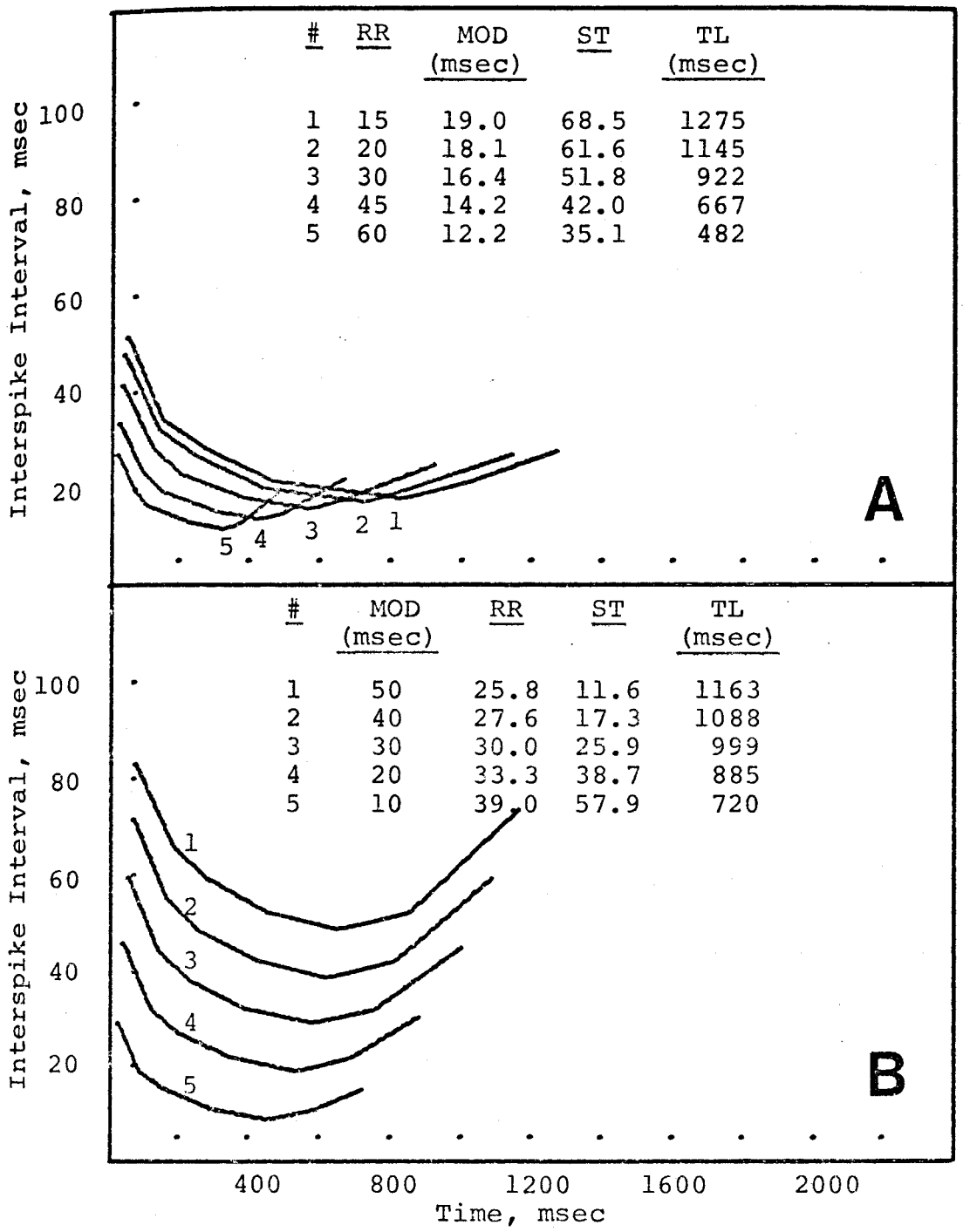

Figure 82. Theoretical reconstruction of interspike interval modulation curves for I-VI cells. Pattern shifts are shown for increasing respiration rate (A) and for decreasing mode (B). Tabular data is given for selected parameters.

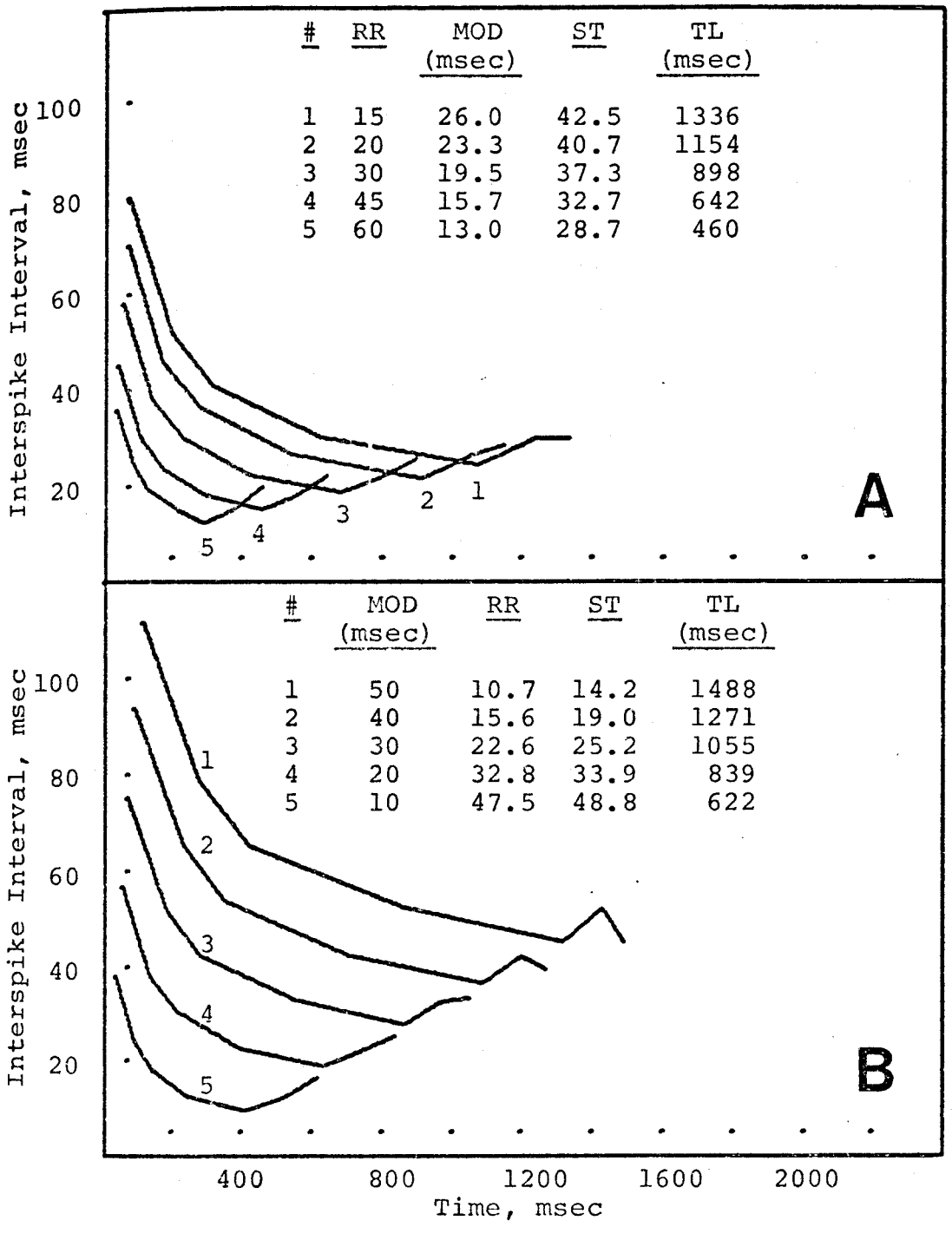

Figure 83. Theoretical reconstruction of interspike interval modulation curves for E-VI cells. Pattern shifts are shown for increasing respiration rate (A) and for decreasing mode (B). Tabular data is given for selected parameters.

different rates and five different modes. Each theoretical curve consists of seven points with the following coordinates:

#	X	Y
1	FI	FI
2	T50	0.5(FI - MI) + MI
3	T70	0.3(FI - MI) + MI
4	T90	0.1(FI - MI) + MI
5	T100	MI
6	T90 + PL	0.1(FI - MI) + MI
7	TL	LI

Corresponding respiration rate, mode, spikes per train and train length parameters are identified for each curve in tabular format. Consistently, the first parameter is the independent variable and the remaining three are dependent variables. For respiration rate plots, MOD $\propto$ TL/(ST-1) $\sim$ k. For mode plots, TL $\propto$ MOD(ST-1) $\sim$ k. Rate and mode curves are plotted in the same figures for each cell population. Panel A represents the projected population response to increasing rates. Panel B predicts the population response to decreasing modes (increasing depths). All plots in Figures 81-83 have identical scalings for easy comparison.

Theoretical interspike interval modulation curves

from I-VO population data are plotted in Figure 81. Panel A shows that the family of curves form a tight distribution group, differing significantly only in train length and possibly first interval as the respiration rate is increased. Only a small decrease in mode is observed due to a simultaneous proportional decrease in train length and spikes per train. Panel B shows significant pattern changes in both horizontal (X-axis) and vertical (Y-axis) interval ordering during decrease in mode time (increase in depth). This is due to the high correlation of many I-VO parameters on mode (Figure 78). As the mode decreases, a minimal increase in respiration rate occurs, presumably due to the simultaneous decrease in train length (TLP $\sim$ k). The latter results from a decrease in mode which is faster than the increase in spikes per train.

Data from the I-VI population are plotted in Figure 82. The curves in panel A show a downward shift as the respiratory rate is increased. Disproportionate decreases in spikes per train and train length produce moderate mode interval shortening. Panel B shows theoretical parallel shifts of the I-VI curves as a function of decreasing mode. The reduction in train length (and, therefore, the increase in respiration rate) follows predicted mode and spikes per train combinations. Comparison of Figures 82

and 81 reveals interesting inspiratory cell pattern differences when the vagi are intact and severed.

The last set of theoretical interspike interval modulation curves are plotted in Figure 83 for E-VI cells. In panel A, an increase in respiration rate is accompanied by a decrease in mode due to a faster decrease in train length than spikes per train. As the mode decreases in panel B, the modulation curve shifts downward in a characteristic activation pattern. Unlike I-VI curves in Figure 82B, E-VI curve shifts are not parallel since a simultaneous decrease in train length occurs. This results from a decreasing mode - spikes per train product as the respiratory depth is increased. Presumably this explains the simultaneous increase in respiration rate as a function of mode. Comparison of E-VI and I-VI patterns in Figures 83 and 82, respectively, demonstrates qualitative similarities between corresponding curves. Quantitatively, however, expiratory cells consistently have lower discharge frequencies than inspiratory cells at equivalent respiratory rates (panel A) as shown by the higher modulation curves for E-VI cells. In mode plots (panel B), expiratory first interval times are significantly longer than those for inspiratory cells.

In summary, the reconstructed discharge patterns

for I-VO, I-VI and E-VI cell groups in Figures 81-83 constitute specific population characteristics corresponding to medullary outputs of respiration rate (panel A) and respiratory depth (1/MOD, panel B). A major conclusion from these data is that respiratory cell discharge patterns have a two-fold dynamic response. In one sense, individual curves represent dynamic modulation of the interspike interval during the train progression as indicated by the "U" shaped quality of all curves. This property of discharge has been recognized by many investigators (51, 69, 72, 74, 91) who have described frequency modulation curves for single respiratory cells. In a second sense, however, respiratory discharge patterns are dynamically locked to the respiration rate and mode outputs. Only a few workers have realized this for rate (31, 127, 129) and depth changes (129). From the data presented in this dissertation, it is suggested that the interpretation of single respiratory cell discharge characteristics must incorporate respiration rate and depth modifications. This suggests that single cell data acquired under differing rate and depth conditions should not be averaged together as Nesland et al. (129) failed to recognize.

B. Single Cell Elements

As previously discussed, all regression plots (Figures 11-34) characteristically possessed standard deviations (error lines) from the mean regression line, indicative of inherent biological variation within each defined population of cells. Selected single cell responses to induced or spontaneous modifications in the breathing pattern were presented in Results to illustrate this cell to cell variability in otherwise homogeneous neuron populations. Figure 46, for example, presents evidence that two cells recorded at the same time can exhibit wide variation in discharge frequency. To summarize single cell differences from and similarities to population characteristics, interspike interval modulation curves for individual units (Figures 44-62) and theoretical units (Figures 81-83) can be compared for corresponding cell types.

Deviations from I-VO population predictions (Figure 81) are seen for inspiratory cell C81UI5L in Figure 54B. After severing both vagi (data points 1 and 2) data points 3-10 represent interspike interval modulation curve response to cummulative doses of pentobarbital. A simultaneous decrease in respiration rate and increase in mode interval time resulted in a predicted

increase in train length, although no overall change in spikes per train was observed. Induced modifications in the latter parameter were masked by significant depression of both rate and depth components by the barbiturate (82, 131).

Many single cell comparisons can be made with the theoretical I-VI population data (Figure 82). Inspiratory pattern responses for two cells, C32UI1R (Figure 44B) and C80UI1R (Figure 45B), show parallel shifts during spontaneous depth increase and decrease, respectively. Since respiration rate modification in each case was at best only minimal, both modulation curve sets match predicted I-VI population patterns as a function of mode (Figure 82B). During a spontaneous increase in respiratory rate with minimal depth change, inspiratory cell C28UI5 (Figure 47B) showed a simultaneous increase in mode interval time. This rendered the single unit pattern response atypical compared to I-VI population characteristics as a function of rate (Figure 82A). For another inspiratory cell, C62UI3R (Figure 48), doxapram-induced increases in respiratory rate revealed typical discharge pattern responses. That is, the interspike interval shifted downward as the mode interval time decreased with a simultaneous decrease in train length and

spikes per train. This response paralleled I-VI population predictions during rate increase (Figure 82A). Finally, inspiratory cells C63UI4R (Figure 50B) and C83UI1L (Figure 52B) were followed during pentobarbital administration. The response pattern of cell C63UI4R during respiration rate decrease closely followed population trends (Figure 82A) with increases in mode, spikes per train and train length. The response pattern of cell C83UI1L, was atypical. In this case, respiration rate was decreased and train length was lengthened, but a significant decrease in the mode interval time caused an exaggerated increase in spikes per train. The modulation curve shift (Figure 52B) appeared to possess characteristics of theoretical I-VI population curves as a function of both rate and mode.

A few single expiratory cell examples can be compared with E-VI population predictions in Figure 83. Cell C64UE4R (Figure 56B) and cell C71UE2R (Figure 58B) were subjected to cumulative doses of pentobarbital. In the former case, only a slight decrease in the mode was observed as the rate was significantly decreased. There was a corresponding increase in spikes per train and train length. With the exception of a peculiar inflection in the interspike interval modulation curve

for the first three data points (Figure 56B), this pattern response resembled theoretical E-VI population trends during rate decrease (Figure 83A). In general, cell C71UE2R pattern shifts paralleled E-VI population constructions as a function of mode (Figure 83B). During pentobarbital accumulation, there was only a slight respiration rate decrease while the mode was significantly increased. The train length was not lengthened as predicted, but spikes per train decreased nevertheless. In Figure 60B, expiratory cell C82UE3R was depressed by cumulative doses of morphine sulphate. With the exception of the control pattern at data point 1, successive injections of morphine produced atypical interspike interval modulation curve shifts which did not correlate with E-VI population projections related to either respiration rate or mode changes (Figure 83). Morphine caused a slight increase in respiration rate which was inconsistent with Ngai's (132) observations. Also, the mode was increased while the spikes per train decreased, producing a significant shortening in the train length. Examination of Figure 60B reveals that morphine, in this case, exerts its greatest effect on the latter portion of the interspike interval modulation curve. Finally, expiratory cell C68UE6R (Figure 62B) was analyzed before (Curve 1)

and after (Curves 2 and 3) unilateral left vagotomy. The mode interval time and spikes per train changed in opposite directions so that train length, and therefore respiration rate, remained relatively constant. Disregarding the latter two characteristics, the single cell pattern shifts resembled E-VI population data as a function of mode (Figure 83B).

From the comparison of inspiratory (I-VI) and expiratory (E-VI) single cell data and population responses, it is difficult to find major differences between these two neuron groups. Both cell types possess indistinguishable variability during barbiturate depression, and interspike interval modulation curves (Figures 82 and 83) reveal distinct similarities as a function of either respiration rate or mode. Interpretation of these data is consistent with the hypothesis that inspiratory and expiratory neurons are functionally similar. It is possible that these cell types belong to a similar reticular formation cell class, differing only in intercellular connections.

Gross characterizations of respiratory cell discharge patterns include assessment of spike frequency, burst duration and phasing with the respiratory cycle. Variations in the first two parameters throughout the

respiratory complex can be explained on the basis of threshold differences among cells (91) and/or differing combinations of neuronal connections (36). The pairing of cell inputs (excitatory and inhibitory) with threshold characteristics of the membrane defines the level of excitability for any given respiratory neuron. This excitability level for individual respiratory cells and grouped neuron populations fluctuates in phase with the respiratory cycle due to oscillating inputs (156) and variations in threshold values (18, 154).

The data presented in this dissertation indicate that expiratory cells have lower discharge frequencies than inspiratory cells at equivalent respiratory rates and modes (compare Figures 82 and 83) suggesting that the former have less excitatory inputs and/or higher firing thresholds than the latter. Also, the observation that expiratory cell parameters correlate better with rate and mode (cf. Figures 76 and 77) indicates that the E-VI population is relatively more homogeneous than the I-VI cell group. This decreased variability in the expiratory population may be indicative of fewer modulatory inputs to these cells, or of the dominance of one or more inputs with relatively lower variability.

Finally, both inspiratory and expiratory cells

tend to fire for a constant fraction of the respiratory cycle (TLP $\sim$ k) irrespective of respiration rate or depth changes (Figures 49-61). A wide variety of percentages are found for I-VO, I-VI and E-VI cell groups (Figures 22, 34 and 43) indicating that all cells in any defined population do not have identical starting and stopping times. Further study into this phenomenon, preferably at the intracellular level, should provide important data on single cell inputs and threshold characteristics.

C. Respiratory Complex Organization

The most consistent definition of apneusis refers to the situation where inspiratory mechanisms are locked in a hold position for an extended period of time. This respiratory pattern can be induced either by appropriate neural transections (112, 113, 114, 116, 117, 136, 167, 176 and Figure 63) or high barbiturate levels (31, 82, 131, 151 and Figure 64). Although both techniques result in prolonged inspiratory times, significant differences occur in the depth of inspiration. Neural transections produce near maximal inspiratory efforts while barbiturate administration produces a prolonged, but shallower inspiratory hold. Although this difference cannot be seen by comparing Figures 63 and 64, this result is presumably due to partial depression of the

inspiratory mechanism by barbiturate.

The production and abolition of apneusis has been useful in modeling the organization of brainstem respiratory mechanisms. For example, localized lesions in the rostral pons in vagotomized prepartions have resulted in apneusis (22, 93, 134, 147, 151, 152, 170, 172). Investigators have suggested that this pneumotaxic area is inhibitory to inspiration. Transection between the medullary-pontine border in apneustically breathing animals converts this pattern into one of gasping (26, 87, 112, 133, 136, 167, 170). Coupled with the former data, this suggests that the lower pons contains a constantly discharging cell population which is excitatory to rhythmically active medullary inspiratory neurons. From this work and similar studies, a general concept of respiratory organization developed which suggested that medullary inspiratory neurons are inhibited by vagal, pneumotaxic, cerebellar and expiratory cell connections and are facilitated by apneustic drives.

The fact that barbiturates can induce apneusis suggests that respiratory inhibitory mechanisms are differentially more susceptible to pharmacologic blockade than facilitatory systems. If this were not the case, barbiturate administration should result in apnea or

expiratory holds as seen with morphine (132). Figure 72 implies that rostral pontine cells are depressed before medullary cells at equivalent barbiturate levels in the same cat. This finding is consistent with the observation that barbiturates act at high levels of the CNS and then work their way down the neuraxis as the dose is increased. Anatomically speaking, then, the pneumotaxic region may be depressed before the apneustic or medullary areas with cumulative barbiturate administration.

When the vagi are intact, it takes a higher dose of barbiturate to induce apneusis than when the vagi are severed (Figure 66). Assuming that pneumotaxic circuits are the first to be blocked as discussed above, this drug level difference suggests that either vagal influences or inspiratory mechanisms are mediated at sub-pneumotaxic stations (lower pons) or inhibitory synapses are more susceptible to barbiturate blockade than facilitatory synapses. In either case, high barbiturate levels appear to disrupt brainstem connections so that unilateral vagal influence cannot cross over to the opposite brainstem side (compare Figures 63 and 67).

The notion that apneusis results from a preponderant influence of facilitatory versus inhibitory drives on inspiration was introduced in Results. This concept

is actually a combination of Gray's (77) multiple factor theory (Σ chemical factors) and Gesell's et al. (71) reflexogenic components (Σ neural factors). For example, removal of inhibition via cerebellectomy (76, 83 and Figure 65), vagotomy (Figure 67) or decreasing carotid sinus pressure (BCO, Figure 73; histamine, Figure 74) all produced apneustic breaths. Similarly, increased facilitatory drive via doxapram (Figure 75) produced identical pattern changes. These results could only be observed when the barbiturate level was significantly higher than the initial anesthetic dosage (30 mg/kg pentobarbital). At lower levels, cerebellectomy, showed little, and vagotomy showed marked rate and depth changes, while decreased sinus pressure (86) and doxapram produced definite rate acceleration and depth increase. From these data it is suggested that pneumotaxic inhibitors must be blocked by barbiturate before apneusis can be induced by various experimental procedures. Krieger, Christensen, Sapru and Wang (105) have recently postulated the presence of another inhibitory afferent pathway in the cervical cord, which modulates pontine apneustic mechanisms. If this is a real entity, it represents another inhibitory input to the inspiratory system.

Results derived from single cell studies support

the conclusion that barbiturates differentially block inhibitory before facilitatory inputs. Figure 68 shows that inspiratory cells fire continuously during apneusis indicating that they are not depressed to an appreciable extent by barbiturate. Expiratory cells, on the other hand, are completely inhibited during the apneustic breath (Figure 69) due to direct barbiturate depression or more probably to reciprocal inhibition from constantly active inspiratory cells. Robson et al. (148) found similar results, but also described constant expiratory activity in some circumstances.

An interesting exception was observed for inspiratory cell C54UI13L as shown in Figure 84. A prolonged apneustic breath was produced one and one-half minutes after pentobarbital injection (new incremental dose level at 19.6 mg/kg). Unlike the inspiratory cell response in Figure 68, cell C54UI13L failed to fire continuously during the inspiratory hold. Rather, the unit turned off at a train length that was not significantly different from control. The cell recording was not lost at this time since the cell fired during succeeding breaths. This atypical unit discharge could arise from an inspiratory cell on the fringe of the I-VO population that was blocked by barbiturate or from a starter neuron

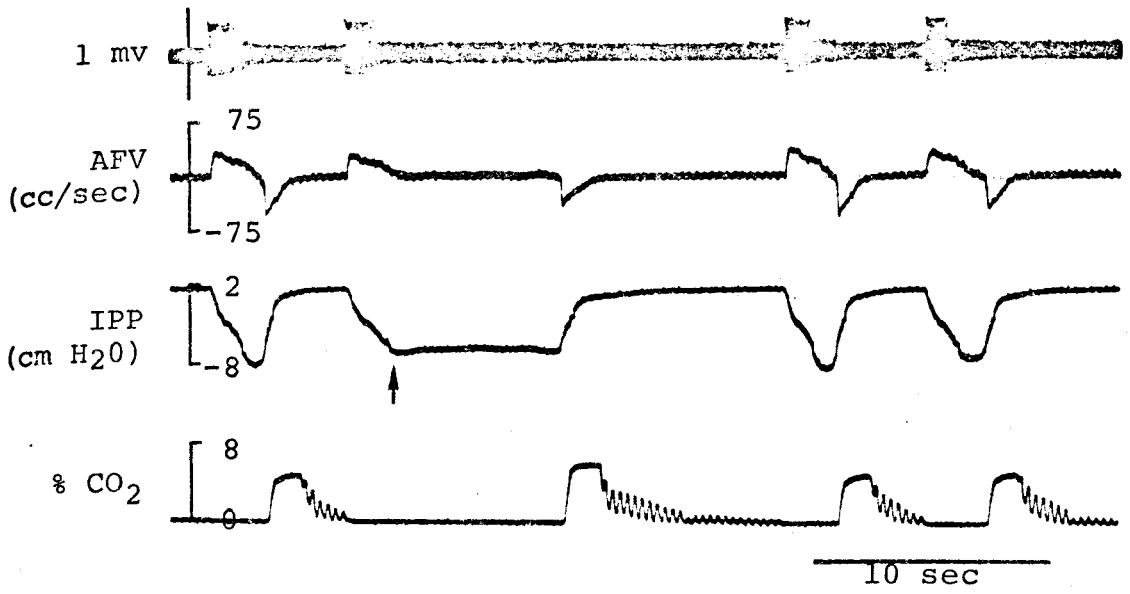

Figure 84. C54UI13L. Single inspiratory cell recording during induction of apneustic breath (arrow) 90 seconds after administration of 1.8 mg/Kg pentobarbital. Note failure of unit to maintain discharge for duration of the inspiratory hold as in Figure 68. Vagi sectioned.

or pacemaker cell responsible for activating the inspiratory complex. The latter speculation is an exciting possibility which merits further investigation.

The triphasic shift in the histogram distribution in Figures 70 and 71 shows that an inspiratory cell with vagi intact can, in fact, be activated during barbiturate accumulation. Since the respiration rate was consistently depressed, the coupling between rate and unit discharge frequency was destroyed. In normal cases, rate and cell discharge frequency change in the same direction (31). Therefore, this uncoupling at medium barbiturate levels represents a significant change in brainstem functional activity during drug depression. More specifically, by comparison of Figures 66 and 71, the inflection in the inspiratory curves in the latter figure can be attributed to pneumotaxic blockade. That is, the inflection occurred at a low barbiturate level (4-7 mg/kg thiopental) not sufficient to block vagal inhibitory feedback (Figure 66). Also, apneusis was not seen at this drug level.

Following apneustic breaths there is usually an elevated end-expiratory % CO_2 (Figures 64, 65, 67, 68, 69, 73, 74). It was suggested that this central chemodrive was of sufficient magnitude to periodically

interrupt inspiratory holds. This view is inconsistent with Stella's (168) data, which showed prolonged apneustic breaths induced by either CO_2 administration or rebreathing. On the other hand, Ngai (130) showed that 10% CO_2 accelerated the apneustic cycling, a response independent of peripheral chemoreceptor drives. Åström (9) has published excellent work on the combined action of CO_2 excess and O_2 deficiency in the regulation of breathing. The work of Mitchell and Herbert (123) should also be considered. These workers showed that CO_2 does have a direct effect on central inspiratory neurons in terms of rhythm generation (increased frequency discharge) although CO_2 does not change the resting membrane potential.

D. Information Transfer

The data presented in this dissertation have established certain quantitative relationships between respiratory cell discharge characteristics and medullary outputs of respiration rate and depth (1/MOD). It is suggested that if this study were repeated at the phrenic motoneuron or vagal afferent level, valuable information on gross properties of intersystem information transfer could be evaluated.

In a control systems approach, it would be ideal to derive transfer functions (ratio of output to input)

relating discharge pattern differences to synaptic processes intervening between successive stations of the respiratory arc. Due to numerous complexities inherent in the system, including proprioceptive modulation of rate and depth outputs at the spinal cord level (7, 54, 159, 160) and rate and depth interactions (37), the application of rigid mathematical criteria in transfer function derivation is quite difficult. Nevertheless, by comparison of idealized interspike interval modulation curves from various respiratory populations (expiratory, inspiratory, internuncial, phrenic, vagal afferent) it may be possible to initiate quantitative description of system couplings.

Gesell et al. (72) studied frequency modulation patterns of respiratory cells and found similar discharge patterns along major arcs of the respiratory system. For two of these components, interspike interval modulation curves for a vagal afferent and phrenic motoneuron were reconstructed in Figure 85A and B from the data of Adrian (2) and Pitts (142), respectively. These curves, generated from single train discharges, have a relatively smooth "U" shaped form which is characteristic of inspiratory and expiratory cells only after averaging of many successive bursts (cf. Figure 9). The regularity

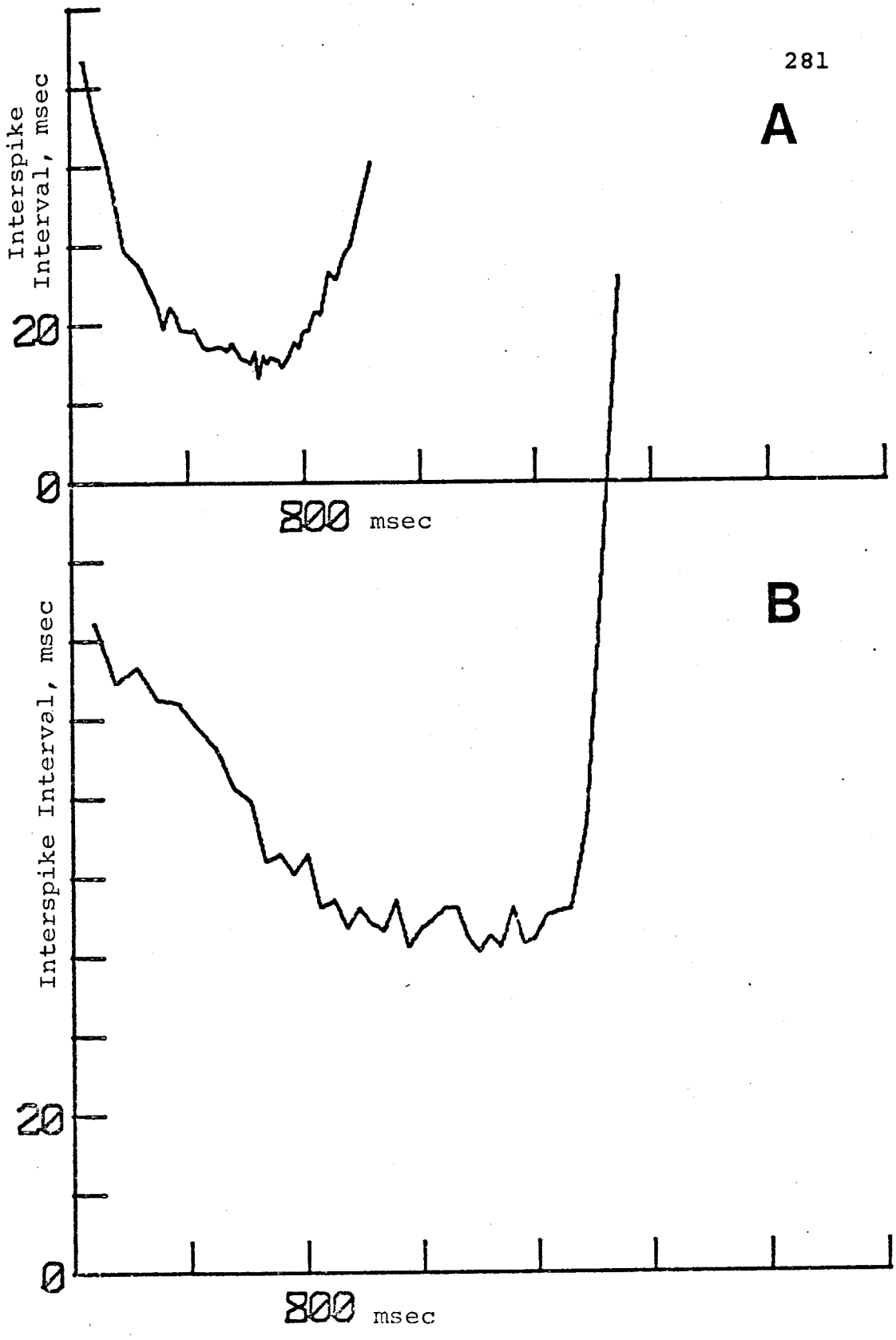

Figure 85. Interspike interval modulation curves for single train of vagal afferent (A) and phrenic motoneuron (B).

in vagal afferent interval ordering for a single burst (Figure 85A) derives from the highly predictable relationships between lung volume and vagal afferent discharge frequency (2). The regular phrenic pattern (Figure 85B) for a single burst indicates that this motoneuron is acting as a physiological integrator. Spatial summation of several respiratory neurons and/or spinal neurons arriving at phrenic cell bodies results in transformation of the variable medullary output into a smoothed pattern before preceeding to the respiratory musculature (75, 143). Comparison of Figure 85B (RR ∿ 15) with Figure 82A (Curve 1) shows that average medullary outputs also undergo frequency depression as they are converted into phrenic outputs. The phrenic motoneuron may act as a frequency converter to provide suitable impulse frequency to muscles of respiration for tidal volume control (144).

Dirken and Woldring (51) suggested that expiratory cells were activated by vagal afferents. If this is so, the inflation reflex which inhibits inspiration may be mediated through expiratory cells which have inhibitory inputs to inspiratory neurons. The data in Table III shows that only a few expiratory cells could be located when the vagus nerves were sectioned. Moreover,

Figure 62 shows that an expiratory discharge could be inhibited by vagotomy, suggesting that some kind of functional connection exists between vagal afferents and expiratory neurons. Assuming this to be true, the greater homogeniety of expiratory than inspiratory cells may be due to the dominence of highly regular input signals carried over vagal afferents (Figure 85A).

If one studies the respiratory system in terms of respiratory rate and depth outputs, it should be recognized that the transfer function for rate is equal to unity between serially-linked components. This is true since all components of the respiratory arc oscillate at the same frequency. The transfer function for depth, however, remains undefined since it is coded and recoded at each level of the respiratory system.

CHAPTER VII

CONCLUSION

1. The experiments presented in this dissertation were designed to investigate three aspects of central respiratory control utilizing computer techniques: (a) population characteristics of inspiratory and expiratory cells in the medulla; (b) characteristics of single elements in the above populations; (c) genesis of apneustic breathing by barbiturate administration and other experimental procedures.

2. The cells examined in these experiments comprised three neuronal populations: inspiratory, vagus nerves sectioned; inspiratory, vagus nerves intact; and expiratory, vagus nerves intact.

3. A new mathematical technique was devised to describe average interspike interval ordering of respiratory trains (interspike interval modulation curves) by temporal summation of consecutive trains discharging under steady state conditions. This technique provides

a capability for detailed analysis of the respiratory train, not possible by histogram analysis.

4. Twenty-five parameters, most of which have not been reported in the literature, were derived from the modulation curves. These parameters describe specific characteristics of the initial, middle and terminal phases of a respiratory train.

5. All parameters for similar populations were correlated with two functional respiratory outputs, rate and depth ($\propto 1/$mode interval time) using regression analyses. The implications of similarities and dissimilarities in the response of inspiratory and expiratory cells were discussed.

6. Theoretical modulation curves were reconstruted from regression equations for each population. These curves predict characteristic alterations in respiratory cell discharge patterns as a function of rate and mode.

7. Single cell parameter responses were analyzed during experimental manipulations designed to modify respiratory rate and depth. Variations in discharge patterns, observed among many single units, were consistent with the expected variation within population distributions.

8. Various experimental procedures were found to

elicit apneustic breathing in cats under pentobarbital anesthesia. Additional doses of depressant drugs appeared to induce apneusis by differential inhibition of negative feedback loops in the brainstem. At appropriate barbiturate levels, decreasing carotid sinus pressure or doxapram administration elicited apneustic breathing, presumably by activation of facilitatory input. In other cases, vagotomy and cerebellectomy also produced apneusis.

9. The data in this study were discussed in the context of possible interneuronal connections within the brainstem respiratory complex.

CHAPTER VIII

BIBLIOGRAPHY

1. Achard, C. and V.M. Bucher. Courants d'action bulbaires a rythme respiratoire. Helv. Physiol. Pharmacol. Acta 12: 265-283, 1954.

2. Adrian, E.D. Afferent impulses in the vagus and their effect on respiration. J. Physiol., London 79: 332-358, 1933.

3. Adrian, E.D. and D.W. Bronk. The discharge of impulses in motor nerve fibres. J. Physiol., London 66: 81-101, 1928.

4. Adrian, E.D. and F.J.J. Buytendijk. Potential changes in the isolated brain stem of the goldfish. J. Physiol., London 71: 121-135, 1931.

5. Amoroso, E.C., J.G. Bainbridge, F.R. Bell, A.M. Lawn, and H. Rosenberg. Central respiratory spike potentials. Nature 167: 603-604, 1951.

6. Amoroso, E.C., F.R. Bell, and H. Rosenberg. The localization of respiratory regions in the rhombencephalon of the sheep. Proc. Roy. Soc., London, Ser. B 139: 128-140, 1951.

7. Andersen, P. and T.A. Sears. Medullary activation of intercostal fusimotor and alpha motorneurones. J. Physiol., London 209: 739-755, 1970.

8. Arnheim, R. Arch. Anat. Physiol., Leipzig: 35, 1894 (Cited in Reference 144).

9. Åström, A. On the action of combined carbon dioxide excess and oxygen deficiency in the regulation of breathing. Acta Physiol. Scand. Suppl. 98, 27: 1-61, 1952.

10. Aviado, D.M., Jr. and C.F. Schmidt. Respiratory burns with special reference to pulmonary edema and congestion. Circulation 6: 666-680, 1952.

11. Baker, A.B., H.A. Matzke, and G.R. Brown. Poliomyelitis. III. Bulbar poliomyelitis; A study of medullary function. Arch. Neurol. Psychiat. 63: 257-281, 1950.

12. Baker, F.L. and D.H. York. A reliable technique for making glass microelectrodes of known resistance. Proc. I.E.E.E. 59: 1711-1712, 1971.

13. Bancroft, J. Features in the Architecture of Physiological Function. Cambridge: University Press, 1938, pp. 368.

14. Batsel, H.L. Localization of bulbar respiratory center by microelectrode sounding. Exptl. Neurol. 9: 410-426, 1964.

15. Batsel, H.L. Some functional properties of bulbar respiratory units. Exptl. Neurol. 11: 341-366, 1965.

16. Baumgarten, R. von. Koordinationsformen einzelner Ganglienzellen der rhombencephalen Atemzentren. Pflügers Arch. 262: 573-594, 1956.

17. Baumgarten, R. von. Zur Technik der Mikroableitung am pulsierenden Gehirn. Naturwiss. 1: 22-23, 1957.

18. Baumgarten, R. von, K. Balthasar, and H.P. Koepchen. Über ein Substrat atmungsrhythmischer Erregungsbildung im Rautenhirn der Katze. Pflügers Arch. 270: 504-528, 1960.

19. Baumgarten, R. von. and E. Kanzow. The interaction of two types of inspiratory neurons in the region of the tractus solitarius of the cat. Arch. Ital. Biol. 96: 361-373, 1958.

20. Baumgarten, R. von, E. Kanzow, H.P. Koepchen, and F. Timm. Beitrag zur Technik der extra- und intracellulären, sowre der stereotaktischen Mikroableitung im Gehirn. Pflügers Arch. 271: 245-256, 1960.

21. Baumgarten, R. von and G.C. Salmoiraghi. Respiratory neurons in the goldfish. Arch. Ital. Biol. 100: 31-47, 1962.

22. Baxter, D.W. and G. Olszewski. Respiratory responses evoked by electrical stimulation of pons and mesencephalon. J. Neurophysiol. 18: 276-287, 1955.

23. Beaton, L.E. and H.W. Magoun. Localization of the medullary respiratory centers in the monkey. Am. J. Physiol. 134: 177-185, 1941.

24. Bertrand, F. and A. Hugelin. Respiratory synchronizing function of nucleus parabrachialis medialis: Pneumotaxic mechanisms. J. Neurophysiol. 34: 189-207, 1971.

25. Borison, H.L. Electrical stimulation of the neural mechanism regulating spasmodic respiratory acts in the cat. Am. J. Physiol. 154: 55-62, 1948.

26. Breckenridge, C.G. and H.E. Hoff. Pontine and medullary regulation of respiration in the cat. Am. J. Physiol. 160: 385-394, 1950.

27. Breckenridge, C.G. and H.E. Hoff. Reflex respiration. Am. J. Physiol. 178: 521, 1954.

28. Breckenridge, C.G., H.E. Hoff, and H.T. Smith. Effect on respiration in midpontine animal of chemical inhibition of facilitatory system. Am. J. Physiol. 162: 74-79, 1950.

29. Breuer, J. Die Selbststeuerung der Atmung durch den Nervus vagus. Sitzber. Akad. Wiss. Wien. 58: 909-937, 1868.

30. Brock, L.G., J.S. Coombs, and J.C. Eccles. The recording of potentials from motorneurones with an intracellular electrode. J. Physiol., London 117: 431-460, 1952.

31. Brodie, D.A. The effect of thiopental and cyanide on the activity of inspiratory neurons. J. Pharmacol. Exptl. Therap. 126: 264-269, 1959.

32. Brodie, D.A. and H.L. Borison. Analysis of central control of respiration by the use of cyanide. J. Pharmacol. Exptl. Therap. 118: 220-229, 1956.

33. Brodie, D.A. and H.L. Borison. Evidence for a medullary inspiratory pacemaker. Functional concept of central regulation of respiration. Am. J. Physiol. 188: 347-354, 1957.

34. Brookhart, J.M. The respiratory effects of localized faradic stimulation of the medulla oblongata. Am. J. Physiol. 129: 709-723, 1940.

35. Burns, B.D. The central control of respiratory movements. Brit. Med. Bull. 19: 7-9, 1963.

36. Burns, B.D. and G.C. Salmoiraghi. Repetitive firing of respiratory neurons during their burst activity. J. Neurophysiol. 23: 27-46, 1960.

37. Clark, F.J. and C. von Euler. On the regulation of depth and rate of breathing. J. Physiol., London 222: 267-295, 1972.

38. Cohen, M.I. Intrinsic periodicity of the pontile pneumotaxic mechanism. Am. J. Physiol. 195: 23-27, 1958.

39. Cohen, M.I. Respiratory periodicity in the paralyzed vagotomized cat: Hypocapnic polypnea. Am. J. Physiol. 206: 845-854, 1964.

40. Cohen, M.I. Discharge patterns of brain-stem respiratory neurons in relation to carbon dioxide tension. J. Neurophysiol. 31: 142-165, 1968.

41. Cohen, M.I. Discharge patterns of brain-stem respiratory neurons during Hering-Breuer reflex evoked by lung inflation. J. Neurophysiol. 32: 356-374, 1969.

42. Cohen, M.I. How respiratory rhythm originates: Evidence from discharge patterns of brainstem respiratory neurons. Ed. Porter. Breathing: Hering Breuer Centenary Symposium. A Ciba Foundation Symposium. London: Churchill, 1970, pp. 125-157.

43. Cohen, M.I. Switching of the respiratory phases and evoked phrenic responses produced by rostal pontine electrical stimulation. J. Physiol., London 217: 133-158, 1971.

44. Cohen, M.I. and P.M. Gootman. Spontaneous and evoked oscillations in respiratory and sympathetic discharge. Brain Res. 16: 265-268, 1969.

45. Cohen, M.I. and S.C. Wang. Respiratory neuronal activity in pons of cat. J. Neurophysiol. 22: 33-50, 1959.

46. Comroe, J.H., Jr. The effects of direct chemical and electrical stimulation of the respiratory center in the cat. Am. J. Physiol. 139: 490-498, 1943.

47. Cooper, G.F., J.G. Robson, and I. Waldron. The action potentials recorded from undamaged nerve fibres with micro-electrodes. J. Physiol., London 200: 9P-11P, 1969.

48. Culberson, J.L. and D.L. Kimmel. Central distribution of primary afferent fibers of the glossopharyngeal and vagal nerves in the opossum, Didelphis virginiana. Brain Res. 44: 325-335, 1972.

49. Davis, H.L., W.S. Fowler, and E.H. Lambert. Effect of volume and rate of inflation and deflation on transpulmonary pressure and response of pulmonary stretch receptors. Am. J. Physiol. 187: 558-566, 1956.

50. Delhez, L. Évolution de l'activité électrique integrée du diaphragme durant l'hyperventilation. Compt. Rend. Soc. Biol. 158: 2496-2500, 1964.

51. Dirken, M.N.J. and S. Woldring. Unit activity in bulbar respiratory centre. J. Neurophysiol. 14: 211-225, 1951.

52. Einthoven, W. On vagus currents examined with the string galvanometer. Quart. J. Exptl. Physiol. 1: 243-245, 1908.

53. Eldridge, F.L. Relationship between phrenic nerve activity and ventilation. Am. J. Physiol. 221: 535-543, 1971.

54. Euler, C. von. Proprioceptive control in respiration. In: Granit R. muscular afferents and motor control. Proc. First Nobel Symposium. Stockholm: Almquist et Wiksell, 1966, pp. 197-207.

55. Euler, C. von, F. Herrero, and I. Wexler. Control mechanisms determining rate and depth of respiratory movements. Resp. Physiol. 10: 93-108, 1970.

56. Eyzaguirre, C. and J.R. Taylor. Respiratory discharge of some vagal motorneurons. J. Neurophysiol. 26: 61-78, 1963.

57. Fallert, M. and R. Mühlemann. Der Hering-Breuer-Reflex bei künstlicher Beatmung des Kaninchens. Pflügers Arch. 330: 162-174, 1971.

58. Fink, B.R., E.C. Hanks, D.A. Holaday, and S.H. Ngai. Monitoring of ventilation by integrated diaphragmatic electromyogram. Determination of carbon dioxide (CO_2) threshold in anesthetized man. J. Am. Med. Assoc. 172: 1367-1371, 1960.

59. Flourens, M.J.P. Recherches Expérimentales sur les Propriétés et les Fonctions du Système Nerveux dans les Animaux Vertébrés. Paris: Crevot, 1842, pp. 331.

60. Flourens, M.J.P. Physiologie animale - note sur le point vital de la moelle allongée. Compt. Rend. Acad. Sci. 33: 437-439, 1851.

61. Foley, J.O. and F.S. DuBois. An experimental study of the rootlets of the vagus nerve in the cat. J. Comp. Neurol. 60: 137-159, 1934.

62. Freeman, J.A. A simple method for producing in quantity, metal micro-electrodes with a desired taper and impedance. Electroenceph. Clin. Neurophysiol. 26: 623-626, 1969.

63. Gabriel, M. and H. Seller. Excitation of expiratory neurons adjacent to the nucleus ambiguus by carotid sinus baroreceptor and trigeminal afferents. Pflügers Arch. 313: 1-10, 1969.

64. Gad, J. and G. Marinesco. Recherches experimentales sur le centre respiratoire bulbaire. Comp. Rend. Acad. Sci. 115: 444-447, 1892.

65. Galen, C. De Anat. Administr. lib. VIII. Cap. IX. (Cited in Reference 144).

66. Gerstein, G.L. Analysis of firing patterns in single neurons. Science 131: 1811-1812, 1960.

67. Gerstein, G.L. and N.Y.S. Kiang. An approach to the quantitative analysis of electrophysiological data from single neurons. Biophysical J. 1: 15-28, 1961.

68. Gerstein, G.L. and B. Mandelbrot. Random walk models for the spike activity of a single neuron. Biophysical J. 4: 41-68, 1964.

69. Gesell, R., A.K. Atkinson, and R.C. Brown. The origin of respiratory activity patterns. Am. J. Physiol. 128: 629-634, 1940.

70. Gesell, R., J. Bricker, and C. Magee. Structural and functional organization of the central mechanism controlling breathing. Am. J. Physiol. 117: 423-452, 1936.

71. Gesell, R. and M.A. Hamilton. Reflexogenic components of breathing. Am. J. Physiol. 133: 694-719, 1941.

72. Gesell, R., C.S. Magee, and J.W. Bricker. Activity patterns of the respiratory neurons and muscles. Am. J. Physiol. 128: 615-628, 1940.

73. Gesell, R., E.H. Steffensen, and J.M. Brookhart. The interaction of the rate and depth components of respiratory control. Am. J. Physiol. 120: 105-120, 1937.

74. Gesell, R. and J.J. Worzniak. On the origin of the expiratory activity patterns. Am. J. Physiol. 131: 681-686, 1941.

75. Gill, P.K. and M. Kuno. Excitatory and inhibitory actions on phrenic motoneurones. J. Physiol., London 168: 274-289, 1963.

76. Glasser, R.L., J.W. Tippett, and V.A. Davidian, Jr. Cerebellar activity, apneustic breathing, and the neural control of respiration. Nature 209: 810-812, 1966.

77. Gray, J.S. The multiple factor theory of the control of respiratory ventilation. Science 103: 739-744, 1946.

78. Green, J.D. A simple microelectrode for recording from the central nervous system. Nature 182: 962, 1958.

79. Haber, E., K.W. Kohn, S.H. Ngai, D.A. Holaday, and S.C. Wang. Localization of spontaneous respiratory neuronal activities in the medulla oblongata of the cat: A new location of the expiratory center. Am. J. Physiol. 190: 350-355, 1957.

80. Hammouda, M. and W.H. Wilson. Reflex slowing of respiration accompanying changes in the intrapulmonary pressure. J. Physiol., London 88: 284-297, 1937.

81. Harris, P.H.P. Electrical activity in medullary respiratory centres. J. Physiol., London 196: 80P-81P, 1968.

82. Harris, T.D. and H.L. Borison. Effect of pentobarbital on electrical excitability of respiratory center in the cat. Am. J. Physiol. 176: 77-82, 1954.

83. Henderson, V.E. and T.A. Sweet. On the respiratory centre. Am. J. Physiol. 91: 94-102, 1929.

84. Hering, E. and J. Breuer. Die Selbststeuerung der Atmung durch den Nervus vagus. Sitzber. Akad. Wiss. Wien. 57: 672, 1862.

85. Hess, W.R. Die Regulierung der Atmung; gleichzeitig ein Beitrag zur Physiologie des vegetativen Nervensystems. Leipzig: Georg Thieme, 1931, pp. 137.

86. Heymans, C. and J.J. Bouckaert. Sinus caroticus and respiratory reflexes. J. Physiol., London 69: 254-266, 1930.

87. Hoff, H.E. and C.G. Breckenridge. The medullary origin of respiratory periodicity in the dog. Am. J. Physiol. 158: 157-172, 1949.

88. Hoff, H.E. and C.G. Breckenridge. Levels of integration of respiratory patterns. J. Neurophysiol. 15: 47-56, 1952.

89. Hubel, D.H. Tungsten microelectrode for recording from single units. Science 125: 549-550, 1957.

90. Hukuhara, T. and S. Nakayama. Further studies on the effects of the transection of the brain stem upon respiratory movements. Jap. J. Physiol. 9: 43-48, 1959.

91. Hukuhara, T., S. Nakayama, and H. Okada. Action potentials in the normal respiratory centers and its centrifugal pathways in the medulla oblongata and spinal cord. Jap. J. Physiol. 4: 145-153, 1954.

92. Joels, N. and M. Samueloff. The activity of the medullary centres in diffusion respiration. J. Physiol., London 133: 360-372, 1956.

93. Johnson, F.H. The locus coeruleus as a pneumotaxic center. Anat. Record 112: 348, 1952.

94. Kahn, N. and S.C. Wang. Descending respiratory pathways in the medulla oblongata of the cat. Am. J. Physiol. 209: 599-603, 1965.

95. Kahn, N. and S.C. Wang. Pontine pneumotaxic center and central respiratory rhythm. Am. J. Physiol. 211: 520-524, 1966.

96. Kahn, N. and S.C. Wang. Electrophysiologic basis for pontine apneustic center and its role in integration of the Hering-Breuer reflex. J. Neurophysiol. 30: 301-318, 1967.

97. Katz, S. and A.D. Horres. Medullary respiratory neuron response to pulmonary emboli and pneumothorax. J. Appl. Physiol. 33: 390-396, 1972.

98. Katz, R.L., S.H. Ngai, G.G. Nahas, and S.C. Wang. Relationship between acid-base balance and the central respiratory mechanisms. Am. J. Physiol. 204: 867-872, 1963.

99. Kerr, D.I.B., C.W. Dunlop, E.D. Best, and J.A. Mullner. Modification of apneusis by afferent vagal stimulation. Am. J. Physiol. 176: 508-512, 1954.

100. Kim, J.K. and F.G. Carpenter. Excitation of medullary neurons by chemical agents. Am. J. Physiol. 201: 1187-1191, 1961.

101. Knight, B.W. Dynamics of encoding in a population of neurons. J. Gen. Physiol. 59: 734-766, 1972.

102. Knight, B.W. The relationship between the firing rate of a single neuron and the level of activity in a population of neurons. J. Gen. Physiol. 59: 767-778, 1972.

103. Knowlton, G.C. and M.G. Larrabee. A unitary analysis of pulmonary volume receptors. Am. J. Physiol. 147: 100-114, 1946.

104. Korczyn, A.D., U. Leibowitz, and F. Bergmann. Effect of pentobarbitone on respiratory responses to nerve stimulation. Confin. Neurol. 25: 183-195, 1965.

105. Krieger, A.J., H.D. Christensen, H.N. Sapru, and S.C. Wang. Changes in ventilatory patterns after ablation of various respiratory feedback mechanisms. J. Appl. Physiol. 33: 431-435, 1972.

106. Lamarre, Y. and J.P. Raynauld. Rhythmic firing in the spontaneous activity of centrally located neurons. A method of analysis. Electroenceph. Clin. Neurophysiol. 18: 87-90, 1965.

107. Legallois, C.J. Expériences sur le Principe de la Vie. Paris: d'Hautel, 1812, pp. 328.

108. Liljestrand, Å. Respiratory reactions elicited from medulla oblongata of the cat. Acta Physiol. Scand. 29, Suppl. 106: 321-393, 1953.

109. Loewy, A. Experimentelle studien über das Athemcentrum in der Medulla oblongata und die Bedingungen seiner Thatigkeit. Pflügers Arch. 42: 245-272, 1888.

110. Longet, F.A. Experiences relatives aux effets de l'inhalation de l'éther sulfurique sur le systéme nerveux. Arch. Gen. Med. 13: 374-412, 1847.

111. Lorry, A.C. Acad. Roy. des Sci. Mem. de Math. et de Physique. 3: 344, 1760 (Cited in Reference 144).

112. Lumsden, T. Observations on the respiratory centres in the cat. J. Physiol., London 57: 153-160, 1923.

113. Lumsden, T. Observations on the respiratory centres. J. Physiol., London 57: 354-367, 1923.

114. Lumsden, T. The regulation of respiration. J. Physiol., London 58: 81-91, 1923.

115. Magoun, H.W. and L.E. Beaton. Respiratory responses from stimulation of the medulla of the cat. Am. J. Physiol. 134: 186-191, 1941.

116. Marckwald, M. Die Athembewegungen und deren Innervation beim Kaninchen. Z. Biol. 23: 149-283, 1887.

117. Marckwald, M. Die Bedsutung des Mittelhirns für die Athmung. Z. Biol. 26: 259-289, 1890.

118. Marckwald, M. and H. Kronecker. Die Athembewegungen des Zwerchfells des Kaninchens. Arch. Physiol., Leipzig., 4: 441-446, 1880.

119. Marczynski, T.J. and C.J. Sherry. A new analysis of trains of increasing or decreasing interspike intervals treated as self-adjusting sets of ratios. Brain Res. 35: 533-538, 1971.

120. Mead, J. Control of respiratory frequency. J. Appl. Physiol. 15: 325-336, 1960.

121. Mead, J. The control of respiratory frequency. Ann. N.Y. Acad. Sci. 109: 724-729, 1963.

122. Merrill, E.G. The lateral respiratory neurons of the medulla: Their associations with nucleus ambiguus, nucleus retroambigualis, the spinal accessory nucleus and the spinal cord. Brain Res. 24: 11-28, 1970.

123. Mitchell, R.A. and D.A. Herbert. Intracellular potentials from medullary respiratory neurons in the cat. Physiologist 14: 196, 1971.

124. Monnier, M. Physiologie des formations réticulées. II. Respiration. Effets de l'excitation faradique du bulbe chez le chat. Rev. Neurol. 69: 517-523, 1938.

125. Naifeh, K.H., S.E. Huggins, and H.E. Hoff. Study of the control of crocodilian respiration by anesthetic dissection. Resp. Physiol. 12: 251-260, 1971.

126. Naifeh, K.H., S.E. Huggins, and H.E. Hoff. Effects of brain stem section on respiratory patterns of crocodilian reptiles. Resp. Physiol. 13: 186-197, 1971.

127. Nelson, J.R. Single unit activity in medullary respiratory centers of cat. J. Neurophysiol. 22: 590-598, 1959.

128. Nesland, R. and F. Plum. Subtypes of medullary respiratory neurons. Exptl. Neurol. 12: 337-348, 1965.

129. Nesland, R.S., F. Plum, J.R. Nelson, and H.D. Siedler. The graded response to stimulation of medullary respiratory neurons. Exptl. Neurol. 14: 57-76, 1966.

130. Ngai, S.H. Pulmonary ventilation studies on pontile and medullary cats. Changes in O_2 consumption, in arterial blood pH, CO_2 tension and O_2 saturation, and in response to CO_2 and cyanide. Am. J. Physiol. 190: 356-360, 1957.

131. Ngai, S.H. Effect of pentobarbital and meperidine on the central respiratory mechanisms in the cat. N.Y. Acad. Sci. Trans. Ser. 2, 22: 252-258, 1960.

132. Ngai, S.H. Effects of morphine and meperidine on the central respiratory mechanisms in the cat; the action of levallorphan in antagonizing these effects. J. Pharm. Exptl. Therap. 131: 91-99, 1961.

133. Ngai, S.H., M.J. Frumin, and S.C. Wang. Organization of the central respiratory mechanism in cats. Federation Proc. 11: 112, 1952.

134. Ngai, S.H. and S.C. Wang. Pneumotaxic center in the cat: Effect of its stimulation and destruction. Am. J. Physiol. 171: 752-753, 1952.

135. Ngai, S.H. and S.C. Wang. Organization of central respiratory mechanisms in the brain stem of the cat: Localization by stimulation and destruction. Am. J. Physiol. 190: 343-349, 1957.

136. Ondina, D.M., W.S. Yamamoto, and W.S. Masland. Respiratory centers in the albino rat. Am. J. Physiol. 198: 389-392, 1960.

137. Otis, A.B., W.O. Fenn, and H. Rahn. Mechanics of breathing in man. J. Appl. Physiol. 2: 592-607, 1950.

138. Paintal, A.S. The conduction velocities of respiratory and cardiovascular afferent fibres in the vagus nerve. J. Physiol. 121: 341-359, 1953.

139. Parrot, T.L. and D.G. Fleming. Analysis of firing patterns in medullary respiratory neurons. Proc. Eng. Med. Biol. 7: 234, 1965.

140. Pitts, R.F. The differentiation of respiratory centers. Am. J. Physiol. 134: 192-201, 1941.

141. Pitts, R.F. Excitation and inhibition of phrenic motor neurones. J. Neurophysiol. 5: 75-88, 1942.

142. Pitts, R.F. The function of components of the respiratory complex. J. Neurophysiol. 5: 403-413, 1942.

143. Pitts, R.F. The basis for repetitive activity in phrenic motoneurons. J. Neurophysiol. 6: 439-454, 1943.

144. Pitts, R.F. Organization of the respiratory center. Physiol. Rev. 26: 609-630, 1946.

145. Pitts, R.F., H.W. Magoun, and S.W. Ranson. Localization of the medullary respiratory centers in the cat. Am. J. Physiol. 126: 673-688, 1939.

146. Pitts, R.F., H.W. Magoun, and S.W. Ranson. Interrelations of the respiratory centers in the cat. Am. J. Physiol. 126: 689-707, 1939.

147. Pitts, R.F., H.W. Magoun, and S.W. Ranson. The origin of respiratory rhythmicity. Am. J. Physiol. 127: 654-670, 1939.

148. Robson, J.G., M.A. Houseley, and O.H. Solis-Quiroga. The mechanism of respiratory arrest with sodium pentobarbital and sodium thiopental. Ann. N.Y. Acad. Sci. 109: 494-504, 1963.

149. Rohrer, F. Handbuch des normalen und pathologischen Pathologie, Vol. 2. Berlin: Springer Verlag, 1925, p. 70.

150. St. John, W.M. Respiratory tidal volume responses of cats with chronic pneumotaxic center lesions. Resp. Physiol. 16: 92-108, 1972.

151. St. John, W.M., R.L. Glasser, and R.A. King. Apneustic breathing after vagotomy in cats with chronic pneumotaxic center lesions. Resp. Physiol. 12: 239-250, 1971.

152. St. John, W.M., R.L. Glasser, and R.A. King. Rhythmic respiration in awake vagotomized cats with chronic pneumotaxic area lesions. Resp. Physiol. 15: 233-244, 1972.

153. Salmoiraghi, G.C. Functional organization of brainstem respiratory neurons. Ann. N.Y. Acad. Sci. 109: 571-585, 1963.

154. Slamoiraghi, G.C. and R. von Baumgarten. Intracellular potentials from respiratory neurons in brainstem of cat and mechanism of rhythmic respiration. J. Neurophysiol. 24: 203-218, 1961.

155. Salmoraghi, G.C. and B.D. Burns. Localization and patterns of discharge of respiratory neurons in brain-stem of cat. J. Neurophysiol. 23: 2-13, 1960.

156. Salmoiraghi, G.C. and B.D. Burns. Notes on mechanism of rhythmic respiration. J. Neurophysiol. 23: 14-26, 1960.

157. Salzano, J. and F.G. Hall. Influence of vagal blockade on respiratory work in the hypoxic and hypercapneic anesthetized dog. J. Appl. Physiol. 14: 348-352, 1959.

158. Scheibel, M.E. and A.B. Scheibel. Periodic sensory nonresponsiveness in reticular neurones. Arch. Ital. Biol. 103: 300-316, 1965.

159. Sears, T.A. Investigations of respiratory motoneurones of the thoracic spinal cord. Prog. Brain Res. 12: 259-273, 1964.

160. Sears, T.A. Breathing: A sensori-motor act. In: The Scientific Basis of Medicine Annual Reviews, 1971. Eds. Gilliland and Francis. London: Athens Press, 1971, pp. 129-147.

161. Shannon, R. and F.W. Zechman. The reflex and mechanical response of the inspiratory muscles to an increased airflow resistance. Resp. Physiol. 16: 51-69, 1972.

162. Shannon, R., F.W. Zechman, and D.T. Frazier. First-breath response of medullary inspiratory neurones to the mechanical loading of inspiration. Resp. Physiol. 16: 70-78, 1972.

163. Sherry, C.J., T.J. Marczynski, and D.J. Wolf. The interdependence series matrix; a method for determining the serial dependence of neuronal interspike intervals. Intern. J. Neurosci. 3: 35-42, 1972.

164. Silver, S.L. Signal averaging techniques. Electronics World, No. 5, 85: 45-53, 1971.

165. Smith, D.R. and G.K. Smith. A statistical analysis of the continual activity of single cortical neurons in the cat unanesthetized isolated forebrain. Biophysical J. 5: 47-74, 1965.

166. Steffensen, E.H., J.M. Brookhart, and R. Gesell. Proprioceptive respiratory reflexes of the vagus nerve. Am. J. Physiol. 119: 517-526, 1937.

167. Stella, G. On the mechanism of production, and the physiological significance of "apneusis." J. Physiol., London 93: 10-23, 1938.

168. Stella, G. The dependence of the activity of the "apneustic centre" on the carbon dioxide of the arterial blood. J. Physiol., London 93: 263-275, 1938.

169. Takagi, K. and T. Nakayama. Respiratory discharge of the pons. Science 128: 1206, 1958.

170. Tang, P.C. Localization of the pneumotaxic center in the cat. Am. J. Physiol. 172: 645-652, 1953.

171. Tang, P.C. Brain stem control of respiratory depth and rate in the cat. Resp. Physiol. 3: 349-366, 1967.

172. Tang, P.C. and T.C. Ruch. Localization of the pneumotaxic center in the cat. Am. J. Physiol. 167: 830-831, 1951.

173. Vasilevskii, V.S. Responses of bulbar respiratory neurons to stimulation of receptive fields in the air passages. Neurophysiol. 3: 463-470, 1971.

174. Waldron, I. Activity patterns in respiratory muscles and in respiratory neurons of the rostral medulla of the cat. J. Physiol., London 208: 373-383, 1970.

175. Wang, S.C. and S.H. Ngai. General organization of central respiratory mechanisms. In: Handbook of Physiology, Section 3, Vol. I., Respiration. Washington, D.C.: American Physiological Society, 1964, pp. 487-505.

176. Wang, S.C., S.H. Ngai, and M.J. Frumin. Organization of central respiratory mechanisms in the brain stem of the cat. Genesis of normal respiratory rhythmicity. Am. J. Physiol. 190: 333-342, 1957.

177. Whitteridge, D. and E. Bülbring. Changes in activity of pulmonary receptors in anesthesia and their influences on respiratory behavior. J. Pharm. Exptl. Therap. 81: 340-359, 1944.

178. Widdicombe, J.G. Respiratory reflexes from the lungs. Brit. Med. Bull. 19: 15-20, 1963.

179. Widdicombe, J.G. Respiratory reflexes. In: Handbook of Physiology, Section 3, Vol. I., Respiration. Washington, D.C.: American Physiological Society, 1964, pp. 585-630.

180. Woldring, S. and M.N.J. Dirken. Site and extension of bulbar respiratory centre. J. Neurophysiol. 14: 227-241, 1951.

181. Wyss, O.A.M. Respiratory effects from stimulation of the afferent vagus nerve in the monkey. J. Neurophysiol. 10: 315-320, 1947.

182. Wyss, O.A.M. Separate localization in the medulla oblongata of the vagal inspiratory and expiratory reflex centers. Science 106: 322-323, 1947.

183. Wyss, O.A.M., P. Andereggen, and R.J.H. Oberholzer. Le mécanisme central des réflexes respiratoires d'origine vagale. Helv. Physiol. Pharmacol. Acta 4: 443-458, 1946.

184. Zechman, F.W., Jr., J. Salzano, and F.G. Hall. Effect of cooling the cervical vagi on the work of breathing. J. Appl. Physiol. 12: 301-304, 1958.

CHAPTER IX

APPENDIX

Table VII. Core memory assignments for program DATA.

LINC Segments	PMODE Fields	Absolute Location	Contents
IF* 0	0	0000 - 0777	Decwriter Output
		1000 - 1777	X - Y Plotter Output
IF 1	0	2000 - 2777, 3000 - 3777	X - Y Plotter Subroutine
IF 2	0	4000 - 4777, 5000 - 5777	Mainline Program and Tape Storage Output
IF 3	0	6000 - 6777, 7000 - 7777	CRT Display HISTO, ISIM, AXIS and TITLE
DF** 4	1	10000 - 10777	Σ Interval Time (LO) Array, Bits 0-11 (LOOP B); ISIM Array (LOOP C)
		11000 - 11777	First Interval (FI) Array
DF 5	1	12000 - 12777	Divisor N (DIV) Array
		13000 - 13777	Σ Interval Time (HI) Array; Bits 12-23 (LOOP B)
DF 6	1	14000 - 14777	Intervals per Train (ST-1) Array
		15000 - 15777	Respiration Rate (RR) Array
DF 7	1	16000 - 16777	HISTO Array
		17000 - 17777	Analog Input Array (LOOP A); ISIM Array (LOOP B)

*Instruction Field

**Data Field

```
0000                    *20
0001                    /PROGRAM ERASE
0002                    /
0003                    /ZERO STORED IN EACH WORD OF
0004                    /1000 OCTAL BLOCK LINC MAGNETIC TAPE
0005                    /
0006        0020  0067  ST,     SET I 7
0007        0021  3777          3777
0010        0022  0011          CLR
0011        0023  1067          STA I 7
0012        0024  0207          XSK 7
0013        0025  6023          JMP .-2
0014        0026  0000          HLT
0015        0027  1020          LDA I
0016        0030  4000          4000
0017        0031  4033          STC W0
0020        0032  0736  A,      WRI I U
0021        0033  0000  W0,     0
0022        0034  1020          LDA I
0023        0035  0001          1
0024        0036  1140          ADM
0025        0037  0033          W0
0026        0040  1460          SAE I
0027        0041  4777          4777
0030        0042  6032          JMP A
0031        0043  0712          RDE U
0032        0044  4000          4000
0033        0045  0000          HLT
0034        0046  0000          HLT
0035        0047  6020          JMP ST

NO ERRORS

A       4032
ST      4020
W0      4033
```

```
0000                    *20
0001                    /PROGRAM DATA
0002                    /
0003                    /TIME SCALED 4X SLOWER
0004                    /
0005                    /LOOP A- DISPLAY CHANNEL 12 INPUT
0006                    /LOOP B- HISTO- ISIM CONSTRUCTION
0007                    /LOOP C- OUTPUT SELECTION
0010                    /
0011                    /ANALOG INPUTS
0012                    /
0013                    /12 A+B- SINGLE UNIT RECORDING
0014                    /04 B  - RATE OF RISE TRIGGER LEVEL
0015                    /00 B  - RESET DELAY 0-4095 MSEC
0016                    /05 A  - POSITION CHANNEL 12 DISPLAY
0017                    /01 C  - SHIFT HISTO DISPLAY U TO D
0020                    /01 C" - SHIFT ISIM DISPLAY R TO L
0021                    /
0022                    /PROGRAM CONTROL
0023                    /
0024                    /LEFT SWITCHES - N FOR HISTOGRAM
0025                    /RIGHT SWITCHES- DATA POINT NUMBER
0026                    /
0027                    /SENSE SWITCHES
0030                    /
0031                    /0 A - CHANNEL 12 DISPLAY FREEZE
0032                    /0 B - MANUAL PULSE REJECTION
0033                    /0 C - HISTO- ISIM DISPLAY SELECTION
0034                    /0 C"- EXIT FROM ANY OUTPUT PROCEDURE
0035                    /1 B - CONTINUOUS HISTOGRAM
0036                    /1 C - START TELETYPE OUTPUT
0037                    /2 C - START XY PLOT
0040                    /3 C - START TAPE STORAGE
0041                    /4 C - PROGRAM RESTART
0042                    /5 A - EXIT CHANNEL 12 DISPLAY LOOP
0043                    /5 B - EXIT HISTO- ISIM CONSTRUCT LOOP
0044                    /5 B"- ENTER OUTPUT LOOP
0045                    /5 C - COMPLETE TELY, XY OR TAPE OUTPUT
0046                    /
0047    0020  0002              PDP
0050                            PMODE
0051    4021  6046              TLS             /CLOCK PRESETS
0052    4022  6135              CLSA
0053    4023  7300              CLA CLL
0054    4024  1235              TAD KCLLR
0055    4025  6132              CLLR
0056    4026  7200              CLA
0057    4027  1236              TAD KCLAB
0060    4030  6133              CLAB
0061    4031  7200              CLA
0062    4032  1237              TAD KCLEN
0063    4033  6134              CLEN
0064    4034  5240              JMP GO
0065    4035  2100  KCLLR,      2100            /100K HZ MODE 1
0066    4036  7730  KCLAB,      -50             /PRESET -40
0067    4037  0300  KCLEN,      300             /ENABLE
0070                    /
0071                    /LOOP A
0072                    /
0073    4040  6141  GO,         LINC
0074                            LMODE
0075    0041  0647              LDF 7
```

```
0076    0042  0073  CO,     SET I 13        /SAMPLE AND
0077    0043  2777          2777            /DISPLAY CHAN 12
0100    0044  0500  D,      IOB
0101    0045  6131          6131            /CLOCK OVERFLOW
0102    0046  6044          JMP .-2         /EVERY 0.1 MSEC
0103    0047  0500          IOB
0104    0050  6135          6135            /CLSA
0105    0051  0112          SAM 12
0106    0052  0341          SCR 1
0107    0053  1073          STA I 13
0110    0054  0213          XSK 13
0111    0055  6044          JMP D
0112    0056  0073  DS,      SET I 13        /START DISPLAY
0113    0057  2777          2777
0114    0060  0445          SNS 5
0115    0061  0456          SKP
0116    0062  6102          JMP ST          /EXIT TO LOOP B
0117    0063  7727          JMP TITL        /TO TITLE
0120    0064  7727          JMP TITL        /ROUTINE
0121    0065  0105  SD,      SAM 5
0122    0066  0341          SCR 1
0123    0067  4072          STC .+3
0124    0070  1033          LDA I 13
0125    0071  1120          ADA I
0126    0072  0000          0
0127    0073  0153          DIS 13
0130    0074  0213          XSK 13
0131    0075  6065          JMP SD
0132    0076  0440          SNS 0
0133    0077  0456          SKP
0134    0100  6056          JMP DS          /FREEZE DISPLAY
0135    0101  6042          JMP CO          /RESAMPLE
0136                  /
0137    0102  0063  ST,      SET I 3         /CLEAR MEMORY
0140    0103  3777          3777
0141    0104  0011          CLR
0142    0105  0644          LDF 4
0143    0106  1063          STA I 3
0144    0107  0645          LDF 5
0145    0110  1043          STA 3
0146    0111  0646          LDF 6
0147    0112  1043          STA 3
0150    0113  0647          LDF 7
0151    0114  1043          STA 3
0152    0115  0203          XSK 3
0153    0116  6105          JMP .-11
0154                  /
0155    0117  5760          STC R1
0156    0120  5761          STC R2
0157    0121  5762          STC R3
0160    0122  5763          STC R4
0161    0123  5766          STC M1
0162    0124  5767          STC M2
0163    0125  5770          STC M3
0164    0126  5757          STC L510
0165                  /
0166    0127  0517          LSW             /SELECT N FOR
0167    0130  1120          ADA I           /HISTO
0170    0131  0001          1
0171    0132  4512          STC HN
0172    0133  5755          STC ZRO
0173                  /
0174    0134  0064          SET I 4         /FI
```

```
0175    0135  2777          2777
0176    0136  0070          SET I 10        /RESP RATE
0177    0137  3000          3000
0200    0140  6145          JMP .+5
0201                /
0202                /LOOP B
0203                /
0204    0141  0011  N,        CLR             /REMOVE RESET
0205    0142  0647            LDF 7           /DELAY TIME
0206    0143  1052            STA 12
0207    0144  0643            LDF 3
0210                /
0211    0145  0063            SET I 3         /LOW
0212    0146  3777            3777
0213    0147  0065            SET I 5         /DIVISOR
0214    0150  3777            3777
0215    0151  0066            SET I 6         /HIGH
0216    0152  3000            3000
0217    0153  0072            SET I 12        /INTERVAL TIMES
0220    0154  3000            3000
0221                /
0222    0155  0223  NA,       XSK I 3         /LOW
0223    0156  0226            XSK I 6         /HIGH
0224    0157  0647            LDF 7
0225    0160  1032            LDA I 12        /INTERVAL TIMES
0226    0161  0643            LDF 3
0227    0162  0450            AZE
0230    0163  0456            SKP
0231    0164  6231            JMP NN          /EXIT
0232    0165  5752            STC CONT
0233                /
0234    0166  0500  NC,       IOB             /CLOCK OVERFLOW
0235    0167  6131            6131            /EVERY 0.1 MSEC
0236    0170  6211            JMP NJ
0237    0171  0500            IOB
0240    0172  6135            6135            /CLSA
0241                /
0242    0173  1020            LDA I
0243    0174  0001            1
0244    0175  1140            ADM
0245    0176  1755            ZRO
0246    0177  1460            SAE I
0247    0200  0144            144             /100
0250    0201  6211            JMP NJ
0251                /
0252    0202  1020            LDA I           /INCREMENT RATE
0253    0203  0001            1               /ARRAY EVERY
0254    0204  0646            LDF 6           /0.01 SEC
0255    0205  1150            ADM 10
0256    0206  0643            LDF 3
0257    0207  0011            CLR
0260    0210  5755            STC ZRO
0261                /
0262    0211  1020  NJ,       LDA I           /TRANSFER INT
0263    0212  0001            1               /TIMES
0264    0213  0644            LDF 4
0265    0214  1203            LAM 3
0266    0215  0643            LDF 3
0267    0216  5747            STC GAR
0270    0217  0645            LDF 5
0271    0220  1206            LAM 6
0272    0221  0643            LDF 3
0273    0222  1020            LDA I
```

```
0274    0223  7776          -1
0275    0224  1140          ADM
0276    0225  1752          CONT
0277    0226  0450          AZE
0300    0227  6166          JMP NC          /CONT TRANSFER
0301    0230  6155          JMP NA          /READ NEW INT
0302                  /
0303    0231  0072  NN,     SET I 12
0304    0232  3000          3000
0305    0233  0011          CLR             /CLEAR INTERVAL
0306    0234  0647          LDF 7           /TIMES ARRAY
0307    0235  1072          STA I 12
0310    0236  0643          LDF 3
0311    0237  0212          XSK 12
0312    0240  6234          JMP .-4
0313    0241  0072          SET I 12
0314    0242  3000          3000
0315                  /
0316    0243  1020          LDA I
0317    0244  0377          377
0320    0245  5742          STC S2
0321    0246  5757          STC L510
0322    0247  0693          LIF 3
0323    0250  6040          JMP DISR        /DISPLAY R
0324                  /
0325    0251  0500  C,       IOB             /CLOCK OVERFOLW
0326    0252  6131          6131            /EVERY 0.1 MSEC
0327    0253  6251          JMP .-2
0330    0254  0500          IOB
0331    0255  6135          6135            /CLSA
0332                  /
0333    0256  1020          LDA I
0334    0257  0001          1
0335    0260  1140          ADM
0336    0261  1755          ZRO
0337    0262  1460          SAE I
0340    0263  0144          144             /100
0341    0264  6274          JMP .+10
0342                  /
0343    0265  1020          LDA I           /INCREMENT RATE
0344    0266  0001          1               /ARRAY EVERY
0345    0267  0646          LDF 6           /0.01 SEC
0346    0270  1150          ADM 10
0347    0271  0643          LDF 3
0350    0272  0011          CLR
0351    0273  5755          STC ZRO
0352                  /
0353    0274  0440          SNS 0           /MANUAL PULSE
0354    0275  0456          SKP             /REJECTION
0355    0276  6251          JMP C
0356                  /
0357    0277  6552          JMP TRIG
0360    0300  0451          APO
0361    0301  6251          JMP C           /NO TRIGGER
0362                  /
0363    0302  0603          LIF 3           /TRIGGER
0364    0303  6016          JMP DISS        /DISPLAY S
0365                  /
0366    0304  1000  QT,      LDA
0367    0305  0512          HN
0370    0306  4314          STC .+6
0371    0307  1000          LDA             /EXIT TO DISPLAY
0372    0310  1770          M3              /IF REACH HISTO
```

```
0373    0311  1120          ADA I           /N AND TRAIN
0374    0312  0001          1               /FINISHED
0375    0313  1460          SAE I
0376    0314  0000          0
0377    0315  0456          SKP
0400    0316  6572          JMP RR
0401                  /
0402    0317  0445          SNS 5           /MANUAL EXIT
0403    0320  0456          SKP             /TO DISPLAY
0404    0321  6572          JMP RR
0405    0322  0230          XSK I 10
0406    0323  0456          SKP             /EXIT IF MORE
0407    0324  6572          JMP RR          /THAN 510 TRAINS
0410                  /
0411    0325  1020          LDA I
0412    0326  0001          1
0413    0327  1140          ADM             /INCREMENT NUM
0414    0330  1763          R4              /TRAINS
0415                  /
0416    0331  1020          LDA I           /SET FI MARKER
0417    0332  0001          1
0420    0333  5743          STC FI
0421                  /
0422    0334  0225  B,        XSK I 5         /DIVISOR
0423    0335  0232          XSK I 12        /INTERVAL TIMES
0424    0336  6342          JMP .+4
0425    0337  1020          LDA I           /TRAIN LENGTH
0426    0340  0007          7               />510 INTERVALS
0427    0341  5757          STC L510        /SET MARKER
0430                  /
0431    0342  1020  E,        LDA I
0432    0343  0377          377
0433    0344  5742          STC S2
0434    0345  5751          STC STOR        /OVERFLOW STORE
0435                  /
0436    0346  0500  A,        IOB             /CLOCK OVERFLOW
0437    0347  6131          6131            /EVERY 0.1 MSEC
0440    0350  6346          JMP .-2
0441    0351  0500          IOB
0442    0352  6135          6135            /CLSA
0443                  /
0444    0353  1020          LDA I           /INCREMENT TIME
0445    0354  0001          1               /COUNTER
0446    0355  1140          ADM
0447    0356  1751          STOR
0450                  /
0451    0357  0100          SAM 0           /RESET DELAY
0452    0360  0451          APO
0453    0361  0011          CLR
0454    0362  0243          ROL 3
0455    0363  1100          ADA
0456    0364  1751          STOR
0457    0365  1460          SAE I           /4095 0.1 MSEC
0460    0366  7777          7777            /MAX DELAY
0461    0367  0456          SKP
0462    0370  6141          JMP N           /EXIT
0463                  /
0464    0371  1000  Y,        LDA             /BYPASS INTERVAL
0465    0372  1757          L510            /INCREMENT IF
0466    0373  1460          SAE I           /TRAIN >510 INT
0467    0374  0007          7
0470    0375  0456          SKP
0471    0376  6410          JMP .+12
```

```
0472                    /
0473    0377  1020      LDA I       /INCREMENT INT
0474    0400  0001      1           /TIME
0475    0401  0647      LDF 7
0476    0402  1152      ADM 12
0477    0403  0643      LDF 3
0500                    /
0501    0404  1020      LDA I
0502    0405  0001      1
0503    0406  1140      ADM
0504    0407  1755      ZRO
0505    0410  1460      SAE I
0506    0411  0144      144         /100
0507    0412  6422      JMP .+10
0510                    /
0511    0413  1020      LDA I       /INCREMENT RATE
0512    0414  0001      1           /ARRAY EVERY
0513    0415  0646      LDF 6       /0.01 SEC
0514    0416  1150      ADM 10
0515    0417  0643      LDF 3
0516    0420  0011      CLR
0517    0421  5755      STC ZRO
0520                    /
0521    0422  0440      SNS 0       /MANUAL PULSE
0522    0423  0456      SKP         /REJECTION
0523    0424  6141      JMP N
0524                    /
0525    0425  6552      JMP TRIG
0526    0426  0451      APO
0527    0427  6346      JMP A       /NO TRIGGER
0530                    /
0531    0430  1000      LDA
0532    0431  1751      STOR
0533    0432  1120      ADA I       /REJECT TRIGGER
0534    0433  7753      -24         /IF <2 MSEC
0535    0434  0451      APO         /SINCE LAST
0536    0435  6346      JMP A       /TRIGGER
0537                    /
0540    0436  0603      LIF 3       /TRIGGER
0541    0437  6027      JMP DIST    /DISPLAY T
0542                    /
0543    0440  1000  TB, LDA         /FI?
0544    0441  1743      FI
0545    0442  1460      SAE I
0546    0443  0001      1
0547    0444  6454      JMP .+10    /NO
0550    0445  1000      LDA         /YES, SAVE FI
0551    0446  1751      STOR
0552    0447  0644      LDF 4
0553    0450  1064      STA I 4
0554    0451  0643      LDF 3
0555    0452  0011      CLR
0556    0453  5743      STC FI
0557                    /
0560    0454  1000      LDA
0561    0455  1757      L510
0562    0456  1460      SAE I       /BYPASS ISIM
0563    0457  0007      7           /CALCULATIONS
0564    0460  0456      SKP         /IF TRAIN
0565    0461  6474      JMP Q       /LENGTH>510 INT
0566                    /
0567    0462  1020      LDA I       /INCREMENT
0570    0463  0001      1           /DIVISOR
```

```
0571    0464  0645          LDF 5
0572    0465  1145          ADM 5
0573    0466  0643          LDF 3
0574                /
0575    0467  1020          LDA I           /INCREMENT N
0576    0470  0001          1               /FOR ISIM
0577    0471  1140          ADM
0600    0472  1766          M1
0601    0473  6476          JMP .+3
0602                /
0603    0474  0441  Q,       SNS 1           /CONTINUE TO
0604    0475  6342          JMP E           /FILL HISTO
0605    0476  1000          LDA             /BYPASS HISTO
0606    0477  1751          STOR            /CONSTRUCTION
0607    0500  1120          ADA I           /IF INTERVAL
0610    0501  6003          -1774           /TIME >102 MSEC
0611    0502  0451          APO
0612    0503  0456          SKP
0613    0504  6544          JMP MS
0614                /
0615    0505  1000          LDA
0616    0506  1770          M3
0617    0507  1120          ADA I
0620    0510  0001          1
0621    0511  1460          SAE I
0622    0512  0000  HN,      0
0623    0513  6522          JMP .+7
0624    0514  1000          LDA
0625    0515  1757          L510
0626    0516  1460          SAE I
0627    0517  0007          7
0630    0520  6334          JMP B
0631    0521  6141          JMP N
0632    0522  1020          LDA I           /INCREMENT N
0633    0523  0001          1               /FOR HISTO
0634    0524  1140          ADM
0635    0525  1770          M3
0636                /
0637    0526  1000          LDA             /CONSTRUCT HISTO
0640    0527  1751          STOR            /0.4 MSEC BINS
0641    0530  0341          SCR 1
0642    0531  1560          BCL I
0643    0532  0001          1
0644    0533  1120          ADA I
0645    0534  2000          2000
0646    0535  4542          STC .+5
0647    0536  1020          LDA I
0650    0537  0001          1
0651    0540  0647          LDF 7
0652    0541  1140          ADM
0653    0542  0000          0
0654    0543  0643          LDF 3
0655                /
0656    0544  1000  MS,      LDA
0657    0545  1757          L510
0660    0546  1460          SAE I
0661    0547  0007          7
0662    0550  6334          JMP B           /RETURN & BUMP
0663    0551  6342          JMP E           /RETURN- NO BUMP
0664                /
0665    0552  1000  TRIG,    LDA             /TRIGGER
0666    0553  1742          S2              /ROUTINE
0667    0554  0017          COM
```

```
0670    0555  5741          STC S1
0671    0556  0104          SAM 4
0672    0557  0341          SCR 1
0673    0560  0017          COM
0674    0561  5746          STC TRG
0675    0562  0112          SAM 12
0676    0563  0341          SCR 1
0677    0564  5742          STC S2
0700    0565  1000          LDA
0701    0566  1741          S1
0702    0567  3742          ADD S2
0703    0570  3746          ADD TRG
0704    0571  6000          JMP 0           /RETURN
0705                  /
0706    0572  0063  RR,       SET I 3         /LOW
0707    0573  3777           3777
0710    0574  0065           SET I 5         /DIVISOR
0711    0575  3777           3777
0712    0576  0066           SET I 6         /HIGH
0713    0577  3000           3000
0714                  /
0715    0600  0645           LDF 5
0716    0601  1025           LDA I 5
0717    0602  0643           LDF 3
0720    0603  0450           AZE
0721    0604  0456           SKP             /EXIT TO DISPLAY
0722    0605  7525           JMP KR          /IF DIV=0
0723    0606  0065           SET I 5
0724    0607  3777           3777
0725                  /
0726    0610  0645  RK,       LDF 5           /CALCULATE MEAN
0727    0611  1025           LDA I 5         /INTERVAL TIMES
0730    0612  0643           LDF 3
0731    0613  0450           AZE
0732    0614  0456           SKP
0733    0615  6634           JMP RP          /EXIT
0734    0616  5015           STC KD
0735    0617  0644           LDF 4
0736    0620  1023           LDA I 3         /LOW
0737    0621  0643           LDF 3
0740    0622  5016           STC KL
0741    0623  0645           LDF 5
0742    0624  1026           LDA I 6         /HIGH
0743    0625  0643           LDF 3
0744    0626  5017           STC KH
0745    0627  7000           JMP DIV
0746    0630  0644           LDF 4
0747    0631  1043           STA 3           /RESTORE AVG
0750    0632  0643           LDF 3
0751    0633  6610           JMP RK
0752                  /
0753    0634  0070  RP,       SET I 10        /CALCULATE
0754    0635  3000           3000            /INDIVIDUAL
0755    0636  0646  PR,       LDF 6           /RESP RATES
0756    0637  1030           LDA I 10
0757    0640  0643           LDF 3
0760    0641  0450           AZE
0761    0642  0456           SKP
0762    0643  6660           JMP RA          /EXIT
0763    0644  5015           STC KD
0764    0645  1020           LDA I
0765    0646  5140           5140            /60000 0.01
0766    0647  5016           STC KL          /SEC/10 MIN
```

```
0767    0650  1020        LDA I
0770    0651  0016        16
0771    0652  5017        STC KH
0772    0653  7000        JMP DIV
0773    0654  0646        LDF 6
0774    0655  1050        STA 10
0775    0656  0643        LDF 3
0776    0657  6636        JMP FR
0777                /
1000    0660  0070  RA,     SET I 10        /CALCULATE MEAN
1001    0661  3000          3000            /RESP RATE
1002    0662  0646  RN,     LDF 6
1003    0663  1030          LDA I 10
1004    0664  0643          LDF 3
1005    0665  0450          AZE
1006    0666  0456          SKP
1007    0667  6707          JMP DV
1010    0670  5751          STC STOR
1011    0671  1020  RU,     LDA I
1012    0672  0001          1
1013    0673  1200          LAM
1014    0674  1762          R3
1015    0675  5747          STC GAR
1016    0676  1200          LAM
1017    0677  1761          R2
1020    0700  1020          LDA I
1021    0701  7776          -1
1022    0702  1140          ADM
1023    0703  1751          STOR
1024    0704  0450          AZE
1025    0705  6671          JMP RU
1026    0706  6662          JMP RN
1027    0707  1000  DV,     LDA
1030    0710  1763          R4
1031    0711  5015          STC KD
1032    0712  1000          LDA
1033    0713  1762          R3
1034    0714  5016          STC KL
1035    0715  1000          LDA
1036    0716  1761          R2
1037    0717  5017          STC KH
1040    0720  7000          JMP DIV
1041    0721  1040          STA
1042    0722  1760          R1              /MEAN RESP RATE
1043                /
1044    0723  0070          SET I 10        /FIND HIGH AND
1045    0724  3000          3000            /LOW RESP RATE
1046    0725  0646          LDF 6
1047    0726  1030          LDA I 10
1050    0727  0643          LDF 3
1051    0730  1040          STA
1052    0731  1762          R3              /LOW RR
1053    0732  1040          STA
1054    0733  1761          R2              /HIGH RR
1055    0734  0646  TR,     LDF 6
1056    0735  1030          LDA I 10
1057    0736  0643          LDF 3
1060    0737  0450          AZE
1061    0740  0456          SKP
1062    0741  7070          JMP KX          /EXIT
1063    0742  0017          COM
1064    0743  1100          ADA
1065    0744  1761          R2              /HIGH RR
```

```
1066    0745  0451          APO
1067    0746  0456          SKP
1070    0747  6756          JMP .+7
1071    0750  0646          LDF 6
1072    0751  1010          LDA 10
1073    0752  0643          LDF 3
1074    0753  1040          STA
1075    0754  1761          R2              /HIGH RR
1076    0755  6734          JMP TR
1077    0756  0646          LDF 6
1100    0757  1010          LDA 10
1101    0760  0643          LDF 3
1102    0761  0017          COM
1103    0762  1100          ADA
1104    0763  1762          R3              /LOW RR
1105    0764  0451          APO
1106    0765  6734          JMP TR
1107    0766  0646          LDF 6
1110    0767  1010          LDA 10
1111    0770  0643          LDF 3
1112    0771  1040          STA
1113    0772  1762          R3              /LOW RR
1114    0773  6734          JMP TR          /EXIT
1115                  /
1116                        *1000
1117    1000  0002  DIV,      PDP             /DIVIDE
1120                        PMODE           /ROUTINE
1121    5001  7300          CLA CLL
1122    5002  1215          TAD KD
1123    5003  3210          DCA .+5
1124    5004  1216          TAD KL
1125    5005  7421          MQL
1126    5006  1217          TAD KH
1127    5007  7407          DVI
1130    5010  0000          0
1131    5011  7200          CLA
1132    5012  7501          MQA
1133    5013  6141          LINC
1134                        LMODE
1135    1014  6000          JMP 0           /RETURN
1136    1015  0000  KD,      0
1137    1016  0000  KL,      0
1140    1017  0000  KH,      0
1141                  /
1142    1020  0064  KX,      SET I 4         /CORRECT FI
1143    1021  2777          2777            /ARRAY
1144    1022  0644  KX2,     LDF 4
1145    1023  1024          LDA I 4
1146    1024  0643          LDF 3
1147    1025  0450          AZE
1150    1026  0456          SKP
1151    1027  7036          JMP AB
1152    1030  1020          LDA I
1153    1031  0001          1
1154    1032  0644          LDF 4
1155    1033  1144          ADM 4
1156    1034  0643          LDF 3
1157    1035  7022          JMP KX2
1160                  /
1161    1036  0063  AB,      SET I 3         /CORRECT FI
1162    1037  2000          2000
1163    1040  1020          LDA I
1164    1041  0001          1
```

```
1165    1042  0644          LDF 4
1166    1043  1143          ADM 3
1167    1044  0643          LDF 3
1170                  /
1171    1045  0065          SET I 5         /CALCULATE ST
1172    1046  2000          2000
1173    1047  0070          SET I 10
1174    1050  3765          3765
1175    1051  0645          LDF 5
1176    1052  1005          LDA 5           /NUM TRAINS
1177    1053  0643          LDF 3
1200    1054  5015          STC KD
1201    1055  5016          STC KL
1202    1056  5017          STC KH
1203    1057  1000  ST1,     LDA
1204    1060  1766          M1              /FMN
1205    1061  5752          STC CONT
1206    1062  1020  ST2,     LDA I
1207    1063  0001          1
1210    1064  1200          LAM
1211    1065  1016          KL
1212    1066  5747          STC GAR
1213    1067  1200          LAM
1214    1070  1017          KH
1215    1071  1020          LDA I
1216    1072  7776          -1
1217    1073  1140          ADM
1220    1074  1752          CONT
1221    1075  0450          AZE
1222    1076  7062          JMP ST2
1223    1077  0230          XSK I 10
1224    1100  7057          JMP ST1
1225    1101  7000          JMP DIV
1226    1102  1120          ADA I
1227    1103  0012          12
1230    1104  5764          STC R5          /ST
1231                  /
1232    1105  0063          SET I 3         /FIND MI
1233    1106  2000          2000
1234    1107  0644          LDF 4
1235    1110  1003          LDA 3
1236    1111  0643          LDF 3
1237    1112  1040          STA
1240    1113  1765          R6              /MI
1241    1114  0644  MI1,     LDF 4
1242    1115  1023          LDA I 3
1243    1116  0643          LDF 3
1244    1117  0450          AZE
1245    1120  0456          SKP
1246    1121  7134          JMP AT          /EXIT
1247    1122  0017          COM
1250    1123  1100          ADA
1251    1124  1765          R6              /MI
1252    1125  0451          APO
1253    1126  7114          JMP MI1
1254    1127  0644          LDF 4
1255    1130  1003          LDA 3
1256    1131  0643          LDF 3
1257    1132  5765          STC R6          /MI
1260    1133  7114          JMP MI1
1261                  /
1262    1134  0011  AT,      CLR             /CALCULATE
1263    1135  5751          STC STOR        /NUMBER OF
```

```
1264    1136  0065          SET I 5         /INTERVALS PER
1265    1137  2000          2000            /TRAIN
1266    1140  0067          SET I 7
1267    1141  3777          3777
1270    1142  1020  KQ,     LDA I
1271    1143  0001          1
1272    1144  1140          ADM
1273    1145  1751          STOR
1274    1146  0645          LDF 5
1275    1147  1005          LDA 5
1276    1150  0643          LDF 3
1277    1151  0450          AZE
1300    1152  0456          SKP
1301    1153  7175          JMP KO          /EXIT
1302    1154  0017          COM
1303    1155  0645          LDF 5
1304    1156  1125          ADA I 5
1305    1157  0643          LDF 3
1306    1160  0450          AZE
1307    1161  0456          SKP
1310    1162  7142          JMP KQ
1311    1163  0017          COM
1312    1164  0646          LDF 6
1313    1165  1067          STA I 7         /NUM TRAINS
1314    1166  0643          LDF 3
1315    1167  1000          LDA
1316    1170  1751          STOR
1317    1171  0646          LDF 6
1320    1172  1067          STA I 7         /NUM INTERVALS
1321    1173  0643          LDF 3
1322    1174  7142          JMP KQ
1323                  /
1324    1175  0071  KO,     SET I 11        /SUM 0.4 MSEC
1325    1176  2001          2001            /BINS TO FORM
1326    1177  0072          SET I 12        /0.8 MSEC BINS
1327    1200  3777          3777
1330    1201  0073          SET I 13
1331    1202  1577          1577
1332    1203  0647          LDF 7
1333    1204  1031          LDA I 11
1334    1205  0231          XSK I 11
1335    1206  0016          NOP
1336    1207  1131          ADA I 11
1337    1210  1072          STA I 12
1340    1211  0643          LDF 3
1341    1212  0231          XSK I 11
1342    1213  0016          NOP
1343    1214  0233          XSK I 13
1344    1215  7203          JMP .-12
1345                  /
1346    1216  0063          SET I 3         /FIND MEAN
1347    1217  3777          3777
1350    1220  0067          SET I 7
1351    1221  3777          3777
1352    1222  0011          CLR
1353    1223  5016          STC KL
1354    1224  5017          STC KH
1355    1225  0646  MN1,     LDF 6
1356    1226  1027          LDA I 7
1357    1227  0643          LDF 3
1360    1230  5753          STC NOM
1361    1231  0646          LDF 6
1362    1232  1027          LDA I 7
```

```
1363    1233  0643          LDF 3
1364    1234  0450          AZE
1365    1235  0456          SKP
1366    1236  7313          JMP MN4         /EXIT
1367    1237  5754          STC LEN
1370    1240  0644  MN2,     LDF 4
1371    1241  1023          LDA I 3
1372    1242  0643          LDF 3
1373    1243  5752          STC CONT
1374    1244  1020  MN3,     LDA I
1375    1245  0001          1
1376    1246  1200          LAM
1377    1247  1016          KL
1400    1250  5747          STC GAR
1401    1251  1200          LAM
1402    1252  1017          KH
1403    1253  1460          SAE I
1404    1254  7777          7777
1405    1255  7261          JMP .+4
1406    1256  0011          CLR             /CLR MEAN IF
1407    1257  5773          STC T2          /SUM > 24 BITS
1410    1260  7320          JMP MO          /EXIT
1411    1261  1020          LDA I
1412    1262  7776          -1
1413    1263  1140          ADM
1414    1264  1752          CONT
1415    1265  0450          AZE
1416    1266  7244          JMP MN3
1417    1267  1020          LDA I
1420    1270  7776          -1
1421    1271  1140          ADM
1422    1272  1754          LEN
1423    1273  0450          AZE
1424    1274  7240          JMP MN2
1425    1275  0063          SET I 3
1426    1276  3777          3777
1427    1277  1020          LDA I
1430    1300  7776          -1
1431    1301  1140          ADM
1432    1302  1753          NOM
1433    1303  0450          AZE
1434    1304  0456          SKP
1435    1305  7225          JMP MN1
1436    1306  0646          LDF 6
1437    1307  1007          LDA 7
1440    1310  0643          LDF 3
1441    1311  5754          STC LEN
1442    1312  7240          JMP MN2
1443    1313  1000  MN4,     LDA
1444    1314  1766          M1              /FMN
1445    1315  5015          STC KD
1446    1316  7000          JMP DIV
1447    1317  5773          STC T2          /MEAN
1450                /
1451    1320  0071  MO,      SET I 11        /FIND MODE
1452    1321  3777          3777
1453    1322  0073          SET I 13
1454    1323  1677          1677
1455    1324  0647          LDF 7
1456    1325  1031          LDA I 11
1457    1326  0643          LDF 3
1460    1327  5772          STC T1
1461    1330  1020          LDA I
```

```
1462    1331  0004          4
1463    1332  5751          STC STOR
1464    1333  0233  KP,     XSK I 13
1465    1334  0456          SKP
1466    1335  7363          JMP KS          /EXIT
1467    1336  1020          LDA I
1470    1337  0010          10              /INCREMENT BY
1471    1340  1140          ADM             /8.8 MSEC
1472    1341  1751          STOR
1473    1342  1000          LDA
1474    1343  1772          T1              /MON
1475    1344  0017          COM
1476    1345  0647          LDF 7
1477    1346  1131          ADA I 11
1500    1347  0643          LDF 3
1501    1350  0451          APO
1502    1351  7333          JMP KP
1503    1352  0647          LDF 7
1504    1353  1011          LDA 11
1505    1354  0643          LDF 3
1506    1355  5772          STC T1          /MON
1507    1356  1000          LDA
1510    1357  1751          STOR
1511    1360  1040          STA
1512    1361  1767          M2              /MOD
1513    1362  7333          JMP KP
1514                  /
1515    1363  0071  KS,     SET I 11        /FIND MEDIAN
1516    1364  3777          3777
1517    1365  1000          LDA
1520    1366  1770          M3              /HSN
1521    1367  0341          SCR 1
1522    1370  1560          BCL I
1523    1371  4000          4000
1524    1372  5745          STC MD
1525    1373  1020          LDA I
1526    1374  0004          4
1527    1375  1040          STA
1530    1376  1771          M4              /MED
1531    1377  0647  KA,     LDF 7
1532    1400  1031          LDA I 11
1533    1401  0643          LDF 3
1534    1402  0017          COM
1535    1403  1140          ADM
1536    1404  1745          MD
1537    1405  0451          APO
1540    1406  7414          JMP KE          /EXIT
1541    1407  1020          LDA I
1542    1410  0010          10
1543    1411  1140          ADM
1544    1412  1771          M4              /MED
1545    1413  7377          JMP KA
1546                  /
1547    1414  0065  KE,     SET I 5         /STORE CONSTANTS
1550    1415  2000          2000            /AT END OF TL
1551    1416  0067          SET I 7         /QUARTER 4
1552    1417  2340          2340
1553    1420  0063          SET I 3
1554    1421  2000          2000
1555    1422  1009          LDA
1556    1423  1760          R1              /MEAN RR
1557    1424  0647          LDF 7
1560    1425  1047          STA 7           /2340-RR
```

```
1561    1426  0645          LDF 5
1562    1427  1005          LDA 5           /NT
1563    1430  0647          LDF 7
1564    1431  1067          STA I 7         /2341-NT
1565    1432  0643          LDF 3
1566    1433  1000          LDA
1567    1434  1764          R5              /ST
1570    1435  0647          LDF 7
1571    1436  1067          STA I 7         /2342-ST
1572    1437  0011          CLR
1573    1440  1067          STA I 7         /2343-SD
1574    1441  1067          STA I 7         /2344-SE
1575    1442  0644          LDF 4
1576    1443  1003          LDA 3           /FI
1577    1444  0647          LDF 7
1600    1445  1067          STA I 7         /2345-FI
1601    1446  0011          CLR
1602    1447  1067          STA I 7         /2346-SD
1603    1450  1067          STA I 7         /2347-SE
1604    1451  0643          LDF 3
1605    1452  1000          LDA
1606    1453  1765          R6              /MI
1607    1454  0647          LDF 7
1610    1455  1067          STA I 7         /2350-MI
1611    1456  0643          LDF 3
1612    1457  1000          LDA
1613    1460  1766          M1              /ISIM N
1614    1461  0647          LDF 7
1615    1462  1067          STA I 7         /2351-FMN
1616    1463  0643          LDF 3
1617    1464  1000          LDA
1620    1465  1770          M3              /HISTO N
1621    1466  0647          LDF 7
1622    1467  1067          STA I 7         /2352-HSN
1623    1470  0643          LDF 3
1624    1471  1000          LDA
1625    1472  1773          T2              /MEAN
1626    1473  0647          LDF 7
1627    1474  1067          STA I 7         /2353-MEN
1630    1475  0643          LDF 3
1631    1476  1000          LDA
1632    1477  1771          M4              /MEDIAN
1633    1500  0647          LDF 7
1634    1501  1067          STA I 7         /2354-MED
1635    1502  0643          LDF 3
1636    1503  1000          LDA
1637    1504  1767          M2              /HISTO MODE
1640    1505  0647          LDF 7
1641    1506  1067          STA I 7         /2355-MOD
1642    1507  0643          LDF 3
1643    1510  1000          LDA
1644    1511  1772          T1              /MON
1645    1512  0647          LDF 7
1646    1513  1067          STA I 7         /2356-MON
1647    1514  0011          CLR
1650    1515  1067          STA I 7
1651    1516  0207          XSK 7
1652    1517  7515          JMP .-2
1653    1520  0643          LDF 3
1654                        /
1655    1521  0445  BB5,     SNS 5           /HLT UNTIL
1656    1522  7525          JMP KR          /RESET SNS 5
1657    1523  0603          LIF 3
```

```
1660    1524  6104          JMP DIS5
1661                        /
1662    1525  7734  KR,     JMP DSPY        /TO DISPLAY
1663    1526  7734          JMP DSPY        /ROUTINE
1664    1527  0603          LIF 3
1665    1530  6366          JMP AXIS        /TO AXIS DISPLAY
1666                        /
1667    1531  7727  KJ,     JMP TITL        /TO TITLE
1670    1532  7727          JMP TITL        /ROUTINE
1671    1533  0441          SNS 1
1672    1534  7547          JMP KW
1673    1535  0440          SNS 0
1674    1536  0456          SKP
1675    1537  7547          JMP KW          /EXIT
1676    1540  0603          LIF 3
1677    1541  6051          JMP DIS1
1700    1542  0445  BB1,     SNS 5
1701    1543  7535          JMP .-6
1702    1544  0002          PDP             /TO TELETYPE
1703                        PMODE           /OUTPUT
1704    5545  4422          JMS I T00
1705    5546  6141          LINC
1706                        LMODE
1707                        /
1710    1547  0442  KW,     SNS 2
1711    1550  7562          JMP KF
1712    1551  0440          SNS 0
1713    1552  0456          SKP
1714    1553  7562          JMP KF          /EXIT
1715    1554  0603          LIF 3
1716    1555  6062          JMP DIS2
1717    1556  0445  BB2,     SNS 5
1720    1557  7551          JMP .-6
1721    1560  0002          PDP             /TO XY PLOT
1722                        PMODE
1723    5561  4405          JMS I XY
1724                        LMODE
1725                        /
1726    1562  0443  KF,     SNS 3           /TAPE STORAGE
1727    1563  7724          JMP KU
1730    1564  0440          SNS 0
1731    1565  0456          SKP
1732    1566  7724          JMP KU          /EXIT
1733    1567  0603          LIF 3
1734    1570  6073          JMP DIS3
1735    1571  0445  BB3,     SNS 5
1736    1572  7564          JMP .-6         /DELAY
1737                        /
1740    1573  1020          LDA I           /CHECK FOR
1741    1574  6000          6000            /OVER WRITING
1742    1575  5622          STC WT0
1743                        /
1744    1576  0516          RSW
1745    1577  1560          BCL I
1746    1600  4000          4000
1747    1601  1120          ADA I
1750    1602  7632          -145            /RETURN IF
1751    1603  0451          APO             /DATA POINT
1752    1604  0456          SKP             /NUMBER > 101
1753    1605  7571          JMP BB3
1754                        /
1755    1606  0516          RSW             /READ DATA POINT
1756    1607  1040          STA             /NUMBER AND MULT
```

```
1757    1610  1613          .+3           /X 5
1760    1611  0242    -     ROL 2
1761    1612  1120          ADA I
1762    1613  0000          0
1763    1614  1040          STA
1764    1615  1750          BLK
1765    1616  1140          ADM
1766    1617  1622          WT0
1767    1620  0647          LDF 7
1770    1621  0712          RDE U
1771    1622  0000  WT0,     0
1772    1623  0072          SET I 12
1773    1624  3000          3000
1774    1625  1012          LDA 12        /FI OF ARRAY
1775    1626  0643          LDF 3
1776    1627  0450          AZE
1777    1630  0456          SKP
2000    1631  7641          JMP SV        /BLOCKS EMPTY
2001                  /
2002    1632  0440          SNS 0         /BLOCKS FILLED
2003    1633  0456          SKP
2004    1634  7724          JMP KU        /EXIT
2005    1635  0603          LIF 3
2006    1636  6115          JMP DISF
2007    1637  0445  BB4,    SNS 5
2010    1640  7632          JMP .-6
2011                  /
2012    1641  1020  SV,      LDA I         /STORE DATA
2013    1642  4000          4000
2014    1643  5652          STC W0
2015    1644  1000          LDA
2016    1645  1750          BLK
2017    1646  1140          ADM
2020    1647  1652          W0
2021    1650  0644          LDF 4
2022    1651  0734          WRC I U       /FIRST HALF FM
2023    1652  0000  W0,      0
2024    1653  0643          LDF 3
2025    1654  1020          LDA I
2026    1655  1001          1001
2027    1656  1140          ADM
2030    1657  1652          W0
2031    1660  5663          STC W1
2032    1661  0644          LDF 4
2033    1662  0734          WRC I U       /LAST HALF FM
2034    1663  0000  W1,      0
2035    1664  0643          LDF 3
2036                  /
2037    1665  1020          LDA I
2040    1666  1001          1001
2041    1667  1140          ADM
2042    1670  1663          W1
2043    1671  5674          STC W2
2044    1672  0644          LDF 4
2045    1673  0734          WRC I U       /FI
2046    1674  0000  W2,      0
2047    1675  0643          LDF 3
2050                  /
2051    1676  1020          LDA I
2052    1677  4003          4003
2053    1700  5707          STC W3
2054    1701  1000          LDA
2055    1702  1750          BLK
```

```
2056    1703  1140          ADM
2057    1704  1707          W3
2060    1705  0646          LDF 6
2061    1706  0734          WRC I U         /TL
2062    1707  0000  W3,     0
2063    1710  0643          LDF 3
2064                  /
2065    1711  1020          LDA I
2066    1712  4004          4004
2067    1713  5722          STC W4
2070    1714  1000          LDA
2071    1715  1750          BLK
2072    1716  1140          ADM
2073    1717  1722          W4
2074    1720  0647          LDF 7
2075    1721  0714          WRC U           /HISTO AND
2076    1722  0000  W4,     0               /CONSTANTS
2077    1723  0643          LDF 3
2100                  /
2101    1724  0444  KU,     SNS 4
2102    1725  7525          JMP KR          /DISPLAY AGAIN
2103    1726  6102          JMP ST          /RESTART
2104                  /
2105    1727  1000  TITL,   LDA             /SAVE RETURN
2106    1730  0000          0               /ADDRESS
2107    1731  5756          STC RETN
2110    1732  0603          LIF 3
2111    1733  6443          JMP LET
2112                  /
2113    1734  1000  DSPV,   LDA             /SAVE RETURN
2114    1735  0000          0               /ADDRESS
2115    1736  5756          STC RETN
2116    1737  0603          LIF 3
2117    1740  6126          JMP DISP
2120                  /
2121    1741  0000  S1,     0
2122    1742  0000  S2,     0
2123    1743  0000  FI,     0
2124    1744  0000  RC,     0
2125    1745  0000  MD,     0
2126    1746  0000  TRG,    0
2127    1747  0000  GAR,    0
2130    1750  0000  BLK,    0
2131    1751  0000  STOR,   0
2132    1752  0000  CONT,   0
2133    1753  0000  NOM,    0
2134    1754  0000  LEN,    0
2135    1755  0000  ZRO,    0
2136    1756  0000  RETN,   0
2137    1757  0000  L510,   0
2140    1760  0000  R1,     0
2141    1761  0000  R2,     0
2142    1762  0000  R3,     0
2143    1763  0000  R4,     0
2144    1764  0000  R5,     0
2145    1765  0000  R6,     0
2146    1766  0000  M1,     0
2147    1767  0000  M2,     0
2150    1770  0000  M3,     0
2151    1771  0000  M4,     0
2152    1772  0000  T1,     0
2153    1773  0000  T2,     0
2154                  /
```

```
2155                                PMODE
2156                                *6014           /IF 3
2157                                LMODE
2160    0014  1000                  1000            /PRESETS FOR
2161    0015  1000                  1000            /TITLE ROUTINE
2162                        /
2163    0016  0011  DISS,   CLR                     /DISPLAY S
2164    0017  0061         SET I 1
2165    0020  0364         364
2166    0021  0062         SET I 2
2167    0022  0646         646
2170    0023  1742         DSC 2
2171    0024  1762         DSC I 2
2172    0025  0602         LIF 2
2173    0026  6304         JMP QT
2174                        /
2175    0027  0011  DIST,   CLR                     /DISPLAY T
2176    0030  0061         SET I 1
2177    0031  0364         364
2200    0032  0062         SET I 2
2201    0033  0650         650
2202    0034  1742         DSC 2
2203    0035  1762         DSC I 2
2204    0036  0602         LIF 2
2205    0037  6440         JMP TB
2206                        /
2207    0040  0011  DISR,   CLR                     /DISPLAY R
2210    0041  0061         SET I 1
2211    0042  0364         364
2212    0043  0062         SET I 2
2213    0044  0644         644
2214    0045  1742         DSC 2
2215    0046  1762         DSC I 2
2216    0047  0602         LIF 2
2217    0050  6251         JMP C
2220                        /
2221    0051  0011  DIS1,   CLR                     /DISPLAY W
2222    0052  0061         SET I 1
2223    0053  0364         364
2224    0054  0062         SET I 2
2225    0055  0656         656
2226    0056  1742         DSC 2
2227    0057  1762         DSC I 2
2230    0060  0602         LIF 2
2231    0061  7542         JMP BB1
2232                        /
2233    0062  0011  DIS2,   CLR                     /DISPLAY P
2234    0063  0061         SET I 1
2235    0064  0364         364
2236    0065  0062         SET I 2
2237    0066  0640         640
2240    0067  1742         DSC 2
2241    0070  1762         DSC I 2
2242    0071  0602         LIF 2
2243    0072  7556         JMP BB2
2244                        /
2245    0073  0011  DIS3,   CLR                     /DISPLAY A
2246    0074  0061         SET I 1
2247    0075  0364         364
2250    0076  0062         SET I 2
2251    0077  0602         602
2252    0100  1742         DSC 2
2253    0101  1762         DSC I 2
```

```
2254    0102  0602          LIF 2
2255    0103  7571          JMP BB3
2256                /
2257    0104  0011  DIS5,    CLR           /DISPLAY 5
2260    0105  0061          SET I 1
2261    0106  0364          364
2262    0107  0062          SET I 2
2263    0110  0752          752
2264    0111  1742          DSC 2
2265    0112  1762          DSC I 2
2266    0113  0602          LIF 2
2267    0114  7521          JMP BB5
2270                /
2271    0115  0011  DISF,    CLR           /DISPLAY F
2272    0116  0061          SET I 1
2273    0117  0364          364
2274    0120  0062          SET I 2
2275    0121  0614          614
2276    0122  1742          DSC 2
2277    0123  1762          DSC I 2
2300    0124  0602          LIF 2
2301    0125  7637          JMP BB4
2302                /
2303    0126  1020  DISP,    LDA I
2304    0127  7400          -377
2305    0130  0061          SET I 1
2306    0131  0000          0
2307    0132  0062          SET I 2
2310    0133  0566          566
2311    0134  1742          DSC 2         /DISPLAY 0
2312    0135  1762          DSC I 2       /X AXIS
2313                /
2314    0136  0440          SNS 0         /SELECT DATA
2315    0137  6265          JMP MK        /DISPLAY
2316                /
2317    0140  1020          LDA I
2320    0141  7540          -237
2321    0142  0061          SET I 1
2322    0143  0000          0
2323    0144  0062          SET I 2
2324    0145  0572          572
2325    0146  1742          DSC 2         /DISPLAY 20
2326    0147  1762          DSC I 2       /Y AXIS
2327    0150  1762          DSC I 2
2330    0151  1762          DSC I 2
2331                /
2332    0152  1020          LDA I
2333    0153  7400          -377
2334    0154  0061          SET I 1
2335    0155  0040          40
2336    0156  0062          SET I 2
2337    0157  0572          572
2340    0160  1742          DSC 2         /DISPLAY 200
2341    0161  1762          DSC I 2       /X AXIS
2342    0162  1762          DSC I 2
2343    0163  1762          DSC I 2
2344    0164  1762          DSC I 2
2345    0165  1762          DSC I 2
2346                /
2347    0166  0101          SAM 1         /R TO L ISIM
2350    0167  0451          APO           /DATA DISPLAY
2351    0170  0011          CLR           /SHIFT
2352    0171  1120          ADA I
```

```
2353    0172  2000          2000
2354    0173  4175          STC .+2
2355    0174  0065          SET I 5
2356    0175  0000          0
2357    0176  6242          JMP SCLE        /SCALE PLOT
2360    0177  4201          STC .+2
2361    0200  0071          SET I 9
2362    0201  0000          0
2363                  /
2364    0202  0644  RE,     LDF 4
2365    0203  1005          LDA 5
2366    0204  0643          LDF 3
2367    0205  1120          ADA I
2370    0206  0005          5
2371    0207  0341          SCR 1           /SCALE INT TIMES
2372    0210  1040          STA
2373    0211  0220          SCL
2374    0212  1120          ADA I
2375    0213  6776          -1001           /BYPASS DISPLAY
2376    0214  0451          APO             /IF >101.4 MSEC
2377    0215  0456          SKP
2400    0216  6224          JMP .+6
2401    0217  1020          LDA I           /DISPLAY
2402    0220  0000  SCL,     0               /INTERVALS
2403    0221  1120          ADA I
2404    0222  7400          -377
2405    0223  0151          DIS 9
2406    0224  0644          LDF 4
2407    0225  1025          LDA I 5         /EXIT ISIM
2410    0226  0643          LDF 3
2411    0227  0450          AZE             /DISPLAY IF
2412    0230  0456          SKP             /INTERVAL = 0
2413    0231  6364          JMP DL
2414    0232  6242          JMP SCLE        /SCALE PLOT
2415    0233  1140          ADM
2416    0234  0011          9               /HORIZONTAL
2417    0235  1120          ADA I           /INCREMENT
2420    0236  7000          -777
2421    0237  0451          APO
2422    0240  6202          JMP RE
2423    0241  6364          JMP DL
2424                  /
2425    0242  1000  SCLE,    LDA             /SCALING ROUTINE
2426    0243  0000          0               /SAVE RETURN ADD
2427    0244  4264          STC BACK
2430    0245  0644          LDF 4
2431    0246  1005          LDA 5
2432    0247  0643          LDF 3
2433    0250  1120          ADA I
2434    0251  0005          5
2435    0252  0343          SCR 3
2436                  /
2437    0253  0002          PDP
2440                        PMODE
2441    0254  7421          MQL
2442    0255  7200          CLA
2443    0256  7407          DVI             /DIV 5
2444    0257  0005          5
2445    0260  7200          CLA
2446    0261  7501          MQA
2447    0262  6141          LINC
2450                        LMODE
2451    0263  6264          JMP BACK
```

```
2452                        /
2453      0264  0000  BACK,   0
2454                        /
2455      0265  0071  HK,     SET I 11        /HISTO START ADD
2456      0266  3777          3777
2457                        /
2460      0267  1020          LDA I
2461      0270  7700          -77
2462      0271  0061          SET I 1
2463      0272  0000          0
2464      0273  0062          SET I 2
2465      0274  0572          572
2466      0275  1742          DSC 2           /DISPLAY 200
2467      0276  1762          DSC I 2         /Y AXIS
2470      0277  1762          DSC I 2
2471      0300  1762          DSC I 2
2472      0301  1762          DSC I 2
2473      0302  1762          DSC I 2
2474                        /
2475      0303  1020          LDA I
2476      0304  7400          -377
2477      0305  0061          SET I 1
2500      0306  0717          717
2501      0307  0062          SET I 2
2502      0310  0564          564
2503      0311  1742          DSC 2
2504      0312  1762          DSC I 2
2505      0313  1762          DSC I 2         /DISPLAY 100
2506      0314  1762          DSC I 2         /X AXIS
2507      0315  1762          DSC I 2
2510      0316  1762          DSC I 2
2511                        /
2512      0317  0073  LB,     SET I 13        /DISPLAY HISTO
2513      0320  0000          0               /0.6 MSEC BINS
2514      0321  0101          SAM 1           /U TO D HISTO
2515      0322  0451          APO             /DISPLAY SHIFT
2516      0323  0011          CLR
2517      0324  0017          COM
2520      0325  4346          STC XC
2521      0326  0647  LK,     LDF 7
2522      0327  1011          LDA 11
2523      0330  0643          LDF 3
2524      0331  0450          AZE
2525      0332  0456          SKP
2526      0333  6352          JMP LY
2527      0334  1040          STA
2530      0335  0344          DT
2531      0336  1120          ADA I
2532      0337  6003          -1774
2533      0340  0451          APO
2534      0341  0456          SKP
2535      0342  6352          JMP LY
2536      0343  1020          LDA I
2537      0344  0000  DT,     0
2540      0345  1120          ADA I
2541      0346  0000  XC,     0
2542      0347  1120          ADA I
2543      0350  7400          -377
2544      0351  0153          DIS 13
2545      0352  0231  LY,     XSK I 11
2546      0353  0016          NOP
2547      0354  1020          LDA I
2550      0355  0004          4
```

```
2551    0356  1140          ADM
2552    0357  0013          13
2553    0360  1120          ADA I
2554    0361  7001          -776
2555    0362  0451          APO
2556    0363  6326          JMP LK
2557    0364  0602  DL,     LIF 2
2560    0365  7756          JMP RETN        /EXIT
2561                /
2562    0366  0063  AXIS,    SET I 3         /HORIZONTAL AXIS
2563    0367  0000          0               /DISPLAY
2564    0370  0070          SET I 10
2565    0371  6777          -1000
2566    0372  1020          LDA I
2567    0373  7400          -377
2570    0374  0073  AK,      SET I 13
2571    0375  7715          -62
2572    0376  0143  BR,      DIS 3
2573    0377  1120          ADA I
2574    0400  0001          1
2575    0401  1460          SAE I
2576    0402  7412          -365
2577    0403  6376          JMP BR
2600    0404  1020          LDA I
2601    0405  7400          -377
2602    0406  0163          DIS I 3
2603    0407  0230          XSK I 10
2604    0410  0456          SKP
2605    0411  6415          JMP BM          /EXIT
2606    0412  0233          XSK I 13
2607    0413  6406          JMP .-5
2610    0414  6374          JMP AK
2611                /
2612    0415  1020  BM,      LDA I           /VERTICAL AXIS
2613    0416  7400          -377            /DISPLAY
2614    0417  0063  RZ,      SET I 3
2615    0420  7000          7000
2616    0421  0070          SET I 10
2617    0422  7715          -62
2620    0423  0073          SET I 13
2621    0424  7767          -10
2622    0425  0143  RT,      DIS 3
2623    0426  1120          ADA I
2624    0427  0001          1
2625    0430  1460          SAE I
2626    0431  0400          400
2627    0432  6435          JMP AM
2630    0433  0692          LIF 2
2631    0434  7531          JMP KJ          /EXIT
2632    0435  0230  AM,      XSK I 10
2633    0436  6425          JMP RT
2634    0437  0163          DIS I 3
2635    0440  0233          XSK I 13
2636    0441  6437          JMP .-2
2637    0442  6417          JMP RZ
2640                /
2641    0443  1020  LET,     LDA I           /TITLE ROUTINE
2642    0444  0200          200             /IN IF 1
2643    0445  0004          ESF
2644    0446  0500  LISN,    IOB
2645    0447  6031          6031            /KSF
2646    0450  6467          JMP TITLE
2647    0451  0500          IOB
```

```
2650    0452  6036          6036          /KRB
2651    0453  0500          IOB
2652    0454  6046          6046          /TLS
2653    0455  1560          BCL I
2654    0456  7700          7700
2655    0457  0241          ROL 1
2656    0460  1120          ADA I
2657    0461  0600          600
2660    0462  1075          STA I 15
2661    0463  1460          SAE I
2662    0464  0706          706
2663    0465  6446          JMP LISN
2664    0466  6515          JMP EXIT
2665    0467  0074  TITLE,  SET I 14
2666    0470  1000          1000
2667    0471  0061          SET I 1
2670    0472  0000          0
2671    0473  1034  INTITL, LDA I 14        /BUMP
2672    0474  1000          LDA
2673    0475  0015          15
2674    0476  0017          COM
2675    0477  1100          ADA
2676    0500  0014          14
2677    0501  0451          APO
2700    0502  6504          JMP .+2
2701    0503  6523          JMP END
2702    0504  1014          LDA 14
2703    0505  4507          STC .+2
2704    0506  0076          SET I 16
2705    0507  0000          0
2706    0510  1020          LDA I
2707    0511  0370          370
2710    0512  1756          DSC 16
2711    0513  1776          DSC I 16
2712    0514  6473          JMP INTITL
2713    0515  0075  EXIT,   SET I 15
2714    0516  1000          1000
2715    0517  0500          IOB
2716    0520  6042          6042          /TCF
2717    0521  0602          LIF 2
2720    0522  7756          JMP RETN
2721    0523  0074  END,    SET I 14
2722    0524  1000          1000
2723    0525  0500          IOB
2724    0526  6042          6042          /TCF
2725    0527  0602          LIF 2
2726    0530  7756          JMP RETN
2727                /
2730                        *564
2731    0564  2101          2101          /1
2732    0565  0177          0177
2733    0566  4136          4136          /0
2734    0567  3641          3641
2735    0570  4136          4136          /0
2736    0571  3641          3641
2737    0572  4523          4523          /2
2740    0573  2151          2151
2741    0574  4136          4136          /0
2742    0575  3641          3641
2743    0576  4136          4136          /0
2744    0577  3641          3641
2745                /
2746                        *602          /IF 3
```

```
2747    0602  4477      4477
2750    0603  7744      7744        /A
2751    0604  5177      5177
2752    0605  2651      2651        /B
2753    0606  4136      4136
2754    0607  2241      2241        /C
2755    0610  4177      4177
2756    0611  3641      3641        /D
2757    0612  4577      4577
2760    0613  4145      4145        /E
2761    0614  4477      4477
2762    0615  4044      4044        /F
2763    0616  4136      4136
2764    0617  2645      2645        /G
2765    0620  1077      1077
2766    0621  7710      7710        /H
2767    0622  7741      7741
2770    0623  0041      0041        /I
2771    0624  4142      4142
2772    0625  4076      4076        /J
2773    0626  1077      1077
2774    0627  4324      4324        /K
2775    0630  0177      0177
2776    0631  0301      0301        /L
2777    0632  3077      3077
3000    0633  7730      7730        /M
3001    0634  3077      3077
3002    0635  7706      7706        /N
3003    0636  4177      4177
3004    0637  7741      7741        /O
3005    0640  4477      4477
3006    0641  3044      3044        /P
3007    0642  4276      4276
3010    0643  0376      0376        /Q
3011    0644  4477      4477
3012    0645  3146      3146        /R
3013    0646  5121      5121
3014    0647  4651      4651        /S
3015    0650  4040      4040
3016    0651  4077      4077        /T
3017    0652  0177      0177
3020    0653  7701      7701        /U
3021    0654  0176      0176
3022    0655  7402      7402        /V
3023    0656  0677      0677
3024    0657  7701      7701        /W
3025    0660  1463      1463
3026    0661  6314      6314        /X
3027    0662  0770      0770
3030    0663  7007      7007        /Y
3031    0664  4543      4543
3032    0665  6151      6151        /Z
3033    0666  4177      4177
3034    0667  0000      0000        /(
3035    0670  2040      2040
3036    0671  0410      0410        /\
3037    0672  0000      0000
3040    0673  7741      7741        /)
3041    0674  2000      2000
3042    0675  2077      2077        /^
3043    0676  3410      3410
3044    0677  1010      1010        /BACK ARROW
3045    0700  0000      0000
```

```
3046    0701  0000        0000    /SPACE
3047    0702  7500        7500
3050    0703  0000        6000    /!
3051    0704  6000        6000
3052    0705  6000        6000    /"
3053    0706  3614        3614
3054    0707  1436        1436    /NUMBER SIGN
3055    0710  7721        7721
3056    0711  4677        4677    /$
3057    0712  1446        1446
3060    0713  6130        6130    /%
3061    0714  5166        5166
3062    0715  0523        0523    /&
3063    0716  5000        5000
3064    0717  0060        0060    /APOSTROPHY
3065    0720  4136        4136
3066    0721  0000        0000    /(
3067    0722  0000        0000
3070    0723  3641        3641    /)
3071    0724  2050        2050
3072    0725  0050        0050    /*
3073    0726  0404        0404
3074    0727  0437        0437    /+
3075    0730  0605        0605
3076    0731  0000        0000    /,
3077    0732  0404        0404
3100    0733  0404        0404    /-
3101    0734  0001        0001
3102    0735  0000        0000    /.
3103    0736  0601        0601
3104    0737  4030        4030    //
3105    0740  4136        4136
3106    0741  3641        3641    /0
3107    0742  2101        2101
3110    0743  0177        0177    /1
3111    0744  4523        4523
3112    0745  2151        2151    /2
3113    0746  4122        4122
3114    0747  2651        2651    /3
3115    0750  2414        2414
3116    0751  0477        0477    /4
3117    0752  5172        5172
3120    0753  0651        0651    /5
3121    0754  1506        1506
3122    0755  4225        4225    /6
3123    0756  4443        4443
3124    0757  6050        6050    /7
3125    0760  5126        5126
3126    0761  2651        2651    /8
3127    0762  5120        5120
3130    0763  3651        3651    /9
3131    0764  2200        2200
3132    0765  0000        0000    /:
3133    0766  2601        2601
3134    0767  0000        0000    /;
3135    0770  2410        2410
3136    0771  0042        0042    /<
3137    0772  1212        1212
3140    0773  1212        1212    /=
3141    0774  4200        4200
3142    0775  1024        1024    />
3143    0776  2000        2000
3144    0777  3045        3045    /?
```

```
3145                    /
3146                            PMODE
3147                            PLOT=JMS I 2
3150                            WRITE=JMS I 3
3151                            MARK=JMS I 4
3152                            NUM=JMS I 20
3153                            DUMP=JMS I 21
3154                            DOWN=CLA
3155                            UP=CLA IAC
3156                            INIT=CLA CMA
3157                            *2                      /8 MODE PAGE 0
3160    0002    3400            PLOTX
3161    0003    3313            TYPLOT
3162    0004    3276            PLT1
3163    0005    1020    XY,     XYPLT
3164    0006    0000    CT,     0
3165                            *10
3166    0010    0000    PXTABLE,        0               /AUTO INDEXES
3167    0011    0000    PYTABLE,        0               /10 AND 11
3170                            *20
3171    0020    3200            DECPLT
3172    0021    2200            PLTSTG
3173                            *1000
3174    1000    7777    KFM,    7777                    /FMODM
3175    1001    5777    KHS,    5777                    /HISTO
3176    1002    1006    PTEXT1, TEXT1
3177    1003    1010    PTEXT2, TEXT2
3200    1004    1012    PTEXT3, TEXT3
3201    1005    1015    PTEXT4, TEXT4
3202    1006    6000
3202                    TEXT1,  TEXT $0$
3203    1007    0000            0
3204    1010    6260
3204                    TEXT2,  TEXT $20$
3205    1011    0000            0
3206    1012    6160
3206    1013    6000
3206                    TEXT3,  TEXT $100$
3207    1014    0000            0
3210    1015    6460
3210    1016    6000
3210                    TEXT4,  TEXT $400$
3211    1017    0000            0
3212    1020    0000    XYPLT,  0                       /START XY-PLOT
3213    1021    7300            CLA CLL                 /ROUTINE
3214    1022    1200            TAD KFM
3215    1023    3010            DCA PXTABLE
3216    1024    1201            TAD KHS                 /RESTORE TABLE
3217    1025    3011            DCA PYTABLE             /START ADDRESSES
3220    1026    7240            INIT
3221    1027    4402            PLOT
3222    1030    7201            UP
3223    1031    4402            PLOT
3224    1032    0074            74                      /0.6"
3225    1033    0106            106                     /0.7"
3226    1034    7200            CLA
3227    1035    1202            TAD PTEXT1              /0
3230    1036    4403            WRITE
3231    1037    0003            0003
3232                    /
3233    1040    7201            UP
3234    1041    4402            PLOT
3235    1042    0055            55                      /0.45"
```

```
3236    1043  0252          252             /1.7"
3237    1044  7200          CLA
3240    1045  1203          TAD PTEXT2      /20
3241    1046  4403          WRITE
3242    1047  0003          0003
3243                  /
3244    1050  7201          UP
3245    1051  4402          PLOT
3246    1052  0074          74              /0.6"
3247    1053  1072          1072            /5.7"
3250    1054  7200          CLA
3251    1055  1202          TAD PTEXT1      /0
3252    1056  4403          WRITE
3253    1057  0003          0003
3254                  /
3255    1060  7201          UP
3256    1061  4402          PLOT
3257    1062  0036          36              /0.3"
3260    1063  1236          1236            /6.7"
3261    1064  7200          CLA
3262    1065  1204          TAD PTEXT3      /100
3263    1066  4403          WRITE
3264    1067  0003          0003
3265                  /
3266    1070  7201          UP
3267    1071  4402          PLOT
3270    1072  0330          330             /2.2"
3271    1073  0062          62              /0.5"
3272    1074  7200          CLA
3273    1075  1205          TAD PTEXT4      /400
3274    1076  4403          WRITE
3275    1077  0003          0003
3276                  /
3277    1100  7201          UP              /ISIM 0,0
3300    1101  4402          PLOT
3301    1102  0120          120
3302    1103  0120          120
3303    1104  7240          INIT
3304    1105  4402          PLOT
3305                  /
3306    1106  7200          DOWN            /Y-AXIS
3307    1107  4402          PLOT
3310    1110  0000          0
3311    1111  1750          1750
3312                  /
3313    1112  7200          CLA
3314    1113  1353          TAD KINC2
3315    1114  3335          DCA INC2
3316    1115  1351          TAD KCT
3317    1116  3006          DCA CT
3320                  /
3321    1117  7200  BACK1,   CLA
3322    1120  1335          TAD INC2
3323    1121  3325          DCA INC1
3324    1122  7200          DOWN
3325    1123  4402          PLOT
3326    1124  0024          24
3327    1125  0000  INC1,    0
3330    1126  7200          CLA
3331    1127  1352          TAD M5
3332    1130  1335          TAD INC2
3333    1131  3335          DCA INC2
3334    1132  7201          UP
```

```
3335    1133  4402          PLOT
3336    1134  0000          0
3337    1135  0000  INC2,    0
3340    1136  2006          ISZ CT
3341    1137  5317          JMP BACK1
3342                /
3343    1140  7201          UP              /ISIM X-AXIS
3344    1141  4402          PLOT
3345    1142  0000          0
3346    1143  0000          0
3347    1144  7200          DOWN
3350    1145  4402          PLOT
3351    1146  1356          1356
3352    1147  0000          0
3353    1150  5377          JMP PAGE1
3354                /
3355    1151  7754  KCT,     -24
3356    1152  7716  M5,      -62
3357    1153  1750  KINC2,   1750
3360                /
3361                          *1177
3362    1177  7200  PAGE1,   CLA
3363    1200  1342          TAD KINC4
3364    1201  3224          DCA INC4
3365    1202  1340          TAD CTK
3366    1203  3006          DCA CT
3367                /
3370    1204  7200  BACK2,   CLA
3371    1205  1224          TAD INC4
3372    1206  3211          DCA INC3
3373    1207  7200          DOWN
3374    1210  4402          PLOT
3375    1211  0000  INC3,    0
3376    1212  0024          24
3377    1213  2006          ISZ CT
3400    1214  7410          SKP
3401    1215  5227          JMP AXS2
3402    1216  7200          CLA
3403    1217  1341          TAD M75
3404    1220  1224          TAD INC4
3405    1221  3224          DCA INC4
3406    1222  7201          UP
3407    1223  4402          PLOT
3410    1224  0000  INC4,    0
3411    1225  0000          0
3412    1226  5204          JMP BACK2
3413                /
3414    1227  7201  AXS2,    UP              /HISTO X-AXIS
3415    1230  4402          PLOT
3416    1231  0000          0
3417    1232  0764          764
3420    1233  7200          DOWN
3421    1234  4402          PLOT
3422    1235  1356          1356
3423    1236  0764          764
3424                /
3425    1237  7201          UP
3426    1240  4402          PLOT
3427    1241  1306          1306            /7.1"
3430    1242  0726          726             /4.7"
3431    1243  7200          CLA
3432    1244  1261          TAD PTEXT5      /100
3433    1245  4403          WRITE
```

```
3434    1246  0003          0003
3435                /
3436    1247  7201          UP
3437    1250  4402          PLOT
3440    1251  1356          1356
3441    1252  0764          764
3442                /
3443    1253  7209          CLA
3444    1254  1342          TAD KINC4
3445    1255  3305          DCA INC6
3446    1256  1340          TAD CTK
3447    1257  3006          DCA CT
3450    1260  5265          JMP BACK3
3451                /
3452    1261  1262  PTEXT5, TEXT5
3453    1262  6160
3453    1263  6000
3453                TEXT5,  TEXT $100$
3454    1264  0000          0
3455                /
3456    1265  7200  BACK3,  CLA
3457    1266  1305          TAD INC6
3460    1267  3272          DCA INC5
3461    1270  7200          DOWN
3462    1271  4402          PLOT
3463    1272  0000  INC5,    0
3464    1273  1010          1010
3465    1274  2006          ISZ CT
3466    1275  7410          SKP
3467    1276  5310          JMP HISP
3470    1277  7200          CLA
3471    1300  1341          TAD M75
3472    1301  1305          TAD INC6
3473    1302  3305          DCA INC6
3474    1303  7201          UP
3475    1304  4402          PLOT
3476    1305  0000  INC6,    0
3477    1306  0764          764
3500    1307  5265          JMP BACK3
3501                /
3502    1310  7201  HISP,    UP              /PLOT HISTO
3503    1311  4402          PLOT
3504    1312  0000          0
3505    1313  0764          764
3506    1314  7300          CLA CLL
3507    1315  3333          DCA PL1
3510    1316  1344          TAD M175        /125
3511    1317  3006          DCA CT
3512    1320  7200  BAK1,   CLA
3513    1321  6211          CDF 10
3514    1322  1411          TAD I PYTABLE   /HISTO START ADD
3515    1323  6201          CDF 0
3516    1324  1345          TAD K764
3517    1325  3334          DCA PL2
3520    1326  1343          TAD PG
3521    1327  1333          TAD PL1
3522    1330  3333          DCA PL1
3523    1331  7200          DOWN
3524    1332  4402          PLOT
3525    1333  0000  PL1,     0
3526    1334  0000  PL2,     0
3527    1335  2006          ISZ CT
3530    1336  5320          JMP BAK1
```

```
3531    1337  5377          JMP PAGE2
3532                  /
3533    1340  7766  CTK,    -12
3534    1341  7665  M75,    -113
3535    1342  1356  KINC4,  1356
3536    1343  0006  P6,     6
3537    1344  7603  M175,   -175          /-125
3540    1345  0764  K764,   764           /5"
3541                  /
3542                        *1377
3543    1377  7201  PAGE2,  UP             /PLOT ISIM
3544    1400  7300          CLA CLL
3545    1401  3276          DCA PL3
3546    1402  1316          TAD N02
3547    1403  3314          DCA KTC
3550    1404  1315          TAD N00
3551    1405  3006          DCA CT
3552    1406  7300  BAK2,   CLA CLL
3553    1407  3274          DCA PL5
3554    1410  6211          CDF 10
3555    1411  1410          TAD I PXTABLE
3556    1412  6201          CDF 0
3557    1413  7450          SNA              /EXIT IF TRAIN
3560    1414  5301          JMP EX           /DONE
3561    1415  1312          TAD K5
3562    1416  3277          DCA PL4
3563                  /
3564    1417  2314          ISZ KTC
3565    1420  5236          JMP .+16
3566    1421  7300          CLA CLL
3567    1422  1277          TAD PL4
3570    1423  7421          MQL
3571    1424  7200          CLA
3572    1425  7407          DVI              /SCALE X AXIS
3573    1426  0032          32
3574    1427  7200          CLA
3575    1430  7501          MQA
3576    1431  1276          TAD PL3
3577    1432  3276          DCA PL3
3600    1433  1316          TAD N02
3601    1434  3314          DCA KTC
3602    1435  5250          JMP .+13
3603                  /
3604    1436  7300          CLA CLL
3605    1437  1277          TAD PL4
3606    1440  7421          MQL
3607    1441  7200          CLA
3610    1442  7407          DVI
3611    1443  0033          33
3612    1444  7200          CLA
3613    1445  7501          MQA
3614    1446  1276          TAD PL3
3615    1447  3276          DCA PL3
3616                  /
3617    1450  7300          CLA CLL          /SCALE Y AXIS
3620    1451  1277          TAD PL4
3621    1452  1317          TAD N4
3622    1453  7110          CLL RAR
3623    1454  3277          DCA PL4
3624                  /
3625    1455  7300          CLA CLL
3626    1456  1276          TAD PL3
3627    1457  1310          TAD M1356
```

```
3630    1460  7500          SMA             /EXIT IF TRAIN
3631    1461  5301          JMP EX          /LENGTH >2 SEC
3632                /
3633    1462  7300          CLA CLL
3634    1463  2006          ISZ CT
3635    1464  5270          JMP .+4
3636    1465  7300          CLA CLL
3637    1466  1311          TAD K1          /UP
3640    1467  3274          DCA PL5
3641                /
3642    1470  7300          CLA CLL
3643    1471  1274          TAD PL5
3644    1472  1313          TAD K7200       /DOWN
3645    1473  3274          DCA PL5
3646    1474  0000  PL5,     0               /PEN POSITION
3647    1475  4402          PLOT
3650    1476  0000  PL3,     0
3651    1477  0000  PL4,     0
3652    1500  5206          JMP BAK2
3653                /
3654    1501  7201  EX,      UP              /REPOSITION PEN
3655    1502  4402          PLOT            /FOR NEXT PLOT
3656    1503  1402          1402
3657    1504  0000          0
3660                /
3661    1505  6141          LINC
3662                        LMODE
3663    1506  0002          LIF 2
3664    1507  7562          JMP KF          /EXIT
3665                /
3666    1510  6421  N1356,   -1356
3667    1511  0001  K1,      1
3670    1512  0005  K5,      5
3671    1513  7200  K7200,   7200
3672    1514  0000  K1C,     0
3673    1515  7777  N00,     7777
3674    1516  7775  N02,     7775
3675    1517  7774  N4,      7774
3676                /
3677                        PMODE
3700                        *2000           /PLOT SUBROUTINE
3701                        PAGE            /IN IF 1
3702    2000  0000  MOVE,    0
3703    2001  1276          TAD NNN5
3704    2002  3301          DCA NNN5GO
3705    2003  3271          DCA OLDRX
3706    2004  1277  TIM1,    TAD NNN2
3707    2005  3300          DCA NNN2GO
3710    2006  1672          TAD I L
3711    2007  3273          DCA N
3712    2010  1273  TIM2,    TAD N
3713    2011  0275          AND LLL7
3714    2012  3265          DCA RARY
3715    2013  1273          TAD N
3716    2014  7012          RTR
3717    2015  7010          RAR
3720    2016  0275          AND LLL7
3721    2017  1276          TAD NNN5
3722    2020  7500          SMA
3723    2021  4703          JMS I RPNUPD
3724    2022  1274          TAD LLL5
3725    2023  3264          DCA RARX
3726    2024  1264          TAD RARX
```

```
3727    2025  3271          DCA OLDRX
3730    2026  4313          JMS SCLPLT
3731    2027  4304          JMS PLOTIT
3732    2030  7200          CLA
3733    2031  1273          TAD M
3734    2032  7012          RTR
3735    2033  7012          RTR
3736    2034  7012          RTR
3737    2035  3273          DCA M
3740    2036  2300          ISZ MMM2GO
3741    2037  5210          JMP TIM2
3742    2040  2301          ISZ MMM5GO
3743    2041  7410          SKP
3744    2042  5245          JMP SPC
3745    2043  2272          ISZ L
3746    2044  5204          JMP TIM1
3747    2045  4703  SPC,    JMS I RPNUPD
3750    2046  7200          CLA
3751    2047  1270          TAD LINRUN
3752    2050  7650          SNA CLA
3753    2051  5256          JMP .+5
3754    2052  1275          TAD LLL7
3755    2053  3265          DCA RAWY
3756    2054  3264          DCA RAWX
3757    2055  5261          JMP .+4
3760    2056  1274          TAD LLL5
3761    2057  3264          DCA RAWX
3762    2060  3265          DCA RAWY
3763    2061  4313          JMS SCLPLT
3764    2062  4304          JMS PLOTIT
3765    2063  5600          JMP I MOVE
3766                  /
3767    2064  0000  RAWX,0
3770    2065  0000  RAWY,0
3771    2066  0000  SCLMLT,0
3772    2067  0000  TRANSQ,0
3773    2070  0000  LINRUN,0
3774    2071  0000  OLDRX,0
3775    2072  0000  L,0
3776    2073  0000  M,0
3777    2074  0005  LLL5,   5
4000    2075  0007  LLL7,   7
4001    2076  7773  MMM5,     -5
4002    2077  7776  MMM2,     -2
4003    2100  0000  MMM2GO,0
4004    2101  0000  MMM5GO,0
4005    2102  0000  CNTR,0
4006    2103  2264  RPNUPD, PNUPDN
4007                  /
4010    2104  0000  PLOTIT, 0
4011    2105  7201  PNSTAT, CLA IAC
4012    2106  4712          JMS I PLUT
4013    2107  0000  XHVT,   0
4014    2110  0000  YHVT,   0
4015    2111  5704          JMP I PLOTIT
4016                  /
4017    2112  3400  PLUT,   PLOTX
4020    2113  0000  SCLPLT, 0
4021    2114  1267          TAD TRANSQ
4022    2115  7450          SNA
4023    2116  5354          JMP STRAIT
4024    2117  1277          TAD MMM2
4025    2120  7450          SNA
```

```
4026    2121  5334          JMP ROTRIT
4027    2122  7510          SPA
4030    2123  5343          JMP INVRT
4031                        /
4032    2124  7200  ROTLFT,  CLA
4033    2125  1264          TAD RAWX
4034    2126  3310          DCA TRY
4035    2127  1265          TAD RAWY
4036    2130  7041          CIA
4037    2131  1275          TAD LLL7
4040    2132  3307          DCA TRX
4041    2133  5360          JMP SCALE
4042                        /
4043    2134  1264  ROTRIT,  TAD RAWX
4044    2135  7041          CIA
4045    2136  1274          TAD LLL5
4046    2137  3310          DCA TRY
4047    2140  1265          TAD RAWY
4050    2141  3307          DCA TRX
4051    2142  5360          JMP SCALE
4052                        /
4053    2143  1264  INVRT,  TAD RAWX
4054    2144  7041          CIA
4055    2145  1274          TAD LLL5
4056    2146  3307          DCA TRX
4057    2147  1265          TAD RAWY
4060    2150  7041          CIA
4061    2151  1275          TAD LLL7
4062    2152  3310          DCA TRY
4063    2153  5360          JMP SCALE
4064                        /
4065    2154  1264  STRAIT,  TAD RAWX
4066    2155  3307          DCA TRX
4067    2156  1265          TAD RAWY
4070    2157  3310          DCA TRY
4071                        /
4072    2160  1266  SCALE,  TAD SCLMLT
4073    2161  3302          DCA CNTR
4074    2162  1307          TAD TRX
4075    2163  2302          ISZ CNTR
4076    2164  5362          JMP .-2
4077    2165  3307          DCA XMYT
4100    2166  1266          TAD SCLMLT
4101    2167  3302          DCA CNTR
4102    2170  1310          TAD TRY
4103    2171  2302          ISZ CNTR
4104    2172  5370          JMP .-2
4105    2173  3310          DCA YMYT
4106    2174  5713          JMP I SCLPLT
4107                        TRX=XMYT
4110                        TRY=YMYT
4111                        /
4112                        PAGE
4113    2200  0000  PLTSTG,  0
4114    2201  3317          DCA STRADD
4115    2202  1731          TAD I OLDX
4116    2203  3327          DCA COLDX
4117    2204  1732          TAD I OLDY
4120    2205  3330          DCA COLDY
4121    2206  1324  RDPACK,  TAD MM2
4122    2207  3320          DCA MM2GO
4123    2210  1717          TAD I STRADD
4124    2211  3321          DCA SAV
```

```
4125    2212  1321  RDPK2,  TAD SAV
4126    2213  7012          RTR
4127    2214  7012          RTR
4130    2215  7012          RTR
4131    2216  0325  RDPK3,  AND LL77
4132    2217  7450          SNA
4133    2220  5256          JMP TYPFIN
4134    2221  3322  BASAD,  DCA CODE
4135    2222  1326          TAD MM5
4136    2223  3323          DCA CNTR2
4137    2224  1322          TAD CODE
4140    2225  2323          ISZ CNTR2
4141    2226  5224          JMP .-2
4142    2227  1336          TAD BASE
4143    2230  3733          DCA I RL
4144    2231  4304  UPDATE, JMS SCL00
4145    2232  3731          DCA I OLDX
4146    2233  1734          TAD I RYMVT
4147    2234  3732          DCA I OLDY
4150    2235  4735          JMS I RMOVE
4151    2236  4304          JMS SCL00
4152    2237  7041          CIA
4153    2240  1731          TAD I OLDX
4154    2241  1327          TAD COLDX
4155    2242  3327          DCA COLDX
4156    2243  1734          TAD I RYMVT
4157    2244  7041          CIA
4160    2245  1732          TAD I OLDY
4161    2246  1330          TAD COLDY
4162    2247  3330          DCA COLDY
4163    2250  1321  RDPK4,  TAD SAV
4164    2251  2320          ISZ MM2GO
4165    2252  5216          JMP RDPK3
4166    2253  7200          CLA
4167    2254  2317          ISZ STRADD
4170    2255  5206          JMP RDPACK
4171    2256  7200  TYPFIN, CLA
4172    2257  1327          TAD COLDX
4173    2260  3731          DCA I OLDX
4174    2261  1330          TAD COLDY
4175    2262  3732          DCA I OLDY
4176    2263  5600          JMP I PLTSTG
4177                /
4200    2264  0000  PNUPDN, 0
4201    2265  1324          TAD MM2
4202    2266  7640          SZA CLA
4203    2267  5273          JMP .+4
4204    2270  1300          TAD DN
4205    2271  3702          DCA I RPNSTA
4206    2272  5275          JMP .+3
4207    2273  1301          TAD PUP
4210    2274  3702          DCA I RPNSTA
4211    2275  1703          TAD I ROLDRX
4212    2276  1326          TAD MM5
4213    2277  5664          JMP I PNUPDN
4214    2300  7200  DN,     CLA
4215    2301  7201  PUP,    CLA IAC
4216    2302  2105  RPNSTA, PNSTAT
4217    2303  2071  ROLDRX, OLDRX
4220                /
4221    2304  0000  SCL00,  0
4222    2305  7200          CLA
4223    2306  3713          DCA I RRAWX
```

```
4224    2307  3714          DCA I RRAWY
4225    2310  4715          JMS I RSCLPL
4226    2311  1716          TAD I RXMVT
4227    2312  5704          JMP I SCL00
4230    2313  2064  RRAWX,  RAWX
4231    2314  2065  RRAWY,  RAWY
4232    2315  2113  RSCLPL, SCLPLT
4233    2316  2107  RXMVT,  XMVT
                    /VARIABLES FOR PLTSTG
4234
4235    2317  0000  STRADD,0
4236    2320  0000  MM2GO,0
4237    2321  0000  SAV,0
4240    2322  0000  CODE,0
4241    2323  0000  CNTR2,0
4242    2324  7776  MM2,        -2
4243    2325  0077  LL77,       77
4244    2326  7773  MM5,        -5
4245    2327  0000  COLDX,0
4246    2330  0000  COLDY,0
4247    2331  3562  OLDX,       PLOTX+162
4250    2332  3563  OLDY,       PLOTX+163
4251    2333  2072  RL,L
4252    2334  2110  RYMVT,      YMVT
4253    2335  2000  RMOVE,      MOVE
4254    2336  2332  BASE,       .-4
4255                /
4256                /MOVEMENT CODES FOR EACH CHARACTER
4257                /
4260    2337  1370  1370;
4260    2340  1333   1333;
4260    2341  4026   4026;
4260    2342  4040   4040;
4260    2343  4040   4040    /A
4261    2344  4676  4676;
4261    2345  3343   3343;
4261    2346  3303   3303;
4261    2347  4042   4042;
4261    2350  4000   4000    /B
4262    2351  4660  4660;
4262    2352  1676   1676;
4262    2353  0105   0105;
4262    2354  4010   4010;
4262    2355  4040   4040    /C
4263    2356  3676  3676;
4263    2357  4145   4145;
4263    2360  0030   0030;
4263    2361  0000   0000;
4263    2362  0000   0000    /D
4264    2363  4676  4676;
4264    2364  0306   0306;
4264    2365  0333   0333;
4264    2366  4000   4000;
4264    2367  4040   4040    /E
4265    2370  4676  4676;
4265    2371  0306   0306;
4265    2372  0333   0333;
4265    2373  0000   0000;
4265    2374  0000   0000    /F
4266    2375  4660  4660;
4266    2376  1676   1676;
4266    2377  0105   0105;
4266    2400  4010   4010;
4266    2401  2242   2242    /G
```

```
4267    2402  0376  0376;
4267    2403  4643   4643;
4267    2404  4040   4040;
4267    2405  4040   4040;
4267    2406  4040   4040    /H
4270    2407  7010  7010;
4270    2410  2030   2030;
4270    2411  1626   1626;
4270    2412  3636   3636;
4270    2413  3636   3636    /I
4271    2414  0072  0072;
4271    2415  3630   3630;
4271    2416  4626   4626;
4271    2417  4646   4646;
4271    2420  4646   4646    /J
4272    2421  0276  0276;
4272    2422  4013   4013;
4272    2423  4613   4613;
4272    2424  4646   4646;
4272    2425  4646   4646    /K
4273    2426  0076  0076;
4273    2427  4040   4040;
4273    2430  4040   4040;
4273    2431  4040   4040;
4273    2432  4040   4040    /L
4274    2433  2376  2376;
4274    2434  4046   4046;
4274    2435  4040   4040;
4274    2436  4040   4040;
4274    2437  4040   4040    /M
4275    2440  4076  4076;
4275    2441  4646   4646;
4275    2442  4646   4646;
4275    2443  4646   4646;
4275    2444  4646   4646    /N
4276    2445  7561  7561;
4276    2446  3616   3616;
4276    2447  4145   4145;
4276    2450  1030   1030;
4276    2451  0501   0501    /O
4277    2452  4676  4676;
4277    2453  0343   0343;
4277    2454  4643   4643;
4277    2455  0006   0006;
4277    2456  0000   0000    /P
4300    2457  1645  1645;
4300    2460  4146   4146;
4300    2461  0030   0030;
4300    2462  2262   2262;
4300    2463  4072   4072    /Q
4301    2464  4676  4676;
4301    2465  0343   0343;
4301    2466  4013   4013;
4301    2467  4040   4040;
4301    2470  4040   4040    /R
4302    2471  3070  3070;
4302    2472  4241   4241;
4302    2473  1333   1333;
4302    2474  0504   0504;
4302    2475  4616   4616    /S
4303    2476  7620  7620;
4303    2477  0646   0646;
4303    2500  0606   0606;
```

```
4303      2501  0606   0606;
4303      2502  0606   0606    /T
4304      2503  7601  7601;
4304      2504  1001   1001;
4304      2505  4130   4130;
4304      2506  4646   4646;
4304      2507  4646   4646    /U
4305      2510  7606  7606;
4305      2511  4620   4620;
4305      2512  4646   4646;
4305      2513  4646   4646;
4305      2514  4646   4646    /V
4306      2515  7606  7606;
4306      2516  2310   2310;
4306      2517  4630   4630;
4306      2520  4646   4646;
4306      2521  4646   4646    /W
4307      2522  4670  4670;
4307      2523  0666   0666;
4307      2524  4076   4076;
4307      2525  4040   4040;
4307      2526  4040   4040    /X
4310      2527  7320  7320;
4310      2530  2306   2306;
4310      2531  4646   4646;
4310      2532  4646   4646;
4310      2533  4646   4646    /Y
4311      2534  7606  7606;
4311      2535  0046   0046;
4311      2536  4040   4040;
4311      2537  4040   4040;
4311      2540  4040   4040    /Z
4312      2541  7030  7030;
4312      2542  1610   1610;
4312      2543  3636   3636;
4312      2544  3636   3636;
4312      2545  3636   3636    /(
4313      2546  7502  7502;
4313      2547  0105   0105;
4313      2550  4341   4341;
4313      2551  4303   4303;
4313      2552  2545   2545    /\
4314      2553  7010  7010;
4314      2554  3630   3630;
4314      2555  1616   1616;
4314      2556  1616   1616;
4314      2557  1616   1616    /)
4315      2560  7303  7303;
4315      2561  4325   4325;
4315      2562  0321   0321;
4315      2563  0303   0303;
4315      2564  0303   0303    /^
4316      2565  7041  7041;
4316      2566  3300   3300;
4316      2567  4606   4606;
4316      2570  4545   4545;
4316      2571  4545   4545    /BACK ARROW
4317      2572  0000  0000;
4317      2573  0000   0000;
4317      2574  0000   0000;
4317      2575  0000   0000;
4317      2576  0000   0000    /SPACE
4320      2577  7101  7101;
-
```

```
4320      2600  6441   6441;
4320      2601  0474   0474;
4320      2602  3664   3664;
4320      2603  2276   2276    /!
4321      2604  7510  7510;
4321      2605  2213   2213;
4321      2606  4332   4332;
4321      2607  4444   4444;
4321      2610  4444   4444    /"
4322      2611  7501  7501;
4322      2612  4145   4145;
4322      2613  0101   0101;
4322      2614  0101   0101;
4322      2615  0101   0101    /NUMBER SIGN
4323      2616  7521  7521;
4323      2617  3424   3424;
4323      2620  1314   1314;
4323      2621  3233   3233;
4323      2622  1212   1212    /$
4324      2623  7525  7525;
4324      2624  1514   1514;
4324      2625  1135   1135;
4324      2626  3231   3231;
4324      2627  2121   2121    /%
4325      2630  7521  7521;
4325      2631  3424   3424;
4325      2632  2314   2314;
4325      2633  3212   3212;
4325      2634  3232   3232    /&
4326      2635  7323  7323;
4326      2636  2615   2615;
4326      2637  2335   2335;
4326      2640  2323   2323;
4326      2641  2323   2323    /APOSTROPHY
4327      2642  7636  7636;
4327      2643  1325   1325;
4327      2644  3021   3021;
4327      2645  3030   3030;
4327      2646  3030   3030    /(
4330      2647  7010  7010;
4330      2650  3321   3321;
4330      2651  1625   1625;
4330      2652  1616   1616;
4330      2653  1616   1616    /)
4331      2654  7521  7521;
4331      2655  1423   1423;
4331      2656  2332   2332;
4331      2657  3412   3412;
4331      2660  2323   2323    /*
4332      2661  7521  7521;
4332      2662  0323   0323;
4332      2663  2343   2343;
4332      2664  2121   2121;
4332      2665  2121   2121    /+
4333      2666  7211  7211;
4333      2667  2122   2122;
4333      2670  2111   2111;
4333      2671  1010   1010;
4333      2672  1010   1010    /,
4334      2673  7313  7313;
4334      2674  6333   6333;
4334      2675  3333   3333;
4334      2676  3333   3333;
```

```
4334    2677  3333   3333    /-
4335    2700  7110  7110;
4335    2701  2021   2021;
4335    2702  1110   1110;
4335    2703  0464   0464;
4335    2704  0404   0404    /.
4336    2705  4670  4670;
4336    2706  4066   4066;
4336    2707  4040  .4040;
4336    2710  4040   4040;
4336    2711  4040   4040    //
4337    2712  7501  7501;
4337    2713  3616   3616;
4337    2714  4145   4145;
4337    2715  1030   1030;
4337    2716  4501   4501    /0
4340    2717  7010  7010;
4340    2720  2030   2030;
4340    2721  1526   1526;
4340    2722  2626   2626;
4340    2723  2626   2626    /1
4341    2724  7505  7505;
4341    2725  3616   3616;
4341    2726  4445   4445;
4341    2727  0001   0001;
4341    2730  4140   4140    /2
4342    2731  7606  7606;
4342    2732  1346   1346;
4342    2733  4334   4334;
4342    2734  3041   3041;
4342    2735  0110   0110    /3
4343    2736  7630  7630;
4343    2737  4333   4333;
4343    2740  0603   0603;
4343    2741  0606   0606;
4343    2742  0606   0606    /4
4344    2743  7646  7646;
4344    2744  0306   0306;
4344    2745  3414   3414;
4344    2746  4143   4143;
4344    2747  0030   0030    /5
4345    2750  1372  1372;
4345    2751  4233   4233;
4345    2752  3041   3041;
4345    2753  0500   0500;
4345    2754  3616   3616    /6
4346    2755  7505  7505;
4346    2756  4616   4616;
4346    2757  3222   3222;
4346    2760  2212   2212;
4346    2761  1010   1010    /7
4347    2762  4472  4472;
4347    2763  0646   0646;
4347    2764  4204   4204;
4347    2765  0040   0040;
4347    2766  0000   0000    /8
4350    2767  7540  7540;
4350    2770  1636   1636;
4350    2771  0405   0405;
4350    2772  3313   3313;
4350    2773  4544   4544    /9
4351    2774  7211  7211;
4351    2775  2122   2122;
```

```
4351      2776  6411   6411;
4351      2777  2575   2575;
4351      3000  1424   1424     /:
4352      3001  7210  7210;
4352      3002  2122   2122;
4352      3003  6410   6410;
4352      3004  2575   2575;
4352      3005  1424   1424     /;
4353      3006  7545  7545;
4353      3007  4103   4103;
4353      3010  4141   4141;
4353      3011  4141   4141;
4353      3012  4141   4141     /<
4354      3013  7202  7202;
4354      3014  6342   6342;
4354      3015  0373   0373;
4354      3016  0303   0303;
4354      3017  0303   0303     /=
4355      3020  7101  7101;
4355      3021  0543   0543;
4355      3022  0505   0505;
4355      3023  0505   0505;
4355      3024  0505   0505     />
4356      3025  7505  7505;
4356      3026  3616   3616;
4356      3027  4445   4445;
4356      3030  2123   2123;
4356      3031  7060   7060     /?
4357                   /
4360                           PAGE
4361      3200  0000  DECPLT,  0
4362      3201  7500           SMA
4363      3202  5207           JMP PLUS
4364      3203  7041           CIA
4365      3204  3261           DCA VALUE
4366      3205  1272           TAD L55
4367      3206  5211           JMP .+3
4370      3207  3261  PLUS,    DCA VALUE
4371      3210  1274           TAD L40
4372      3211  4276           JMS PLT1
4373      3212  3270           DCA SKPF
4374      3213  1253           TAD M7
4375      3214  3271           DCA CNT4
4376      3215  3262           DCA DIGIT
4377      3216  1253           TAD CNTRZA
4400      3217  3263           DCA CNTRZB
4401      3220  1252           TAD ADDRZA
4402      3221  3226           DCA ARROW
4403      3222  7410           SKP
4404      3223  3261           DCA VALUE
4405      3224  7100           CLL
4406      3225  1261           TAD VALUE
4407      3226  1254  ARROW,   TAD TENPWR
4410      3227  7430           SZL
4411      3230  2262           ISZ DIGIT
4412      3231  7430           SZL
4413      3232  5223           JMP ARROW-3
4414      3233  7200           CLA
4415      3234  1262           TAD DIGIT
4416      3235  2271           ISZ CNT4
4417      3236  7410           SKP
4420      3237  5242           JMP .+3
4421      3240  7450           SNA
```

```
4422    3241  5264          JMP CK
4423    3242  2270          ISZ SKPF
4424    3243  1275          TAD K60
4425    3244  4276  OUT,    JMS PLT1
4426    3245  3262          DCA DIGIT
4427    3246  2226          ISZ ARROW
4430    3247  2263          ISZ CNTRZB
4431    3250  5225          JMP ARROW-1
4432    3251  5600          JMP I DECPLT
4433    3252  1254  ADDRZA, TAD TENPWR
4434    3253  7774  CNTRZA, -4
4435    3254  6030  TENPWR, -1750
4436    3255  7634          -0144
4437    3256  7766          -0012
4440    3257  7777          -0001
4441    3260  7777          -0001
4442    3261  0000  VALUE,  0
4443    3262  0000  DIGIT,  0
4444    3263  0000  CNTRZB, 0
4445    3264  1270  CK,     TAD SKPF
4446    3265  7650          SNA CLA
4447    3266  1273          TAD M20
4450    3267  5243          JMP OUT-1
4451    3270  0000  SKPF,   0
4452    3271  0000  CNT4,   0
4453                        M7=CNTRZA
4454    3272  0055  L55,    55
4455    3273  7760  M20,    -20
4456    3274  0040  L40,    40
4457    3275  0060  K60,    60
4460    3276  0000  PLT1,   0
4461    3277  7006          RTL
4462    3300  7006          RTL
4463    3301  7006          RTL
4464    3302  0312          AND L7700
4465    3303  3310          DCA STG
4466    3304  1311          TAD STG+1
4467    3305  4743          JMS I RPLTST
4470    3306  7300          CLA CLL
4471    3307  5676          JMP I PLT1
4472    3310  0000  STG,    0
4473    3311  3310          STG
4474    3312  7700  L7700,  7700
4475    3313  0000  TYPLOT, 0
4476    3314  3346          DCA S
4477    3315  1713          TAD I TYPLOT
4500    3316  0344          AND L77
4501    3317  7041          CIA
4502    3320  3740          DCA I RSCLNL
4503    3321  1713          TAD I TYPLOT
4504    3322  7012          RTR
4505    3323  7012          RTR
4506    3324  7012          RTR
4507    3325  0345          AND L7
4510    3326  3741          DCA I RTRANS
4511    3327  1713          TAD I TYPLOT
4512    3330  7006          RTL
4513    3331  7006          RTL
4514    3332  0345          AND L7
4515    3333  3742          DCA I RLINRU
4516    3334  2313          ISZ TYPLOT
4517    3335  1346          TAD S
4520    3336  4743          JMS I RPLTST
```

```
4521    3337  5713          JMP I TYPLOT
4522                        /
4523    3340  2066  RSCLML, SCLMLT
4524    3341  2067  RTRANS, TRANSQ
4525    3342  2070  RLINRU, LINRUN
4526    3343  2200  RPLTST, PLTSTG
4527    3344  0077  L77,    77
4530    3345  0007  L7,     7
4531    3346  0000  S,      0
4532                        /
4533                        PLSF=6501
4534                        PLCF=6502
4535                        PLPU=6504
4536                        PLPR=6511
4537                        PLDU=6512
4540                        PLDD=6514
4541                        PLPL=6521
4542                        PLUD=6522
4543                        PLPD=6524
4544                        PAGE
4545    3400  0000  PLOTX,  0
4546    3401  7510          SPA
4547    3402  5220          JMP PLOTA
4550    3403  1361          TAD PLOTPN
4551    3404  7112          CLL RTR
4552    3405  7710          SPA CLA
4553    3406  5227          JMP PLOT1
4554    3407  7620          SNL CLA
4555    3410  5214          JMP .+4
4556    3411  3361          DCA PLOTPN
4557    3412  6504          PLPU
4560    3413  5216          JMP .+3
4561    3414  2361          ISZ PLOTPN
4562    3415  6524          PLPD
4563    3416  4370          JMS PLOTNT
4564    3417  5227          JMP PLOT1
4565    3420  7200  PLOTA,  CLA
4566    3421  6504          PLPU
4567    3422  3361          DCA PLOTPN
4570    3423  3362          DCA PLOTNX
4571    3424  3363          DCA PLOTNY
4572    3425  4370          JMS PLOTNT
4573    3426  5600          JMP I PLOTX
4574    3427  1362  PLOT1,  TAD PLOTNX
4575    3430  7141          CIA CLL
4576    3431  1600          TAD I PLOTX
4577    3432  7420          SNL
4600    3433  7041          CIA
4601    3434  3364          DCA PLOTDX
4602    3435  7004          RAL
4603    3436  3367          DCA PLOTNY
4604    3437  1600          TAD I PLOTX
4605    3440  3362          DCA PLOTNX
4606    3441  2200          ISZ PLOTX
4607    3442  1363          TAD PLOTNY
4610    3443  7141          CIA CLL
4611    3444  1600          TAD I PLOTX
4612    3445  7420          SNL
4613    3446  7041          CIA
4614    3447  3365          DCA PLOTDY
4615    3450  1367          TAD PLOTNY
4616    3451  7004          RAL
4617    3452  3367          DCA PLOTNY
```

```
4620    3453  1600          TAD I PLOTX
4621    3454  3363          DCA PLOTNY
4622    3455  2200          ISZ PLOTX
4623    3456  1364          TAD PLOTDX
4624    3457  7141          CIA CLL
4625    3460  1365          TAD PLOTDY
4626    3461  7620          SNL CLA
4627    3462  5275          JMP PLOT2
4630    3463  1364          TAD PLOTDX
4631    3464  3366          DCA PLOTNA
4632    3465  1365          TAD PLOTDY
4633    3466  3364          DCA PLOTDX
4634    3467  1366          TAD PLOTNA
4635    3470  3365          DCA PLOTDY
4636    3471  7001          IAC
4637    3472  0367          AND PLOTNY
4640    3473  1342          TAD PLOT11
4641    3474  5300          JMP .+4
4642    3475  1367  PLOT2,  TAD PLOTNY
4643    3476  7110          CLL RAR
4644    3477  1345          TAD PLOT12
4645    3500  3366          DCA PLOTNA
4646    3501  1766          TAD I PLOTNA
4647    3502  3340          DCA PLOT4
4650    3503  1365          TAD PLOTDY
4651    3504  7640          SZA CLA
4652    3505  5310          JMP .+3
4653    3506  1766          TAD I PLOTNA
4654    3507  5314          JMP .+5
4655    3510  1367          TAD PLOTNY
4656    3511  1350          TAD PLOT13
4657    3512  3367          DCA PLOTNY
4660    3513  1767          TAD I PLOTNY
4661    3514  3334          DCA PLOTDB
4662    3515  1365          TAD PLOTDY
4663    3516  7041          CIA
4664    3517  3365          DCA PLOTDY
4665    3520  1364          TAD PLOTDX
4666    3521  7040          CMA
4667    3522  3367          DCA PLOTNY
4670    3523  1364          TAD PLOTDX
4671    3524  7110          CLL RAR
4672    3525  2367  PLOT3,  ISZ PLOTNY
4673    3526  7410          SKP
4674    3527  5600          JMP I PLOTX
4675    3530  7100          CLL
4676    3531  1365          TAD PLOTDY
4677    3532  7430          SZL
4700    3533  5340          JMP PLOT4
4701    3534  0000  PLOTDB, 0
4702    3535  1364          TAD PLOTDX
4703    3536  4370          JMS PLOTNT
4704    3537  5325          JMP PLOT3
4705    3540  0000  PLOT4,  0
4706    3541  5336          JMP .-3
4707    3542  3543  PLOT11, .+1
4710    3543  6511          PLPR
4711    3544  6521          PLPL
4712    3545  3546  PLOT12, .+1
4713    3546  6512          PLDU
4714    3547  6514          PLDD
4715    3550  3551  PLOT13, .+1
4716    3551  6513          PLDU!PLPR
```

```
4717    3552  6523          PLUD!PLPL
4720    3553  6515          PLDD!PLPR
4721    3554  4355          JMS .+1
4722    3555  0000          0
4723    3556  6514          PLDD
4724    3557  6521          PLPL
4725    3560  5755          JMP I .-3
4726    3561  0000  PLOTPN,  0
4727    3562  0000  PLOTNX,  0
4730    3563  0000  PLOTNY,  0
4731    3564  0000  PLOTDX,  0
4732    3565  0000  PLOTDY,  0
4733    3566  0000  PLOTNR,  0
4734    3567  0000  PLOTNV,  0
4735    3570  0000  PLOTNT,  0
4736    3571  6501          PLSF
4737    3572  5371          JMP .-1
4740    3573  6502          PLCF
4741    3574  5770          JMP I PLOTNT
4742                        /
4743                        MQL=7421
4744                        DVI=7407
4745                        MQA=7501
4746                        /
4747                        PMODE
4750                        *177
4751    0177  0000  OUT0,   0
4752    0200  6046          TLS
4753    0201  7300          CLA CLL
4754    0202  4162          JMS CRLF
4755    0203  4162          JMS CRLF
4756    0204  1062          TAD K322        /R
4757    0205  4154          JMS TYPE
4760    0206  1066          TAD K240        /SPACE
4761    0207  4154          JMS TYPE
4762    0210  1062          TAD K322        /R
4763    0211  4154          JMS TYPE
4764    0212  1050          TAD K301        /A
4765    0213  4154          JMS TYPE
4766    0214  1064          TAD K324        /T
4767    0215  4154          JMS TYPE
4770    0216  1052          TAD K305        /E
4771    0217  4154          JMS TYPE
4772    0220  1066          TAD K240        /SPACE
4773    0221  4154          JMS TYPE
4774    0222  1066          TAD K240        /SPACE
4775    0223  4154          JMS TYPE
4776    0224  1057          TAD K315        /M
4777    0225  4154          JMS TYPE
5000    0226  1066          TAD K240        /SPACE
5001    0227  4154          JMS TYPE
5002    0230  1426          TAD I PR1       /MEAN RESP RATE
5003    0231  4114          JMS TYP
5004    0232  1054          TAD K310        /H
5005    0233  4154          JMS TYPE
5006    0234  1066          TAD K240        /SPACE
5007    0235  4154          JMS TYPE
5010    0236  1427          TAD I PR2       /HIGH
5011    0237  4114          JMS TYP
5012    0240  1056          TAD K314        /L
5013    0241  4154          JMS TYPE
5014    0242  1066          TAD K240        /SPACE
5015    0243  4154          JMS TYPE
```

```
5016    0244  1430        TAD I PR3       /LOW
5017    0245  4114        JMS TYP
5020    0246  1060        TAD K316        /N
5021    0247  4154        JMS TYPE
5022    0250  1066        TAD K240        /SPACE
5023    0251  4154        JMS TYPE
5024    0252  1431        TAD I PR4       /NUMBER TRAINS
5025    0253  4114        JMS TYP
5026    0254  6211        CDF 10
5027    0255  1045        TAD K5000       /INDIVID RATES
5030    0256  4423        JMS I TO1
5031    0257  6201        CDF 0
5032    0260  1064        TAD K324        /T
5033    0261  4154        JMS TYPE
5034    0262  1062        TAD K322        /R
5035    0263  4154        JMS TYPE
5036    0264  1050        TAD K301        /A
5037    0265  4154        JMS TYPE
5040    0266  1055        TAD K311        /I
5041    0267  4154        JMS TYPE
5042    0270  1060        TAD K316        /N
5043    0271  4154        JMS TYPE
5044    0272  1063        TAD K323        /S
5045    0273  4154        JMS TYPE
5046    0274  1066        TAD K240        /SPACE
5047    0275  4154        JMS TYPE
5050    0276  1066        TAD K240        /SPACE
5051    0277  4154        JMS TYPE
5052    0300  1055        TAD K311        /I
5053    0301  4154        JMS TYPE
5054    0302  1060        TAD K316        /N
5055    0303  4154        JMS TYPE
5056    0304  1064        TAD K324        /T
5057    0305  4154        JMS TYPE
5060    0306  1066        TAD K240        /SPACE
5061    0307  4154        JMS TYPE
5062    0310  1066        TAD K240        /SPACE
5063    0311  4154        JMS TYPE
5064    0312  1063        TAD K323        /S
5065    0313  4154        JMS TYPE
5066    0314  1064        TAD K324        /T
5067    0315  4154        JMS TYPE
5070    0316  1066        TAD K240        /SPACE
5071    0317  4154        JMS TYPE
5072    0320  1432        TAD I PR5       /ST
5073    0321  4114        JMS TYP
5074    0322  1060        TAD K316        /N
5075    0323  4154        JMS TYPE
5076    0324  1066        TAD K240        /SPACE
5077    0325  4154        JMS TYPE
5100    0326  6211        CDF 10
5101    0327  1443        TAD I K2000     /NUMBER TRAINS
5102    0330  4114        JMS TYP
5103    0331  1044        TAD K3777       /TRAIN LENGTH
5104    0332  4425        JMS I TO3
5105    0333  6201        CDF 0
5106    0334  1053        TAD K306        /F
5107    0335  4154        JMS TYPE
5110    0336  1055        TAD K311        /I
5111    0337  4154        JMS TYPE
5112    0340  1062        TAD K322        /R
5113    0341  4154        JMS TYPE
5114    0342  1063        TAD K323        /S
-
```

```
5115    0343  4154    JMS TYPE
5116    0344  1064    TAD K324        /T
5117    0345  4154    JMS TYPE
5120    0346  1066    TAD K240        /SPACE
5121    0347  4154    JMS TYPE
5122    0350  1055    TAD K311        /I
5123    0351  4154    JMS TYPE
5124    0352  1060    TAD K316        /N
5125    0353  4154    JMS TYPE
5126    0354  1064    TAD K324        /T
5127    0355  4154    JMS TYPE
5130    0356  6211    CDF 10
5131    0357  1042    TAD K777        /FIRST INTERVALS
5132    0360  4423    JMS I T01
5133    0361  6201    CDF 0
5134    0362  1057    TAD K315        /M
5135    0363  4154    JMS TYPE
5136    0364  1066    TAD K240        /SPACE
5137    0365  4154    JMS TYPE
5140    0366  1055    TAD K311        /I
5141    0367  4154    JMS TYPE
5142    0370  1060    TAD K316        /N
5143    0371  4154    JMS TYPE
5144    0372  1064    TAD K324        /T
5145    0373  4154    JMS TYPE
5146    0374  1052    TAD K305        /E
5147    0375  4154    JMS TYPE
5150    0376  1062    TAD K322        /R
5151    0377  4154    JMS TYPE
5152    0400  1065    TAD K326        /V
5153    0401  4154    JMS TYPE
5154    0402  1050    TAD K301        /A
5155    0403  4154    JMS TYPE
5156    0404  1056    TAD K314        /L
5157    0405  4154    JMS TYPE
5160    0406  1063    TAD K323        /S
5161    0407  4154    JMS TYPE
5162    0410  1066    TAD K240        /SPACE
5163    0411  4154    JMS TYPE
5164    0412  1066    TAD K240        /SPACE
5165    0413  4154    JMS TYPE
5166    0414  1057    TAD K315        /M
5167    0415  4154    JMS TYPE
5170    0416  1052    TAD K305        /E
5171    0417  4154    JMS TYPE
5172    0420  1060    TAD K316        /N
5173    0421  4154    JMS TYPE
5174    0422  1066    TAD K240        /SPACE
5175    0423  4154    JMS TYPE
5176    0424  1441    TAD I PT2       /MEAN
5177    0425  4114    JMS TYP
5200    0426  1057    TAD K315        /M
5201    0427  4154    JMS TYPE
5202    0430  1055    TAD K311        /I
5203    0431  4154    JMS TYPE
5204    0432  1066    TAD K240        /SPACE
5205    0433  4154    JMS TYPE
5206    0434  1433    TAD I PR6       /MI
5207    0435  4114    JMS TYP
5210    0436  1060    TAD K316        /N
5211    0437  4154    JMS TYPE
5212    0440  1066    TAD K240        /SPACE
5213    0441  4154    JMS TYPE
```

```
5214    0442  1434        TAD I PM1       /NUMBER INT
5215    0443  4114        JMS TYP
5216    0444  6211        CDF 10
5217    0445  1047        TAD K7777       /AVG INTERVALS
5220    0446  4423        JMS I TO1
5221    0447  6201        CDF 0
5222    0450  1055        TAD K311        /I
5223    0451  4154        JMS TYPE
5224    0452  1063        TAD K323        /S
5225    0453  4154        JMS TYPE
5226    0454  1055        TAD K311        /I
5227    0455  4154        JMS TYPE
5230    0456  1054        TAD K310        /H
5231    0457  4154        JMS TYPE
5232    0460  1066        TAD K240        /SPACE
5233    0461  4154        JMS TYPE
5234    0462  1066        TAD K240        /SPACE
5235    0463  4154        JMS TYPE
5236    0464  1057        TAD K315        /M
5237    0465  4154        JMS TYPE
5240    0466  1061        TAD K317        /O
5241    0467  4154        JMS TYPE
5242    0470  1051        TAD K304        /D
5243    0471  4154        JMS TYPE
5244    0472  1066        TAD K240        /SPACE
5245    0473  4154        JMS TYPE
5246    0474  1435        TAD I PM2       /MODE
5247    0475  4114        JMS TYP
5250    0476  1057        TAD K315        /M
5251    0477  4154        JMS TYPE
5252    0500  1061        TAD K317        /O
5253    0501  4154        JMS TYPE
5254    0502  1060        TAD K316        /N
5255    0503  4154        JMS TYPE
5256    0504  1066        TAD K240        /SPACE
5257    0505  4154        JMS TYPE
5260    0506  1440        TAD I PT1       /MON
5261    0507  4114        JMS TYP
5262    0510  1057        TAD K315        /M
5263    0511  4154        JMS TYPE
5264    0512  1052        TAD K305        /E
5265    0513  4154        JMS TYPE
5266    0514  1051        TAD K304        /D
5267    0515  4154        JMS TYPE
5270    0516  1066        TAD K240        /SPACE
5271    0517  4154        JMS TYPE
5272    0520  1437        TAD I PM4       /MEDIAN
5273    0521  4114        JMS TYP
5274    0522  1060        TAD K316        /N
5275    0523  4154        JMS TYPE
5276    0524  1066        TAD K240        /SPACE
5277    0525  4154        JMS TYPE
5300    0526  1436        TAD I PM3       /NUMBER INT
5301    0527  4114        JMS TYP
5302    0530  6211        CDF 10
5303    0531  1046        TAD K5777       /HISTO TABLE
5304    0532  4424        JMS I TO2
5305    0533  6201        CDF 0
5306    0534  4162        JMS CRLF        /SPACE PAPER
5307    0535  4162        JMS CRLF
5310    0536  4162        JMS CRLF
5311    0537  4162        JMS CRLF
5312    0540  4162        JMS CRLF
-
```

```
5313    0541  4162          JMS CRLF
5314    0542  4162          JMS CRLF
5315    0543  4162          JMS CRLF
5316    0544  4162          JMS CRLF
5317    0545  4162          JMS CRLF
5320    0546  4162          JMS CRLF
5321    0547  5577          JMP I OUT0      /EXIT
5322                  /
5323                        *600
5324    0600  0000  OUT1,    0               /TELETYPE OUT
5325    0601  3012          DCA 12
5326    0602  6046          TLS             /ROUTINE
5327    0603  7300          CLA CLL
5330    0604  4162          JMS CRLF
5331    0605  4162          JMS CRLF
5332    0606  7200          CLA
5333    0607  1072          TAD M12
5334    0610  3073          DCA DON
5335    0611  7200  AX,     CLA
5336    0612  1412          TAD I 12
5337    0613  7440          SZA
5340    0614  5220          JMP .+4
5341    0615  4162          JMS CRLF
5342    0616  4162          JMS CRLF
5343    0617  5600          JMP I OUT1
5344    0620  4114          JMS TYP
5345    0621  2073          ISZ DON
5346    0622  5227          JMP DB
5347    0623  4162          JMS CRLF
5350    0624  7200          CLA
5351    0625  1072          TAD M12
5352    0626  3073          DCA DON
5353    0627  4101  DB,     JMS KEY
5354    0630  7440          SZA
5355    0631  5211          JMP AX
5356    0632  1070          TAD K260
5357    0633  3074          DCA CP
5360    0634  4162          JMS CRLF
5361    0635  4162          JMS CRLF
5362    0636  5600          JMP I OUT1
5363                  /
5364    0637  0000  OUT2,    0
5365    0640  3012          DCA 12
5366    0641  6046          TLS
5367    0642  7300          CLA CLL
5370    0643  4162          JMS CRLF
5371    0644  4162          JMS CRLF
5372    0645  7200          CLA
5373    0646  1072          TAD M12
5374    0647  3073          DCA DON
5375    0650  1076          TAD N175
5376    0651  3077          DCA CNT
5377    0652  7200  AX2,    CLA
5400    0653  1412          TAD I 12
5401    0654  4114          JMS TYP
5402    0655  2077          ISZ CNT
5403    0656  5260          JMP .+2
5404    0657  5637          JMP I OUT2
5405    0660  2073          ISZ DON
5406    0661  5266          JMP DB2
5407    0662  4162          JMS CRLF
5410    0663  7200          CLA
5411    0664  1072          TAD M12
```

```
5412    0665  3073          DCA DON
5413    0666  4101  DB2,    JMS KEY
5414    0667  7440          SZA
5415    0670  5252          JMP AX2
5416    0671  1070          TAD K260
5417    0672  3074          DCA CP
5420    0673  5637          JMP I OUT2
5421                  /
5422    0674  0000  OUT3,    0
5423    0675  3012          DCA 12
5424    0676  6046          TLS
5425    0677  7300          CLA CLL
5426    0700  4162          JMS CRLF
5427    0701  4162          JMS CRLF
5430    0702  7200          CLA
5431    0703  1071          TAD N2
5432    0704  3073          DCA DON
5433    0705  7200  AX3,    CLA
5434    0706  1412          TAD I 12
5435    0707  7440          SZA
5436    0710  5313          JMP .+3
5437    0711  4162          JMS CRLF
5440    0712  5674          JMP I OUT3
5441    0713  4114          JMS TYP
5442    0714  1066          TAD K240        /SPACE
5443    0715  4154          JMS TYPE
5444    0716  1066          TAD K240        /SPACE
5445    0717  4154          JMS TYPE
5446    0720  2073          ISZ DON
5447    0721  5305          JMP AX3
5450    0722  4162          JMS CRLF
5451    0723  7200          CLA
5452    0724  1071          TAD N2
5453    0725  3073          DCA DON
5454    0726  4101          JMS KEY
5455    0727  7440          SZA
5456    0730  5305          JMP AX3
5457    0731  1070          TAD K260
5460    0732  3074          DCA CP
5461    0733  4162          JMS CRLF
5462    0734  5674          JMP I OUT3
5463                  /
5464                  *22
5465    0022  0177  TO0,     OUT0            /8 MODE PAGE 0
5466    0023  0600  TO1,     OUT1
5467    0024  0637  TO2,     OUT2
5470    0025  0674  TO3,     OUT3
5471    0026  5760  PR1,     R1
5472    0027  5761  PR2,     R2
5473    0030  5762  PR3,     R3
5474    0031  5763  PR4,     R4
5475    0032  5764  PR5,     R5
5476    0033  5765  PR6,     R6
5477    0034  5766  PH1,     H1
5500    0035  5767  PH2,     H2
5501    0036  5770  PH3,     H3
5502    0037  5771  PH4,     H4
5503    0040  5772  PT1,     T1
5504    0041  5773  PT2,     T2
5505    0042  0777  K777,    777
5506    0043  2000  K2000,   2000
5507    0044  3777  K3777,   3777
5510    0045  5000  K5000,   5000
```

```
5511    0046  5777  K5777,  5777
5512    0047  7777  K7777,  7777
5513    0050  0301  K301,   301          /A
5514    0051  0304  K304,   304          /D
5515    0052  0305  K305,   305          /E
5516    0053  0306  K306,   306          /F
5517    0054  0310  K310,   310          /H
5520    0055  0311  K311,   311          /I
5521    0056  0314  K314,   314          /L
5522    0057  0315  K315,   315          /M
5523    0060  0316  K316,   316          /N
5524    0061  0317  K317,   317          /O
5525    0062  0322  K322,   322          /R
5526    0063  0323  K323,   323          /S
5527    0064  0324  K324,   324          /T
5530    0065  0326  K326,   326          /Y
5531    0066  0240  K240,   240          /SPACE
5532    0067  0257  K257,   257          //
5533    0070  0260  K260,   260          /0
5534    0071  7776  N2,     -2
5535    0072  7766  M12,    -12
5536    0073  0000  DON,    0
5537    0074  0000  CP,     0
5540    0075  7455  M323,   -323
5541    0076  7603  N175,   -175
5542    0077  0000  CNT,    0
5543    0100  0000  REM,    0
5544          /
5545    0101  0000  KEY,    0            /CHECK FOR HIT
5546    0102  6031        KSF            /S (STOP) KEY
5547    0103  5106        JMP .+3
5550    0104  6036        KRB
5551    0105  3074        DCA CP
5552    0106  6032        KCC
5553    0107  6046        TLS
5554    0110  7200        CLA
5555    0111  1074        TAD CP
5556    0112  1075        TAD M323
5557    0113  5501        JMP I KEY
5560          /
5561    0114  0000  TYP,   0            /OCTAL TO
5562    0115  7421        MQL            /DECIMAL
5563    0116  7407        DVI            /CONVERSION
5564    0117  1750        1750           /ROUTINE
5565    0120  3100        DCA REM
5566    0121  7501        MQA
5567    0122  1070        TAD K260
5570    0123  4154        JMS TYPE
5571    0124  1100        TAD REM
5572    0125  7421        MQL
5573    0126  7407        DVI
5574    0127  0144        144
5575    0130  3100        DCA REM
5576    0131  7501        MQA
5577    0132  1070        TAD K260
5600    0133  4154        JMS TYPE
5601    0134  1100        TAD REM
5602    0135  7421        MQL
5603    0136  7407        DVI
5604    0137  0012        12
5605    0140  3100        DCA REM
5606    0141  7501        MQA
5607    0142  1070        TAD K260
```

```
5610      0143  4154          JMS TYPE
5611      0144  1100          TAD REM
5612      0145  1070          TAD K260
5613      0146  4154          JMS TYPE
5614      0147  1066          TAD K240
5615      0150  4154          JMS TYPE
5616      0151  1066          TAD K240
5617      0152  4154          JMS TYPE
5620      0153  5514          JMP I TYP
5621                    /
5622      0154  0000  TYPE,   0               /TYPE ROUTINE
5623      0155  6041          TSF
5624      0156  5155          JMP .-1
5625      0157  6046          TLS
5626      0160  7200          CLA
5627      0161  5554          JMP I TYPE
5630                    /
5631      0162  0000  CRLF,   0               /CARRIAGE RETURN
5632      0163  1170          TAD CR          /LINE FEED
5633      0164  4154          JMS TYPE        /ROUTINE
5634      0165  1171          TAD LF
5635      0166  4154          JMS TYPE
5636      0167  5562          JMP I CRLF
5637      0170  0215  CR,     215
5640      0171  0212  LF,     212

NO ERRORS

A       4346
AB      5036
ADDR2A  3252
AK      6374
AM      6435
ARROW   3226
AT      5134
AX      0611
AXIS    6366
AX52    1227
AX2     0652
AX3     0705
B       4334
BACK    6264
BACK1   1117
BACK2   1204
BACK3   1265
BAK1    1320
BAK2    1406
BASAD   2221
BASE    2336
BB1     5542
BB2     5556
BB3     5571
BB4     5637
BB5     5521
BLK     5750
BM      6415
BR      6376
C       4251
CK      3264
CNT     0077
CNTR    2102
CNTR2A  3253
CNTR2B  3263
-
```

```
CNTR2   2323
CNT4    3271
CO      4042
CODE    2322
COLDX   2327
COLDY   2330
CONT    5752
CP      0074
CR      0170
CRLF    0162
CT      0006
CTK     1340
D       4044
DB      0627
DB2     0666
DECPLT  3200
DIGIT   3262
DISF    6115
DISP    6126
DISR    6040
DIS5    6016
DIST    6027
DIS1    6051
DIS2    6062
DIS3    6073
DIS5    6104
DIV     5000
DL      6364
DN      2300
DON     0073
DOWN    7200
DS      4056
DSPY    5734
DT      6344
DUMP    4421
DV      4707
DVI     7407
E       4342
END     6523
EX      1501
EXIT    6515
FI      5743
GAR     5747
GO      4040
HISP    1310
HN      4512
INC1    1125
INC2    1135
INC3    1211
INC4    1224
INC5    1272
INC6    1305
INIT    7240
INTITL  6473
INVRT   2143
KA      5377
KCLAB   4036
KCLEN   4037
KCLLR   4035
KCT     1151
KD      5015
KE      5414
KEY     0101
```

```
KF      5562
KFM     1000
KH      5017
KH5     1001
KINC2   1153
KINC4   1342
KJ      5531
KL      5016
KO      5175
KP      5333
KQ      5142
KR      5525
KS      5363
KTC     1514
KU      5724
KW      5547
KX      5020
KX2     5022
K1      1511
K2000   0043
K240    0066
K257    0067
K260    0070
K301    0050
K304    0051
K305    0052
K306    0053
K310    0054
K311    0055
K314    0056
K315    0057
K316    0060
K317    0061
K322    0062
K323    0063
K324    0064
K326    0065
K3777   0044
K5      1512
K5000   0045
K5777   0046
K60     3275
K7200   1513
K764    1345
K777    0042
K7777   0047
L       2072
LB      6317
LEN     5754
LET     6443
LF      0171
LINRUN  2070
LISN    6446
LK      6326
LLL5    2074
LLL7    2075
LL77    2325
LY      6352
L40     3274
L510    5757
L55     3272
L7      3345
L77     3344
```

```
PLOTDY 3565
PLOTIT 2104
PLOTMV 3567
PLOTNA 3566
PLOTNX 3562
PLOTNY 3563
PLOTPN 3561
PLOTT1 3542
PLOTT2 3545
PLOTT3 3550
PLOTWT 3570
PLOTX  3400
PLOT1  3427
PLOT2  3475
PLOT3  3525
PLOT4  3540
PLPD   6524
PLPL   6521
PLPR   6511
PLPU   6504
PLSF   6501
PLTSTG 2200
PLT1   3276
PLUD   6522
PLUS   3207
PLUT   2112
PL1    1333
PL2    1334
PL3    1476
PL4    1477
PL5    1474
PM1    0034
PM2    0035
PM3    0036
PM4    0037
PNSTAT 2105
PNUPDN 2264
PR     4636
PR1    0026
PR2    0027
PR3    0030
PR4    0031
PR5    0032
PR6    0033
PTEXT1 1002
PTEXT2 1003
PTEXT3 1004
PTEXT4 1005
PTEXT5 1261
PT1    0040
PT2    0041
PUP    2301
PXTABL 0010
PYTABL 0011
P6     1343
Q      4474
Q1     4304
RA     4660
RANX   2064
RANY   2065
RC     5744
RDPACK 2206
RDPK2  2212
```

TIM2	2010
TITL	5727
TITLE	6467
T00	0022
T01	0023
T02	0024
T03	0025
TR	4734
TRANSQ	2067
TRG	5746
TRIG	4552
TRX	2107
TRY	2110
TYP	0114
TYPE	0154
TYPFIN	2256
TYPLOT	3313
T1	5772
T2	5773
UP	7201
UPDATE	2231
V	4371
VALUE	3261
WRITE	4403
W10	5622
W0	5652
W1	5663
W2	5674
W3	5707
W4	5722
XC	6346
XMVT	2107
XY	0005
XYPLT	1020
YMVT	2110
ZRO	5755

```
*L L,$CALC1,0
*W
C FOCAL-12

01.10 L D,F1,U,#0,1
01.20 A !!,"FDP",PF,"LDP",PL
01.30 F DP=PF,PL;D 2
01.40 T !!;L C,F1;Q

02.10 S J=(DP*5+4)*256+221;S NT=F1(J+4);S ST=F1(J+5)/10
02.20 S MI=F1(J+11);S L=MI+(F1(J+8)-MI)/10;S D=ST-FITR(ST)
02.30 D 3
02.40 S J=DP*5*256;S SL=(F1(J+1)-F1(J))/F1(J+1)
02.50 D 4
02.60 D 5

03.10 S K=0;S C1=0;S C2=0
03.20 S J=(DP*5+3)*256;S C3=F1(J+K)
03.30 S C1=C1+C3*F1(J+K+1);S C2=C2+C3*F1(J+K+1)^2
03.40 S K=K+2;S C3=F1(J+K);I (F1(J+K))3.5,3.5,3.3
03.50 S DF=FSQT((C2-C1^2/NT)/(NT-1))
03.55 S DS=DF
03.60 D 3.1;S J=(DP*5+2)*256;S K=-1;S C3=1
03.70 D 3.3
03.80 S K=K+1;I (F1(J+K))3.9,3.9,3.7
03.90 D 3.5

04.10 D 3.1;S C3=0
04.20 I (K-ST+2)4.3,4.3,4.7
04.30 S C1=C1+F1(J+K)
04.40 I (F1(J+K)-L)4.5,4.6,4.6
04.50 S C2=C2+F1(J+K)
04.60 S K=K+1;G 4.2
04.70 S C=F1(J+K)*D;S C1=C1+C
04.80 S LI=D*(F1(J+K)-F1(J+K-1))+F1(J+K-1)

05.10 S J=(DP*5+4)*256+221
05.20 S F1(J+1)=C1/10+.5;S F1(J+2)=60000/F1(J+3)+.5
05.30 S F1(J+6)=DS*10+.5;S F1(J+7)=100*DS/FSQT(NT)+.5
05.40 S F1(J+9)=DF+.5;S F1(J+10)=10*DF/FSQT(NT)+.5
05.50 S F1(J+16)=C2/10+.5;S F1(J+19)=LI+.5;S F1(J+20)=-SL*100+.5
05.60 S F1(J+33)=C2*1000/C1+.5;S F1(J+34)=C1*10/F1(J+2)+.5
*
```

```
*L L,$CALC2,0
*W
C FOCAL-12
01.10 L 0,F1,U,#0,1
01.20 A !!,"FDP",PF,"LDP",PL
01.30 F DP=PF,PL;D 2
01.40 T !!;L C,F1;Q

02.10 S J=(DP*5+4)*256+221
02.20 S MI=F1(J+11);S D=F1(J+8)-MI
02.30 S K5=.5*D+MI;S K7=.3*D+MI;S K9=.1*D+MI
02.40 D 4
02.50 D 6

04.10 S K=0;S T=0;S J=DP*5*256;S L=K5;D 5
04.20 S T5=D;S N5=N;S L=K7;D 5
04.30 S T7=D;S N7=N;S L=K9;D 5
04.40 S T9=D;S N9=N;S L=MI;D 5
04.50 S T1=D;S N1=N

05.10 I (F1(J+K)-L)5.3,5.3,5.2
05.20 S T=T+F1(J+K);S K=K+1;G 5.1
05.30 S M=(F1(J+K)-F1(J+K-1))/F1(J+K)
05.40 S D=T+(L-F1(J+K-1))/M
05.50 S N=K-(F1(J+K-1)-L)/(F1(J+K)-F1(J+K-1))

06.10 S J=(DP*5+4)*256+221
06.20 S F1(J+21)=T5/10+.5;S F1(J+22)=T7/10+.5
06.30 S F1(J+23)=T9/10+.5;S F1(J+24)=T1/10+.5
06.40 S F1(J+25)=N5*10+.5;S F1(J+26)=N7*10+.5
06.50 S F1(J+27)=N9*10+.5;S F1(J+28)=N1*10+.5
06.60 S D=F1(J+1)/100;S F1(J+29)=T5/D+.5
06.70 S F1(J+30)=T7/D+.5;S F1(J+31)=T9/D+.5
06.80 S F1(J+32)=T1/D+.5
*
```

```
*L L,$READ,0
*W
C FOCAL-12
01.10 L 0,F1,U,#0,1
01.20 A !!,"TAPE",T,"FDP",PF,"LDP",PL
01.30 F DP=PF,PL;D 2
01.40 D 2.05;T %8.04;L C,F1;Q

02.05 S J=(DP*5+4)*256+221;F I=1,31;T "  ",!
02.10 T %3,"DATA POINT",DP+(T-1)*100
02.15 T !!,%11,"TL",F1(J+1),!,"CT",F1(J+2)*10
02.20 T !,%10.01,"RR",F1(J+3)/10,!,%11,"NT",F1(J+4)
02.25 T !,%10.01,"ST",F1(J+5)/10,!,"SD",F1(J+6)/10
02.30 T !,%11.02,"SE",F1(J+7)/100,!,%10.01,"FI",F1(J+8)/10
02.35 T !,"SD",F1(J+9)/10,!,%11.02,"SE",F1(J+10)/100
02.40 T !,%10.01,"MI",F1(J+11)/10,!,%10,"FMN",F1(J+12)
02.45 T !,"HSN",F1(J+13),!,%9.01,"MEN",F1(J+14)/10
02.50 T !,"MED",F1(J+15)/10,!,"MOD",F1(J+16)/10
02.55 T !,%10,"HON",F1(J+17),!,%11,"PL",F1(J+18)
02.60 T !,%10.01,"LI",F1(J+19)/10,!,%4.02,"SL        ",-F1(J+20)/100
02.65 T !,%10,"T50",F1(J+21),!,"T70",F1(J+22)
02.70 T !,"T90",F1(J+23),!,%9.0,"T100",F1(J+24)
02.75 T !,%9.01,"N50",F1(J+25)/10,!,"N70",F1(J+26)/10
02.80 T !,"N90",F1(J+27)/10,!,%8.01,"N100",F1(J+28)/10
02.85 T !,%9.01,"T5P",F1(J+29)/10,!,"T7P",F1(J+30)/10
02.90 T !,"T9P",F1(J+31)/10,!,%8.01,"T10P",F1(J+32)/10
02.95 T !,%9.01,"PLP",F1(J+33)/10,!,"TLP",F1(J+34)/10
*
```

```
*L L,$SUM1,0
*W
C FOCAL-12

01.10 L 0,F1,U,#0,1
01.20 A "TAPE",T,"FDP",PF,"LDP",PL
01.30 T !!,"  DP       RR       NT       ST       SD"
01.40 T "       SE       FI       SD       SE       MI"
01.50 F DP=PF,PL;D 2
01.60 T !!,%8.04;L C,F1;Q

02.10 S J=(DP*5+4)*256+221
02.20 T !,%3,DP+(T-1)*100
02.30 T %6.01,F1(J+3)/10,%7,F1(J+4),%6.01,F1(J+5)/10
02.40 T F1(J+6)/10,%6.02,F1(J+7)/100,%6.01,F1(J+8)/10
02.50 T F1(J+9)/10,%6.02,F1(J+10)/100,%6.01,F1(J+11)/10
*
```

```
*L L,$SUM2,0
*W
C FOCAL-12

01.10 L 0,F1,U,#0,1
01.20 A "TAPE",T,"FDP",PF,"LDP",PL
01.30 T !!,"  DP      FMN      HSN      MEN      MED"
01.40 T "       MOD      MON       PL       LI"
01.50 F DP=PF,PL;D 2
01.60 T !!,%8.04;L C,F1;Q

02.10 S J=(DP*5+4)*256+221
02.20 T !,%3,DP+(T-1)*100
02.30 T %7,F1(J+12),F1(J+13),%6.01,F1(J+14)/10
02.40 T F1(J+15)/10,F1(J+16)/10,%7,F1(J+17)
02.50 T F1(J+18),%6.01,F1(J+19)/10
*
```

```
*L L,$SUM3,0
*W
C FOCAL-12

01.10 L 0,F1,U,#0,1
01.20 A "TAPE",T,"FDP",PF,"LDP",PL
01.30 T  !!,"   DP       SL      T50      T70      T90"
01.40 T "     T100      N50      N70      N90     N100"
01.50 F DP=PF,PL;D 2
01.60 T !!,%8.04;L C,F1;Q

02.10 S J=(DP*5+4)*256+221
02.20 T !,%3,DP+(T-1)*100,"    "
02.30 T %3.02,-F1(J+20)/100,%7,F1(J+21),F1(J+22)
02.40 T F1(J+23),F1(J+24),%6.01,F1(J+25)/10
02.50 T F1(J+26)/10,F1(J+27)/10,F1(J+28)/10
*
```

```
*L L,$SUM4,0
*W
C FOCAL-12

01.10 L 0,F1,U,#0,1
01.20 A "TAPE",T,"FDP",PF,"LDP",PL
01.30 T !!,"   DP       TL       CT      T5P      T7P"
01.40 T "      T9P     T10P      PLP      TLP"
01.50 F DP=PF,PL;D 2
01.60 T !!,%8.04;L C,F1;Q

02.10 S J=(DP*5+4)*256+221
02.20 T !,%3,DP+(T-1)*100
02.30 T %7,F1(J+1),F1(J+2)*10,%6.01,F1(J+29)/10,F1(J+30)/10
02.40 T F1(J+31)/10,F1(J+32)/10,F1(J+33)/10,F1(J+34)/10
*
```

```
*L L,$REORD,0
*W
C FOCAL-12

01.10 L O,F0,U,#0,0
01.20 A !!,"TAPE",T,"FDP",PF,"LDP",PL;S T=(T-1)*100
01.30 D 2
01.40 F R=1,34;S L=R*1000;F DP=PF,PL;D 3
01.50 T !!;L C,F0;Q

02.10 S A(1)=2;S A(2)=21;S A(3)=22;S A(4)=23
02.20 S A(5)=24;S A(6)=18;S A(7)=1;S A(8)=3
02.30 S A(9)=5;S A(10)=8;S A(11)=11;S A(12)=19
02.40 S A(13)=14;S A(14)=15;S A(15)=16;S A(16)=25
02.50 S A(17)=26;S A(18)=27;S A(19)=28;S A(20)=29
02.60 S A(21)=30;S A(22)=31;S A(23)=32;S A(24)=33
02.70 S A(25)=34;S A(26)=20;S A(27)=7;S A(28)=10
02.80 S A(29)=6;S A(30)=9;S A(31)=4;S A(32)=12
02.90 S A(33)=13;S A(34)=17

03.10 L O,F1,U,#0,1
03.20 S J=(DP*5+4)*256+221
03.30 S F1(L+DP+T)=F0(J+A(R))
03.40 L C,F1
*
```

```
*L L,$IVO,0
*W
C FOCAL-12
01.10 L 0,F0,U,#0,0
01.20 F J=1,34;S N=0;S L=J*1000;F K=1,50;S N=N+1;D 2;D 3
01.30 T !!!;L C;F0;Q

02.10 I (N-2)2.2,2.15,2.2
02.15 S N=N+41;R
02.20 I (N-50)2.3,2.25,2.3
02.25 S N=N+32;R
02.30 I (N-85)2.4,2.35,2.4
02.35 S N=N+10;R
02.40 I (N-112)2.5,2.45,2.5
02.45 S N=N+6;R
02.50 I (N-120)2.6,2.55,2.6
02.55 S N=N+11;R
02.60 I (N-140)2.7,2.65,2.7
02.65 S N=N+37;R
02.70 I (N-179)2.8,2.75,2.8
02.75 S N=N+11;R
02.80 I (N-191)2.9,2.85,2.9
02.85 S N=N+7
02.90 R

03.10 L 0,F1,U,#0,1
03.20 S F1(L+K)=F0(L+N)
03.30 L C,F1
*
```

```
*L L,$IVI,0
*W
C FOCAL-12
 ...
01.10 L 0,F0,U,#0,0
01.20 F J=1,34;S N=0;S L=J*1000;F K=1,175;S N=N+1;D 2;D 3
01.30 T !!!;L C,F0;Q

02.05 I (N-1)2.15,2.1,2.15
02.10 S N=N+1;R
02.15 I (N-43)2.25,2.2,2.25
02.20 S N=N+7;R
02.25 I (N-82)2.35,2.3,2.35
02.30 S N=N+3;R
02.35 I (N-95)2.45,2.4,2.45
02.40 S N=N+17;R
02.45 I (N-118)2.55,2.5,2.55
02.50 S N=N+2;R
02.55 I (N-131)2.65,2.6,2.65
02.60 S N=N+9;R
02.65 I (N-177)2.75,2.7,2.75
02.70 S N=N+2;R
02.75 I (N-190)2.85,2.8,2.85
02.80 S N=N+1;R
02.85 I (N-198)2.95,2.9,2.95
02.90 S N=N+8
02.95 R

03.10 L 0,F1,U,#0,1
03.20 S F1(L+K)=F0(L+N)
03.30 L C,F1
*
```

```
*L L,$EVO,0
*W
C FOCAL-12

01.10 L O,F0,U,#0,0
01.20 F J=1,34;S N=0;S L=J*1000;F K=1,3;S N=N+1;D 2;D 3
01.30 T !!!;L C,F0;Q

02.10 I (N-1)2.3,2.2,2.3
02.20 S N=N+19;R
02.30 I (N-21)2.5,2.4,2.5
02.40 S N=N+45;R
02.50 I (N-67)2.7,2.6,2.7
02.60 S N=N+15
02.70 R

03.10 L O,F1,U,#0,1
03.20 S F1(L+K)=F0(L+N)
03.30 L C,F1
*
```

```
*L L,$EVI,0
*W
C FOCAL-12

01.10 L O,F0,U,#0,0
01.20 F J=1,34;S N=0;S L=J*1000;F K=1,105;S N=N+1;D 2;D 3
01.30 T !!!;L C,F0;Q

02.10 I (N-20)2.3,2.2,2.3
02.20 S N=N+1;R
02.30 I (N-66)2.5,2.4,2.5
02.40 S N=N+1;R
02.50 I (N-82)2.7.2.6,2.7
02.60 S N=N+1
02.70 R

03.10 L O,F1,U,#0,1
03.20 S F1(L+K)=F0(L+N)
03.30 L C,F1
*
```

```
*L L,$ROWM,0
*W
C FOCAL-12
 ...
01.10 L 0,F1,U,#0,1
01.20 A !!,"FC",CF,"LC",CL
01.30 F U=CF,CL;D 2;D 3;D 4
01.40 T !!!;L C,F1;Q

02.10 I (U-1).15,2.15,2.2
02.15 S D=.1;R
02.20 I (U-7)2.25,2.25,2.3
02.25 S D=1;R
02.30 I (U-25)2.35,2.35,2.4
02.35 S D=10;R
02.40 I (U-28)2.45,2.45,2.5
02.45 S D=100;R
02.50 I (U-30)2.55,2.55,2.6
02.55 S D=10;R
02.60 S D=1

03.10 S N=0;S C1=0;S C2=0;S H=0
03.20 S K=U*1000+1;S L=F1(K)/D
03.30 S X=F1(K+N)/D
03.35 I (X)3.4,3.7,3.4
03.40 I (X-L)3.45,3.5,3.5
03.45 S L=X
03.50 I (H-X)3.55,3.6,3.6
03.55 S H=X
03.60 S N=N+1;S C1=C1+X;S C2=C2+X^2;G 3.3
03.70 S M=C1/N;S SD=FSQT((C2-C1^2/N)/(N-1))

04.10 T !!!!,%3"ROW",U,!!,%8.04,"MEAN ",M,!,"SD    ",SD
04.20 T !,"SE    ",SD/FSQT(N),!,"RANGE",H-L
04.30 T !,"LOW   ",L,!,"HIGH ",H
*
```

```
*L L,$RLIN,0
*W
C FOCAL-12
 ...
01.10 L 0,F1,U,#0,1
01.20 A !!,"FC",CF,"LC",CL
01.30 F U=CF,CL;D 2
01.40 D 5;T %8.04;L C,F1;Q

02.10 D 5
02.20 F V=1,13;D 3
02.30 D 5
02.40 F V=14,26;D 3

03.10 S A=U;D 6
03.20 S XD=D
03.30 S A=V;D 6
03.40 S YD=D
03.50 D 4

04.10 S N=0;S C1=0;S C2=0;S C3=0;S C4=0;S C5=0
04.15 S XL=U*1000+1;S YL=V*1000+1
04.20 S X=F1(XL+N)/XD;S Y=F1(YL+N)/YD
04.25 I (X)4.3,4.45,4.3
04.30 S N=N+1
04.35 S C1=C1+X;S C2=C2+X^2;S C3=C3+Y
04.40 S C4=C4+Y^2;S C5=C5+X+Y;G 4.2
04.45 S DX=C2-C1^2/N;S DY=C4-C3^2/N
04.50 S NU=C5-C1*C3/N;S R=NU/FSQT(DX*DY)
04.55 S M=NU/DX;S B=(C3-C1*M)/N
04.60 S S=DY-DX*M^2;S E=FSQT(S/(N-2))
04.65 T !!!,%2.0,"X",U,"    Y",V,%9.04
04.70 T "    B",B,"    M",M*1000,"    E",E,"    R",R,
04.75 T !,"                N",N,"    D",DX,"    S",S,"    V",R^2

05.10 F I=1,14;T "   ",!
05.20 T "LINEAR FIT-   Y=B+X*M/1000+E"

06.10 I (A-1)6.2,6.2,6.3
06.20 S D=.1;R
06.30 I (A-7)6.4,6.4,6.5
06.40 S D=1;R
06.50 I (A-25)6.6,6.6,6.7
06.60 S D=10;R
06.70 S D=100
*
```

```
#L L,$REXP,0
#N
C FOCAL-12
 .
01.10 L D,F1,U,#0,1
01.20 A !!,"FC",CF,"LC",CL
01.30 F U=CF,CL;D 2
01.40 D 5;T %8.04;L C,F1;Q

02.10 D 5
02.20 F V=1,13;D 3
02.30 D 5
02.40 F V=14,26;D 3

03.10 S A=U;D 6
03.20 S XD=D
03.30 S A=V;D 6
03.40 S YD=D
03.50 D 4

04.10 S N=0;S C1=0;S C2=0;S C3=0;S C4=0;S C5=0
04.15 S XL=U*1000+1;S YL=V*1000+1
04.20 S X=F1(XL+N)/XD;S Y=F1(YL+N)/YD
04.25 I (X)4.3,4.45,4.3
04.30 S Y=FLOG(Y);S N=N+1
04.35 S C1=C1+X;S C2=C2+X^2;S C3=C3+Y
04.40 S C4=C4+Y^2;S C5=C5+X*Y;G 4.2
04.45 S DX=C2-C1^2/N;S DY=C4-C3^2/N
04.50 S NU=C5-C1*C3/N;S R=NU/FSQT(DX*DY)
04.55 S M=NU/DX;S B=(C3-C1*M)/N
04.60 S S=DY-DX*M^2;S E=FSQT(S/(N-2))
04.65 T !!!,%2.0,"X",U,"    Y",V,%9.04
04.70 T "    B",B,"    M",M*1000,"    E",E,"    R",R
04.75 T !,"                N",N,"    D",DX,"    S",S,"    Y",R^2

05.10 F I=1,14;T "   ",!
05.20 T "EXPONENTIAL FIT-    Y=EXP(B+X*M/1000+E)"

06.10 I (A-1)6.2,6.2,6.3
06.20 S D=.1;R
06.30 I (A-7)6.4,6.4,6.5
06.40 S D=1;R
06.50 I (A-25)6.6,6.6,6.7
06.60 S D=10;R
06.70 S D=100
*
```

```
*L L,$RLOG,0
*W
C FOCAL-12

01.10 L D,F1,U,#0,1
01.20 A !!,"FC",CF,"LC",CL
01.30 F U=CF,CL;D 2
01.40 D 5;T %8.04;L C,F1;Q

02.10 D 5
02.20 F V=1,13;D 3
02.30 D 5
02.40 F V=14,26;D 3

03.10 S A=U;D 6
03.20 S XD=D
03.30 S A=V;D 6
03.40 S YD=D
03.50 D 4

04.10 S N=0;S C1=0;S C2=0;S C3=0;S C4=0;S C5=0
04.15 S XL=U*1000+1;S YL=V*1000+1
04.20 S X=F1(XL+N)/XD;S Y=F1(YL+N)/YD
04.25 I (X)4.3,4.45,4.3
04.30 S X=FLOG(X);S N=N+1
04.35 S C1=C1+X;S C2=C2+X^2;S C3=C3+Y
04.40 S C4=C4+Y^2;S C5=C5+X*Y;G 4.2
04.45 S DX=C2-C1^2/N;S DY=C4-C3^2/N
04.50 S NU=C5-C1*C3/N;S R=NU/FSQT(DX*DY)
04.55 S M=NU/DX;S B=(C3-C1*M)/N
04.60 S S=DY-DX*M^2;S E=FSQT(S/(N-2))
04.65 T !!!,%2.0,"X",U,"    Y",V,%9.04
04.70 T "    B",B,"    M",M,"    E",E,"    R",R
04.75 T !,"                N",N,"    D",DX,"    S",S,"    Y",R^2

05.10 F I=1,14;T "  ",!
05.20 T "LOGARITHMIC FIT-    Y=B+LN(X)*M+E"

06.10 I (A-1)6.2,6.2,6.3
06.20 S D=.1;R
06.30 I (A-7)6.4,6.4,6.5
06.40 S D=1;R
06.50 I (A-25)6.6,6.6,6.7
06.60 S D=10;R
06.70 S D=100
*
```

```
*L L,$RLLG,0
*N
C FOCAL-12
 . . .
01.10 L 0,F1,U,#0,1
01.20 A !!,"FC",CF,"LC",CL
01.30 F U=CF,CL;D 2
01.40 D 5;T %8.04;L C,F1;Q

02.10 D 5
02.20 F V=1,13;D 3
02.30 D 5
02.40 F V=14,26;D 3

03.10 S A=U;D 6
03.20 S XD=D
03.30 S A=V;D 6
03.40 S YD=D
03.50 D 4

04.10 S N=0;S C1=0;S C2=0;S C3=0;S C4=0;S C5=0
04.15 S XL=U*1000+1;S YL=V*1000+1
04.20 S X=F1(XL+N)/XD;S Y=F1(YL+N)/YD
04.25 I (X)4.3,4.45,4.3
04.30 S X=FLOG(X);S Y=FLOG(Y);S N=N+1
04.35 S C1=C1+X;S C2=C2+X^2;S C3=C3+Y
04.40 S C4=C4+Y^2;S C5=C5+X*Y;G 4.2
04.45 S DX=C2-C1^2/N;S DY=C4-C3^2/N
04.50 S NU=C5-C1*C3/N;S R=NU/FSQT(DX*DY)
04.55 S M=NU/DX;S B=(C3-C1*M)/N
04.60 S S=DY-DX*M^2;S E=FSQT(S/(N-2))
04.65 T !!!,%2.0,"X",U,"    Y",V,%9.04
04.70 T "    B",B,"    M",M*1000,"    E",E,"    R",R
04.75 T !,"                N",N,"    D",DX,"    S",S,"    Y",R^2

05.10 F I=1,14;T "  ",!
05.20 T "LOG-LOG FIT-    Y=EXP(B+LN(X)*M/1000+E)"

06.10 I (A-1)6.2,6.2,6.3
06.20 S D=.1;R
06.30 I (A-7)6.4,6.4,6.5
06.40 S D=1;R
06.50 I (A-25)6.6,6.6,6.7
06.60 S D=10;R
06.70 S D=100
*
```

```
*L L,$REGSD,0
*W
C FOCAL-12

01.10 A !!,"N1",N1,!,"N2",N2
01.20 A !,"D1",D1,!,"D2",D2
01.30 A !,"S1",S1,!,"S2",S2
01.40 A !,"M1",M1,!,"M2",M2
01.50 S DF=N1+N2-4;S S=(S1+S2)/DF
01.60 S DI=FSQT(S/(D1+D2))
01.70 S T=FABS((M1-M2)/DI)

02.10 S C=.63661977
02.20 S D=FSQT(DF)
02.30 S TH=FATN(T/D);S X=DF/(DF+T^2)
02.40 I (DF-1)2.5,2.5,3.1
02.50 S A=C*TH;G 4.5

03.10 S TS=FITR(DF/2);S TS=2*TS
03.20 I (DF-TS)3.3,3.3,3.4
03.30 S IX=1;G 3.5
03.40 S IX=2
03.50 S A=1;S Y=1;S Z=IX;S W=Z+1
03.60 I (DF-W)4.1,4.1,3.7
03.70 S Y=X*Y*Z/W
03.80 S A=A+Y;S Z=Z+2;S W=W+2;G 3.6

04.10 I (2-IX)4.2,4.2,4.4
04.20 S N=FSQT(X-X^2)
04.30 S A=C*(TH+A*N);G 4.5
04.40 S N=FSQT(1-X);S A=A*N
04.50 S P=1-A

05.10 T !!,"DF=",DF,!,"T= ",T,!,"P= ",P,!!!
*
```

```
#L L,$RSIGD,0
#W
C FOCAL-12

01.10 A !!,"N1",N1,"N2",N2,"R1",R1,"R2",R2
01.20 S Z1=(FLOG(1+R1)-FLOG(1-R1))/2
01.30 S Z2=(FLOG(1+R2)-FLOG(1-R2))/2
01.40 S S=1/(N1-3)+1/(N2-3)
01.50 S C=FABS((Z1-Z2)/FSQT(S));T !,"C=",C
01.60 D 2
01.70 G 1.1

02.10 I (C-1.959964)2.14,2.17,2.2
02.14 T "    NS  P>.05";R
02.17 T "    S  P=.05";R
02.20 I (C-2.053749)2.24,2.27,2.3
02.24 T "    S  P<.05";R
02.27 T "    S  P=.04";R
02.30 I (C-2.170090)2.34,2.37,2.4
02.34 T "    S  P<.04";R
02.37 T "    S  P=.03";R
02.40 I (C-2.326348)2.44,2.47,2.5
02.44 T "    S  P<.03";R
02.47 T "    S  P=.02";R
02.50 I (C-2.575829)2.54,2.57,2.6
02.54 T "    S  P<.02";R
02.57 T "    S  P=.01";R
02.60 T "    S  P<.01";R
*
```

```
*L L,$PVALR,0
*W
C FOCAL-12

01.10 A !!,"N",N,!,"R",R
01.20 S DF=N-2;S D=FSQT(DF)
01.30 S T=FSQT(1-R^2);S T=R*D/T

02.10 S C=.63661977
02.20 S D=FSQT(DF)
02.30 S TH=FATN(T/D);S X=DF/(DF+T^2)
02.40 I (DF-1)2.5,2.5,3.1
02.50 S A=C*TH;G 4.5

03.10 S TS=FITR(DF/2);S TS=2*TS
03.20 I (DF-TS)3.3,3.3,3.4
03.30 S IX=1;G 3.5
03.40 S IX=2
03.50 S A=1;S Y=1;S Z=IX;S W=Z+1
03.60 I (DF-W)4.1,4.1,3.7
03.70 S Y=X*Y*Z/W
03.80 S A=A+Y;S Z=Z+2;S W=W+2;G 3.6

04.10 I (2-IX)4.2,4.2,4.4
04.20 S N=FSQT(X-X^2)
04.30 S A=C*(TH+A*N);G 4.5
04.40 S N=FSQT(1-X);S A=A*N
04.50 S P=1-A

05.10 T !,"DF=",DF,!,"T= ",T
05.20 T !,%10.10,"P= ",P,%8.04
05.30 G 1.1
*
```

```
*L L,$STTEST,0
*W
C FOCAL-12

01.10 S C1=0;S C2=0;S R=0
01.20 A !!,"NX",N
01.30 F J=1,N;A !,V;S C1=C1+V;S C2=C2+V^2
01.40 S MX=C1/N;S K=(C2-C1^2/N)/(N-1);S DX=FSQT(K)
01.50 S EX=DX/FSQT(N);S DF=N
01.60 D 1.1;A !!,"NY",N;D 1.3
01.70 S MY=C1/N;S K=(C2-C1^2/N)/(N-1);S DY=FSQT(K)
01.80 S EY=DY/FSQT(N);S DF=DF+N-2
01.85 A !!,"PAIRED?",Y;I (Y-25)1.95,1.9,1.95
01.90 A !,"R",R;S DF=DF/2
01.95 S T=FABS((MX-MY)/FSQT(EX^2+EY^2-2*R*EX*EY))

02.10 S C=.63661977
02.20 S D=FSQT(DF)
02.30 S TH=FATN(T/D);S X=DF/(DF+T^2)
02.40 I (DF-1)2.5,2.5,3.1
02.50 S A=C*TH;G 4.5

03.10 S TS=FITR(DF/2);S TS=2*TS
03.20 I (DF-TS)3.3,3.3,3.4
03.30 S IX=1;G 3.5
03.40 S IX=2
03.50 S A=1;S Y=1;S Z=IX;S W=Z+1
03.60 I (DF-W)4.1,4.1,3.7
03.70 S Y=X*Y*Z/W
03.80 S A=A+Y;S Z=Z+2;S W=W+2;G 3.6

04.10 I (2-IX)4.2,4.2,4.4
04.20 S N=FSQT(X-X^2)
04.30 S A=C*(TH+A*N);G 4.5
04.40 S N=FSQT(1-X);S A=A*N
04.50 S P=1-A

05.10 T !!,"MX=",MX,!,"SD=",DX,!,"SE=",EX
05.20 T !!,"MY=",MY,!,"SD=",DY,!,"SE=",EY
05.30 T !!,"DF=",DF,!,"T= ",T,!,"P= ",P,!!!;Q
*
```

```
*L L,$TIMFOL,0
*W
C FOCAL-12

01.10 S M=0;S D=0;S S=0;T %8.02
01.20 T !,"TL          MIN       DIFF"
01.30 A !!,L;D 5;S Z=T;T M,D
01.40 A !!,L;D 5;S M=T-Z;S D=M-S
01.45 I (L)1.5,1.6,1.5
01.50 T M,D;S S=M;G 1.4
01.60 T !!!,%8.04;Q

05.10 I (L-50)5.15,5.15,5.2
05.15 S T=(L-8)/10.5;R
05.20 I (L-130)5.25,5.25,5.3
05.25 S T=(L-10)/10;R
05.30 I (L-206)5.35,5.35,5.4
05.35 S T=(L-16)/9.5;R
05.40 I (L-278)5.45,5.45,5.5
05.45 S T=(L-26)/9;R
05.50 I (L-380)5.55,5.55,5.6
05.55 S T=(L-40)/8.5;R
05.60 I (L-476)5.65,5.65,5.7
05.65 S T=(L-60)/8;R
05.70 I (L-596)5.75,5.75,5.8
05.75 S T=(L-86)/7.5;R
05.80 I (L-708)5.85,5.85,5.95
05.85 S T=(L-120)/7;R
05.95 S T=(L-162)/6.5;R
*
```

```
*L L,%PLOT,0
*W
C FOCAL-12
 .
01.10 L D,F0,I,#0,0
01.15 L D,F1,I,#0,1
01.20 D C
01.25 A !!,"PEN DOWN",G;S P=0;S C1=0;S C2=0;S T=0
01.30 S A=FDIS(0,0);S A=FDIS(0,.68)
01.35 S A=FDIS(1.02,.68);S A=FDIS(1.02,0)
01.40 S A=FDIS(0,0);D P
01.45 D C
01.50 S A=FDIS(0,.34);S A=FDIS(1.02,.34);D P
01.55 D C
01.60 S A=FDIS(.34,0);S A=FDIS(.34,.68);D P
01.65 D C
01.70 S A=FDIS(.68,0);S A=FDIS(.68,.68);D P
01.75 D C
01.80 A "PEN UP",G

02.10 S P=P+1;S C1=FABS(C1-.34)
02.20 I (P-3)2.4,2.3,2.4
02.30 S C2=.34;S T=1
02.40 I (P-5)2.6,2.5,2.6
02.50 S C2=.68;S T=0
02.60 I (P-6)3.1,3.1,2.7
02.70 D R
02.80 T !!!;S G=F0(0);L C,F0;L C,F1;Q

03.10 T !!!,%2,"PLOT",P,%8.04
03.20 A !,"X ROW",XR,!,"X SCALE",XS
03.30 S U=XR*1000;S D=XR;D 5;S XS=XS*D
03.40 A !,"Y ROW",YR,!,"Y SCALE",YS
03.50 S V=YR*1000;S D=YR;D 5;S YS=YS*D

04.10 S K=0
04.15 S K=K+1
04.20 I (T)4.25,4.25,4.3
04.25 S X=F0(U+K);S Y=F0(V+K);G 4.35
04.30 S X=F1(U+K);S Y=F1(V+K)
04.35 I (X)4.4,4.65,4.45
04.40 S X=X+4096
04.45 I (Y)4.5,4.65,4.55
04.50 S Y=Y+4096
04.55 S A=FDIS(C2+X*.34/XS,C1+Y*.34/YS)
04.60 G 4.15
04.65 D P
04.70 D C
04.75 G 2.1

05.10 I (D-1)5.2,5.2,5.3
05.20 S D=.1;R
05.30 I (D-7)5.4,5.4,5.5
05.40 S D=1;R
05.50 I (D-25)5.6,5.6,5.7
05.60 S D=10;R
05.70 S D=100
*
```

```
*L L,%REGP1,0
*W
C FOCAL-12

01.10 A !!!,"PEN DOWN",G
01.20 S P=0;S C1=0;S C2=0
01.30 S P=P+1;S C1=FABS(C1-.34)
01.40 I (P-3)1.6,1.5,1.6
01.50 S C2=.34
01.60 I (P-5)1.8,1.7,1.8
01.70 S C2=.68
01.80 I (P-6)2.1,2.1,1.9
01.90 D R
01.95 G 1.2

02.10 D C
02.15 T !!!,%2.0,"PLOT",P,%8.04
02.20 A !,"REG FIT",R,!,"B",B,!,"M",M,!,"E",E
02.25 A !,"X LOW",XL,!,"X HIGH",XH;S B=B-2*E
02.30 A !,"X SCALE",XS,!,"Y SCALE",YS;S S=(XH-XL)/25
02.35 I (R-1)2.4,2.4,2.5
02.40 F I=1,3;D 3
02.45 G 1.3
02.50 I (R-2)2.55,2.55,2.65
02.55 F I=1,3;D 4
02.60 G 1.3
02.65 I (R-3)2.7,2.7,2.8
02.70 F I=1,3;D 5
02.75 G 1.3
02.80 I (R-4)2.85,2.85,2.15
02.85 F I=1,3;D 6
02.90 G 1.3

03.10 S B=B+E
03.20 D C
03.30 F J=XL,S,XH;S Y=(B+M*J)*.34/YS;D 7
03.40 D P

04.10 S B=B+E
04.20 D C
04.30 F J=XL,S,XH;S Y=FEXP(B+M*J)*.34/YS;D 7
04.40 D P

05.10 S B=B+E
05.20 D C
05.30 F J=XL,S,XH;S Y=(B+M*FLOG(J))*.34/YS;D 7
05.40 D P

06.10 S B=B+E
06.20 D C
06.30 F J=XL,S,XH;S Y=FEXP(B+M*FLOG(J))*.34/YS;D 7
06.40 D P

07.10 I (Y)7.4,7.2,7.2
07.20 I (Y-.34)7.3,7.3,7.4
07.30 S A=FDIS(C2+J*.34/XS,C1+Y)
07.40 R
*
```

```
*L L,%REGP2,0
*W
C FOCAL-12

01.10 A "PEN DOWN",G,!!!;O C
01.15 S P=0;S C1=0;S C2=0
01.20 S A=FDIS(0,0);S A=FDIS(0,.68)
01.25 S A=FDIS(1.02,.68);S A=FDIS(1.02,0)
01.30 S A=FDIS(0,0);O P
01.35 O C
01.40 S A=FDIS(0,.34);S A=FDIS(1.02,.34);O P
01.45 O C
01.50 S A=FDIS(.34,0);S A=FDIS(.34,.68);O P
01.55 O C
01.60 S A=FDIS(.68,0);S A=FDIS(.68,.68);O P
01.65 O C

02.10 S P=P+1;S C1=FABS(C1-.34)
02.15 I (P-3)2.25,2.2,2.25
02.20 S C2=.34
02.25 I (P-5)2.35,2.3,2.35
02.30 S C2=.68
02.35 I (P-6)2.5,2.5,2.4
02.40 O R
02.45 G 1.15
02.50 A !!!,"N",N
02.55 F K=1,N;D 3
02.60 O C
02.65 G 2.1

03.10 O C
03.15 T !!,%2,"PLOT",P,%8.04
03.20 A !,"REG FIT",R,!,"B",B,!,"M",M
03.25 A !,"X LOW",XL,!,"X HIGH",XH
03.30 A !,"X SCALE",XS,!,"Y SCALE",YS;S S=(XH-XL)/25
03.35 I (R-1)3.4,3.4,3.5
03.40 O C
03.42 F J=XL,S,XH;S Y=(B+M*J)*.34/YS;D 4
03.44 O P
03.46 R
03.50 I (R-2)3.55,3.55,3.65
03.55 O C
03.57 F J=XL,S,XH;S Y=FEXP(B+M*J)*.34/YS;D 4
03.59 O P
03.61 R
03.65 I (R-3)3.7,3.7,3.8
03.70 O C
03.72 F J=XL,S,XH;S Y=(B+M*FLOG(J))*.34/YS;D 4
03.74 O P
03.76 R
03.80 I (R-4)3.85,3.85,3.1
03.85 O C
03.87 F J=XL,S,XH;S Y=FEXP(B+M*FLOG(J))*.34/YS;D 4
03.89 O P

04.10 I (Y)4.4,4.2,4.2
04.20 I (Y-.34)4.3,4.3,4.4
04.30 S A=FDIS(C2+J*.34/XS,C1+Y)
04.40 R
*
```

```
*L L.%LINEP.0
*W
C FOCAL-12
01.10 L 0,F1,I,#0,1
01.20 A !!,"PEN DOWN",G
01.30 D 7
01.40 A !!!,"FDP",PF,!,"LDP",PL

02.10 A !!,"T100",D;S M=.34
02.20 F J=2,5;D 5
02.30 A !!,"TL",D;S M=.68
02.40 F J=6,7;D 5
02.50 A !!,"FI/LI",D;S D=D*10;S M=1.02
02.60 F J=10,12;D 5
02.70 O R
02.80 D 7

03.10 A !!,"MEN",D;S D=D*10;S M=.34
03.20 F J=13,15;D 5
03.30 A !!,"N100",D;S D=D*10;S M=.68
03.40 F J=16,19;D 5
03.50 A !!,"RR/ST",D;S D=D*10;S M=1.02
03.60 F J=8,9;D 5
03.70 O R
03.80 D 7

04.10 A !!,"SL",D;S D=-D*100;S M=.34
04.20 S J=26;D 5
04.30 S D=1000;S M=.68
04.40 F J=20.23;D 5
04.50 S M=1.02
04.60 F J=24,25;D 5
04.70 O R
04.80 G 1.3

05.10 S L=J*1000
05.20 F K=PF,PL;S V=F1(L+K);D 6
05.30 O P
05.40 O C

06.10 I (V)6.2,6.3,6.3
06.20 S V=V+4096
06.30 S A=FDIS(M-V*.34/D,.68*(K-PF)/(PL-PF))

07.10 O C
07.20 S A=FDIS(0,0);S A=FDIS(0,.68)
07.30 S A=FDIS(1.02,.68);S A=FDIS(1.02,0)
07.40 S A=FDIS(0,0);O P
07.50 O C
07.60 S A=FDIS(.34,0);S A=FDIS(.34,.68);O P
07.70 O C
07.80 S A=FDIS(.68,0);S A=FDIS(.68,.68);O P
07.90 O C
*
```

Table VIII. Regression equations of 24 parameters on respiration rate for I-VO cells.

1. T50 = 147.2220 + 21.1092 · ln(RR) ± 98.7780
2. T70 = 156.0950 + 63.3316 · ln(RR) ± 165.1760
3. T90 = 405.9660 + 44.2711 · ln(RR) ± 253.2590
4. T100 = EXP[6.8533 - 0.0193(RR ± 0.7480]
5. PL = 792.7180 - 16.8713(RR) ± 273.1040
6. TL = EXP[7.9172 - 0.0355(RR) ± 0.2342]
7. FI = 88.0191 - 1.5262(RR) ± 25.5480
8. MI = 36.6944 - 4.5819 · ln(RR) ± 10.8402
9. LI = 75.3811 - 13.1186 · ln(RR) ± 12.7498
10. MEN = 52.9135 - 7.5962 · ln(RR) ± 12.4183
11. MED = 43.3729 - 5.4107 · ln(RR) ± 11.9047
12. MOD = 35.1646 - 3.3601 · ln(RR) ± 10.9786
13. N50 = -0.0234 + 1.4496 · ln(RR) ± 1.7945
14. N70 = -1.4086 + 3.1496 · ln(RR) ± 4.4809
15. N90 = 3.9172 + 3.4890 · ln(RR) ± 6.5986
16. N100 = EXP[3.3038 - 0.0088(RR) ± 0.4769]
17. ST = 124.0940 - 24.1712 · ln(RR) ± 25.8741
18. SL = EXP[-0.6432 - 0.0583(RR) ± 0.9638]
19. T5P = -6.4697 + 7.1477 · ln(RR) ± 6.0545
20. T7P = -14.6178 + 12.9528 · ln(RR) ± 9.6405
21. T9P = 14.2368 + 17.3266 · ln(RR) ± 14.9481
22. T10P = 6.1723 + 16.8245 · ln(RR) ± 21.9979
23. PLP = EXP[2.4491 + 0.3447 · ln(RR) ± 0.4723]
24. TLP = EXP[2.3434 + 0.4872 · ln(RR) ± 0.2374]

Table IX. Regression equations of 24 parameters on respiration rate for I-VI cells.

1. T50 = EXP[5.2791 - 0.0168(RR) ± 0.4879]
2. T70 = EXP[5.9359 - 0.0207(RR) ± 0.4527]
3. T90 = 544.7000 - 5.3169(RR) ± 110.3810
4. T100 = 1822.4400 - 367.3070 · ln(RR) ± 151.5740
5. PL = EXP[8.9515 - 0.9727 · ln(RR) ± 0.5897]
6. TL = EXP[7.4751 - 0.0216(RR) ± 0.3241]
7. FI = EXP[4.1577 - 0.0144(RR) ± 0.4247]
8. MI = EXP[3.0236 - 0.0097(RR) ± 0.4929]
9. LI = EXP[3.4636 - 0.0084(RR) ± 0.5742]
10. MEN = EXP[3.3497 - 0.0103(RR) ± 0.4487]
11. MED = EXP[3.2064 - 0.0101(RR) ± 0.4596]
12. MOD = EXP[3.0901 - 0.0097(RR) ± 0.4704]
13. N50 = EXP[1.3283 - 0.0029(RR) ± 0.5420]
14. N70 = EXP[2.1464 - 0.0079(RR) ± 0.6085]
15. N90 = EXP[3.2366 - 0.1684 · ln(RR) ± 0.5423]
16. N100 = EXP[4.4251 - 0.3482 · ln(RR) ± 0.5332]
17. ST = 133.7710 - 24.1028 · ln(RR) ± 26.2316
18. SL = 0.2676 + 0.0009(RR) ± 0.1664
19. T5P = EXP[1.6797 + 0.2574 · ln(RR) ± 0.6053]
20. T7P = 13.8721 + 3.2756 · ln(RR) ± 12.3565
21. T9P = 14.4688 + 8.2056 · ln(RR) ± 14.5038
22. T10P = 44.8520 + 5.2108 · ln(RR) ± 15.8760
23. PLP = 53.8008 - 5.4440 · ln(RR) ± 13.9808
24. TLP = EXP[3.1710 + 0.1823 · ln(RR) ± 0.3230]

Table X. Regression equations of 24 parameters on respiration rate for E-VI cells.

1. $T50 = 414.4040 - 80.5027 \cdot \ln(RR) \pm 49.1951$
2. $T70 = 675.8920 - 133.5940 \cdot \ln(RR) \pm 78.0391$
3. $T90 = 1438.1000 - 299.7580 \cdot \ln(RR) \pm 147.7610$
4. $T100 = 2617.3300 - 569.2290 \cdot \ln(RR) \pm 219.7980$
5. $PL = 1495.4300 - 325.7690 \cdot \ln(RR) \pm 162.7690$
6. $TL = 3048.0900 - 632.1220 \cdot \ln(RR) \pm 203.9220$
7. $FI = 164.2190 - 31.3311 \cdot \ln(RR) \pm 15.0115$
8. $MI = 47.4782 - 8.5725 \cdot \ln(RR) \pm 5.9890$
9. $LI = 50.0437 - 7.2535 \cdot \ln(RR) \pm 7.5328$
10. $MEN = 63.2751 - 11.2802 \cdot \ln(RR) \pm 7.1998$
11. $MED = 55.7401 - 10.0034 \cdot \ln(RR) \pm 6.7460$
12. $MOD = 51.5672 - 9.4249 \cdot \ln(RR) \pm 6.4786$
13. $N50 = 2.8954 + 0.0026(RR) \pm 1.0860$
14. $N70 = EXP[1.9225 - 0.0856 \cdot \ln(RR) \pm 0.4301]$
15. $N90 = EXP[3.3632 - 0.2598 \cdot \ln(RR) \pm 0.5371]$
16. $N100 = EXP[4.8054 - 0.4883 \cdot \ln(RR) \pm 0.5994]$
17. $ST = EXP[3.8809 - 0.0087(RR) \pm 0.4402]$
18. $SL = 0.3539 - 0.0007(RR) \pm 0.1330$
19. $T5P = 12.1021 + 0.1206(RR) \pm 5.9030$
20. $T7P = 18.5201 + 0.1848(RR) \pm 8.2920$
21. $T9P = 41.1972 + 0.1200(RR) \pm 12.9830$
22. $T10P = 105.7470 - 9.9173 \cdot \ln(RR) \pm 16.8018$
23. $PLP = 49.2392 - 0.2522(RR) \pm 13.3991$
24. $TLP = 31.3642 + 0.3127(RR) \pm 12.2442$

Table XI. Regression equations of 24 parameters on mode for I-VO cells.

1. T50 = EXP[1.0320 + 1.2984 · ln(MOD) ± 0.4121]
2. T70 = EXP[0.8938 + 1.4780 · ln(MOD) ± 0.4866]
3. T90 = EXP[1.3322 + 1.4884 · ln(MOD) ± 0.5060]
4. T100 = EXP[2.8979 + 1.1556 · ln(MOD) ± 0.4785]
5. PL = EXP[4.8709 + 0.3974 · ln(MOD) ± 0.4734]
6. TL = EXP[6.9655 + 0.0141(MOD) ± 0.2555]
7. FI = EXP[1.6716 + 0.7526 · ln(MOD) ± 0.2953]
8. MI = EXP[-0.2865 + 1.0628 · ln(MOD) ± 0.0819]
9. LI = EXP[3.1848 + 0.0164(MOD) ± 0.3305]
10. MEN = EXP[0.6723 + 0.8603 · ln(MOD) ± 0.0963]
11. MED = EXP[0.1401 + 0.9860 · ln(MOD) ± 0.0701]
12. RR = EXP[2.8361 - 0.0035(MOD) ± 0.3519]
13. N50 = EXP[-0.2682 + 0.4897 · ln(MOD) ± 0.3919]
14. N70 = EXP[-0.3260 + 0.6783 · ln(MOD) ± 0.5045]
15. N90 = EXP[0.5364 + 0.6099 · ln(MOD) ± 0.5160]
16. N100 = EXP[2.7940 + 0.1159 · ln(MOD) ± 0.4755]
17. ST = EXP[5.7306 - 0.5586 · ln(MOD) ± 0.2817]
18. SL = 1.5777 - 0.4054 · ln(MOD) ± 0.1762
19. T5P = EXP[-0.7570 + 1.0007 · ln(MOD) ± 0.4944]
20. T7P = EXP[-0.9009 + 1.1821 · ln(MOD) ± 0.5395]
21. T9P = EXP[-0.4554 + 1.1903 · ln(MOD) ± 0.5328]
22. T10P = EXP[1.1015 + 0.8601 · ln(MOD) ± 0.4767]
23. PLP = EXP[3.0794 + 0.1005 · ln(MOD) ± 0.4852]
24. TLP = 9.3865 + 10.1569 · ln(MOD) ± 10.7925

Table XII. Regression equations of 24 parameters on mode for I-VI cells.

1. T50 = EXP[3.4807 + 0.4385 · ln(MOD) ± 0.4992]
2. T70 = EXP[4.2152 + 0.3596 · ln(MOD) ± 0.5112]
3. T90 = EXP[5.0715 + 0.2638 · ln(MOD) ± 0.4108]
4. T100 = EXP[5.5763 + 0.2304 · ln(MOD) ± 0.4115]
5. PL = 118.0350 + 74.1879 · ln(MOD) ± 214.8230
6. TL = EXP[5.8916 + 0.2984 · ln(MOD) ± 0.4226]
7. FI = EXP[1.8325 + 0.6608 · ln(MOD) ± 0.3431]
8. MI = EXP[-0.1469 + 1.0296 · ln(MOD) ± 0.0848]
9. LI = EXP[0.5052 + 0.9691 · ln(MOD) ± 0.3438]
10. MEN = EXP[0.4260 + 0.9319 · ln(MOD) ± 0.1187]
11. MED = EXP[0.1874 + 0.9697 · ln(MOD) ± 0.0754]
12. RR = 57.9943 - 8.2390 · ln(MOD) ± 13.6773
13. N50 = EXP[1.5490 - 0.0186(MOD) ± 0.5220]
14. N70 = 12.3624 - 0.2541(MOD) ± 5.6031
15. N90 = EXP[3.2714 - 0.0358(MOD) ± 0.4619]
16. N100 = EXP[3.9485 - 0.0425(MOD) ± 0.4265]
17. ST = EXP[4.4601 - 0.0402(MOD) ± 0.4317]
18. SL = 0.4408 - 0.0518 · ln(MOD) ± 0.1649
19. T5P = EXP[2.4029 + 0.0101(MOD) ± 0.6075]
20. T7P = EXP[3.0127 + 0.0048(MOD) ± 0.5512]
21. T9P = 49.1428 - 2.1869 · ln(MOD) ± 14.7922
22. T10P = 75.3259 - 4.4685 · ln(MOD) ± 15.8466
23. PLP = EXP[3.5634 - 0.0067(MOD) ± 0.4934]
24. TLP = EXP[3.5274 + 0.1022 · ln(MOD) ± 0.3264]

Table XIII. Regression equations of 24 parameters on mode for E-VI cells.

1. T50 = 43.8866 + 4.6491(MOD) $\pm$ 51.7531
2. T70 = 75.7932 + 6.8930(MOD) $\pm$ 87.0515
3. T90 = 92.4733 + 15.4179(MOD) $\pm$ 171.5270
4. T100 = 178.3820 + 22.8032(MOD) $\pm$ 312.2210
5. PL = 205.4960 + 7.1587(MOD) $\pm$ 224.2730
6. TL = 406.0200 + 21.6303(MOD) $\pm$ 336.7980
7. FI = 19.3363 + 1.8472(MOD) $\pm$ 15.9847
8. MI = EXP[0.0741 + 0.9541 · ln(MOD) $\pm$ 0.0576]
9. LI = EXP[1.4074 + 0.6132 · ln(MOD) $\pm$ 0.2543]
10. MEN = 2.9307 + 1.1204(MOD) $\pm$ 1.7804
11. MED = 1.4173 + 1.0386(MOD) $\pm$ 1.1502
12. RR = EXP[4.2340 - 0.0372(MOD) $\pm$ 0.4073]
13. N50 = 4.1876 - 0.4250 · ln(MOD) $\pm$ 1.0718
14. N70 = 8.5037 - 1.0773 · ln(MOD) $\pm$ 2.2008
15. N90 = 24.4363 - 4.1020 · ln(MOD) $\pm$ 5.6749
16. N100 = 58.5247 - 11.7915 · ln(MOD) $\pm$ 13.4960
17. ST = 98.2588 - 21.4823 · ln(MOD) $\pm$ 16.2235
18. SL = 0.3880 - 0.0034(MOD) $\pm$ 0.1308
19. T5P = EXP[2.2873 + 0.1666 · ln(MOD) $\pm$ 0.3945]
20. T7P = EXP[2.8490 + 0.1194 · ln(MOD) $\pm$ 0.3965]
21. T9P = 37.6028 + 0.4654(MOD) $\pm$ 12.6321
22. T10P = 60.9340 + 0.5264(MOD) $\pm$ 17.0150
23. PLP = 52.2560 - 4.6586 · ln(MOD) $\pm$ 14.0615
24. TLP = EXP[4.6441 - 032.46 · ln(MOD) $\pm$ 0.2601]

Table XIV. Best fitting regression equations for 24 parameters on respiration rate and mode for I-VO, I-VI and E-VI cells: linear (LIN); exponential (EXP); logarithmic (LOG); log-log (LLG).

	Parameter	I-VO (RR)	I-VI (RR)	E-VI (RR)	I-VO (MOD)	I-VI (MOD)	E-VI (MOD)
1	T50	LOG	EXP	LOG	LLG	LLG	LIN
2	T70	LOG	EXP	LOG	LLG	LLG	LIN
3	T90	LOG	LIN	LOG	LLG	LLG	LIN
4	T100	EXP	LOG	LOG	LLG	LLG	LIN
5	PL	LIN	LLG	LOG	LLG	LOG	LIN
6	TL	EXP	EXP	LOG	EXP	LLG	LIN
7	FI	LIN	EXP	LOG	LLG	LLG	LIN
8	MI	LOG	EXP	LOG	LLG	LLG	LLG
9	LI	LOG	EXP	LOG	EXP	LLG	LLG
10	MEN	LOG	EXP	LOG	LLG	LLG	LIN
11	MED	LOG	EXP	LOG	LLG	LLG	LIN
12	MOD (RR)	LOG	EXP	LOG	(EXP)	(LOG)	(EXP)
13	N50	LOG	EXP	LIN	LLG	EXP	LOG
14	N70	LOG	EXP	LLG	LLG	LIN	LOG
15	N90	LOG	LLG	LLG	LLG	EXP	LOG
16	N100	EXP	LLG	LLG	LLG	EXP	LOG
17	ST	LOG	LOG	EXP	LLG	EXP	LOG
18	SL	EXP	LIN	LIN	LOG	LOG	LIN
19	T5P	LOG	LLG	LIN	LLG	EXP	LLG
20	T7P	LOG	LOG	LIN	LLG	EXP	LLG
21	T9P	LOG	LOG	LIN	LLG	LOG	LIN
22	T10P	LOG	LOG	LOG	LLG	LOG	LIN
23	PLP	LLG	LOG	LIN	LLG	EXP	LOG
24	TLP	LLG	LLG	LIN	LOG	LLG	LLG

APPROVAL SHEET

The dissertation submitted by Charles Lewis Webber, Jr., has been read and approved by the following Committee:

Dr. Clarence N. Peiss, Chairman
Professor, Physiology and
Associate Dean, Graduate School, Loyola

Dr. Walter C. Randall
Professor and Chairman, Physiology, Loyola

Dr. Robert D. Wurster
Associate Professor, Physiology, Loyola

Dr. Syogoro Nishi
Professor, Pharmacology, Loyola

Dr. Joseph D. Brain
Assistant Professor, Harvard University, Boston

The final copies have been examined by the director of the dissertation and the signature which appears below verifies the fact that any necessary changes have been incorporated and that the dissertation is now given final approval by the Committee with reference to content and form.

The dissertation is therefore accepted in partial fulfillment of the requirements for the degree of Doctor of Philosophy.

August 9, 1973
Date

Clarence N. Peiss
Signature of Advisor